

NASA Contractor Report 172387

(NASA-CR-172387-Phase-2) A STUDY OF
ENVIRONMENTAL CHARACTERIZATION OF
CONVENTIONAL AND ADVANCED ALUMINUM ALLOYS
FOR SELECTION AND DESIGN. PHASE 2: THE
BREAKING (Aluminum Co. of America, Alcoa

N85-11219

Unclas
G3/26 24312

A Study of Environmental Characterization of Conventional and Advanced Aluminum Alloys for Selection and Design

Phase II -The Breaking Load Test Method

**D. O. Sprowls, R. J. Bucci, B. M. Ponchel
R. L. Brazill, and P. E. Bretz**

**Aluminum Company of America
Alcoa Laboratories
Alcoa Center, PA 15069**

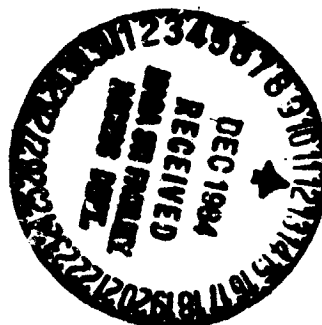
**Contract NAS1-16424
(Period: May 1, 1982 - Aug. 31, 1984)**

August 31, 1984



**National Aeronautics and
Space Administration**

**Langley Research Center
Hampton, Virginia 23665**



FINAL REPORT

A Study of Environmental Characterization
of Conventional and Advanced Aluminum
Alloys for Selection and Design

Phase II - The Breaking Load Test Method

by

D. O. Sprowls, R. J. Bucci, B. M. Ponchel,
R. L. Brazill and P. E. Bretz

Aluminum Company of America
Alcoa Laboratories
Alcoa Center, PA 15069

Prepared for:

National Aeronautics and Space Administration
Langley Research Center
Hampton, VA 23665

Contract NAS1 16424
(Period: May 1, 1982 - August 31, 1984)
NASA Contractor Report No. 172397

August 31, 1984

SYNOPSIS

A new technique is demonstrated for accelerated stress corrosion testing of high strength aluminum alloys. The new procedure offers a higher degree of precision and shorter exposure test periods than the traditional time-to-failure approach, which is useful for characterization of alloys with claims of improved resistance to stress corrosion cracking (SCC). The new approach uses data from tension tests performed on replicate groups of smooth specimens after various lengths of exposure to static stress. The breaking strength measures degradation in the test specimen load carrying ability due to the environmental attack. Analysis of breaking load data by extreme value statistics enables the calculation of survival probabilities and a statistically defined threshold stress applicable to the particular sample of material and the specified testing conditions.

An elastic-plastic fracture mechanics model is given which quantifies damage in a stress corroded specimen by an "effective flaw size" calculated from the measured breaking stress and the strength and fracture toughness properties of the test material. The effective flaw corresponds to the "weakest link" in the specimen test section at the time of the tension test, and it estimates the maximum penetration of SCC attack. An advantage to using flaw depth as the parameter to rank SCC performance is that the potential biases of alloy strength and toughness and of specimen size are removed. In contrast, breaking strength or lifetime under exposure is dependent on the above mechanical

factors. A second advantage of the fracture mechanics interpretation is that the rate of growth of SCC flaws can be estimated from breaking loads obtained from smooth specimens subjected to various exposure intervals. Thus, it is possible to acquire from a single test method the following quantitative types of SCC characterization data: probability of initiation and growth of SCC to an arbitrary shallow depth, and a SCC growth rate that can be correlated to the plateau or average crack velocity measured in traditional precracked specimen tests (DCB or WOL type). The engineering potential of these data is discussed in terms of probabilistic fracture mechanics and application to design and material selection for structural durability.

Comparisons are made with experimental results on three tempers of 7075 alloy plate tested by the breaking load method and by traditional tests of statically loaded smooth tension bars and conventional precracked specimens. Limited data are included for the new Alcoa powder metallurgy alloys 7090 and 7091.

In summary, the breaking load test is shown to be a promising new tool for characterization of SCC in high strength aluminum alloys. The procedures developed in this study bring together for the first time and in a single unified approach, a wide spectrum of aspects that are important to measurement of SCC as follows: statistics, extreme value theory, fracture mechanics (linear-elastic and elastic-plastic), small cracks, shorter test times, fewer specimens, high measurement precision and completely quantitative descriptors of SCC initiation and crack growth.

NASA CONTRACT NAS1-16424 - PHASE II
NASA CONTRACTOR REPORT - NASA CR 172387

TABLE OF CONTENTS

	<u>PAGE</u>
SYNOPSIS	i
TABLE OF CONTENTS	iii
LIST OF TABLES	viii
LIST OF FIGURES	xii
FOREWORD	xx
I. GENERAL OBJECTIVES	1
II. INTRODUCTION (Interpretation of the Problem)	2
A. General Mechanism of SCC in Aluminum Alloys ...	2
B. Purposes of SCC Testing	6
C. State of the Art of Accelerated SCC Testing ...	7
1. Environmental Factors	8
2. Mechanical Concepts	10
3. Materials Selection	15
4. Problems with Accelerated SCC Testing	16
D. New Approach to Smooth Specimen Testing (The Breaking Load Test)	17
E. Summary	18
III. EXPERIMENTAL APPROACH (General Philosophy and Test Procedures)	21
A. Strategy	21
B. Test Materials	24
C. Mechanical Property Test Methods	25
D. Stress Corrosion Test Methods	26
1. Smooth Tension Specimens - Traditional Pass- Fail Tests	26

	<u>PAGE</u>
2. Smooth Tension Specimens - Breaking Load Tests	27
a. Test Program	27
b. Statistical Procedure	28
3. Fracture Mechanics Specimens (DCB and WOL) ..	33
a. DCB Specimen Tests (K-decreasing)	34
b. WOL Specimen Tests (K-increasing)	36
E. Fractographic Procedures	39
F. Correlation of Fracture Stress with Flaw Size..	40
1. Analytical Relationships for the Cylindrical Tension Specimen	41
a. Limit Analysis Solutions	44
b. LEFM Stress-Intensity-Factor Solutions.	45
2. Supplementary Tests of Cylindrical Tension Specimens Containing Fatigue Cracks	49
IV. TEST RESULTS	51
A. Mechanical Properties	51
B. Stress Corrosion Tests of 7075 Alloy Plate.....	52
1. Smooth Tension Specimens - Traditional Pass-Fail Analyses...	52
2. Smooth Tension Specimens - Breaking Load Analyses	52
a. Comparison of the Three Tempers of 7075 Alloy Plate	53
b. Effect of Specimen Diameter on Test Performance of the Intermediate Resistance T7X1 Temper	54
c. Effects of Grain Orientation in Tests of 7075-T651	55

	<u>PAGE</u>
3. Fracture Mechanics Specimens	56
a. Bolt Loaded DCB Specimens (K-decreasing Test)	56
b. Ring Loaded WOL Specimens (K-increasing Test)	62
C. Metallographic and Fractographic Examinations..	66
1. Type of Corrosion and Fracture Characterization	66
2. Flaw Size Measurements on SCC Specimens ...	67
D. Correlation of Fracture Stress with Flaw Size..	71
1. Analytical Relationships for the Cylindrical Tension Specimen Containing an Elliptical Surface Crack	71
2. Fatigue Cracked Tension Specimens, Supplementary Tests	72
a. Effect of Bending Stress on Breaking Load-Flaw Size Correlation	74
3. Equivalent Flaw Sizes Calculated from Breaking Load Tests of SCC Test Specimens..	75
a. Effect of SCC Geometry on Breaking Load-Flaw Size Correlation	76
b. Reduction of SCC Test Results in Terms of Effective Flaw Depth	79
V. DISCUSSION OF TEST RESULTS	82
A. Further Analysis of SCC Breaking Load Test Results	82
1. Comparison of Probabilities of Survival Calculated from Breaking Load and Traditional Pass-Fail Data	82
2. Increased Precision for Characterization of SCC Resistant Materials	82
3. Optimum Length of Environmental Exposure for Breaking Load Tests	85

	<u>PAGE</u>
4. Fracture Mechanics Interpretations	91
a. Effects of Alloy Strength and Toughness	91
b. Effect of Specimen Size	97
5. Mechanistic Implications	99
a. Magnitude of Exposure Stress	99
b. Comparison of Trends in Apparent 0.2% Yield Strength and Tensile Strength (Gross Fracture Stress)	101
6. Breaking Load Test Data on P/M Products ...	106
B. Comparison of SCC Test Methods	111
VI. COMPATIBILITY OF THE BREAKING LOAD TEST APPROACH WITH MATERIAL EVALUATION FOR STRUCTURAL DURABILITY	116
VII. SUMMARY AND CONCLUSIONS	123
VIII. RECOMMENDATIONS	129
A. Recommended Methodology for SCC Characteriza- tion of High Strength Aluminum Alloys	129
1. SCC Tests for Alloy Selection and Design ..	129
2. Screening Tests for Alloy Development	130
B. Future Work - Breaking Load Test Approach	130
1. Additional Verification	131
2. Test/Evaluation Methods	132
3. Fundamental Understanding (Mechanisms)	134
4. Applications	135
XI. REFERENCES	136
XI. TABLES	144
XII. FIGURES	156

	<u>PAGE</u>
XIII. APPENDICES	245
A. Glossary of Symbols	245
B. Calculation of a Statistically Defined Threshold Stress from Breaking Load Test Data..	247
C. Detailed Breaking Load SCC Test Results and a Description of the Probability Plotting Method Used to Statistically Analyze Breaking Load Data	257
1. Breaking Load Test Results	257
2. Description of the Probability Plotting Method for Determining the Extreme Value Distribution Parameters $\hat{\mu}$ and $\hat{\sigma}$	257
D. Detailed Test Data and Analytical Procedures for the Fracture Mechanics Type Stress Corrosion Tests	278
XIV. REPORT DOCUMENTATION PAGE	288

LIST OF TABLES

<u>NO.</u>	<u>PAGE</u>
I Resistance to stress-corrosion ratings for high strength aluminum alloy products.....	144
II Composition and mechanical properties of 2.5 in. thick aluminum alloy 7075-T651 plate used as the basis for the SCC testing program.....	145
III Outdoor SCC tests of short transverse specimens of 7075-T651 plate.....	146
IV Breaking load test program for 7075 alloy plate in three tempers.....	147
V Short transverse tensile and fracture toughness (K_{Ic}) properties of 7X75-type alloys.....	148
VI Summary of breaking load specimen failures of 7075 alloy specimens incurred during exposure to 3.5% NaCl solution by alternate immersion per ASTM G44.	149
VII 99% survival stress and statistical threshold stress values calculated from breaking load tests of three temper variants of 2.5 in. thick 7075 alloy plate exposed to 3.5% NaCl solution by alternate immersion (ASTM G44).....	150
VIII Graphical development of stress corrosion crack growth rate curves from DCB specimens of 7075 alloy plate.....	151
IX Results of SCC tests on fatigue precracked WOL specimens of 7075 alloy plate.....	152
X Flaw size measurements from breaking load specimens oriented in short transverse direction and exposed to 3.5 percent sodium chloride by alternate immersion.....	153
XI Results of breaking load experiments on fatigue precracked, short transverse, 0.125 in. diameter tensile bars of aluminum 7X75 plate alloys.....	154
XII SCC comparisons of three temper variants of 7075 alloy plate by different accelerated SCC test methods - short transverse stress.....	155

LIST OF TABLES (CONTINUED)

<u>NO.</u>		<u>PAGE</u>
B-1	Calculated threshold stresses (point estimates) determined from breaking load test results obtained on three temper variants of alloy 7075 exposed to 3.5% NaCl by alternate immersion.....	252
B-2	Estimation of statistical threshold stress from breaking load test results obtained on three temper variants of aluminum alloy 7075 exposed to 3.5% NaCl by alternate immersion.....	253
C-1	Tensile properties of 0.125 inch diameter short transverse specimens of 7075-T651 alloy exposed to 3.5% sodium chloride solution by alternate immersion.....	263
C-2	Mean and standard deviation of tensile properties for 0.125 inch diameter short transverse specimens of 7075-T651 exposed to 3.5% sodium chloride solution by alternate immersion.....	264
C-3	Extreme value analysis of tensile property data for 0.125 inch diameter short transverse specimens of 7075-T651 exposed to 3.5% sodium chloride solution by alternate immersion.....	265
C-4	Apparent tensile properties of 0.125 inch diameter short transverse specimens of 7075-T7X1 alloy exposed to 3.5% sodium chloride solution by alternate immersion.....	266
C-5	Mean and standard deviation of tensile properties for 0.125 inch diameter short transverse specimens of 7075-T7X1.....	267
C-6	Extreme value analysis of tensile property data for 0.125 inch diameter short transverse specimens of 7075-T7X1 exposed to 3.5% sodium chloride solution by alternate immersion.....	268
C-7	Apparent tensile properties of 0.125 inch diameter short transverse specimens of 7075-T7X2 alloy exposed to 3.5% sodium chloride solution by alternate immersion.....	269
C-8	Mean and standard deviation of tensile properties for 0.125 inch diameter short transverse specimens of 7075-T7X2.....	270

LIST OF TABLES (CONTINUED)

<u>NO.</u>		<u>PAGE</u>
C-9	Extreme value analysis of tensile property data for 0.125 inch diameter short transverse specimens of 7075-T7X2 exposed to 3.5% sodium chloride solution by alternate immersion.....	271
C-10	Apparent tensile properties of 0.225 inch diameter short transverse specimens of 7075-T7X1 alloy exposed to 3.5% sodium chloride solution by alternate immersion.....	272
C-11	Mean and standard deviation of tensile properties for 0.225 inch diameter short transverse specimens of 7075-T7X1.....	273
C-12	Extreme value analysis of tensile property data for 0.225 inch diameter short transverse specimens of 7075-T7X1 exposed to 3.5% sodium chloride solution by alternate immersion.....	274
C-13	Apparent tensile properties of 0.225 inch diameter long transverse specimens of 7075-T651 alloy exposed to 3.5% sodium chloride solution by alternate immersion.....	275
C-14	Mean and standard deviation of tensile properties for 0.225 inch diameter long transverse specimens of 7075-T651 exposed to 3.5% sodium chloride solution by alternate immersion.....	276
C-15	Extreme value analysis of tensile property data for 0.225 inch diameter long transverse specimens of 7075-T651 exposed to 3.5% sodium chloride solution by alternate immersion.....	277
D-1	Environmental crack growth data for 7075-T651, DCB specimen SL-1.....	280
D-2	Environmental crack growth data for 7075-T651, DCB specimen SL-2.....	281
D-3	Environmental crack growth data for 7075-T7X1, DCB specimen SL-1.....	282

LIST OF TABLES (CONTINUED)

<u>NO.</u>		<u>PAGE</u>
D-4	Environmental crack growth data for 7075-T7X1, DCB specimen SL-2.....	283
D-5	Environmental crack growth data for 7075-T7X2, DCB specimen SL-1.....	284
D-6	Environmental crack growth data for 7075-T7X2, DCB specimen SL-2.....	285
D-7	Comparison of data reduction methods for calculating crack growth rates in DCB specimens.	286
D-8	Summary of crack length measurements and stress intensity factor calculations for ring-loaded WOL specimens exposed to 3.5% NaCl solution introduced dropwise into the crack three times a day.....	287

LIST OF FIGURES

<u>NO.</u>	<u>PAGE</u>
1 Causes of premature fracture influenced by corrosion of a structural component.....	156
2 Effects of the magnitude of sustained tensile stress and its orientation relative to the grain structure on the SCC resistance of a metallurgically susceptible material.....	157
3 Effect of temper on SCC performance of alloy 7075 plate stressed in the critical short transverse direction.....	158
4 Effect of variations in geographic atmospheric environment on the probability and time to failure by SCC of a material with intermediate susceptibility.....	159
5 The relative influences of electrochemical and mechanical factors in the corrosion and SCC damage to a susceptible material.....	160
6 Application of linear elastic fracture mechanics (LEFM) to the propagation of SCC.....	161
7 Comparison of SCC growth in 7075 alloy plate for various geographic locations within the continental United States.....	162
8 Schematic diagram of a concept for combining stress corrosion thresholds obtained on smooth and LEFM specimens to give a conservative assessment of materials.....	163
9 Proposed linear-elastic and elastic-plastic models for describing critical combinations of stress and flaw size at SCC thresholds and at the onset of rapid tensile fracture.....	164
10 Schematic representation showing the effect of stress corrosion crack growth and the concurrent crack tip stress and strain field intensity (ie., K or J) on specimen breaking stress after exposure to environment under sustained stress.....	165
11 Effect of applied stress and length of exposure on daily probability of survival of alloy 7075-T651.....	166
12 Grain structure at mid-plane of 2.5 in. thick plate of 7075-T651.....	167

LIST OF FIGURES (CONTINUED)

<u>NO.</u>		<u>PAGE</u>
13	Alcoa stress corrosion stressing frame and loading device.....	168
14	Results of notch tensile tests on three flaw configurations in 0.125 inch diameter 7075-T7351 specimens showing that the net section stress required to cause fracture is notch configuration dependent.....	169
15	Face grooved double cantilever beam (DCB) specimen.....	170
16	Stress intensity factor vs. crack length for the DCB specimen, crack line loaded by constant displacement.....	171
17	Ultrasonic crack measurement system used for DCB specimens.....	172
18	Detailed geometry of the pin-loaded, modified WOL specimens.....	173
19	Stress intensity factor solution for the modified WOL specimen.....	174
20	Ring-loaded WOL specimen test setup.....	175
21	Normalized compliance relationship for the modified WOL specimen.....	176
22	Nomenclature for three practical flaw configurations within a cylindrical tension specimen....	177
23	Limit load, LEFM, and estimated EPFM (wide range) failure criteria for 0.125 in. diameter, short transverse 7075-T651 tension specimens containing an elliptical flaw of depth a and aspect ratio $a/c=0.8$	178
24	Normalized limit solutions for the axial loaded cylindrical tension specimen with various crack configurations and depths.....	179
25	Stress intensity factor solutions for various crack configurations in an axial loaded cylindrical tension specimen.....	180

LIST OF FIGURES (CONTINUED)

<u>NO.</u>		<u>PAGE</u>
26	Typical fracture surface appearance of chord-notched and fatigue precracked 0.125 in. diameter tension specimens as observed under the scanning electron microscope.....	181
27	Typical curve fits through digitized data from SEM fractographs of fatigue cracks in 0.125 in. diameter tension specimens.....	182
28	Comparison of actual and fitted short transverse true stress-true strain behavior of 7075 plate alloys.....	183
29	Comparison of actual and fitted short transverse true stress-true strain behavior of 7475 plate alloys.....	186
30	SCC failure results of short transverse smooth 0.125 in. tension specimens of 7075 alloy plate...	189
31	Mean breaking stress vs. exposure times for short transverse 0.125 in. diameter tension specimens exposed to 3.5% NaCl solution by alternate immersion (ASTM G44) at various exposure stress levels.....	190
32	99% survival stress vs. exposure time corresponding to the mean breaking stresses shown in Figure 31.....	191
33	Standard deviations vs. exposure times corresponding to the mean breaking stresses shown in Figure 31.....	192
34	Effect of specimen diameter on breaking stresses in 7075-T7X1 short transverse specimens.....	193
35	Effect of grain orientation on breaking stresses in 7075-T651 specimens.....	194
36	Crack growth in bolt-loaded DCB specimens exposed to 3.5% NaCl solution introduced dropwise into the crack three times a day.....	195
37	Photograph of fracture surface appearance of 7075 alloy DCB specimens exposed to 3.5% NaCl solution introduced dropwise into the crack three times a day.....	196

LIST OF FIGURES (CONTINUED)

<u>NO.</u>		<u>PAGE</u>
38	Graphically produced crack growth rate curves from bolt-loaded DCB specimens exposed to 3.5% NaCl solution introduced dropwise into the crack three times a day.....	197
39	Comparison of crack growth rate curves obtained with various data reduction techniques.....	198
40	Raw and adjusted crack mouth opening data for ring-loaded, modified WOL specimen of 7075-T7X2...	199
41	Adjusted crack growth curves from ring-loaded WOL specimens exposed to 3.5% NaCl solution introduced dropwise into the crack three times a day.....	200
42	SCC propagation rates from ring-loaded WOL specimens of 7075-T651 alloy exposed to 3.5% NaCl solution introduced dropwise into the crack three times a day.....	201
43	Photomicrographs of tips of fatigue precracks in WOL specimens exposed 1580 hr with no indication of environmental crack growth.....	202
44	Load-displacement records from fracture tests of 7075 WOL specimens after SCC tests.....	203
45	Typical forms of surface attack in smooth tension specimens of the three tempers of 7075 alloy plate exposed six days with no applied stress to 3.5% NaCl alternate immersion and then tension tested..	204
46	Fracture surface of 7075-T651 breaking load specimen ST67, which failed during alternate immersion under 20 ksi exposure stress.....	205
47	Fracture surface maps of several breaking load specimens illustrating the range of flaw sizes and shapes observed [(a)-(h)].....	206
48	SCC flaw sizes corresponding to largest and smallest breaking loads measured in groups of five 7075-T651 alloy 0.125 in. diameter tension specimens exposed to 3.5% NaCl solution by alternate immersion at various levels of exposure stress.....	210

LIST OF FIGURES (CONTINUED)

<u>NO.</u>		<u>PAGE</u>
49	SCC flaw sizes corresponding to largest and smallest breaking loads measured in groups of five 7075-T7X1 alloy 0.125 and 0.225 in. diameter tension specimens exposed to 3.5% NaCl solution by alternate immersion at 40 ksi exposure stress.....	211
50	SCC flaw sizes corresponding to largest and smallest breaking loads measured in groups of five 7075-T7X2 alloy 0.125 in. diameter tension specimens exposed to 3.5% NaCl solution by alternate immersion at 0 and 40 ksi exposure stress.....	212
51	Fracture surface of breaking load specimen of 7075-T651 (ST63) showing: (a) dimples in tensile fracture region and (b) plateau structure in SCC region.....	213
52	Transition from SCC to tensile fracture surface in breaking load specimen of 7075-T651 (ST60).....	214
53	Transition from SCC to tensile fracture in breaking load specimen of 7075-T7X1 (ST80).....	215
54	Limit load, LEFM, and estimated wide-range EPFM failure criteria for 0.125 in. diameter, short transverse 7075-T651 and 7075-T7X2 tension specimens containing an elliptical surface flaw of depth a and aspect ratio $a/c=0.8$	216
55	Limit load, LEFM, and estimated wide-range EPFM failure criteria for 0.125 and 0.225 in. diameter, short transverse 7075-T7X1 tension specimens containing an elliptical surface flaw of depth a and aspect ratio $a/c=0.8$	217
56	Limit load, LEFM, and estimated wide-range EPFM failure criteria for 0.125 diameter, short transverse 7475-T651, 7475-T7651, and 7475-T7351 tension specimens containing an elliptical surface flaw of depth a and aspect ratio $a/c=0.8$	218
57	Comparison of observed fracture stress-flaw size combinations in fatigue cracked short transverse 0.125 in. diameter tension specimens of 7475 and 7075 plate alloys.....	220

LIST OF FIGURES (CONTINUED)

<u>NO.</u>		<u>PAGE</u>
58	Comparison of actual and predicted fracture stress-flaw size combinations in fatigue precracked, 0.125 in. diameter, short transverse tension specimens of commercial 7X75 plate alloys.....	221
59	Comparison of various plasticity-based predictions with actual fracture stress-flaw size combinations in 0.125 in. diameter fatigue precracked tension specimens of 7475-T651 alloy.....	223
60	Comparison of actual and predicted fracture stress vs. maximum SCC flaw depth in stress corroded, 0.125 in. diameter, short transverse tension specimens of alloys 7075-T651 and 7075-T7X2.....	224
61	Comparison of actual and predicted fracture stress vs. maximum SCC flaw depth in stress corroded, 0.125 and 0.225 in. diameter, short transverse tension specimens of alloy 7075-T7X1...	225
62	Comparison of actual and predicted fracture stress vs. depth of equivalent annular crack in stress corroded 0.125 in. diameter short transverse tension specimens of alloys 7075-T651 and 7075-T7X2.....	226
63	Comparison of actual and Predicted fracture stress vs. depth of equivalent annular crack in stress corroded 0.125 and 0.225 in. diameter, short transverse tension specimens of alloy 7075-T7X1.....	227
64	Estimated SCC flaw growth in 7075 alloy tension specimens calculated from breaking load data and the EPFM wide-range model.....	228
65	Comparisons of estimated mean SCC flaw growth in 7075 alloy tension specimens calculated from breaking load data and wide-range EPFM model.....	229
66	Calculated 99% penetration limits for 0.125 in. diameter specimens of 7075-T651, 7075-T7X1, and 7075-T7X2, and for 0.225 in. diameter specimens of 7075-T7X1.....	230

LIST OF FIGURES (CONTINUED)

<u>NO.</u>	<u>PAGE</u>
67	Comparison of survival probabilities for two specimen diameters, calculated from breaking load and traditional pass-fail data for short transverse specimens of 7075-T7X1 exposed to 3.5% NaCl alternate immersion (ASTM G44) for various exposure times and then tensile tested..... 231
68	Comparison of probability of survival calculated from breaking load and traditional pass-fail data for short transverse 0.125 in. diameter specimens of 7075-T651 exposed to 3.5% NaCl alternate immersion (ASTM G44) for various exposure times and then tensile tested..... 232
69	Effect of sample size on lower limit of 95% confidence interval of the estimated probability of survival (P) using pass-fail (binomial) data when all samples survive (P=1)..... 233
70	Summary of breaking load data for short transverse SCC tests of 7075 alloy plate showing the variation in standard deviation and change in mean breaking strength relative to the unexposed data set for each temper..... 234
71	Breaking stress-flaw size relationships developed from EPFM wide-range estimates showing effects of alloy toughness (7075-T7X1 vs. 7475-T7651) and strength (7075-T651 vs. 2014-T651) on results of 0.125 in. diameter tension specimens which contain an elliptical partial thickness crack ($a/c=0.8$)... 235
72	Estimated gross fracture (breaking) stress-flaw size behaviors for various I/M and P/M 7XXX series alloys aged to a T7-type temper condition..... 236
73	Effect of specimen diameter (0.125 in. vs. 0.225 in.) on predicted EPFM wide-range estimate of breaking stress-flaw size behavior in 7075-T7X1 tension specimens containing an elliptical partial thickness crack ($a/c=0.8$)..... 237
74	Comparative trends of mean breaking stress and mean apparent yield strength for 7075-T651 and 7075-T7X1 short transverse 0.125 in. diameter tension specimens exposed to 3.5% NaCl solution by alternate immersion (ASTM G44)..... 238

LIST OF FIGURES (CONTINUED)

<u>NO.</u>		<u>PAGE</u>
75	Comparative trends of mean breaking stress and apparent yield strength of short transverse 0.125 in. diameter specimens of 707-T7X2 and long transverse 0.225 in. diameter specimens of 7075-T651.....	239
76	Influence of progressive amounts of corrosion and SCC damage on load vs. deflection behavior of breaking load test specimens.....	240
77	Comparative SCC performances of various tempers of P/M alloy 7091.....	241
78	Comparative performances of P/M 7090 and 7091 in various tempers at several exposures stress levels.....	242
79	Comparison of breaking load test results from 0.125 in. diameter short transverse tension specimens of I/M and P/M aluminum alloys exposed to 3.5% NaCl solution at 30 ksi exposure stress by alternate immersion (ASTM G44) for various times and then tensile tested.....	243
80	Conceptual usage of small crack data for durability life assessment.....	244
B1	Calculated 99% survival stress vs. exposure stress for 0.125 in. diameter 7075-T651 tension specimens.....	254
B2	Calculated 99% survival stress vs. exposure stress for 0.125 in. diameter 7075-T7X1 tension specimens.....	255
B3	Calculated 99% survival stress vs. exposure stress for 0.225 in. diameter 7075-T7X1 tension specimens.....	256

FOREWORD

The problems arising with proliferating stress corrosion cracking (SCC) test methods and a need to relate various types of laboratory test results with each other and with service requirements has long been recognized. Technical direction at Alcoa Laboratories identified the situation as an industrial problem, and D. O. Sprowls conceived this contracted effort (funded by NASA Langley with W. B. Lisagor, monitor) with the objective of clarifying relationships between various SCC testing techniques and providing guidance on optimum characterization methodology for aluminum alloys.

Under the direction of J. P. Lyle, Alcoa initiated a concurrent experimental program around a new "breaking load" testing approach with smooth specimens developed by B. M. Ponchel, coupled with fracture mechanics interpretations developed by R. J. Bucci and R. L. Brazill. After completion of the literature review under Phase I of the present contract, the breaking load method was viewed to hold considerable promise as a much improved quantitative approach for assessing aluminum alloy SCC behavior. Consequently, the second phase of the contracted program was structured to advance the breaking load testing approach and to verify the claimed advantages of this method over current state-of-the-art SCC characterization procedures.

Experimental and analytical work was performed by the following group: breaking load SCC tests and statistical analyses

of results by B. M. Ponchel, R. L. Brazill, P. R. Ziman, and J. J. Liput, Jr.; correlation of gross fracture stress (breaking load) with the sizes of SCC flaws and of fatigue flaws by R. J. Bucci, R. L. Brazill, P. E. Bretz, and R. E. Burns; fracture mechanics SCC (WOL and DCB) tests and statistical analysis of results by R. L. Brazill and P. R. Ziman. Mechanical tests, fractographic, and metallographic examinations were directed by R. H. Wygonik, P. E. Bretz, and R. H. Stevens, respectively.

The literature review and preparation of the Phase I report was performed by D. O. Sprowls with assistance from R. J. Bucci and R. L. Brazill on mechanical aspects and their interpretation. Summary and recommendations from the literature survey, coordination of the experimental program and editing of the Phase I and Phase II reports was done by D. O. Sprowls and R. J. Bucci. Reviews of the Phase II manuscript were made by J. W. Clark, T. L. Hartman, B. W. Lifka, S. R. Novak and J. T. Staley, as well as by the co-authors of the report.

Acknowledgement also is made of breaking load SCC data on powder metallurgy alloys (obtained by G. Sowinski); the supplementary breaking load investigation on fatigue cracked tension specimens (performed by R. L. Brazill and R. J. Bucci); and development of statistical methods (by B. M. Ponchel and R. L. Brazill) that were outside the funding scope of this contract and were contributed by Alcoa Laboratories.

The authors gratefully acknowledge the assistance of Ms. Henrietta Hyde who typed the manuscript of the report.

I. GENERAL OBJECTIVES

1. Determine the type or combination of accelerated tests most suitable for alloy selection and design of high strength aluminum alloys.
2. Perform tests with advanced and conventional alloys to support recommendations for optimum characterization methodology.
3. Identify the relationships between various stress corrosion testing techniques with regard to both specimen design and chemical environment for low, intermediate, and high susceptibility aluminum alloys.

II. INTRODUCTION (Interpretation of the Problem)

This section represents an overview of the literature survey performed in Phase I of this contract.

A. General Mechanism of SCC in Aluminum Alloys

Stress-corrosion cracking (SCC) is a time dependent process that involves the interaction of a sustained tensile stress (which may be aggravated by superimposed dynamic loading) and a corrodent at the surface of a susceptible material. SCC is recognized as a potential problem with certain alloys and tempers of all structural metals. However, it is but one of a number of causes of premature fracture influenced by corrosion of a structural component, as illustrated in Figure 1.

In susceptible aluminum alloys, the SCC generally proceeds along grain boundaries, and if allowed to continue, the strength of the part may be reduced to the point where fracture occurs. Because most high strength aluminum alloy products used in aerospace structures have a directional grain structure, the resistance to SCC of a susceptible alloy and temper is influenced by the direction of stressing relative to the macrostructure. This is illustrated for 7075-T651 rolled plate in Figure 2. Most occurrences of SCC have been in thick products because of the opportunity or ease of inducing short transverse surface tensile stresses in finish machined parts (1).* The interaction between the magnitude of sustained tensile stress and the metallurgical susceptibility of the material is illustrated in Figure 3 (1) by the comparative performance of different tempers of 7075 alloy plate (1).

* Numbers in brackets refer to references listed in Section XI.

SCC will not occur in a vacuum or in a dry atmosphere (less than about 0.1% relative humidity). In typical environments, water is the essential ingredient, present as vapor in the atmosphere or as liquid in aqueous and organic solutions. Both the initiation and propagation of SCC in typical environments are accelerated by increases in moisture, temperature, chlorides (traces of which are present almost everywhere), and various industrial contaminants. Examples of the wide range of effects of variation in atmospheric environments on the SCC of an intermediate susceptibility material is shown in Figure 4 (1).

Various specific mechanisms by which stress corrosion occurs in aluminum alloys have been proposed over the years, but none has been universally accepted. Different models have involved various assumptions of the rate-controlling processes, such as: (a) anodic dissolution, (b) repeated rupture of a protective film at the crack tip, (c) hydrogen embrittlement, (d) environment-induced failure of highly stressed metal-to-metal bonds at the crack tip (chemisorption), and (e) combinations of these. Speidel presented a detailed discussion of these models and concluded that no single model provided a quantitative explanation of all the observed facts (2). In a recent review (3) of the current status of the role of hydrogen in SCC, Thompson concluded that the weight of evidence for most susceptible aluminum alloys now favors the cooperation of hydrogen assisted cracking with anodic dissolution processes. However, this evidence exists only for Al-Zn-Mg, Al-Zn-Mg-Cu, and Al-Mg alloys, and not for Al-Cu or Al-Cu-Mg alloys.

Moreover, the actual mechanism of the embrittlement by hydrogen has yet to be established, not only for aluminum, but also for other metals where hydrogen-assisted cracking has long been recognized.

A generalized theory for the stress corrosion of alloys, proposed forty years ago by Mears, Brown, and Dix (4), still is consistent with many experimental observations concerning the effect of heat treatments on resistance to SCC of aluminum alloys, and may be used as a framework for filling in more recently hypothesized processes. According to this theory, corrosion along localized paths produces fissures with normal components of tensile stress becoming concentrated at their tips. These preferentially corroded paths may represent strata having relatively low inherent resistance to corrosion or they may be (as is usually the case) electrochemically more active than the contiguous metal. In aluminum-base alloys, such pre-existent paths generally are associated with specific metallurgical structures at the grain boundaries. With sufficient concentration of stress to cause localized plastic deformation at certain grain boundaries, the fissures widen at the tips, exposing fresh unfilmed metal to the corrodent. Because this unfilmed metal is still more electrochemically active, an increase in current flow is induced from the tips of the fissures, causing an acceleration of corrosion. This strain-assisted corrosion results in an increased rate of penetration, further separation of the metal, and the nucleation of SCC. While the metallurgical state of the metal may be conducive to such corrosion, cracking may not occur

or cracks will not grow appreciably when a large number of nearly equal fissures are present in close enough proximity to prevent localized concentration of stress. On the other hand, SCC will occur rapidly under conditions favoring more widely separated fissures. A schematic diagram suggesting the relative influences of the electrochemical and mechanical driving forces in the SCC process is shown in Figure 5 (5). This figure indicates a change as SCC proceeds, with the role of stress being negligible at first and then becoming dominant as subcritical cracking advances. Environmental action must always be involved although it may be dominant only at first. The pre-existence of a mechanical flaw or crack in the stressed metal may, of course, alter the initiation stage. Application of the fracture mechanics based stress intensity factor (J or K) as a driving force for the propagation of SCC is illustrated schematically in Figure 5 and 6 (2).

In the published literature (5) the process of SCC is frequently discussed in terms of initiation and propagation, and sketches similar to Figure 5 may be found; however, a precise model has not been established. There may be a gradual transition to crack nucleation (initiation) and growth, with no distinct separation of stages; or there might be a repeated succession of short steps of initiation and growth. Recent fractographic work by Scamans (6) revealed striations that indicate a discontinuous advance of SCC. He has proposed a model with anodic dissolution causing wedging by aluminum oxide followed by a short burst of

hydrogen-assisted cracking. Additional studies are desirable because fractographic work by others has not shown such striations (7). There may, in fact, not be a general case, but rather a changing scenario influenced in large measure by varied metallurgical structures. In any event, from an engineering sense, it is convenient to hypothesize the process in two generic stages, i.e., initiation and propagation, and this terminology will be used subsequently in the report.

B. Purposes of SCC Testing

With the increasing recognition of SCC as an important cause of premature fracture and catastrophic failure of structural components during the 1950's and 60's, the stress corrosion testing of materials became increasingly important. The purpose of such tests fall into two broad categories, namely, commercial and academic. The basic incentive in the commercial category is the estimating of risks, or the prediction of serviceability of an alloy or mill product. Valid environmental characterization of materials is vital to engineers who are responsible for materials selection and structural integrity, on the one hand, and for alloy development on the other--that is, to both user and producer alike. Thus, the use in the laboratory of accelerated SCC tests has become widespread.

It is the objective in the academic category to develop understanding of stress corrosion mechanisms. This increased

understanding, of course, enables the choice of appropriate testing methods, a more reliable estimation of risks, and prediction of service behavior.

C. State of the Art of Accelerated SCC Testing

Many articles on stress corrosion testing methods have been published in the last forty years, beginning with the ASTM/AIME Joint Symposium in 1943. The following quotations by Mr. E. H. Dix, Jr. written a generation ago are even more applicable today:

"With the coming of a more universal recognition of the general susceptibility to SCC of many commercially useful materials, metallurgists and engineers have become SCC conscious... Along with this interest and hyperconsciousness of SCC has come a variety of accelerated SCC tests... Accelerated corrosion tests, at best, are something of a hazard and accelerated SCC tests are a hazard to the nth degree..." (8), and "... While it is relatively easy to determine if a product is susceptible to SCC, it is far more difficult to determine if it possesses a 'degree of susceptibility' which will restrict its general usefulness..." (9).

Testing methods proliferated as SCC problems in industry increased substantially in the 1950's and 60's, while investigators studied the problem and metal producers pushed to develop improved alloys. Even though it became evident that characterization of the SCC performance of metals was influenced by the testing procedures, efforts to standardize were not made until about 1965. A number of ASTM standards have been developed since then (10). Standard tests also have been developed in England and Europe (11), and more uniform testing methods are presently being developed on a broader basis through the

International Standards Organization (ISO/TC156), WG2 on Stress Corrosion Cracking. Efforts to standardize, however, have not resulted in adequate reproducibility or improved mechanistic understanding, at least in comparison to other standardized mechanical tests.

A review of the published literature on SCC testing methods for aluminum alloys was conducted as part of this contractual study. One of the conclusions is that there still is a need for realistic accelerated tests, and preferably ones able to provide quantitative test data which can be used to more realistically evaluate service performance.

1. Environmental Factors

It is generally recognized that environmental variables can have a profound effect, both detrimental and beneficial, on tendencies for stressed components to crack. Each one or a combination of these variables can affect the thermodynamics and the kinetics of the electrochemical processes that influence SCC.

Chloride, bromide, and iodide anions are unique pitting agents for aluminum alloys, and they also accelerate intergranular and crevice corrosion. Chloride solutions are generally favored for accelerated tests because sodium chloride is widely distributed in nature, and the test results are potentially relatable to

stress corrosion behavior in natural environments, particularly seacoast atmospheres. Exposure to 3.5% sodium chloride or to synthetic ocean water by alternate immersion is a widely used procedure for testing aluminum alloys (ASTM G44, G47, G64) (10). Aeration of specimens, achieved by the intermittent immersion, enhances the corrosion potential and produces more rapid SCC than when specimens are continuously immersed (12).

Although nitrates and sulfates when dissolved in distilled water tend to retard rather than to accelerate SCC, their presence in chloride environments can produce a synergistic stimulation of intergranular corrosion and SCC (13, 14). This effect has been observed at geographic locations such as Los Angeles even though conditions there are not considered as corrosive as at locations such as Point Judith, R.I., or Cape Canaveral (15). The results in Figure 4 were obtained with small sized axially loaded tension specimens which are highly influenced by the initiation of localized corrosion and SCC. When similar materials were tested with mechanically precracked double cantilever beam (DCB) specimens in which the propagation of SCC was monitored (Figure 7), the performance at Los Angeles with reference to Point Judith was reversed. Thus, the assessment of the effects of environmental chemistry can be markedly influenced by other factors including climatic conditions, the type of test specimens, and the method of measuring the damage due to SCC.

While it is recognized that the local environment generated inside a crevice or corrosion fissure can be quite different from the bulk environment at the metal surface, and that it changes with the progress of the electrochemical reactions, detailed knowledge of "crack-tip" chemistry and reactions still is speculative. Knowledge of this type is required before quantitative predictive models of SCC performance can be developed.

The lack of quantitative correlations of test results in accelerated test media with service experience has led many investigators to the use of SCC tests in outdoor or other service-type environments. Tests in such environments provide realistic assurance to the investigators, but they are quite time consuming and not ideally suited for alloy development. The simulated service tests also provide guidance to interpreting accelerated tests.

2. Mechanical Concepts

Traditional descriptors of high strength aluminum alloy SCC resistance are expressed in terms of survival time after exposure to environment under stress, or in terms of a maximum (threshold) stress (σ_{th}) below which failure did not occur under the conditions used. These data are typically obtained in the laboratory with small scale smooth tension or beam specimens subjected to various sustained stress levels in a suitable corrodent (1, 2, 5,

11). Failure time in the smooth specimen test, however, includes both crack initiation and subcritical crack growth components which are seldom distinguished owing to the generally imprecise definition of crack initiation. It has been observed that comparative rankings of SCC resistance among materials may change under different conditions of test. The test dependence can be influenced by factors such as specimen size and geometry, magnitude of the applied stress, form of loading (i.e, fixed load or fixed displacement), and the combination of material strength and toughness. Threshold stress values developed from the simple laboratory test can be misleading if interpreted for use in design (1).

The application of linear-elastic fracture mechanics (LEFM) to cracked bodies allows stresses and strains near the crack tip to be determined when the crack tip plasticity is small relative to other important dimensions of the body. The mechanical driving force for cracks then can be quantified in terms of the crack tip stress intensity factor, K , which is expressed in terms of the remotely applied loads, crack size and test specimen geometry. This approach is attractive because conditions of crack tip similitude imply that the rate of crack growth in two geometrically distinct bodies will be identical when their respective K values are equivalent, assuming that environmental conditions also are equivalent at the crack tip. In theory, therefore, behavior

of a stress corrosion crack in a service component can be predicted conservatively from laboratory characterization of the material's crack growth rate (da/dt) vs. K relationship and knowledge of the K solution for the crack in the actual part (2, 5, 11, 16). In actuality, environmental conditions within a crack in a laboratory test specimen may be quite different than in the service component. Moreover, this LEFM approach may be too conservative and unjustified when flaw or crack free material can be assured by non-destructive examination.

Current state-of-the-art LEFM characterization of material susceptibility to SCC sometimes involves the measurement of a threshold stress intensity factor (K_{ISCC} or K_{th}) which identifies combinations of stress and flaw size below which environmental crack growth will not occur. To obtain K_{th} values, or the full da/dt vs. K relationship above threshold, precracked specimens are loaded in the environment of interest. A requirement of LEFM-type testing is that the specimen starting crack length be sufficiently large (typically greater than 0.5 in.) to preclude undesirable interactions of the loading arrangement and machined starter notch with the crack tip stress field (17, 18). In service, large initial defects of this size are rare. For example, damage-tolerant design criteria for military aircraft specify a flaw on the order of 0.05 in. as the initial "worst case" damage assumption upon introduction of a new part into service (19). Hence, it is reasonable to question the appropriateness of using

LEFM specimen (large crack) data to quantify behavior of small flaws which are representative of naturally induced corrosion cracks. For example, the composite diagram in Figure 8 represents a concept of combining stress corrosion "thresholds" obtained on smooth and LEFM specimens to give a conservative assessment of materials for design (20). It is evident that the small flaw portion of the K_{th} analysis is unconservative, as the potential exists for development of SCC at stresses above the smooth specimen threshold.

The question of similitude between long and short crack behaviors has been studied more intensively in the area of fatigue than in corrosion (21-23). Analogous to the corrosion example of Figure 8, disparity exists between smooth specimen fatigue endurance strength and the fatigue crack propagation threshold (ΔK_{th}) developed from compact-type specimen da/dN data (24, 25). It therefore appears reasonable that advances in understanding related to characterization of small fatigue cracks under a fracture (or continuum) mechanics framework may be equally appropriate to characterization of small stress corrosion cracks.

There are several factors which bound the mechanics description of short cracks (23), namely: (a) when the cracks are small compared to the scale of relevant microstructural dimensions (a continuum mechanics limitation); (b) when they are small relative to the scale of local plasticity, either of the crack or as the result of a nearby stress concentrator (an LEFM limitation); or

(c) when they are physically small, that is, small enough to invalidate the idealized assumptions of crack tip geometry and loading conditions, despite the crack being large enough for LEFM to be valid. Geometrical changes in crack tip shape (e.g., sharpening, blunting, branching) or localized stress effects (e.g., residual stress, corrosion product wedging) are examples which can promote the latter.

The evolution of elastic-plastic fracture mechanics (EPFM) within the last decade has extended the validity range of the fracture mechanics approach to cases of more extensive plasticity. The development of EPFM was motivated by the need to estimate toughness in ductile materials for which very large specimens were needed to meet with LEFM requirements. Hutchinson, Rice, and Rosengren (26, 27) developed local crack tip stress and strain field equations for linear elastic hardening solids. These equations form the basis for an EPFM crack driving force parameter that is directly relatable to the LEFM crack tip stress intensity factor when conditions of limited plasticity are met. Although EPFM limitations have not been totally explored, various investigators have shown that the approach yields improved descriptions of toughness and subcritical crack growth behaviors when the small scale yielding assumptions of LEFM are violated (23, 28-30). It, therefore, is anticipated that application and further development of elastic-plastic fracture mechanics theory will lead to improved "wide-range" estimates of critical stress/flaw size combinations for onset of SCC and mechanical fracture, as suggested in Figure 9.

3. Materials Selection

Recent developments of higher strength alloys and tempers with improved resistance to SCC have made the selection of materials increasingly difficult in attempts to avoid SCC. Stress corrosion behavior is not a property of the material that can be measured precisely and tabulated like mechanical properties. Moreover, published information on new alloys and advanced products can be confusing because of the variety of testing techniques that are used. The traditional descriptors of SCC behavior are test dependent, as mentioned in previous sections, and the experimental variables may not be related to the performance expected of particular engineering structures. Thus, because improved materials usually are not truly immune to SCC, comparisons among various materials must be made with caution.

An ASTM standard classification of the resistance to SCC of high strength aluminum alloys (G64-80) was recently developed to assist designers with materials selection (10). This involves qualitative SCC ratings for various alloys, tempers, and mill products based on service experience where available, or on laboratory tests of standardized smooth specimens at specified levels of exposure stress. Table I contains an example from ASTM G64-80 of the ratings applicable to products of 7075 alloy and an interpretation of the ratings in terms of typical or expected service experience. To establish preliminary ratings for experimental materials, the results of laboratory tests of a specified number of production lots must be used.

Various branches of the Department of Defense have issued documents containing lists of approved and restricted alloys, also based on service experience and laboratory testing (1).

It is anticipated that, as standardization of the newer types of accelerated tests progresses, additional guidelines will be developed to aid in materials selection.

4. Problems with Accelerated SCC Testing

Experimental difficulties associated with various testing techniques and the interpretation of test results have been discussed in previous reports (5). These problems can be grouped as follows:

- a. Quantitative measurement of the degree of susceptibility - Need for realistic descriptors that are amenable to statistical analysis.
- b. Correlation of test results - Lab tests vs. real life structures, and relationships among testing methods.
- c. Defining service needs and estimating risks; life assessment.
- d. Lack of general acceptance of standardized test methods.

These problems are particularly troublesome in the characterization of advanced materials with relatively high resistance to SCC. The idealized schematic diagrams shown in Figures 5 and 6 for highly susceptible test specimens assume different form; and test results are more difficult to interpret.

D. New Approach to Smooth Specimen Testing (The Breaking Load Test)

An enticing approach to optimizing SCC testing techniques being explored at Alcoa Laboratories is to monitor the damage due to SCC in statically loaded smooth tension specimens. This is done by performing tension tests on replicate groups of specimens after appropriate periods of environmental exposure. The effects of SCC are measured with minimum extraneous corrosion and without the need of waiting for actual specimen failure. The following practical advantages appeared in earlier Alcoa tests:

- a. Advantageous for statistical treatment of data for materials with relatively high resistance to SCC.
- b. Utilizes shorter exposure periods than traditional "pass-fail" tests.
- c. Amenable to fracture mechanics interpretation using elastic-plastic fracture mechanics (EPFM) characterization of "small" cracks.
- d. Quantifies SCC damage in terms of an effective flaw size which can be calculated from the breaking strength. The effective flaw corresponds to the "weakest link" or largest crack in the specimen test section at the time of fracture.

E. Summary

The following summary is based on the literature survey performed in Phase I, highlights of which were discussed above:

1. Accelerated SCC test data are at best imprecise, test dependent and, therefore, must be qualified with test conditions.
2. Interpretation of accelerated test results and their correlation with in-service expectations may be approached through recognition of both the probability of initiation of SCC and the rate of SCC growth; however, the experimental distinction of crack initiation (incubation) and growth is generally imprecise and must be defined arbitrarily.
3. The most appropriate descriptor(s) of SCC susceptibility in alloy selection for a structural part depends upon the mechanical property design requirements, the type of service loading, the extent of tolerable SCC damage, environmental considerations, and the expected life time.
4. To assist alloy development and/or selection, the following, currently available, accelerated test methods should be considered in keeping with the purpose of this investigation.
 - a. Smooth Specimens - Statically Loaded
 - Valuable for screening alloy resistance to SCC "initiation".

- Most effective when propagation component of test life is small; i.e., small cross-section specimens.
 - Interpreted in terms of threshold stress (σ_{th}) and probability of survival (or failure) under specified testing conditions.
- b. Smooth Specimens - Dynamically Loaded
- Useful research tool, moreso for studying environments than evaluating metals. Broader acceptance requires that correlation with traditional test methods be established, and that the role of initiation vs. propagation on test response be better understood.
- c. Precracked LEFM Specimens - Statically Loaded
- Offers quantitative information in form of crack velocity vs. stress intensity.
 - Useful material screening parameters:
 SCC propagation threshold - K_{ISCC} (from K-increasing test).
 Plateau velocity and crack arrest threshold- K_{th} (from K-decreasing test).
- d. Precracked LEFM Specimens - Dynamically Loaded
- Still in research stage.
 - Limited experience; limited principally to steel.
5. A promising new accelerated testing technique involving statically loaded smooth tension specimens is being explored at Alcoa Laboratories. This new approach involves breaking

load tests of stressed specimens exposed for various lengths of time in a suitable corrosive, thereby measuring the damage due to SCC as it occurs and avoiding the necessity of waiting for test specimens to fail. Data obtained from these tests appear to have an additional advantage of being amenable to fracture mechanics interpretation in terms of effective flaw (SCC) size. The merits of this approach should be investigated further.

The new breaking load testing technique is the primary basis for the experimental program to be described in the following sections of this report.

III. EXPERIMENTAL APPROACH (General Philosophy & Test Procedures)

A. Strategy

Although there is controversy on the mechanisms involved, it is obvious that SCC must involve a time - dependent deterioration in the ability of a structural component or specimen to support a specific load. Accordingly, determination of the change in load carrying ability as a function of exposure time would seem to be a logical and direct way to evaluate stress corrosion damage. This approach is sensitive to localized corrosion and stress concentration effects when the specimen cross section is small, and the fracture will be that where SCC damage is maximum, i.e., the "weakest link." Moreover, it is far simpler to measure maximum load to fracture than the maximum depth of corrosion fissures and cracks. Various investigators have considered such a procedure for investigating stress corrosion susceptibility (31-33); however, their use of the method has been limited to the calculation of stress corrosion indices and determination of the condition of specimens at the completion of an exposure test.

The concurrent change in breaking load with growth of a hypothetical stress corrosion flaw in a small diameter tension specimen is schematically described for two types of material response in Figure 10. The first response is illustrated by solid lines and is the behavior expected for a material with high

susceptibility to SCC. In this "worst-case" example, failure would occur rapidly in the exposure test, and tension testing prior to this event would reveal a rapid decline in breaking load due to crack penetration with increase in exposure time. The dashed curves in Figure 10 illustrate behavior of a second material having improved resistance to SCC. In the latter example, corrosion damage is initiated and continues with extended exposure; but because the rate of advance of SCC is slower in the more resistant material, there is time for relaxation of localized stress and strain as the result of various processes, such as crack-tip blunting, branching of initial fissures, or by formation of secondary corrosion sites. Thus, it would be possible for the material to display an apparent decreasing rate of SCC damage (indicated by the inflections in dashed breaking load curve in Figure 10), although metal continues to be dissolved at an approximately constant rate (34). It is anticipated, therefore, that for a given material/environment combination and test specimen configuration there is a critical time interval at which the maximum susceptibility to SCC will be detected by the breaking load. In general, the critical exposure interval should span a time that is long enough to assure significant SCC damage, but short enough to avoid the confounding caused by competing and extraneous corrosion processes, i.e., between times t_A and t_B in Figure 10. Thus, exposure times beyond t_B are expected to be of little value for evaluation purposes. The circumstances described above have been considered as a partial explanation of previously

noted observations of increasing survival probabilities with increased exposure times in aggressive environments, as illustrated in Figure 11 by data from a previous investigation (35).

A potential advantage to using "apparent tensile strength" after exposure as a criterion for SCC damage is that the value can be used with fracture mechanics theory to calculate an "effective" terminal flaw (crack) size which triggers ultimate tensile fracture. Moreover, by computing flaw sizes corresponding to various exposure times, the generated data are believed to be amenable to flaw growth rate analysis and life assessment, although the latter is beyond the scope of the present investigation. Additional engineering significance of data developed from breaking load tests is discussed in more detail in Section VI.

Although the determination of the average breaking stress of a group of replicate specimens can provide a sensitive measure of the stress corrosion damage, these data do not per-se reveal specific SCC mechanisms. From these data, however, mechanistic inferences can be made through considerations of factors influencing localized initiation of fracture (cracking), the theory of fracture mechanics, changes of the crack-tip stress-strain field, and the criterion of tensile failure (strength or toughness related). To examine these inferences more closely, supporting information was sought by fractographic studies and correlation of breaking stress with flaw size.

State-of-the-art SCC tests were also made under conditions of static loading with both smooth tension specimens and fracture mechanics type specimens to investigate correlations among current and the breaking load test methods.

B. Test Materials

A sample of commercial production 2.5 inch thick plate of 7075-T651 alloy manufactured at Alcoa's Davenport Works was chosen for the primary experimental work. Mechanical properties and the resistance to SCC in various environments had been determined in previous Alcoa investigations (Tables II, III). Samples of the same lot of material were used in an ASTM interlaboratory test program using fracture mechanics type specimens under the direction of Subcommittees G01.06 and E24.04; the test program was started in early 1983.

Two portions of the 7075-T651 plate were given additional precipitation treatments so that materials with low, intermediate and high levels of resistance to SCC (T651, T7X1 and T7X2 tempers, respectively) but with the same composition and grain structure could be evaluated. The special aging treatments were applied at Alcoa Laboratories to 15" x 24" blocks sawed from nearby positions in the same production plate. Identification of the samples used for testing is given in Table II. The hot worked partially recrystallized grain structure of the T651 temper material, which is the same for the T7X temper samples, is illustrated in Figure 12.

Samples of Davenport production 3 in. thick 7475-T651, 7475-T7651 and 7475-T7351 plate were used for supplementary breaking load studies of fatigue cracked specimens.

C. Mechanical Property Test Methods

Duplicate tensile, true-stress versus true-strain, and fracture toughness (K_{IC}) test specimens of the short transverse orientation were taken from the center thickness of each temper variant of the 7075 and 7475 plate materials. Mechanical properties were characterized in the short transverse orientation because this is of greatest practical significance to SCC characterization of aluminum alloys.

Tensile properties were determined in accordance with ASTM Method B557-81 (36) using standard 0.25 in. tapered seat specimens with a mounted extensometer having a 1 in. gauge length.

The true-stress versus true-strain data were obtained using standard tensile test procedures (36) employing 0.25 in. and 0.125 in. diameter tapered seat specimens for alloys 7075 and 7475, respectively. Extensometers of 1 in. and 0.50 in. gauge length were affixed to the 0.25 in. and 0.125 in. diameter specimens, respectively, and a 0.1 in./min. displacement rate was employed. The strain hardening coefficients κ and n were determined using an empirical representation of the true stress-true strain curve over

the region of interest. The mathematical form of the representation is given as:

$$\sigma = \kappa \cdot \epsilon^n \quad [1]$$

where σ is the true stress, ϵ the true plastic strain, κ the strength coefficient, and n the strain hardening exponent. The procedures used for determining κ and n were in accordance with ASTM method E646-78 (37).

The fracture toughness tests were made in accordance with ASTM Method E399-83 (38) using 1 in. thick standard short transverse (S-L) compact specimens.

D. Stress Corrosion Test Methods

1. Smooth Tension Specimens - Traditional Pass-Fail Tests

Conventional stress corrosion tests were performed on smooth 0.125 in. diameter x 2 in. long threaded end tension specimens in accordance with ASTM standard G47 (10). Stressed specimens were loaded in uniaxial tension stressing frames (Figure 13) by applying a predetermined amount of elastic strain.* Although this stressing frame represents a fixed-displacement method of loading, there is a significant amount of elastic strain energy developed in frames holding highly stressed specimens. Thus, as cracks develop and grow in the test specimen, the average stress in the net (uncracked) section will increase as shown in Figure 14, while the nominal exposure stress can decrease as the flawed area fraction becomes large. As long as the flawed area fraction is

* A nominal value of 10.3×10^3 ksi was used for the elastic modulus (E) to convert elastic strain to stress.

small, the average net section stress will be practically the same as it would be in a fixed load arrangement. In a study of the effect of various types of simulated corrosion flaws using machined V-notches (34), it was shown that as the average tensile stress on the net section increased with deepening notches, the net fracture stress was markedly influenced by the type of notch as shown by points A, B and C in Figure 14. Thus, it can be inferred that the distribution of stress corrosion cracks or pits could have a marked effect on times to failure; e.g., an isolated flaw of a given total area developed on only one side would be more severe and cause the specimen to fail much sooner than specimens for which corrosion tends to occur symmetrically around the specimen.

The stressed specimens were exposed to 3.5% NaCl solution by alternate immersion per ASTM standard G44. They were inspected daily and any fractured specimens removed. The specimens were solvent cleaned before exposure.

The number of specimens tested and the stress levels for each of the three 7075 test materials are included with the breaking load test program in Table IV.

2. Smooth Tension Specimens - Breaking Load Tests

a. Test Program

The test program was concentrated on short transverse 0.125 in. diameter tension specimens. Additional tests also were

performed on long transverse 0.225 in. diameter specimens of 7075-T651 and the same larger diameter short transverse specimens of 7075-T7X1. The schedule of the breaking load tests is given in Table IV.

Sets of five specimens were removed from the alternate immersion test after the scheduled lengths of exposure, rinsed in water, dried and tension tested within one hour. The apparent tensile strength and 0.2% yield strength for each specimen was calculated on the basis of the original cross section area (gross fracture stress). Appendix C contains the raw data along with the mean and standard deviation of each test group. Specimens that failed during exposure were excluded from statistical analysis.

b. Statistical Procedure

The statistical characterization of fracture data has been studied for many years (38, 39), with much effort devoted to the statistics of extreme values (40-47). The rationale behind the latter approach is that materials contain weakening flaws and that, although there may be a wide spectrum of flaw sizes in a specimen, the fracture seeks out the largest flaw (weakest link). Thus, for statistical characterization of fracture processes of this kind, the distribution of all flaw sizes within a specimen group is not as important as the distribution of the largest flaws (the extreme value distribution). However, if the distribution of all flaw sizes (the parent distribution) is known and of the

exponential type, the related extreme value distribution is readily obtained.

That the extreme value distribution is appropriate for fracture resulting from corrosion related phenomena is supported by the works of Mears and Brown (48) and Aziz (49, 50). Mears and Brown determined that pitting frequency followed the Poisson distribution, which is related to an exponential distribution. Aziz characterized pitting depth with an exponential distribution, and showed that the maximum depth measurements followed the related extreme value distribution. The frequency and depth of pitting are related to the microstructure, as is SCC. Thus, in the absence of suitable tension test data from stress corroded specimens, it was assumed that stress corrosion flaw sizes would follow an exponential parent distribution, and the related extreme value distribution could be used to characterize the fracture process.

Since fracture stress is related to the largest flaw size in an inverse manner, the appropriate distribution for fracture stress would be an extreme value distribution of smallest values. This distribution is bell-shaped but skewed (longer tail) to the left. This means that a group of replicate tests is likely to produce a wider range of fracture stresses below the average than above. This commonly occurs in corrosion assisted fracture, where an outlier with low fracture stress relative to the remaining replicates is often observed.

When the parent distribution is of exponential type, the probability for survival (no fracture at the stress of interest) can be determined from the extreme value distribution of smallest values. This can be expressed by equation [2] (47), attributed to Gompertz,

$$P = \exp [-e^Z] \quad [2]$$

where P is the probability of survival and Z is the reduced variate. The reduced variate is of the form

$$Z = (S - \hat{\mu})/\hat{\sigma} \quad [2a]$$

where S is the stress of interest (e.g., exposure stress) and $\hat{\mu}$ and $\hat{\sigma}$ are estimates of the distribution location and scale parameters calculated from the sample size, N , the mean breaking strength, \bar{S} , and the standard deviation, δ , as shown below.

$$\hat{\sigma} = \delta/\sigma_N, \text{ and } \hat{\mu} = \bar{S} + \hat{\sigma} \cdot \bar{y}_N \quad [2b]$$

where the parameters σ_N and \bar{y}_N are functions of N and can be found in Gumbel's text for $N > 7$ (47). Appendix C contains a table of σ_N and \bar{y}_N values for $N = 2$ to 7 extrapolated from Gumbel's table.

A more general, although more conservative, method for determining the distribution parameters $\hat{\mu}$ and $\hat{\sigma}$ is probability plotting. The advantage of this method is the ability to satisfactorily handle truncated data sets, such as test groups containing specimens that failed prior to tensile testing. Probability plotting was used to analyze the breaking load data in this report, and the results are tabulated in Appendix C. The probability plotting procedure for determining $\hat{\mu}$ and $\hat{\sigma}$ from the breaking load data is described more fully in Appendix C.

An additional benefit of probability plotting is that it provides verification that the extreme value distribution is appropriate for describing the breaking load data. Although the sample size was small for each test group ($N = 5$), the probability plots of all the breaking load data showed nearly linear relationships on probability paper, indicating that the assumption of extreme value behavior was reasonable.

The probability of a specimen surviving a given exposure period can be calculated from equations 2 and 2a by substituting the exposure stress for S and using $\hat{\mu}$ and $\hat{\sigma}$ determined by an appropriate method (probability plotting in this case). An advantage to evaluating SCC performance by the breaking load method and the statistical procedure described above is the ability to estimate survival probabilities with reasonable confidence as the actual probability of survival approaches 1.0. Resistant materials normally display very few failures in traditional time-to-failure testing. As the actual probability of survival approaches 1.0, traditional pass-fail testing (binomial sampling) becomes inefficient since a prohibitively large number of specimens would be required to determine a value of P with reasonable confidence.

A more meaningful use of breaking load data can be obtained by calculating the tensile stress at which 99% of the specimens could be expected to survive at a specified exposure stress and time. This 99% survival (gross fracture) stress not only permits

a direct comparison of stressed and unstressed specimen performances, but also provides a numerical value for comparing materials. Moreover, the 99% survival stress can be used with fracture mechanics theory to estimate the equivalent flaw size that would not be exceeded in 99% of the unfailed SCC specimens.

The 99% survival stress, S_{99} , for a sample of replicate specimen breaking stresses is determined as follows:

- (a) Calculate the sample mean and standard deviation, \bar{S} and δ .
- (b) Calculate the extreme value distribution scale and location parameters, $\hat{\sigma}$ and $\hat{\mu}$, using the probability plotting method in Appendix C or using equations [2a and 2b] with the appropriate σ_N and \bar{y}_N for the sample size used.
- (c) Determine the 99% survival stress by substituting 0.99 for P in equation [2] and solving equations [2 and 2a] for S as follows:

$$\begin{aligned} S_{99} &= \hat{\mu} + \hat{\sigma} \ln[\ln(0.99)^{-1}] \\ &= \hat{\mu} - 4.60 \hat{\sigma} \end{aligned} \quad [3]$$

The 99% survival stress obtained for a given material at a specified exposure stress and time does not generally correspond to a threshold stress below which SCC would not be expected to occur within the specified exposure time. A series of 99% survival stresses, however, can be used to derive a statistically-defined threshold stress, such as the stress for which there is a 95% confidence of a probability of survival greater than 99%. This concept and the analytical procedure is discussed in detail in Appendix B. It must be remembered, of course, that any such threshold stress would apply only to a random sampling of specimens and should be qualified by the testing conditions.

3. Fracture Mechanics Specimens (DCB and WOL) *

Stress-corrosion crack propagation resistance was evaluated in the three temper variants of 7075 material using two types of fracture mechanics test specimens in which the mechanical crack driving force was characterized by the crack-tip stress-intensity factor, K . The first type of test utilized bolt-loaded, double cantilever beam (DCB) specimens in which K decreases with crack extension. The second type was an increasing K test with ring loaded, wedge-opening loaded (WOL) specimens. Both types of specimens were machined in the S-L orientation; i.e., the crack propagation plane was at the mid-thickness-plane of the plate and crack growth was in the rolling direction. These specimens were of similar configuration and dimensions as those selected for use in a concurrent interlaboratory testing program conducted jointly by ASTM subcommittees G01.06 and E24.04.

The environment used in all of the SCC propagation tests was a 3.5% NaCl solution which was introduced into the crack with an

* These specimen designations, commonly used in the stress corrosion literature, will be used throughout this report. However, recently adopted ASTM Standard Terminology Relating to Fracture Testing (ASTM E616-82) provides standard designation codes for these specimen configurations, loading, and orientation. The DCB specimen has the standard designation of chevron DB(W_p) (S-L), and the modified WOL specimen has the standard designation of precracked MC(T) (S-L).

eyedropper during the initial loading of the specimens and then three times daily during the test exposure, except only once each day on week-ends. All of the tests were performed in laboratory air at $72^{\circ} \pm 3^{\circ}\text{F}$ with 50-70% relative humidity.

a. DCB Specimen Tests (K-decreasing)

A drawing of the DCB specimen used for these tests is shown in Figure 15. Two specimens were taken from each of the three materials. Shallow side grooves were provided to guide crack growth in a plane perpendicular to the applied loading direction. Specimen crack-opening displacements were measured at the load line with micrometer calipers.

Each specimen was precracked by mechanical pop-in produced by tightening the loading bolts equal amounts until a crack initiated in the chevron notch. Under conditions of fixed-displacement loading, the crack-tip stress-intensity factor decreases with increasing crack length, as shown in Figure 16. Thus, after pop-in, the crack arrests, and further loading is required to advance the pop-in crack. After advancing the precrack to a point about 0.1 inch (2 mm) beyond the chevron notch, the loading was increased slightly to ensure that the crack tip stress intensity factor was nearly equal to the material fracture toughness, K_{IC} . At this point, the load-line displacement and crack length were measured, and the stress intensity factor was calculated according to the following equation after Hyatt (51):

$$K_I = \frac{VEH [3H(a + 0.6H)^2 + H^3]^{1/2}}{4 [(a + 0.6H)^3 + H^2a]} \quad [4]$$

where V is the total load-line displacement relative to the unloaded specimen, E is the elastic modulus of the material which is nominally 10.3×10^3 ksi for 7075 alloys, H is the half-height of the specimen, and a is the crack length measured from the load line.

Crack length measurements were made periodically during the test. Measurements were made visually to the nearest 0.005 in. along the specimen faces after rinsing the corrosion product and salt off the specimen surface with deionized water. Measurements also were made ultrasonically at the mid- and quarter-thickness points using the arrangement shown in Figure 17. In this system, the specimen is mounted on a translation stage which moves the specimen under an ultrasonic transducer. The ultrasonic transducer sends a high frequency stress wave down through the specimen and detects its reflection off of interfaces such as cracks, discontinuities, or the bottom of the specimen. The distances (times) between the transducer and the reflecting interfaces are displayed on an oscilloscope. The specimen is manually moved back and forth beneath the transducer until the position of the crack front is fixed. The translation stage is equipped with a digital readout of position so the location of the crack front can be determined. This system has a crack growth resolution (minimum detectable change in crack length) of approximately 0.005 in. and an absolute crack length

measurement error less than 0.1 in. The measurement error can be decreased by comparison with measurements on a calibration block, but actual crack length accuracy is influenced by extraneous reflections produced by crack branching, irregular crack front shape, or voids in the metal. At the conclusion of the exposure test, the specimens were broken open for examination of the fractures and measurement of the final crack lengths.

Stress corrosion crack propagation rates are expected to decrease continuously with crack growth in these tests since K decreases with crack advance. However, it has been observed (16, 52, 53) that corrosion product buildup within the crack can wedge open the specimen and impose an additional, internally produced stress-intensity component on the crack-tip region. This additional component upsets the determination of the true mechanical driving force and can produce crack acceleration under supposed K -decreasing conditions. The implications of the wedging problem will be discussed in Section IV.B.3.

b. WOL Specimen Tests (K-increasing)

The wedge-opening-loaded (WOL) specimen geometry is shown in Figure 13. Under fixed load conditions, K increases with crack extension, as shown in Figure 19. As with the DCB specimen, a chevron notch and side grooves were machined in the specimen to facilitate precracking and to restrict the plane of crack growth to be normal to the applied loading direction. The specimens were

fatigue precracked in air according to the ASTM recommended practice (ASTM E399-81) for precracking fracture toughness specimens.

The specimens were statically loaded for the environmental exposure test by loading rings which were instrumented with strain gages and calibrated to provide continuous load measurement. The compliance of a ring, being much higher than that of a specimen, maintained a nearly constant load on the specimen even when appreciable crack growth occurred (54). The crack-mouth-opening displacement of each specimen was measured with a calibrated clip gage affixed to integral knife edges machined in the specimen.

The load and displacement on each specimen were continuously monitored with an automatic logging system (Figure 20) so crack propagation could be followed without visual observation. Crack length was determined from the normalized compliance of the specimen according to the following equation (55):

$$\ln \left(\frac{EV \sqrt{BB_n}}{P} \right) = [1.83 + 4.307 (a/W) + 5.871 (a/W)^2 - 17.53 (a/W)^3 + 14.57 (a/W)^4] \quad [5]$$

where V is the crack-mouth-opening displacement, P is the load, B is the specimen thickness, B_n is the specimen net thickness between the side grooves, E is the tensile elastic modulus, W is the specimen width, and a is the crack length measured from the load-line. This equation was solved iteratively for a at each load-displacement data pair. The relationship given in equation [5] is plotted in Figure 21.

The stress intensity factor, K, for the WOL specimen is given by the following equation (55):

$$K = \frac{P [2 + a/W]}{\sqrt{B B_n W} [1 - a/W]^{3/2}} [1.308 + 5.278 (a/W) - 19.67 (a/W)^2 + 24.57 (a/W)^3 - 10.27 (a/W)^4] \quad [6]$$

The ratio K/P is plotted as a function of crack length in Figure 19.

Three specimens of each alloy 7075 temper were loaded to various initial stress intensities in order to estimate K_{Isc} (the stress intensity below which stress corrosion crack growth could not be detected) and to determine crack growth kinetics. Both the K_{Isc} estimate and the crack growth kinetics from the K-increasing test on modified WOL specimens will be compared to data obtained from the K-decreasing DCB specimen tests.

The nine crack growth tests were run for about 60 days. At that time, two specimens had indications of crack growth and were removed from the stressing rings along with a third specimen in which no crack growth was indicated and mechanically fractured. Two specimens were removed for metallographic sectioning and one specimen was removed, fatigue cracked an additional increment, and placed back in the stressing ring at higher stress intensity. The tests were continued for another 30 days, at which time the remaining specimens were removed and mechanically fractured for final crack length measurements and fracture surface examination.

E. Fractographic Procedures

Fracture surfaces were examined to characterize the SCC morphology in the various materials and specimen types, and to measure SCC flaw sizes and shapes in selected breaking load specimens. The bulk of this work was done using a scanning electron microscope (SEM) operated at 30 kV accelerating voltage. For the most part, no special cleaning or coating procedures were required, other than a short rinse in acetone to remove loose debris. Any special preparation techniques are noted in the appropriate figure captions.

The primary purpose of measuring flaw sizes and shapes was to provide benchmarks against which the fracture-mechanics estimates of flaw geometry could be checked. For this reason, both the range of flaw sizes for any exposure stress/time combination and the change in flaw size with time were characterized. To do this, the two specimens with the highest and lowest breaking stresses from a group of five replicates were examined from selected temper, exposure stress and exposure time combinations.

The measurement procedure started with a low magnification (25x) fractograph of each specimen. The actual flawed area was then drawn on this photograph with the specimen still in the SEM, using whatever magnification was necessary to determine the local crack-front shape. Thus, for each specimen examined, there was a 25x "map" of the fracture surface. Two measurements of flaw size were taken; the maximum depth of penetration along a diameter

(a_{\max}), and the total cracked area (A_c). The area measurement was made by cutting out the circular fracture image, weighing it on a balance (W_T), and then reweighing the photo after cutting off the flawed areas (W_U). The total cracked area was then calculated from the following equation:

$$A_c = \frac{\pi D^2}{4} \left[1 - \frac{W_U}{W_T} \right] \quad [7]$$

where D is the original specimen diameter.

F. Correlation of Fracture Stress with Flaw Size

The conceptual advantage of using cracked-body mechanics to estimate decrease in fracture stress (apparent tensile strength) with increase in flaw size has been mentioned in preceding discussion (section III.A.). In the context of the breaking load test, this implies that damage accumulated with time can be quantified in terms of an equivalent "small-size" flaw which can be estimated from the specimen's apparent tensile strength after exposure to a corrosive environment. In order to relate the apparent tensile strength to an equivalent flaw size, mathematical equations were developed to describe the relationship between specimen fracture stress, flaw size, and the material strength-toughness properties. These equations are given below in Section III.F.1. The effectiveness of this analytical approach was verified in a supplementary program to establish fracture stress

and flaw geometry data from tension tests of cylindrical specimens containing partial thickness fatigue cracks. The supplementary test program is described in Section III.F.2. Breaking load data developed from the stress corroded tensile bars of the three temper variants of alloy 7075 were then examined similarly. In addition, flaw sizes calculated from these test results were compared with corresponding dimensions of actual flaws measured fractographically on selected SCC breaking-load specimens.

1. Analytical Relationships for the Cylindrical Tension Specimen

Nomenclature for three practical flaw configurations in a cylindrical tension specimen is shown in Figure 22. The assumed elliptical flaw shape of Figure 22(a) is representative of most individual partial thickness cracks observed, while the circumferential crack geometry of Figure 22(c) models the case where multiple cracks form and link around the specimen circumference. The flaw shapes in Figure 22 are supported by fractographic evidence given in Section IV.C.2. For a given fracture stress, the crack depth, a , accompanying fracture would be greatest and least respectively, for the assumed flaw geometries of Figure 22(a) and Figure 22(c). Thus, if damage is to be quantified by the depth of flaw penetration from the specimen surface, then the elliptical part through crack represents a "worst-case" assumption for use in the breaking load calculations.

For the flawed-specimen geometry and test material of interest, a first approximation of the critical flaw at fracture is given by the smaller of the two sizes predicted by tension limit-load or linear-elastic fracture mechanics (LEFM) analysis, as shown in Figure 23. Under the former failure criterion, fracture is the result of the net-section stress reaching the material tensile strength in the specimen uncracked ligament. In general, a limit load failure would be expected when the crack(s) are so small and/or the material so tough that localized concentrations of stress are, simply speaking, "washed out" by gross plastic deformation in the net section. At the other extreme, LEFM predicts failure when the combination of stress and flaw size produces a crack-tip stress-intensity factor (K) which exceeds the material toughness (K_{Ic} or K_{Ic}). The application of LEFM is valid when dimensions of the critical flaw and remaining uncracked ligament are sufficient for the assumptions of small scale yielding to apply. The results of elastic-plastic analyses, however, indicate that deviation from the small-scale yielding assumptions of LEFM begin to break down at applied stresses of about 70% of the material yield strength (30, 56). Thus, LEFM is expected to be most applicable for deep flaws and materials with low toughness.

Elastic-plastic fracture mechanics (EPFM) was developed to allow extension of the concept of a crack driving force to accommodate large-scale plasticity (26-28). Thus, in principle, concepts of EPFM can be applied to intermediate stress and flaw size combinations in the breaking load test for which both the extremes of limit-load and LEFM failure criteria break down. It has been shown that three dimensional elastic-plastic finite element models can be employed to describe crack driving forces for small partial thickness cracks on the scale of interest (57, 58). Rigorous elastic-plastic crack driving force solutions for the specimen configuration and crack geometries of interest are currently under development and, unfortunately, are not available at this writing. In lieu of these solutions, a simple empirical approach was used to approximate the elastic-plastic failure criterion for the breaking load tests. Accordingly, critical combinations of fracture stress and flaw size in the intermediate EPFM regime were modeled using the following weighting expression:

$$\sigma_{EPFM} = \sigma_L \left[1 - \left(\frac{a}{R} \right)^q \right] + \sigma_{LEFM} \left(\frac{a}{R} \right)^s \quad [8]$$

where:

σ_{EPFM} = the EPFM fracture (or breaking) stress (wide range approximation).

σ_L = the fracture stress predicted by the limit load failure criterion.

σ_{LEFM} = the fracture stress predicted by the LEFM failure criterion.

a = flaw depth, refer to Figure 22.

R = the specimen radius.

q, s = weighting exponents.

The values q and s are to be chosen to produce a smooth transition between and tangent to the limiting solutions σ_L and σ_{LEFM} at very shallow and very deep flaw sizes, respectively, as illustrated in Figure 23. Analytical equations used for describing the extremes of limit load and LEFM failure criteria for various crack configurations follow.

a. Limit-Analysis Solutions

An upper bound approximation of the tensile limit-load, P_L , is given when specimen failure is assumed to occur at a net-section stress, σ_{net} , equal to the material's ultimate tensile strength, σ_{UTS} . Thus, the gross limit stress, $\sigma_L = 4 P_L / \pi D^2$, can be calculated for each of the crack configurations of Figure 22 as follows:

$$\sigma_L = (4 \sigma_{UTS} / \pi D^2) \times (\text{Net Cross Section Area}) \quad [9]$$

where the remaining net cross section area (A_{net}) is given by the following equations:

(1) Elliptical Crack (Figure 22(a))

$$A_{net} = \frac{\pi D^2}{4} - (A_1 + A_2) \quad [10]$$

where: $A_1 = \frac{D^2}{4} \left(\theta - \frac{\sin 2\theta}{2} \right)$, and

$$A_2 = \frac{\pi}{2} ac - \frac{c}{a} \left[\frac{D (1 - \cos \theta)}{2} \sqrt{a^2 - \frac{D^2 (1 - \cos \theta)^2}{4}} + a^2 \sin^{-1} \left(\frac{D (1 - \cos \theta)}{2a} \right) \right]$$

and where $\theta = 2s/D$ and the values of c and s can be related by

$$c = \frac{a \sin \left(\frac{2s}{D} \right)}{\sqrt{4 \left(\frac{a}{D} \right)^2 - [\cos \left(\frac{2s}{D} \right) - 1]^2}} \quad [11]$$

(2) Chord Crack (Figure 22(b))

$$A_{\text{net}} = \frac{D\theta}{4} - \left(\frac{D-2a}{2} \right) \left(\frac{D \sin \theta}{2} \right) \quad [12]$$

where $\theta = \cos^{-1} \left(1 - \frac{2a}{D} \right)$; $0 \leq \theta \leq \pi$

(3) Circumferential Crack (Figure 22(c))

$$A_{\text{net}} = \frac{\pi}{4} (D - 2a)^2 \quad [13]$$

For the chord crack configuration, a lower bound limit load solution was approximated by assuming failure of a fully plastic hinge in an assumed elastic-perfectly-plastic material. The gross failure stress in this case is given by:

$$\sigma_L = \sigma_{\text{UTS}} \left[1 - \frac{2\alpha - \sin 2\alpha}{\pi - \theta + 0.5 \sin 2\theta} \right] \left[1 - \frac{\theta}{\pi} + \frac{1}{\pi} \left(1 - \frac{2a}{D} \right) \sin \theta \right] \quad [14]$$

where, $\alpha = \sin^{-1} (0.7937 \sin \theta)$, and

$$\theta = \cos^{-1} \left(1 - \frac{2a}{D} \right)$$

Normalized tension limit-load solutions for each of the above approximations are shown in Figure 24.

b. LEFM Stress-Intensity-Factor Solutions

Under the LEFM failure criterion, fracture is predicted when the stress intensity factor, K , equals or exceeds the critical toughness of the material (taken as K_{IC} in this report). A

variety of K solutions exist for an elliptical surface crack in a finite rectangular plate subjected to uniform tension (59). Athanassiadis (60) and Astiz (61) have independently produced finite element solutions for discrete elliptical flaw configurations in 12 mm and 7 mm diameter tensile bars, respectively. At present, however, there does not exist a K solution for an elliptical surface crack in cylindrical tension specimens which can be generalized to consider any combination of specimen diameter and flaw aspect ratio (a/c). For the round bar geometry, it has been shown (62) that at the point of maximum crack depth, the calculated K value for a partial thickness chord crack is reasonably close to empirically derived K values for the elliptical partial thickness crack. Daoud, et al (63) used finite element analysis to develop the following generalized strain energy release rate, G, equation for the chord crack geometry of Figure 22(b).

$$\frac{\sqrt{EG}}{\sigma\sqrt{\pi a}} = 1.11 - 3.59 \left(\frac{a}{D}\right) + 24.87 \left(\frac{a}{D}\right)^2 - 53.39 \left(\frac{a}{D}\right)^3 + 57.23 \left(\frac{a}{D}\right)^4 \quad [15]$$

$$\text{when:} \quad (0.06 < a/D \leq 0.7)$$

Strain energy release rate, G, can be converted to K according to the following equations (64):

$$K = \sqrt{EG'} (\text{plane stress}), \text{ and } K = \sqrt{EG/(1 - \nu^2)} (\text{plane strain}) \quad [16]$$

where E and ν are the material elastic modulus and Poisson ratio, respectively.

Values of $E = 10.3 \times 10^3$ ksi and $\nu = 0.33$, which are typical for 7X75-type alloys, were used in all computations. Substitution of these values into equation [16] gives a plane strain K solution about 6 percent higher than the plane stress solution. The relationship in equation [15] was verified with compliance data obtained from round bar specimens containing chord cracks machined to various depths (63).

For the elliptical crack geometry of Figure 22(a), K at the point of maximum crack depth can be reasonably estimated by reducing the stress term in the chord crack solution, equation [15], by the ratio of the net section area of the chord crack geometry to the net area of an equivalent diameter section containing an elliptical crack of the same depth,

that is,

$$K_{\text{ellipse}} = K_{\text{chord}} \times \left(\frac{A_{\text{net, C}}}{A_{\text{net, E}}} \right) \quad [17]$$

where:

K_{ellipse} = the adjusted stress intensity factor for the elliptical crack geometry at the point of maximum crack depth, a.

K_{chord} = the stress intensity factor for the chord crack geometry at the point of maximum crack depth, a , (from equations [15] and [16]).

$A_{\text{net, C}}$ = the net area of a cylindrical specimen of diameter D containing a chord crack of depth a , (from equation [12]).

$A_{\text{net, E}}$ = the net area of a cylindrical specimen of diameter D containing an elliptical crack of depth a and aspect ratio a/c , (from equations [10] and [11]).

The above estimate presumes that the elliptical crack stress-intensity solution is more strongly dependent on the average net-section stress in the uncracked ligament ahead of the crack than on the increase in crack-opening constraint associated with change from the chord-crack to elliptical-crack geometry.

The K solution for a round bar with a circumferential crack (Figure 22(c)) is approximated by Harris (65) as:

$$\frac{K}{\sigma\sqrt{\pi a}} = \left\{ 2 \left(1 - \frac{2a}{D} \right) \sqrt{0.2 + \frac{2a/D}{1 - 2a/D}} \right\}^{-1} \quad [18]$$

Stress intensity factor solutions for the chord and circumferentially cracked cylindrical specimen are graphically presented in Figure 25.

2. Supplementary Tests of Cylindrical Tension Specimens Containing Fatigue Cracks

To gain confidence in the ability to analytically relate fracture stress to flaw size, cylindrical tension specimens containing small partial thickness fatigue cracks were loaded to failure in tension. The test specimens were prepared from four commercial variants of 7X75-type alloys; namely, 7075-T651, 7475-T651, 7475-T7651, and 7475-T7351. Alloy 7075-T651 used in this portion of the investigation was from the identical lot of material employed for the SCC evaluations. Alloy 7475 was selected for its high toughness at equivalent strength to alloy 7075 (66, 67). Thus, by comparing results of alloy 7475 to 7075 in the comparable T651 temper condition, the effect of fracture toughness on breaking load calculations could be studied.

Axial 0.125 in. diameter tension specimens oriented in the short transverse direction were removed from each of the four plate materials. The specimen geometry was identical to that used in the SCC portion of this program. To assist fatigue crack initiation, a nominal 0.005 in. deep surface chord defect was machined into the round cross section. The nominal tip radius of the machined defect was 0.005 in. Fatigue cracks of varying sizes were then introduced by subjecting the test specimens to cyclic loading in an electrohydraulic test machine. Cyclic loads were applied at 25 Hz, and at no time did the maximum cyclic load exceed 40 percent of the material yield strength. Crack

initiation was detected visually with a 30X microscope focused at the machined starter notch, or by detecting a change in specimen compliance using a 0.125 in. gage length extensometer and a digital oscilloscope. When a fatigue crack became apparent, cyclic loading was terminated and the specimen pulled to failure. After failure, the specimen fractures were photographed under the scanning electron microscope (SEM). Typical fracture topography revealed in these photos is shown in Figure 26. Dimensions of the fatigue precracks were obtained by generating an elliptical curve fit through digitized locations along the crack front determined in the photographs; see, for example, Figure 27. Dimensions of actual flaws determined by fractography were then compared against predicted sizes calculated from the breaking loads.

IV. TEST RESULTS

A. Mechanical Properties

Short transverse tensile properties for each of the program materials are summarized in Table V. The properties of the commercial plate alloys 7075-T651, 7475-T651, 7475-T7651 and 7475-T7351 exceed the minimum short transverse property limits specified in USAF MIL-Handbook 5 (68). Tensile properties of the specially overaged samples of 7075-T7X1 and 7075-T7X2 do not correspond to any standard T7 type temper; the tensile and yield strengths are lower than for the T651, as expected, considering the electrical conductivities shown in Table II.

The true stress-true strain curves established for the three temper variants of alloys 7075 and 7475 are shown in Figure 28 and 29, respectively. The derived strain hardening coefficients κ and n for each material are given in Table V. Figures 28 and 29 show that agreement of the fitted and actual true stress-true strain behaviors is quite good for all alloys.

Short transverse (S-L) plane strain fracture toughness (K_{IC}) values for the program materials also are given in Table V. All K_{IC} measurements were determined to be valid according to ASTM Method E399-83 (17). The K_{IC} values obtained for each material are representative of commercial plate product in the respective 7X75 alloy designation and temper.

B. Stress Corrosion Tests of 7075 Alloy Plate

1. Smooth Tension Specimens - Traditional Pass-Fail Analyses

The failure records of various groups of smooth tension specimens exposed until failure are summarized in Table VI. A graphical summary of the times to failure of the short transverse 0.125 inch diameter specimens at each of the exposure stress levels for the three temper variants of 7075 alloy is presented in Figure 30. It is obvious that the performances of the three tempers were different, but it is difficult from these few tests to assign a numerical value to each. Crude estimates of threshold stresses for these samples of plate tested under the present conditions per ASTM standard G49-76 (10) are indicated as follows:

7075-T651	$20 > \sigma_{th} > 10$ ksi
7075-T7X1	$40 > \sigma_{th} > 20$ ksi
7075-T7X2	$\sigma_{th} > 40$ ksi

This "ball park" classification of the three materials is sufficient to indicate a substantial improvement of the two T7X tempers over the T651 temper but does not provide a precise description of the behavior of improved materials. Many additional tests would be required to attempt the latter, as described in Appendix B.

2. Smooth Tension Specimens - Breaking Load Analyses

The breaking load data for the individual test specimens and the results of the statistical analyses are summarized in Tables 1-15 of Appendix C. The basic data followed expected trends for

the most part, and these are illustrated graphically in Figures 31-35. The graphs for the more highly stressed short transverse specimens of 7075-T651 and 7075-T7X1 signify the occurrence of SCC as they diverge from the graphs for the specimens exposed with no applied stress. The actual occurrence of SCC was confirmed by the failure of some stressed specimens during exposure and by fractographic examination of broken specimens. A record of the individual failures is given in Table VI, and results of the fractographic examinations are described in Section IV.C. Special grouping of the results were plotted or tabulated to illustrate the comparisons discussed below. Further discussion on significant aspects of the breaking load test results is given in Section V.

a. Comparison of the Three Tempers of 7075 Alloy Plate

Changes in mean breaking stress (gross fracture stress) with length of exposure for 0.125 in. diameter short transverse specimens of the three temper variants of 7075 alloy are shown in Figure 31. The expected wide range in performances of the three tempers at several levels of exposure stress is evident. This is shown also by graphs of 99% survival stresses presented in Figure 32. These stresses represent the lower limit of gross fracture stress for 99% of a large population of specimens under the specific conditions of exposure stress and time indicated. Values of these survival stresses were averaged over a range of exposure periods that appear most appropriate (see Section V.A.3) and are

summarized along with statistical threshold stresses in Table VII. These ranking parameters, which are consistent with the "pass-fail" rankings described in Section IV.B.1., give more discriminating comparisons between the materials.

It is noteworthy that the breaking load test data contain decreasing variance in test results for materials with improved resistance to SCC, and thus could afford greater precision in this important area of interest for alloy development studies. The variance trends are illustrated by the graphs of standard deviation for the mean breaking stresses in Figure 33. This feature is in direct contrast to the traditional "pass-fail" method of test which, because of the dependence on complete specimen failure, requires higher replication of tests to detect susceptibility in materials with improved resistance to SCC. Additional discussion of the precision of breaking load test results is presented in Section V.A.2.

b. Effect of Specimen Diameter on Test Performance of the Intermediate Resistance T7X1 Temper

Two specimen diameters were used for the 7075-T7X1 materials because of previous observations in "pass-fail" tests that the comparisons of materials can be influenced by the choice of specimen size (35). Comparative test results obtained with 0.125 in. and 0.225 in. diameter tension specimens are shown in Figure 34 and Tables VI and VII. The behaviors of the two sizes of specimens were similar, although a slightly longer exposure time

was required for the larger specimen to register the same reduction in 99% survival stress and time to failure as the smaller specimen. This trend can be noted at 40 ksi exposure stress (see Figure 34 and Table VII). Further discussion of the specimen size effect is contained in Sections IV.D.3. and V.A.4. in connection with the correlation of fracture stress with flaw size.

c. Effects of Grain Orientation in Tests of 7075-T651

The expected difference in performances of long and short transverse specimens is shown in Figure 35. The striking difference also is shown by the 99% survival stress and threshold stress values listed in Table VII. The 7075-T651 thresholds are of the same order as the minimum failure stresses shown in Figure 2 for many lots of 7075-T651 plate.

On the basis of the small difference observed between behaviors of the 0.125 in. and 0.225 in. specimen tests of alloy 7075-T7X1, it can be inferred that the size difference of the short and long transverse direction specimens of alloy 7075-T651 probably did not have an appreciable effect on the comparison of test orientations.

It is clear from each of the above comparisons that breaking load test data gives a more quantitative description of SCC resistance at shorter exposure times than would be required for traditional pass-fail interpretation.

3. Fracture Mechanics Specimens

The detailed SCC test data from the fracture mechanics type specimens are contained in Appendix D. Graphical summaries representing the performances of the three 7075 alloy tempers in the two types of test used are discussed in the following section. Theoretically, graphs like the idealized sketch in Figure 6 can provide two useful types of data for the characterization of the resistance to SCC under the conditions of test, namely, a threshold stress intensity factor (K_{th}) for the growth of SCC, and the rate of SCC growth (da/dt). The "plateau velocity" is a significant measurement that relates to the rate of SCC growth a material will sustain for an appreciable crack extension. Comparisons of various data reduction techniques for determining the growth rates were also made.

a. Bolt Loaded DCB Specimens (K-decreasing Test)

Environmental crack growth as a function of exposure time is presented graphically in Figure 36 for each of the DCB specimens. At the conclusion of the environmental exposure, the specimens were broken open by further tightening of the loading bolts, and final crack lengths were measured on the fracture surfaces. Photographs of the specimen fracture surfaces are shown in Figure 37. The crack lengths at conclusion of the test are listed in Appendix D. These data, like the results of the smooth specimens presented above showed expected differences in behavior of the three materials.

The determination of K_{th} with a K-decreasing test depends upon the investigator's ability to, first, induce the initiation and growth of SCC and, secondly, to identify a significant crack arrest. Because the advancing crack tip may not come to a complete stop, an arrest usually is arbitrarily defined by a vanishingly small growth rate that is dependent upon the precision of crack measurement and the patience of the investigator. A review of published articles on DCB testing aluminum alloys indicates that a crack growth rate of about 1 to 2×10^{-5} in./hr. is practicable for estimates of K_{th} , as it is consistent with both crack measurement capability and test results expected for a highly resistant alloy, such as 7075-T73 (51, 53, 69). It would also be desirable to relate a limiting crack growth rate chosen in this way to service requirements, but there are presently no published guidelines for doing this.

The difficulty in identifying true SCC arrests in laboratory tests is frequently compounded by severe corrosion of the crack faces: the wedging action of insoluble corrosion products forming at the crack tip can become very powerful. Exposure of SCC-resistant materials to chloride solutions can produce wedges powerful enough to advance the mechanical precrack by purely mechanical fracture, which can be mistaken for SCC unless verified by fractographic or metallographic examinations (53, 69). Also, wedging action can enhance the crack tip stress-intensity factor and force the extension of SCC in susceptible materials, thereby preventing arrest or causing a series of temporary arrests with

extended exposure (69, 70). In either case, when gross wedging effects are observed, the true mechanical driving force at the crack tip is not indicated by the K relationship [Equation 4], and estimates of K_{th} would be erroneous. Under these conditions, the best estimate of K_{th} (though risky) would appear to be that taken at the first significant arrest (70). With the crack length measurement precision used in this investigation, an arrest would be indicated by inability to detect crack growth over a period of at least 500 hours.

It is evident in Figure 36 that crack arrest was not attained in either of the 7075-T651 specimens, although it appears that the crack growth rate began to decrease after about 500 hours and then increased after 700-900 hours. It is questionable whether arrest would occur with extended exposure and, if so, whether the apparent K_{th} values would be meaningful. Both of the T7X1 temper specimens reached apparent arrests: specimen #1 after 300-800 hours, and specimen #2 after 1200-1700 hours. Although both developed apparent arrests at the same crack length (confirmed by fractography), they had different initial pop-in crack lengths and dissimilar crack length vs. time curves. The performances of the T7X2 temper specimens were similar to those of the T7X1 temper except there was less total crack growth; the T7X2 specimen #1 arrested at 100-600 hours and specimen #2 after 1200-1700 hours. Rough estimates of the minimum K_{th} for each of the three materials based on these apparent arrests were as follows, referring to Tables 1-6 in Appendix D for the K values:

<u>Plate-Temper</u>	Estimates of K_{th}	
	<u>ksi$\sqrt{in.}$</u>	<u>% K_O *</u>
7075-T651	Indeterminate	
7075-T7X1	16	83
7075-T7X2	18	96

* K_O is the stress intensity factor at the beginning of environmental exposure.

There is no generally accepted procedure for calculating crack growth rate as a function of stress intensity from the crack growth curves. Various approaches (often not described) can be observed in the literature, the simplest being a graphical technique. Based on considerable test experience with highly susceptible materials such as 7075-T651, a "constant" rate of growth is observed first (plateau velocity), followed by a decreasing rate of growth with decreasing stress intensity factor (2). The procedure used in the present investigation was to divide the crack length vs. time curves into segments of approximately constant slope represented by straight lines (this involves smoothing of some parts of the crack length curves). The slopes of these segments were computed and corresponding K values were calculated for crack lengths at the end of each segment (Table VIII). The first segment was considered as an estimate of the plateau velocity illustrated in Figure 6.

Segmented growth rate curves were plotted in Figure 38 for the individual specimens, and estimates of representative curves

sketched for each temper. Average values are shown for plateau velocities and minimum values for K_{th} . Plausible growth rate curves could not be drawn for the T7X2 temper, although it is obvious in Figure 36 that there was only a slight amount of crack growth and no appreciable sustained crack growth rate. Examination of the crack tip with a light microscope (40x) and the scanning electron microscope revealed only corrosion and isolated minute sites of SCC. Therefore, a representative curve was estimated assuming that the short time high growth rate at the beginning of each crack growth curve was a transient effect associated with very high K_o values (Figure 16), rather than an indication of a plateau velocity (possibly an artifact caused by the "pop-in" method of precracking).

A convenient computer technique for developing crack growth rate curves involves a curve fitting method by a polynomial function fitted to the entire crack length vs. time curve. Derivatives of the smoothed crack length vs. time relationships were made at points along the fitted curve to determine instantaneous crack growth rates. Two other techniques taken from fatigue crack growth testing experience also were used: one, a secant method, and the other, an incremental polynomial method. These three methods are described in more detail in Table 7 of Appendix D. A comparison of the results using these various data reduction techniques is shown in Figure 39.

All the methods used to calculate crack growth rates produced the same general results which are confused by large amounts of scatter resulting from the use of small crack growth increments. The results for the T651 temp : were clearly separate from those of the more resistant T7X1 and T7X2 tempers, but the latter were indistinguishable. Moreover, the actual significance of such graphs is open to question when the corrosivity of the environment and the length of exposure can cause gross corrosion product wedging effects and/or crack branching, both confusing the estimation of K. Blind reduction of raw crack length measurement data can be useless without prior interpretation of crack length vs. time curves. Allowances should be made for extraneous effects caused by erratic or apparent beginnings of SCC growth, simple scatter in the measurement data due to excessive crack front curvature, multiple crack planes, crack tip branching, and gross wedging by corrosion products.

A simple way to compare the materials using the crack length vs. time curves is by the use of growth rates averaged from time zero (immediately after the mechanical precrack) to an arbitrary time sufficient to achieve significant crack extension in most SCC-susceptible materials (69). In this instance, a comparison of the 7075 alloy materials after an exposure of 1000 hours compared to plateau velocities shown in Figure 38 is as follows:

<u>Plate Temper</u>	<u>Average Growth Increment, in.</u>	<u>Average Growth Rate, in./hr.</u>	<u>Estimated Average Plateau Velocity, in./hr.</u>
T651	0.398	4.0×10^{-4}	4.5×10^{-4}
T7X1	0.056	5.6×10^{-5}	1.1×10^{-4}
T7X2	0.032	3.2×10^{-5}	1.5×10^{-5}

b. Ring Loaded WOL Specimens (K-increasing Test)

Crack lengths in the WOL specimens were determined by monitoring the load and crack-mouth-opening-displacements on each specimen (Figure 20). It was necessary to correct the displacement data because the clip gages used to monitor crack-mouth-opening-displacement showed excessive long-term drift. Post-test corrections were made by averaging the clip gage data from three specimens which exhibited no crack extension (highly resistant T7X1 and T7X2 tempers at low initial stress intensities), and subtracting this pure drift component from data taken from the other clip gages. This adjustment satisfactorily corrected the crack-mouth-opening-displacement for all of the specimens as shown, for example, in Figure 40. Adjusted crack growth curves for the three tempers of 7075 alloy are shown in Figure 41. SCC propagation rates obtained by the five-point incremental polynomial method (Appendix D) are shown in Figure 42 for the three 7075-T651 specimens. Growth rates calculated for all specimens of the T7X1 and T7X2 tempers were below the growth rate resolution limit of the measurement system (about 5×10^{-5} in./hr.) and are not included in Figure 42. Detailed notes concerning the performance of these tests are contained in Table 8 of Appendix D.

Specimens of 7075-T651 were started at initial K_0 levels of 9.4, 6.9, and 4.0 $\text{ksi}/\sqrt{\text{in.}}$. For the test started at $K_0 = 9.4$ $\text{ksi}/\sqrt{\text{in.}}$, crack growth initiated rapidly and rose to a plateau velocity around 8×10^{-4} in./hr. The second specimen, started at $K_0 = 6.9$ $\text{ksi}/\sqrt{\text{in.}}$, showed lower initial growth rates than the first specimen, but the crack growth was accelerated later in the test as K increased. The third specimen showed no crack growth when put in test at $K_0 = 4.0$ $\text{ksi}/\sqrt{\text{in.}}$. Therefore, it was removed from test after about 1340 hours, fatigue cracked an additional 0.1 inch and re-exposed at $K_0 = 7.9$ $\text{ksi}/\sqrt{\text{in.}}$. Crack growth started immediately (Figure 41). Since no crack growth was indicated at $K_0 = 4.0$ $\text{ksi}/\sqrt{\text{in.}}$ and growth did occur at $K_0 = 6.9$ $\text{ksi}/\sqrt{\text{in.}}$, the threshold stress intensity, K_{th} , under the stated environmental conditions was estimated at about 5 $\text{ksi}/\sqrt{\text{in.}}$ (26% of K_{IC}).

Specimens of the 7075-T7X1 temper were started at $K_0 = 6.7$, 9.4, and 14.0 $\text{ksi}/\sqrt{\text{in.}}$. No crack growth was detected in any of the specimens. However, post-test fracture surface examination with a light microscope (40X) revealed significant environmental crack growth in the most highly stressed specimen after a 2330 hour (97 day) exposure time. Total crack growth was about 0.030 inch, or an average growth rate of 1.3×10^{-5} in./hr., which is at about the limit of crack growth rate detection of the test setup under ideal conditions. The 7075-T7X1 temper specimen beginning with the intermediate K_0 level (9.4 $\text{ksi}/\sqrt{\text{in.}}$) was removed from test after 1580 hours with no indication of crack growth, sectioned along the midplane, and examined metallographically. No indication of intergranular SCC was found, although there were

minute discontinuous transgranular and intergranular branches at the crack tip, possibly produced during precracking (Figure 43). The threshold stress intensity for this material was estimated at approximately $13 \text{ ksi}\sqrt{\text{in.}}$ (67% of K_{IC}) for the test conditions stated.

The 7075-T7X2 specimens were tested at initial K_0 levels of 14.9, 15.4, and 18.8 $\text{ksi}\sqrt{\text{in.}}$. No real crack growth was noted during exposure of these specimens except for a slight indication in the most highly stressed specimen (Figure 41). Visual inspection and SEM examination of the mechanically fractured specimen after a 1580 hour exposure, however, failed to verify SCC growth. Metallographic examination of the specimen tested at an initial K_0 of 14.9 $\text{ksi}\sqrt{\text{in.}}$, showed no evidence of intergranular SCC (Figure 43). The threshold stress intensity for environmental crack growth was estimated at about 19 $\text{ksi}\sqrt{\text{in.}}$ (94% K_{IC}) for the test conditions used.

Table IX summarizes the crack growth results for the WOL specimen tests. It was noted that the estimates of K_{th} from these tests were reasonably similar to those from the DCB tests, but additional tests would be required to obtain more definitive estimates.

Oxide wedging, which occurred in the DCB specimen tests, did not appear to be a factor in the WOL specimen tests. However,

evidence of substantial oxide buildup was noted in the 7075-T651 specimens. This evidence is shown in Figure 44 where load-displacement curves obtained during mechanical fracture after exposure are compared. Oxide buildup in the three 7075-T651 specimens is indicated by a marked change in slope of load versus deflection curves. The change in load-deflection slope at low loads indicates that the specimen responds as though the crack length is shortened due to the presence of corrosion products between opposing fracture faces. As loading is increased, the crack progressively opens, and eventually the influence of corrosion product wedging decreases to zero when the crack becomes fully open (above the break in the curve, Figure 44). Since the breaks in these curves were below the exposure loads marked on each curve, it appears unlikely that the oxide was causing crack face interference during exposure (assuming that the initial unloading of the specimen did not alter the position of the break in the load versus displacement curves by permanently deforming the oxide). For the T7X1 and T7X2 temper specimens, little deviation from linearity was seen in the load-displacement curves, indicating little or no oxide buildup during exposure. It is suspected that the increased tendency for buildup in the T651 specimens was the result of their susceptibility to intergranular attack giving rise to exfoliation effects on the crack faces. Note in Figure 45 the reduced tendency for intergranular attack in the T7X tempers, as discussed in Section IV.C.1.

C. Metallographic and Fractographic Examinations

1. Type of Corrosion and Fracture Characterization

Longitudinal sections of corroded tension specimens were examined metallographically to observe the type of attack in all three tempers of 7075 alloy exposed in the absence of applied stress, and to search for evidence of secondary stress-corrosion cracks in failed specimens of 7075-T651 and T7X1.

Profiles of localized corrosion sites in all specimens exhibited a directional appearance as the attack tended to follow the grain structure in the rolling plane of the plate (Figure 45). The type of attack in the stressed specimens of 7075-T651 and T7X1 that failed after 4-5 days exposure in the 3.5% NaCl alternate immersion test was the same as in the specimens exposed with no applied stress, except that the secondary intergranular fissures of the stressed specimens typically penetrated deeper than those of the zero stress specimens. The intergranular fissures in the stressed specimens were considered to be cracks when they were seen to be significantly longer than the fissures in specimens exposed with no applied stress.

In the case of the T651 temper, corrosion proceeded primarily along grain boundaries, as shown by the fine network in Figure 45(a), although directional pitting also was present. The propensity for intergranular attack is normally less in overaged T7-type tempers (71) and, as expected, was reduced in specimens of

the T7X1 temper, Figure 45(b), and practically non-existent in the T7X2 temper, Figure 45(c). Thus, in the T7X2 temper specimens, the corrosion took the form of relatively shallow directional pitting perpendicular to the axis of the specimen with only traces of grain boundary attack associated with some of the pits.

Figure 46 shows a typical SCC fracture surface from a specimen which failed during alternate immersion exposure. The smooth plateau-like areas were found near the outer surface of the specimen (Figure 46(b)) as well as at the maximum depth of SCC flaw penetration (Figure 46(c)).

2. Flaw Size Measurements on SCC Specimens

Representative measurements of SCC flaws on fracture surfaces of stress corroded specimens broken in the tension tests are summarized in Table X. The last four columns of the table contain the pertinent flaw size/geometry information. Deepest flaw penetration (a_{\max}) and the flawed area fraction (A_c/A_o) are the two direct measurements of flaw size described in Section III.E. "Equivalent flaw depth (a_e)" is the depth of an annular crack, Figure 22(c), of equal flawed area fraction; and is calculated from the following equation:

$$a_e = \frac{D}{2} \left[1 - \sqrt{1 - (A_c/A_o)} \right] \quad [19]$$

where D is the specimen diameter, A_0 the original cross section area, and A_c is given by equation [7] in Section III.E. The last column in Table X indicates whether the actual SCC flaw shape is best idealized as a single dominant crack or an annular (ring-like) crack. A number of these fracture surfaces are shown in Figure 47, illustrating the range of flaw depths and shapes observed.

The data in Table X are graphically illustrated in Figures 48 through 50 for the T651, T7X1, and T7X2 tempers, respectively. Data are presented as SCC flaw size (a_{\max} or a_e) plotted against length of exposure. These graphs are analagous to the breaking load curves as they illustrate the degree of total damage (which may or may not include SCC) in terms of flaw depth as a function of exposure time. The bars for each exposure time represent the range of flaw sizes corresponding to the highest and lowest fracture stresses measured in that group of five specimens. When only one point is plotted with an arrow, it represents the one specimen which survived the designated exposure time, and is therefore the smallest flaw of the group of five specimens exposed; the arrow extending upwards indicates the estimated critical flaw depth, a_{cr} , that would result in rapid fracture at the exposure stress. An arrow shown with two plotted points indicates the estimated critical size flaw in the single specimen that failed during exposure. The estimated critical flaw sizes indicated by the arrows were calculated according to equation [8] with the breaking stress equated to the exposure stress, and

inserting the limit stress and LEFM failure solutions for either the elliptical or annular shaped flaw, as appropriate.

These graphs illustrate several expected trends in the data. First, the flaw size generally increased with length of exposure. A notable exception to this is shown by the decrease in flaw size observed in the 0.225 in. specimens of 7075-T7X1 exposed for twelve days (Figure 49); this decrease in flaw size corresponds to a measured increase in average breaking stress noted in Section IV.B.2. (Figure 34), and will be discussed in a later section of the report (V.A.3). Second, data on the highly SCC susceptible 7075-T651 alloy (Figure 48) show that for a given exposure time the flaw size increased with exposure stress, again corresponding to a decrease in breaking load (Figure 31). In contrast, flaw sizes in the highly SCC resistant T7X2 temper material (Figure 50) showed no effect of exposure stress on flaw size, indicating that the increasing level of degradation of this material at the longer exposure was due only to corrosion rather than to stress corrosion. A third point to be made addresses the effect of specimen size (0.125 in. vs. 0.225 in. diameter) on flaw depth. The limited data obtained on specimens broken in tension tests showed that flaw depths in specimens of both diameters span similar ranges (Figure 49). This observation is supported by the effective flaw size calculations discussed later in Section IV.D.3. It appears, however, that measurements should be made on specimens from additional exposure periods to confirm this point. The more rapid decrease in breaking load and the shorter failure times observed

for the 0.125 in. specimens do not necessarily indicate that the growth of stress-corrosion flaws occurred faster in the 0.125 in. specimens; rather it is merely a reflection of a shorter critical flaw size for the smaller specimen. Further discussion of this point is presented in Section V.A.4.

A final point regarding the flaw size measurements made from fractographs such as Figure 47 concerns the accuracy with which the SCC and final (tensile) fracture regions could be distinguished. Both regions had a somewhat stepped or plateau-like topography, primarily due to the short transverse specimen orientation. The final tensile fracture region was characterized by a void coalescence mechanism (Figure 51(a)), whereas the SCC region contained relatively flat plateaus, occasional corrosion debris and "mud-cracking" patterns, but no microvoids (Figure 51(b)). This was generally true for all breaking load specimens, regardless of temper, exposure stress, or exposure time. At lower magnification the SCC region was often darker (Figure 52(a)); this also was true when viewed through an optical microscope. The transition from SCC to final tensile fracture was very abrupt in specimens which were pulled apart after the alternate immersion exposure, and the transition was often marked by very steep inclines (Figure 52(b)). These walls show evidence of shearing and seem to predominantly consist of very fine microvoids. Since this transition is so clear, it was relatively straightforward (although tedious) to map the fracture surfaces and measure SCC flaw sizes and areas. It was noted also that the morphology of

the SCC flaws in the specimens broken in tension tests was similar to that of SCC in specimens that failed during exposure.

A related concern was the possibility of crack extension (a "pop-in") during tension testing. Since the leading edge of SCC flaws usually occur in or along grain boundaries and is likely to be quite irregular, some intergranular pop-ins might be expected. This behavior would most likely occur in short transverse specimens of near peak strength tempers. However, the only evidence of such pop-in was observed in the T651 and T7X1 materials and was in the form of minute areas of local extension where the flaw appeared to be trying to catch up to the points of deepest penetration, rather than growth along the entire flaw contour. Thus, the flaw area A_c could be increased slightly, but a_{max} would not be expected to change. Figure 53 shows a small plateau of fine dimples adjacent to an SCC flaw. This region may indicate a local pop-in of the SCC flaw, but the additional area contributed by even a large number of such pop-in sites would be insignificant in determining the fracture mechanics flaw size, a_{max} .

D. Correlation of Fracture Stress with Flaw Size

1. Analytical Relationships for the Cylindrical Tension Specimen Containing an Elliptical Surface Crack

Analytical relationships involving three different failure criteria were calculated for six 7X75 alloy-temper variants using the following equations presented in Section III.F.:

- a. Limit-Load Analysis - Equation [9] with the appropriate net section area determined with Equation [10].
- b. LEFM - Equation [17] adjusted with the finite-element chord crack solution of Equation [15], under the condition of plane strain Equation [16] with $\nu = 0.33$.
- c. EPFM (Wide-Range Estimate) - Equation [8] with the following empirical exponents q and s chosen to fair in a reasonable transition curve between the two extreme solutions.

<u>Alloy</u>	<u>Specimen Diameter, in.</u>	<u>q</u>	<u>s</u>
7075	0.125	2	4
7075	0.225	1.5	4
7475	0.125	2	3

These relationships are shown in Figures 54-56 and are used in the next two sections as reference curves for the evaluation of the combinations of fracture stress and flaw size for the fatigue and SCC test specimens. These results, which apply to the short transverse orientation, are based on the strength and toughness properties given in Table V. For the calculations, a flaw aspect ratio, a/c , of 0.8 was used to approximate the configuration of interest, as explained in the next section.

2. Fatigue Cracked Tension Specimens, Supplementary Tests

Results of the supplementary breaking load investigation performed using fatigue precracked round tension bars of four commercial plate alloys, namely, 7075-T651, 7475-T651, 7475-T7651

and 7475-T7351 are given in Table XI. All test specimens were 0.125 in. diameter and oriented in the short transverse direction. Table XI gives the breaking loads and the gross fracture stresses obtained in the individual tests, and the corresponding fatigue precrack dimensions determined from the post fracture examination. A wide range of fatigue flaw depths (from about 6 to 60 mils) was generated by the precracking. The mean terminal fatigue crack aspect ratio, a/c , for all specimens analyzed was 0.80. Consequently, this value of a/c was assumed to represent the equilibrium elliptical shape for use in the fracture mechanics correlations of breaking stress to flaw size.

The individual specimen breaking strengths normalized by their respective material yield strengths are shown plotted against the observed fatigue flaw depths in Figure 57. As would be expected, the plot shows that high toughness 7475 alloy products give combinations of breaking stress and flaw size which are greater than those observed for alloy 7075-T651. The influence of alloy toughness and strength on the interpretation of the breaking load test will be discussed in more detail in Section V.A.4.

Experimental and predicted gross fracture stress versus flaw size behaviors of the four 7X75 commercial plate alloys are compared in Figure 58. The predicted behaviors in this figure correspond to the estimated wide-range EPFM solutions shown in Figures 54(a) and 56(a), (b), (c) for the respective alloys and

temperatures. Despite the simplicity of analytical assumptions used in the predictive model, the agreement between the calculated behavior and actual test data is excellent. In theory, further refinements to the predictive procedures under a more rigorous elastic-plastic fracture mechanics approach should reduce the degree of empiricism in the model. These refinements, however, are beyond the scope of the present work. Nevertheless, it can be concluded on the basis of this supplementary investigation that:

(a) small single crack-like flaws can be readily detected in small-scale tension specimens by measuring degradation in breaking strength, and (b) the depth of such flaws can be reasonably calculated from measured breaking strengths and the material strength and toughness properties.

a. Effect of Bending Stress on Breaking Load-Flaw Size

Correlation

To examine the possible influence of eccentricity due to bending on the correlation of breaking load with flaw size, the plastic hinge and tensile limit-load solutions (Equations [14] and [9], respectively) were compared with actual breaking load data from the fatigue-precracked tension specimens. The plastic hinge solution accommodates the bending influence attributed to non-symmetry of the elliptically cracked cross section, whereas the tensile limit-load solution does not. The comparison was made on alloy 7475 for which limit-load is the dominant failure criterion in the breaking load test (see for example, Figure 56). Predicted fracture-stress/flaw-size combinations according to the

different limit-load failure criteria are shown in Figure 59 with data from alloy 7475-T651 fatigue-precracked test bars. It is clear from the figure that the plastic hinge failure criterion grossly under-estimates the observed breaking stress/flaw-size combinations, whereas predictions given by the tensile limit-load criterion appear more applicable. This observation suggests that the specific threaded-end specimen and grip arrangements used for tension testing in this investigation supplied adequate constraint against bending so that its possible effect on the correlation of breaking load with flaw size can be ignored.

3. Equivalent Flaw Sizes Calculated from Breaking Load Tests of SCC Test Specimens

The results of the supplementary investigation reported in the preceding section showed that the wide-range EPFM model accurately predicted the combination of breaking strength and flaw size observed in specimens containing a single, elliptically-shaped, surface crack introduced by fatigue. Building on this success, it is of interest to consider extension of the model to correlate crack-like SCC damage (note, there is often more than one SCC flaw in a single specimen) to the breaking strength of stress corroded test specimens of the three temper variants of alloy 7075.

First, however, comparisons were made of actual fracture-stress/flaw-size combinations with the estimated wide-range EPFM relationships, just as was done with the fatigue cracked

specimens. These are shown for the T651 (most SCC susceptible) and T7X2 (least susceptible) temper conditions in Figure 60, and for the two specimen diameters (0.125 in. and 0.225 in.) of the intermediate T7X1 temper material in Figure 61. The wide-range EPFM model employed in these estimates was identical to that used in the fatigue specimen calculations with assumptions of an elliptical partial thickness crack with an aspect ratio (a/c) of 0.8. Again, the agreement between predicted and actual behaviors under each of the evaluated conditions appears quite good, although there is the tendency for predicted elliptical flaws to be slightly deeper than observed maximum depths of actual SCC flaws.

a. Effect of SCC Geometry on Breaking Load-Flaw Size Correlation

As reported in Section IV.C., the SCC portion of the tension specimen fractures (shown in Figure 47 and noted in the last column of Table X) are not always characterized by a single elliptical flaw. In fact, it is often common for multiple cracking to occur around the circumference, giving the SCC fracture the assumed 2-dimensional annular appearance modeled by Figure 22(c). It, therefore, is interesting to examine how well the equivalent annular flaw depth, a_e , calculated from the SCC area fraction with equation [19] compares with predicted values developed from the circumferential crack geometry assumption of Figure 22(c).

Since limit-load is the dominant failure criterion for short circumferential crack depths on the order of those corresponding to the calculated a_e values in Table X, the fracture-stress/ flaw-size data plotted in Figures 62 and 63 were compared to the appropriate limit-load solutions. The Figures show that the correlation of predicted flaw depths to a_e values calculated from the specimen SCC area fraction is also reasonable. The slashed data points in Figures 62 and 63 correspond to specimen fracture surfaces in which a single SCC flaw was observed to be dominant over other cracked areas. The slashed data points consistently fall below, or to the left of the predicted line (Figures 62 and 63), suggesting that fracture in each case is more dependent on depth of the major flaw than the total flawed area. The above bias is less apparent when the maximum depth of SCC penetration was plotted against the calculated elliptical flaw depth given by the EPFM wide-range model shown in Figures 60 and 61. These figures indicate that the wide-range EPFM model for the single elliptical flaw estimates actual breaking stress-flaw depth combinations equally well regardless of whether the observed SCC fracture is composed of singular or multiple cracks. This is believed to be so because in reality the SCC fracture is 3-dimensional. That is, the multiple SCC flawed areas are not of the same cross-sectional plane as tends to be suggested by the 2-dimensional SEM photos of Figure 47. In 3-dimension, the individual flaws would tend to behave more as isolated events, with maximum penetration (depth) a more controlling factor than flawed area; at least moreso than would be suggested by the

2-dimensional annular crack approximation. Moreover, for engineering purposes, it is safer to characterize SCC damage by the maximum depth of penetration (worst probable flaw), rather than by the equivalent area crack. This view is totally consistent with the extreme value statistical approach selected earlier (Section III.D.2b) for calculation of survival probabilities and the 99% survival stress. Therefore, the maximum depth of an assumed elliptical flaw, calculated from breaking load test results and the wide-range EPFM model, gives a physical dimension (maximum depth of attack) for describing SCC susceptibility of materials. The advantages of this truly quantitative characterization approach will be discussed in the next section and in Sections V and VI.

b. Reduction of SCC Test Results in Terms of Effective Flaw Depth

The wide-range EPFM model was used to estimate depth, a , (Figure 22(a)) of hypothetical elliptical shaped SCC cracks ($a/c = 0.8$) corresponding to breaking strength measurements made on the various groups of stress corrosion test specimens. The results of these computations are presented in Figure 64 as the range and mean estimated flaw depths for each group of five specimens used for breaking load tests. Whenever specimen failure occurred prior to completion of the scheduled number of exposure days, the gross section exposure stress was used to calculate a critical flaw size, a_{cr} , that would produce rapid fracture. This value of a_{cr} was then used to estimate the maximum flaw size corresponding to the specimen group of interest.*

The comparison of mean trends observed for the three 7075 alloy tempers and the two specimen diameters are given in

*The stressing frame used in this investigation (Figure 13) is relatively stiff, and accordingly, the gross exposure stress at the time of SCC failure will be less than the originally applied stress. This reduction in applied stress is more pronounced when the ratio of flaw size to specimen diameter is large, and the specimen is more compliant. The value of a_{cr} calculated by using the original stress can, therefore, be considered a lower bound approximation, since the estimated flaw size would be larger for any smaller value of stress used in the calculation (see Figures 60 and 61).

Figure 65. The ordering of SCC resistance among the 7075 alloy tempers is consistent with experience. That is, increased degree of aging from the T651 to the T7X2 temper condition in all cases decreased the mean flaw depth calculated for the group of five specimens subjected to a given exposure stress and time period. Moreover, the ease with which the relative SCC resistances of the T7X1 and T7X2 temper conditions can be distinguished at higher exposure stress levels (30 and 40 ksi) appears to be a particularly attractive feature of this method of presentation. It is also noteworthy that, when flaw size is plotted against exposure time, the 7075-T7X1 alloy 0.125 in. and 0.225 in. diameter specimen results are practically identical (Figure 65). This is in agreement with the fractographic observations discussed in Section IV.C.2.

In order to estimate the SCC flaw depth that would not be exceeded in 99 percent of the specimens subjected to the designated combination of exposure period and stress, hereafter referred to as a_{99} , the 99% survival stresses (developed in Section IV.B.2.) were substituted into the wide range EPFM model. The results of these computations are shown in Figure 66 and, like the preceding illustrations, the predicted trends are consistent with experience, except for the 0.225 in. diameter specimens of 7075-T7X1 exposed at a stress of 40 ksi. The a_{99} values correspond to a statistical measure of the upper limits of the distributions of flaw depths shown in Figure 64. These distributions are wider in the case of the larger diameter

7075-T7X1 specimen because the analytical solutions from which flaw depths were calculated (Figure 61) indicate that a small change in breaking stress causes variation in the calculated flaw size to be greater for the large specimen diameter. That is, the calibration curve of the larger diameter specimen is more nearly horizontal than that of the small diameter specimen (see Figure 55), and therefore, the calculation of flaw size will be more precise with the smaller diameter specimen.

V. DISCUSSION OF TEST RESULTS

A. Further Analysis of SCC Breaking Load Test Results

1. Comparison of Probabilities of Survival Calculated from Breaking Load and Traditional Pass-Fail Data

Probabilities of survival calculated according to equations [2 and 2a] and the probability plotting method for defining the extreme value distribution parameters, $\hat{\mu}$ and $\hat{\sigma}$, are summarized for each of the tested conditions in Tables 3, 6, 9, 12, and 15 of Appendix C. For another check on the breaking load test method, comparisons were made between probabilities of survival calculated from gross fracture stresses and those obtained from traditional pass-fail data. Pass-fail results for days when failures actually occurred were plotted on the calculated probability of survival graphs for short transverse specimens of 7075-T7X1 and 7075-T651 in Figures 67 and 68, respectively. Good agreement was observed, particularly for the specimens of 7075-T7X1, although the comparisons were quite limited. A significant advantage of the breaking load procedure is the capability of determining the probability of survival without requiring specimens to fail in the environment of interest. This is of particular value in the evaluation of materials with relatively high resistance to SCC under the specified test conditions.

2. Increased Precision for Characterization of SCC-Resistant Materials

With pass-fail test results, more sensitive screening of alloy performance can be obtained only by increasing the number of

replicates. This is illustrated by the graph in Figure 69, which shows the lower 95% confidence limit for the estimated probability of survival determined when all specimens survive for various numbers of replicate tests. One of the most practical advantages of the breaking load test method is that the numerical results provide improved ability to discriminate the performance of materials with improved resistance to SCC--without requiring a prohibitive number of replicate tests. To illustrate this point, consider the case where five replicates each of three 7075 tempers are exposed in test and all specimens survive the designated exposure conditions. The estimated survival probability (P) determined from the pass-fail data would equal 1.0 for all three tempers (i.e., five survivors/five specimens tested). Moreover, Figure 69 shows that for five specimens, the 95% confidence limits are $0.55 \leq P \leq 1.0$. That is, with the estimate $P = 1.0$, the actual probability of survival, P, can be said to lie within 0.55 and 1.0 with 95% confidence. Thus, not only is the confidence interval large, but the test has shown no differences between the tempers. In contrast, the table below illustrates additional discriminating information that can be derived from analysis of breaking load data:

<u>Plate Temper</u>	<u>Exposure Conditions</u>	<u>Probability of Survival, %</u>	<u>99% Survival Stress, ksi</u>
T651	20 ksi, 4 days	93	0
T7X1	30 ksi, 9 days	99	31
T7X2	30 ksi, 9 days	100	63

Data are from Tables 3, 6, and 9 in Appendix C.

The probability of survival calculated from breaking load data is a statistic and should be qualified with a measure of variability (or variance). This requires additional test replication, which is beyond the scope of the present program. Qualitatively, the variance of the probability of survival determined from breaking load data is expected to be much less than that determined from pass-fail analysis of similar sample sizes. Though added replication would reduce probable errors in estimating the population mean breaking strength and standard deviation, high replication may not be necessary for discriminating levels of SCC performance among materials, as shown to be the case for the three temper variants of alloy 7075 plate considered in the current program.

Reproducibility of breaking load measurements was mentioned previously in Section IV.B.2a and the variation in standard deviations was presented in Figure 33. Large standard deviations were associated with large reductions in breaking strength (high SCC susceptibility), as can be seen by comparing Figures 33 and 31. This trend is shown more directly in Figure 70 by plotting fracture strength standard deviations against the mean reduction in apparent tensile strength for all of the test groups in this investigation. Generally speaking, high precision is not required to discriminate good from bad materials because appreciable degradation in breaking strengths are readily detectable in poorly performing materials. Detecting differences in the behavior of materials that are relatively resistant to SCC and exhibit a small

reduction in apparent tensile strength is facilitated by the generally smaller scatter in the data (Figure 70).

The capability of calculating a statistical threshold stress for specified test conditions is another aspect which makes breaking load test results more discriminating than pass-fail data. The concept and calculation procedure for this statistical threshold is described in Appendix B. From a quantitative standpoint, SCC flaw penetration can be calculated from breaking load data, and the advantages of this approach are discussed later in Sections V.A.4. and VI.

3. Optimum Length of Environmental Exposure for Breaking Load Tests

When an aggressive environment is used in an accelerated SCC test, it is important to establish optimum exposure periods that produce a measured SCC response without also causing gross pitting corrosion, which can confuse interpretation of the test. It was for this reason that the recommended period of exposure in ASTM Standard G47 (10) for 0.125 in. diameter tension specimens of 7075 alloy materials was set at 20 days rather than periods such as 30, 90, or 180 days formerly used by various investigators (35).

When SCC-susceptible specimens are exposed to 3.5% NaCl under alternate immersion conditions, corrosion fissures develop which, with continued exposure, will change shape, depth, and distribution under influence of the sustained exposure stress. There will be a "critical time interval" during which notch

sensitivity develops with increasing intensity, thereby causing specimens either to fail while exposed or to fracture in breaking load tests at apparent tensile strength values decreasing toward the exposure stress. This is indicated by times lying between t_A and t_B in the schematic diagram of Figure 10. In either case, fracture occurs through the specimen cross section where the notch effect (i.e., SCC damage) is greatest. If the exposure of surviving specimens is continued beyond the critical interval (i.e., beyond time, t_B in Figure 10), the average fracture stress is sometimes observed to increase toward that of specimens exposed with no applied stress (see for example, the test results of the 0.225 in. diameter 7075-T7X1 specimens after 12 days exposure at 30 and 40 ksi, Figure 34).

An examination of Figures 31-34 indicates that the critical time interval for short transverse 0.125 in. diameter specimens was about 2 to 6 days for 7075-T651 and from 3 to about 9 days for the T7X1 temper, depending upon the exposure stress. The same 3 to 9 day critical time applies to the 0.225 in. diameter specimens of 7075-T7X1. These intervals are in good agreement with the times to failure summarized in Table VI, although failures for the T7X1 temper specimens continued on to longer times. No critical interval was indicated for the highly resistant T7X2 temper specimens, and none would be expected. A single exposure period to determine the maximum SCC tendency by means of breaking load tests should be near the end of this critical time interval. Indications are, however, that this period will depend on the material and exposure environment.

Therefore, it would be advantageous to expose groups of replicate specimens for two or three time periods within the expected critical range and to determine the rate of decline in breaking load. Additionally, by converting the gross fracture stresses to effective flaw sizes, the SCC behavior could then be examined in terms of SCC growth during the critical time period.

Several tenable explanations are proposed for the higher breaking strengths observed in some tests made after exposure periods longer than the critical time interval. Certain of these involve a decrease in the notch stress concentrations and/or flaw-tip stress intensity factor caused by the blunting effects of additional corrosion or by crack-tip branching. The decrease in stress concentration or stress intensity depends upon the SCC flaw, during the "critical time interval", attaining sufficient depth to make the LEFM component (second term) of equation [8] important. In contrast, when a stress corrosion flaw is first initiated and is very shallow, the limit-load is the dominant failure criterion (i.e., the first term of equation [8] overrides), and the geometric shape and acuity of the flaw stress concentration are of negligible importance to breaking strength; all that matters is the area of unflawed cross section. Comparing dimensions of actual SCC flaws (Table X) against the fracture criteria shown in Figures 54 and 55, it is evident that SCC flaws do develop to depths sufficient for the LEFM component of equation [8] to be important.

Another tenable explanation for an apparent "recovery" of breaking strength after exceeding the critical exposure time interval is that strain hardening occurs at the localized concentrations of stress, thereby requiring added stress to induce failure. Alternatively, the strengthening effect may simply be the consequence of enhanced triaxial constraint, thus minimizing the propensity for gross necking within the test section during the breaking load test. Under this hypothesis, "recovery" would be most likely when SCC damage is very shallow and limit-load (first term of equation [8]) the overriding fracture criterion. If either of these hypotheses is correct, it can be visualized that notch acuity might have an influence even with very shallow flaws; and they may help to explain the slight but distinct increase in fracture stress of the SCC resistant T7X2 temper after very short exposures, as shown in Figure 31. Refer to the further discussion along this line in Section V.A.5.b.

Still another proposed explanation of the "recovery" in breaking strength is hydrogen-hardening. This is an effect reportedly observed with pure iron under certain conditions involving dislocation movement and strain hardening (72). However, there is currently little evidence to support this behavior in aluminum alloys.

Another factor to consider is that given the fixed-displacement-type stressing frame used in this investigation (see

Figure 13), the possibility exists for the specimen load, and hence gross section stress, to decrease as multiple fissures/ cracks form and grow with exposure time. The lower the exposure stress and the more flaw tolerant the material, the greater the potential for specimen load relaxation with continued exposure. This would not contribute to a higher breaking load directly, but would reduce the mechanical driving force, thereby tending to decelerate crack growth and enhance the opportunity for general corrosion to proceed. The effects of alloy strength and toughness on breaking load-SCC behavior will be discussed more fully in Section V.A.4.

Actual SCC flaws measured on the fracture surfaces of specimens tension tested after the critical time interval (e.g., 12 days for 0.225 in. diameter specimens of 7075-T7X1 stressed at 40 ksi) were shallower than those from specimens tested in the critical interval. These data, which do not support any of the above explanations, are very limited. Perhaps the apparent "recovery" of breaking strength with longer exposures is merely an indication that those particular specimens were "slow starters" and simply had not yet reached a critical length of exposure. Unfortunately, in planning the layout of test specimens for this investigation, there was no randomization of individual test specimens. Thus, all specimens in a set of five were taken from adjacent positions, and it might be speculated that this apparent effect of exposure time could be related to local variation in the

test material. Other unpublished investigations conducted at Alcoa Laboratories, however, suggest that the apparent "recovery" effect is real, although the reason has not been satisfactorily explained. Test data also showing this effect in advanced powder metallurgy aluminum alloys is presented in Section V.A.6.

Thus, the optimum length of environmental exposure for the breaking load method of evaluation depends upon the relative SCC tendencies in the test material and other factors such as the exposure stress, size of test specimen, etc. The maximum precision in breaking load test results will be obtained when the SCC flaw size is significant (i.e., reliably detectable by loss in specimen breaking strength) but short enough to avoid other confounding influences. A pilot series of tests would be advisable when undertaking study of unfamiliar materials. There appears to be no advantage in extending the exposure beyond an observed critical interval for a given test material and specimen size. It appears that optimum length of exposure will be substantially shorter than the recommended periods in ASTM G47, which are based on the pass-fail interpretation. Advantages in expressing comparative SCC behaviors in terms of the basic parameter of flaw (crack) size will be discussed in the following section.

4. Fracture Mechanics Interpretations

The fracture mechanics analysis of flawed tensile specimens (Section IV.D.) showed that the depth of subcritical cracks introduced either by fatigue or stress corrosion can be reasonably correlated with the specimen breaking strength. The significance of this observation is that penetration of crack-like damage within the material can be tracked in time by periodically making tension tests of replicate specimens after selected intervals of exposure and/or stress history. Thus, SCC damage can be quantified in terms of flaw depth, as was done to compare the SCC performances of three temper variants of alloy 7075 in Figure 65(a). The potential advantages of this new approach are discussed below by examining the influence of alloy strength and toughness and specimen size on the breaking strength.

a. Effects of Alloy Strength and Toughness

The depth and rate of stress-corrosion cracking within the specimen of interest is dependent primarily upon the details of the exposure test conditions (environment, time, stress); see for example, Figures 4,11 and 65. In contrast, the breaking strength of a flawed (cracked) specimen depends significantly on alloy toughness as well as the strength, the more important of the two being determined by the cross sectional area and the dimensions of flaw(s) present, as shown by equation [8]. For the purpose of quantifying resistance to SCC it would be desirable to express SCC damage in terms, such as subcritical flaw depth, that are independent of the mechanical properties of the material.

The effect of alloy strength and toughness on the 0.125 in. diameter tension specimen breaking (fracture) stress versus flaw-size relationship is now examined for some typical materials of interest. The example in Figure 71(a) compares the response of two materials (7075-T7X1 and 7475-T651) having different levels of toughness, but similar strength and SCC performances. The two alloy behaviors diverge with increasing flaw size; and the breaking strength differential, favoring the tougher alloy, is greater for deeper flaws, where the σ_{LEFM} term of equation [8] is dominant. In contrast, the example in Figure 71(b) illustrates a case where the two (7075-T651 and 2014-T651) alloys have comparable toughness and SCC resistance (53,67) but different strengths. In the latter example, the initially divergent breaking load test response of the two materials converge with increasing flaw depth; that is, the breaking strength differential is most pronounced at small flaw depths where the limit-load (σ_L) term of equation [8] is dominant. Thus, if the materials of Figures 71(a) and (b) were assumed to develop an equivalent rate of attack to depth a_1 , then the material strength-toughness properties alone, and not SCC resistance, would determine the gross fracture strength differential between materials.

To better appreciate the significance of these examples to SCC characterization, consider first that the portion of the σ - a curve having greatest practical interest is that which is bounded by σ_{UTS} as the upper limit and σ_{th} as the lower bound; and secondly, the specimen's breaking strength cannot be less than

its exposure stress.* With reference to Figure 71(a), consider, for example, that the estimated threshold stress for alloy 7075-T7X1 is about 31 ksi (see Table VII and Appendix B). At this level of exposure stress, however, the figure illustrates that the 7475-T7651 specimen could withstand a subcritical flaw about 1.4 times the depth of that which could be supported by the 7075-T7X1 specimen. Thus, if after SCC exposure, both alloys were to show identical breaking stress values approaching 31 ksi, then the extent of SCC in the tougher 7475-T7651 material would be substantially greater, and breaking strength alone could not discriminate this difference. However, as the terminal SCC flaw depth** detected by the breaking load becomes smaller (as would

* This assumption is entirely correct for the case of fixed (constant) loading; however, under fixed displacement loading conditions the actual gross section exposure stress may decrease with time below the initial value due to multiple crack formation and specimen load relaxation.

**The terminal SCC flaw depth is correlated to the breaking stress by equation [8]. If failure occurs during exposure, the terminal SCC flaw depth would correspond to the critical size flaw depth predicted to cause unstable fracture at the exposure stress. In the case of materials with high resistance to SCC, it is, of course, imperative to verify the nature of the flaw as SCC rather than pitting corrosion.

be the case for (1) failure under high exposure stress, (2) shorter exposure times, or (3) more SCC resistant tempers), then the bias introduced by toughness would become less a factor in rating SCC performance of materials by their breaking strength. On the other hand, when there is a strength differential between materials (as in Figure 71(b)), and if the terminal SCC flaw is very small, then improved breaking strength would merely be a reflection of higher material strength rather than superior SCC resistance. Here again, the use of breaking stress alone would be inadequate. Conversely, if in the above examples the measured breaking stresses were converted to flaw (crack) dimensions, then the strength and toughness differential between alloys could be normalized, and a more meaningful performance comparison based on accumulated SCC damage (maximum depth of attack) would result.

A most interesting situation exists when the alloys subject to examination possess reversed ordering of strength and toughness properties. The trade-off of toughness and strength is frequently encountered when comparing the relative merits of many structural aluminum alloys. The potential impact of this trade-off on the breaking load test response is illustrated by the examples in Figure 72. The figure shows breaking stress versus flaw size response curves calculated for two 7XXX powder metallurgy (P/M) alloys, 7090 and 7091, overaged to a commercial T7-type temper

condition*, and for comparison, the 7075-T7X1 and 7475-T7651 relationships from Figure 71(a). If breaking (gross fracture) stress is taken to be the descriptor of SCC resistance, then Figure 72 suggests that rankings would be ordered in favor of the high strength 7090 P/M alloy if the flaw depths were equal and small (a_1), while the tough alloys, namely 7091 or 7475, would be favored if the flaw depths were equal and large (a_2). Of course, the time to produce a flaw of given depth varies with the kinetics of SCC damage for each material, which would influence the performance ratings. However, if the rate of damage were assumed to be equal for all the materials considered, then the previous point can be made that performance rated on the basis of breaking strength alone can lead to different rankings at different flaw sizes. In contrast, damage measured in terms of flaw depth would be exact. As a point of reference, the statistical threshold stress determined in this investigation (Appendix B) for alloys 7075-T7X1 and 7075-T7X2 are 31 and 54 ksi, respectively.

* The P/M alloy mechanical properties listed in Figure 2 were developed from Alcoa plant fabricated extrusions evaluated in conjunction with a U. S. Air Force cooperation test program on aluminum P/M products, reference: D. J. Brownhill, R. J. Bucci, S. F. Collis, R. E. Davis, J. C. Kuli, R. C. Malcolm, and G. Sowinski. "Mechanical Property, Corrosion and Exfoliation Data on P/M Alloys 7090-T7E71 and 7091-T7E69 Extrusions", Alcoa Laboratories Report No. 56-3978, 1983 June 21.

The response curves shown in Figure 72 reveal "crossovers" at breaking (fracture) stress values above these 7075 thresholds, thereby indicating that, in addition to breaking strength, its rate of change with time (i.e., the slope of the breaking stress versus time curve (e.g., Figure 31) must be considered in order to develop meaningful comparisons of SCC performances among materials possessing different strength-toughness property combinations. The rate of breaking strength decrease with exposure time can then be correlated to SCC crack growth rates by using equation [8].

In conclusion, flaw depth in concert with alloy strength and toughness properties has major impact on the specimen breaking stress. Alloy strength and toughness, however, may have little or no bearing on the size of the SCC flaw present in the material. The use of fracture mechanics to supplement interpretation of the breaking load test accommodates a more direct assessment of SCC damage in terms of an "effective" flaw depth which correlates well with actual behavior (refer to Section IV.D.3.). Under this approach, breaking load data established from multiple specimens, tension tested after various exposure times, can be translated to give statistical flaw size distributions and their variation with time as an improved quantitative measure of SCC performance. The effective flaw size concept to compare materials eliminates possible confounding influences of strength and toughness that may be present when performances are rated with only a stress

parameter (e.g., threshold stress or breaking strength) or by pass-fail criteria. Consequently, a more representative quantitative comparison of SCC performances among materials is facilitated. More discussion of the potential engineering significance of the effective flaw size approach as it relates to SCC characterization is given in Section VI.

b. Effect of Specimen Size

Though in this study the influence of specimen diameter (0.125 vs. 0.225 in.) on SCC rankings appears to be small, it is well known from fracture mechanics principles that specimen geometry has influence on subcritical crack propagation rates and on the critical combination of stress and flaw size that causes terminal fracture. Thus in theory, specimen size, like alloy strength and toughness, can influence the estimated degree of SCC damage (i.e., subcritical flaw size) given by the breaking load test. Evidence of this influence is given in Figure 73, which compares calculated relationships of fracture stress and flaw size for the 0.125 in. and 0.225 in. diameter tensile bars of alloy 7075-T7X1. The predicted trends described in the figure are in good agreement with results of the breaking load-SCC tests reported in Section IV.D.3. and shown in Figure 61.

The gross fracture stress from the EPFM wide-range model depends strongly on the dimensionless ratio of flaw size to specimen diameter (a/D), especially at deep flaw depths where the LEFM term of equation [8] dominates. In this regime and at a

given absolute flaw depth, the breaking strengths are distinctly dependent on specimen diameter. It is illustrated in Figure 73 that when the 0.125 in. and 0.225 in. diameter specimens of the same material are tested to the same breaking strength (σ_1), the effective flaw size is greater in the larger specimen. Conversely, for the same absolute level of penetration (a_1) in Figure 73--a more likely case for SCC--the breaking strength will be greater in the specimen with the larger diameter. This trend can be observed in Figure 34, particularly so at the 40 ksi exposure stress.

The relationships in Figure 73 show that early indications of SCC damage can more sensitively be determined by using the smaller diameter specimen as it gives a greater reduction in breaking strength than the larger specimen for the same SCC flaw depth. It can also be seen from Figure 73 that as the terminal subcritical flaw depth becomes vanishingly small, the influence of specimen size on breaking stress is negligible. However, breaking stress becomes increasingly specimen size dependent if test conditions are arranged such that the terminal flaw size approaches its maximum limit (as controlled, for example, by the SCC threshold stress). To normalize the specimen size influence, it is useful to invoke fracture mechanics (i.e., equation [8]) to translate the breaking load-SCC characterization to flaw size variation with exposure time. Figure 65(b) shows that when SCC performance of the 0.125 in. and the 0.225 in. diameter 7075-T7X1 tensile bars are characterized in this manner, the results are virtually identical. Moreover, the flaw size versus exposure time

representation correlates well with actual SCC measurements as noted in Section IV.D.3.

5. Mechanistic Implications

Although the present investigation was not planned for studying SCC mechanisms, some mechanistic implications are evident in the test results. The greater precision of the breaking load method for assessing SCC susceptibility opens new possibilities for studying such mechanisms.

a. Magnitude of Exposure Stress

Higher levels of exposure stress applied to short transverse specimens of the SCC-susceptible materials (7075-T651 and T7X1) increased SCC damage, as expected, depending upon the magnitude of the nominal stress relative to the threshold stress, σ_{th} , and the length of exposure. Illustrations of the effects of exposure stress level are shown by the gross fracture stresses and the 99% survival stresses in Figures 31-35, measured SCC flaws on the fracture surfaces in Figures 48-50, and the calculated effective flaw depths based on the gross fracture stresses and the wide-range EPFM relationship from equation [8] in Figures 64-66. The following observations were made from these illustrations in relation to the statistical σ_{th} values contained in Table VII.

- When the exposure stress was slightly below σ_{th} (as in the tests of 7075-T7X1 at 30 ksi), there was a progressive mild acceleration of SCC damage.

- When exposure stress was considerably below σ_{th} (as in tests of 7075-T7X1 at 20 ksi, short transverse tests of 7075-T651 at 10 ksi and long transverse tests of 7075-T651 at 30 and 40 ksi), there was an early mild increase in corrosion damage but no acceleration of damage with continued exposure during the "critical time interval" indicated by tests at exposure stress greater than σ_{th} . The statistical significance of these observations was verified by analyses of variance of the fracture stresses and a regression comparison of the negative slopes of the fracture stress plots in Figures 31 and 35.
- When exposure stress was considerably below σ_{th} and the 99% survival stress approached the material tensile strength (as in the tests of 7075-T7X2), there was no increased corrosion damage caused by the highest stress used (40 ksi, 68% of σ_{YS}). In fact, there was a statistically significant increase in breaking strength that was directly proportional to the magnitude of the exposure stress; refer to Figures 31 and 32. Although it is not clear what causes the apparent strengthening effect, it can be concluded that, for all practical purposes, this sample of 7075-T7X2 is immune to SCC (e.g., nominal gross section stresses as high as the 0.2% offset yield strength are rarely encountered in structural components). The virtual immunity to SCC of this material was shown also by the SCC tests with fracture mechanics

specimens (Section IV.B.3.). Further discussion of the apparent strengthening effect is presented in Section V.A.5.b.

The evidence of SCC damage noted in the first two examples above are no doubt related to the observations of non-propagating SCC cracks reported by Wearmouth, et al (73). The analagous development of non-propagating cracks in originally unflawed material has been studied more extensively in the area of fatigue (74-76). For example, examinations on aluminum alloys conducted at high magnification by Hunter and Fricke (75, 76) clearly revealed formation of crack-like flaws at cyclic stresses well below the fatigue endurance limit (analagous to the SCC threshold) which did not grow to larger sizes. Their observations indicated microstructural features and crack branching to be significant factors in causing arrest of cracks which had been previously observed to grow ten fold in size.

b. Comparison of Trends in Apparent 0.2% Yield Strength vs.
Tensile Strength (Gross Fracture Stress)

Apparent 0.2% offset yield strength values were determined from load versus deflection data taken during the post exposure tensile tests of breaking load specimens and are reported along with apparent tensile strengths in Appendix C. Decreases in apparent yield strength generally paralleled those of the gross fracture stress after exposure periods greater than 2 to 4 days.

The above trend, however, was not consistently observed in specimens exposed for shorter periods, and this observation probably reflects the nature of the operative SCC mechanism of nucleation and early growth of damage in the 7075 alloy materials.

The 0.2% offset yield strength is determined by a specified amount of deviation from linearity of the stress-strain curve. In smooth undamaged specimens, the 0.2% offset yield strength is associated with the onset of homogeneous irrecoverable plastic strains. However, in corroded and stress-corrosion-cracked specimens, deviation from linearity in the stress-strain curve can be attributed to localized plastic strains and variable elastic compliance due to localized plasticity and/or crack growth, two different phenomena that cannot be easily distinguished from each other in the standard tensile test. Therefore, comparison of apparent 0.2% offset yield strength in SCC specimens may not be on the same basis and, therefore, may not be valid.

While the utility of determining offset yield strengths in specimens containing crack-like damage is questionable, several observations are noted below, followed by speculative explanations.

(a) The gross fracture stress of the more SCC susceptible short transverse, 0.125 in. diameter specimens of 7075-T651 and T7X1 appeared to remain unchanged during the beginning of the exposure (particularly for the low levels of applied stress) and

then decreased more or less rapidly, as shown in Figure 74. In most cases, however, the apparent yield strength distinctly increased before it started to decrease. With very susceptible specimens, such as those of 7075-T651 stressed at 30 ksi, the tendency for increasing yield strength was not detected, apparently due to the more rapid rate of attack under these conditions. With more advanced SCC, fracture occurred before the 0.2% offset load was reached, and a yield strength could not be determined.

(b) With the highly SCC-resistant long transverse 0.225 in. specimens of 7075-T651, there was no significant increase in strength at the beginning of the exposure, nor was there any accelerating effect of the exposure stress on the loss in strength after the four-day exposure period, as shown in Figure 75(b). The statistical significance of these observations was verified by analysis of variance. This contrasting effect of grain orientation is probably due to a reduced local concentration of tensile stress because the directional corrosion fissures in the long transverse specimen are parallel to, rather than perpendicular to, the specimen loading axis. That is, the SCC fissures tend to occur in a fixed direction regardless of specimen orientation. The absence of an increase in yield strength at the beginning of the exposure may be attributed in part to the large diameter of the long transverse specimens, as this effect was also absent in most of the 0.225 in. short transverse specimens of 7075-T7X1 (Table 11 of Appendix C).

(c) The behavior of the highly SCC-resistant 7075-T7X2 short transverse 0.125 in. specimens was different still. Statistically significant increases of both the apparent yield and tensile strengths directly proportional to the exposure stresses were observed after the two-day exposure, and these were generally followed by more gradual strength reductions as noted in Figure 75(a). The exposure period over which the strength of the T7X2 specimens is apparently enhanced by static stress extended for at least nine days, which is significant because it includes the critical exposure interval where appreciable degradation in load carrying ability was observed in comparably tested T7X1 and T651 temper specimens.

The anticipated effects of progressive corrosion and SCC on the load-deflection curves of breaking load test specimens are shown schematically in Figure 76. In each example, the load-deflection curve for an unexposed specimen is included for comparison with the corrosion specimen, and the notes on each sketch describe the probable behavior.*

Several alternative explanations have been offered for the apparent strengthening effects observed during the initial exposure of these materials, including the following:

* In the present investigation, the tension test procedure was not tuned to detect small differences in elastic stiffness and total area under the load-deflection curve.

(1) restricted deformation attributed to increasing triaxial stress state at the tips of multiple stress concentrations (directional pits and intergranular fissures--see Figure 45), (2) loss of specimen stiffness (slope of the load vs. deflection curve) associated with advancing corrosion, (3) localized strain hardening at these sites, and (4) hydrogen hardening. Additional studies are needed to determine which of these (or other) mechanisms, acting singly or in combination, is responsible.

Despite varying behaviors of the three different materials in the present investigation, shown by the changing "apparent" tensile properties during the first two to four days of environmental exposure, each seems to conform to the theorized build-up of localized stress concentrations at pits and fissures, particularly in specimens of the short transverse orientation. In SCC-susceptible specimens, these stress concentrations promote crack-like defects which reduce breaking strength. The breaking load test, thus, provides a promising new tool for the study of SCC mechanisms, and it appears that much insight would be gained from more detailed examination of specimen load versus deflection behaviors in selected critical experiments.

6. Breaking Load Test Data on P/M Products

One of Alcoa's major R&D thrusts of this decade is the development of aluminum alloys by combining powder metallurgy (P/M) technology with special processing techniques. The wrought P/M process produces attractive combinations of properties and microstructure not attainable with conventional cast ingot metallurgy (I/M) practices. At the forefront of Alcoa's P/M effort are alloys 7090 and 7091 designed for use in high strength structures. The chemical composition limits of these alloys are as follows:

Weight Percent														
Alloy	Si	Fe	Cu	Mn	Mg	Cr	Zn	Co	O	Ti	Zr	Others		Aluminum
												Each	Total	
7090	0.12*	0.15*	0.6- 1.3	--	2.0- 3.0	--	7.3- 8.7	1.0- 1.9	0.2- 0.5	--	--	0.05	0.15	Remainder
7091	0.12*	0.15*	1.1- 1.8	--	2.0- 3.0	--	5.8- 7.1	0.2- 0.6	0.2- 0.5	--	--	0.05	0.15	Remainder

* Maximum allowable

An engineering property data base is currently being generated on P/M materials. As part of this effort, the SCC resistance of alloys 7090 and 7091 is being examined using the same breaking load test procedures as in the current program. Two extruded bars, one each of 7090 and 7091, aged to the peak strength (T6E192) were chosen as starting materials for the SCC characterization. The bars had a 1.5 in. x 4.5 in. rectangular cross section and were fabricated at Alcoa's Extrusion Works (Lafayette, IN) from 145 lb. billets produced at the Alcoa Technical Center.

Each bar was subdivided into pieces which were given additional aging to improve SCC resistance. Four pieces of 7090 and five pieces of 7091 were treated as follows:

<u>Alloy</u>	<u>Experimental Temper Designation</u>	<u>Additional Aging Time At Temperature</u>
7090	T6E192	None
7090	T7X1 (T7E71)	1 Hour
7090	T7X4	4 Hours
7090	T7X6	6 Hours
7091	T6E192	None
7091	T7X2	2 Hours
7091	T7X4 (T7E69)	4 Hours
7091	T7X14	14 Hours
7091	T7X20	20 Hours

The improved resistance to SCC in P/M alloys after extended second step aging treatments is similar to that of the ingot metallurgy (I/M) alloy 7075, and this trend is readily observed from the 99% survival stress values for P/M alloy 7091 in Figure 77 and comparison of these data to corresponding 7075 results in Figure 32. Data comparing 99% survival stress as a function of exposure stress for P/M alloys 7090 and 7091 are shown in Figure 78. It is evident that good SCC resistance is obtained for both alloys in the overaged tempers, even at the relatively high exposure stress of 50 ksi (approximately equal to 70-75% of the actual short transverse yield strength).

Comparative assessments of P/M alloys vs. I/M alloy 7075 SCC performance are shown in Figure 79. Two ranking criteria are shown: one based on mean breaking stress and the other based on the corresponding effective flaw sizes. The effective flaw sizes in Figure 79(b) were calculated using the relationships shown in Figure 72 for P/M alloys 7090-T7E71 and 7091-T7E69 and those shown in Figures 60 and 61 for the three temper variants of alloy 7075. When respective mean-breaking strengths are compared, the results of Figure 79(a) indicate that the P/M alloys outperform all three 7075 tempers. In contrast, when the same breaking load results are compared on the basis of effective flaw depth, Figure 79(b) shows that the amount of SCC damage (as quantified by effective flaw depth) of the P/M alloys lie between those of the T651 and T7X2 tempers of alloy 7075, with 7091-T7E69 being identical to 7075-T7X1.

An explanation of this difference in alloy rating is that the high breaking stresses observed for the P/M alloys are, in part, a reflection of their superior tensile strengths. It is shown in Figure 72 that at shallow flaw depths the breaking stress of the P/M alloys, by virtue of their higher strength, should always be greater than that of alloy 7075-T7X1 for the same flaw depth. On the other hand, the discussion of Section V.4.a. disclosed that the influences of alloy strength and toughness on SCC performance ratings given by breaking load results can be systematically taken into account (normalized) when the effective flaw interpretation

is used. For these reasons, it is believed that the SCC ratings given by the effective flaw size comparison of Figure 79(b) are closer to reality with respect to characterizing SCC depth and rate of attack than the corresponding ratings of Figure 79(a) given by comparison of only mean breaking strengths. It is, however, essential in the case of SCC-resistant materials to identify the type of flaws producing the reduction in breaking strength. Fractographic examination may be necessary to distinguish between actual SCC and corrosion pits or other types of flaws that could be present in the metal. In the present case, it is instructive to compare the performances of selective material conditions using specimens exposed both with and without applied stress as follows:

Exposure Stress(ksi)	Mean Breaking Stress* (ksi)			Estimated Mean Flaw Depth* (in.)		
	7075- T7X1	7090- T7E71	7091- T7E69	7075- T7X1	7090- T7E71	7091- T7E69
0	68.6	85.7	76.3	0.007	<<0.0005	0.015
30	63.6	80.5	76.3	0.017	0.008	0.015
40	52.2	78.3	75.2	0.026	0.010	0.017
50	--	78.0	75.1	--	0.011	0.018

* From 5 replicate 0.125 in. diameter, short transverse tensile specimens after 4 days exposure to 3.5% NaCl alternate immersion.

It can be seen, that within the critical exposure period of 4 days, neither the mean breaking stress nor the mean effective flaw depths of the 7091-T7E69 alloy were appreciably affected by the level of exposure stress, indicating no appreciable SCC damage.

In the cases of 7075-T7X1 and 7090-T7E71, however, increasing the level of exposure stress resulted in moderate but distinct reduction of specimen mean breaking strength and increase in flaw depth. Fractographic examination of the broken 7075-T7X1 specimens verified that SCC was present. The broken P/M specimens were not examined fractographically and further work in this area is needed.

Although it is evident from Figure 79(b) that P/M 7091-T7E69 and I/M 7075-T7X1 have a similar rate of flaw growth, Figure 72 shows that the tougher and stronger 7091-T7E69 will have the advantage that it can endure considerably more subcritical crack growth before fracture than the 7075-T7X1 alloy. This direct comparison of the P/M 7091 and I/M 7075-T7X1 alloys serves as a clear example in illustrating three important points as follows:

(1) SCC breaking stress used alone is inadequate.

(2) SCC kinetics or damage rate is important but may also be somewhat inadequate without verification of the primary corrosion mechanism (i.e., pitting vs. SCC fissures).

(3) Estimating the true potential for SCC damage tolerance of a material in a given specimen configuration or structural component requires that the damage rate or crack velocity be related to a geometry specific crack driving force.

B. Comparison of SCC Test Methods

Three tempers of the same lot of 7075 alloy plate (i.e., same composition and macrostructure) were used in this investigation in order to compare the abilities of several testing methods to distinguish between different degrees of SCC resistance. A summary of the different measures of susceptibility under the short transverse stress orientation being considered is presented in Table XII.

All of the methods distinguished the relatively high SCC susceptibility of the T651 temper and the very low susceptibility (virtual immunity) of the T7X2 temper under the environmental conditions used. The performances of most interest, however, are those involving comparison of the intermediate T7X1 temper with the two extremes. Some of the more meaningful comparisons involving a 30 ksi exposure condition have been taken from Table XII and listed below for convenience in this discussion.

Ranking Criteria	Measure of SCC		
	T651	T7X1	T7X2
• From Traditional Pass-Fail Analysis:			
95% Confidence Interval on			
Probability of Survival, % (a)	0-31	74-100	74-100
Approximate Threshold Stress, ksi (b)	$20 > \sigma_{th} > 10$	$40 > \sigma_{th} > 20$	$\sigma_{th} > 40$
• From Analysis of Breaking Load Data: (a)			
Probability of Survival, %	0	100	100
99% Probability Survival Stress, ksi	0	53	69
Statistical Threshold Stress, ksi	17	31	54
Mean Depth of SCC, in.	> 0.052	0.018	0.001
99% Penetration Limit, in.	∞	0.028	0.006
SCC Growth Rate, $\times 10^{-5}$ in./hr.	54(c)	6.9(c)	3.3(d)
• From Fracture Mechanics Specimen Data:			
DCB, Plateau Velocity $\times 10^{-5}$ in./hr.	45	11	1.5
WOL, K_{th} , ksi/in. (best estimate)	5	13	19

-
- (a) Exposure to 3.5% NaCl alternate immersion, 6 days at 30 ksi.
 (b) Exposure to 3.5% NaCl alternate immersion, 20 days per ASTM G47.
 (c) Over 2 to 6 days at 30 ksi.
 (d) Over 2 to 9 days at 30 ksi.

The breaking load method of measuring SCC damage not only permits a determination of probability of survival similar to that obtainable from the traditional pass-fail analysis, but it also provides other more useful and more discriminating ways to compare materials, as described in Section V.A.2. A definitive comparison of the T7X1 and T7X2 tempers is shown with the 99% survival stress. For example, at the selected exposure stress of 30 ksi, the 99% survival stresses for the T7X1 and T7X2 tempers are 53 and 69 ksi, respectively. This is consistent with the rating given at the higher level of 40 ksi, 57 and 64 ksi, respectively, Table XII.

A statistically defined threshold stress for the test conditions used can be determined from analytical treatment of the breaking load data (ref. Appendix B). Rating the alloys by their statistical thresholds puts the T7X1 temper about midway between the most (T651) and least (T7X2) susceptible tempers.

With use of the wide range EPFM relationship (Equation [8]), the mean breaking load data can be converted into mean effective SCC flaw depths, which are not only discriminating, but have better potential for relating the test data to service requirements of a part through the application of probabilistic fracture mechanics. Moreover, SCC growth rates calculated from breaking load test results agree reasonably well with the plateau or average growth rate determined with the fracture mechanics DCB specimen. These growth rates rank the T7X1 temper closer to the

T7X2 temper than to the T651 condition. The K_{th} thresholds for SCC growth also rank the T7X1 temper closer to T7X2.

While failure probability and stress threshold numbers (σ_{th}) are useful for rating materials, they are strictly qualitative assessments because they depend upon too many test conditions (e.g., exposure stress, specimen size/configuration and loading arrangement) to be reliable for selecting materials for design, except in a very conservative way. For example, threshold values from the small-sized 0.125 in. diameter tension specimens are very dependent on the initiation component of SCC. Such conservative data is unrealistic in an engineering sense for selecting materials to be used in thick components, where the rate of SCC growth is more likely to control the usable component lifetime. The potential for initiation is of greater concern in thin parts, while the rate of SCC growth probably gives a more realistic selection criterion for thick parts. However, both the SCC initiation and SCC growth phenomena are quite important, and the ability to distinguish between the two is often not at all clear. Thus, in the development of new alloys, it is desirable to obtain information about both the depth and rate of SCC growth in materials as well as to compare them on the basis of small specimen threshold stresses and failure probabilities.

A long-standing controversy has existed over whether it is more appropriate to express stress corrosion thresholds in absolute terms or in terms of ratios of threshold values normalized with

respect to strength or fracture toughness.* Normalizing may give reversed SCC ranking when the materials differ substantially in their mechanical properties. Such reversal was not observed for the three tempers of 7075 alloy used in this investigation (see Table XII). However, such reversals did occur in comparisons of I/M and P/M alloys (Section V.A.6). As to which is the more appropriate way to express thresholds, it depends upon the source and the magnitude of the service stresses anticipated in the component for which a choice of alloy is to be made. When it is expected that the component may experience high sustained tensile stress approaching the yield strength (as may well be the case in poorly fitted assemblies or welded structures with high residual stress), then it is advisable to compare alloys on the basis of ratings normalized by the yield strength. If, on the other hand, the anticipated service stresses are low-level elastic in nature (well below the proportional limits of the materials under consideration), then absolute numbers are likely to be appropriate.

* There is often no clear reason why a single choice needs to be made, as both measures of SCC performance are useful or can relate to different quantities. For example, σ_{th} or K_{th} relates to load carrying ability, while $(K_{th}/\sigma_{YS})^2$ relates to a critical flaw size or damage tolerance capability.

The preceding dilemma of characterizing materials' SCC performance in terms of a qualitative ranking is largely removed when the breaking load approach is used, and assessment is made in terms of effective flaw depths and SCC rates. Rating SCC performances in these terms also has the added advantage of being independent of biases caused by varying combinations of alloy toughness and strength. These biases exist when smooth specimen SCC performances are expressed as failure probabilities or in terms of the threshold or fracture stress (breaking strength or 99% survival stress). The breaking load test, therefore, provides a highly versatile and meaningful approach to characterizing performance of aluminum alloys with improved SCC resistance, particularly so when the data are translated into effective flaw depths and growth rates.

VI. COMPATABILITY OF THE BREAKING LOAD TEST APPROACH
WITH MATERIAL EVALUATION FOR STRUCTURAL DURABILITY

A major use of fracture mechanics is in the design and verification of a safe structural life by assuming the pre-existence of crack-like flaws. Damage-tolerant design requirements stipulate that pre-existing cracks of specified length and shape shall not propagate to critical dimensions within a specified lifetime, and are now commonplace in the aircraft industry, U. S. Air Force MIL-A-83444 (19) being a notable example. To minimize the number of problems in advanced metallic airframe structures, the U. S. Air Force currently imposes requirements to ensure that the structure is "durable" in addition to being "damage-tolerant" (77-79). Whereas the purpose of damage tolerance is to safeguard against catastrophic fracture of cracked structure, the structural durability requirement aims to inhibit initiation and/or growth of subcritical cracks (of any type, e.g., SCC or fatigue) to sizes which result in unacceptable life-cycle costs (of the part, component, airframe or entire fleet) due to excessive maintenance or loss in operational readiness/capability (80, 81).

For damage tolerance purposes, an assumed initial flaw size is set at a level exceeding the lower limit of reliable non-destructive inspection (typically on the order of 0.05 in.), and represents a "worst-case" initial crack size which, if undetected in service, could grow to a critical length and cause rapid fracture. However, relatively few locations in a structure

are designed for a full service life under the presumption of crack-like flaws at the initial damage tolerant size. Durability-based design requirements are concerned with narrowing the probability of relatively small (0.0005-0.05 in.) initial flaws (of whatever origin) growing in sufficient numbers to sizes exceeding the economic repair limit.* Durability size flaws are typically smaller than the lower limits of reliable non-destructive examination. Yet, this level of cracking is of primary importance because it represents a prelude to major cracking problems, and must be accounted for to confidently assure that airframe design will satisfy durability certification tests (79) with only minor adjustments to the final design. Moreover, the usable in-service lifetime for the majority of metal in the structural airframe is most often governed by the time required to initiate and grow small cracks to the durability (economic) size limit (80-86).

Recent applications of probabilistic fracture mechanics principles to model the growth of small cracks has led to improvements in manufacturing quality for extending economic

* The economic flaw size repair limit for a fastener hole, for example, is governed by largest radial crack size that can be removed by reaming to the next fastener size. Thus, by repairing in time to avoid major damage, "quality" of the structural detail after repair can be considered restored to its prior service condition.

lifetimes of mechanically fastened aircraft systems (82-84). The potential for more meaningful evaluations of design trade-offs and user options relative to reducing life-cycle costs of airframe and engine components via statistical interpretation of small-crack behavior has likewise been demonstrated and verified on full-scale test articles (81, 85, 86). The analytical premise in these studies is that that crack size is an indicator of structural quality, and that small crack data measured in replicate laboratory tests can be converted to predictions of time-varying flaw-size distributions at structural details (e.g., holes, cutouts, fillets, fitups, etc.) of the actual part, component, airframe, or entire fleet. Given statistical small crack data of this type, Figure 80(a), it is conceptually possible to perform crack growth analysis via conventional fracture mechanics procedures and arrive at the probability for cracks extending beyond a given size, Figure 80(b), or alternatively compute the distribution of times for a known distribution of flaws at time, t_1 , to attain a prescribed length in service, Figure 80(c). The critical flaw, a_{cr} , in Figure 80(c), for example, might correspond to the economic flaw size limit. Conversely, another useful rating of initial (or early life) product "quality" is the distribution of hypothetical flaw sizes estimated by extrapolating growth of larger detectable flaws "back in time". Evaluation procedures for obtaining each of the above statistical characterizations of short crack behavior are described in detail elsewhere (80-85). In all cases, however, reliable life assessments using

the above procedures require short crack test data (as in Figure 80(a)) as the basic material input. This is exactly the type of information that can be provided via fracture mechanics interpretations of breaking load test results. See, for example, Figures 64, 65, 66 in Section IV.

It was demonstrated in Section IV that when fracture mechanics is used to interpret the data, the breaking load test can be quite effective for detecting and quantifying dimensions of small crack-like damage introduced into a material as a result of the prior specimen load/environment history. Moreover, the breaking load test is (a) simple, (b) seeks the "weakest link" or largest crack, and (c) readily lends itself to statistical treatment of results since copious amounts of data can be generated at relative low cost. In concept, hypothetical flaw size distributions and their variance with test time (Figure 80(a)) can be estimated from breaking load data. The statistical flaw size data can then be expanded to predict probabilities of crack size exceedence (Figure 80(b)) or distributions of time to attain a specific "critical" crack length (Figure 80(c)). Thus, results generated from the breaking load test can be entirely compatible with requirements for probabilistic fracture mechanics analysis of small crack growth. As such, the breaking load test represents a potentially useful laboratory tool for establishing meaningful assessments of structural material performance when design (alloy selection) objectives are based on optimization of life-cycle economics.

With attention to life-cycle economics being a growing trend, the emergence of fracture mechanics based durability design guidelines, coupled with increasing availability of short crack data, will undoubtedly stimulate re-examination of alloy selection criteria for fracture control. This raises an interesting question--does alloy selection for good crack growth resistance at inspectable crack sizes (i.e., damage tolerance) exact too great a penalty (either economic or excessive weight) when performance is projected over the serviceable lifetime of an entire aircraft fleet? Let us suppose that damage tolerance (safety) can be assured by design, inspection, and minimum fracture toughness guarantees. If so, it is likely that life cycle economics can then be optimized by selecting alloys which are relatively free of "microdefects" upon introduction into service and, additionally, offer good resistance to early stage crack growth. Moreover, the material selection process must recognize microstructure-dependent trade-offs in propagation resistances of large versus small cracks. For example, it has been shown within a number of alloy systems that grain size refinement generally increases resistance to fatigue crack initiation and early stage growth while decreasing the propagation resistance of established (long) cracks in conventional fracture mechanics test specimens (23, 87, 88). Provisionally, the small crack data established from the breaking load test is compatible with life-cycle cost estimation procedures given in references 80 and 81. The life-cycle costs can then be traded, in quantitative terms, against damage-tolerant considerations addressed by data obtained from traditional fracture mechanics (long-crack) specimens.

To summarize, it appears reasonable to expect that, in the future, material selection needs will attach much greater importance to satisfying fracture-mechanics-based durability design criteria based on small crack behavior. Such an approach would attempt to optimize material performance in durability terms, while still satisfying the corresponding structural damage tolerance requirements. Though this may imply major revision to current alloy selection strategies, factors supporting the above projection are:

- Increasing awareness of economic penalties associated with excessive maintenance and downtime due to numerous in-service encounters with "nuisance size" flaws (89-91).
- Sensitivity of a specific material to alloy microstructure should be greatest when the crack sizes of interest are comparable to microstructural-feature dimensions and smaller. Therefore, life extension via optimum alloy selection should be more attainable when design objectives emphasize resistance to initiation and early stage growth of many small cracks (durability) rather than resistance to rapid growth of a single large crack (damage tolerance).
- A much greater volume of structural airframe material is controlled by durability performance objectives rather than damage-tolerant performance objectives.

- Recent advances in probabilistic fracture mechanics, coupled with promising new inexpensive testing approaches (e.g., References 80-84) for characterizing short crack behavior, now allows quantitative evaluation of material crack growth potential in statistical terms (e.g., crack exceedance probabilities) amenable to design optimization and cost-benefit studies.

Based on the findings of this investigation, the breaking load test approach, coupled with fracture mechanics interpretation, provides an attractive and cost effective alternative for determining the resistance to formation and growth of small cracks in originally unflawed material. This should, of course, significantly aid the designer confronted with the problem of material selection. In particular, the breaking load approach appears to be a powerful new tool for evaluating materials that must comply with durability-based performance objectives.

VII. SUMMARY AND CONCLUSIONS

An extensive review of state-of-the-art SCC test procedures identified the need for improved accelerated SCC characterization methods which more quantitatively measure degree of susceptibility in terms amenable to statistics and fracture mechanics interpretations. A noted shortcoming of existing methods is the relative inability to discriminate levels of SCC performance among the more resistant materials without requiring a prohibitive number of replicate tests. It was concluded that a new method for analysing SCC data from statically loaded, small diameter smooth tension specimens showed considerable promise for removing the recognized deficiencies. The second phase of this contracted effort was undertaken to advance this new approach and to verify the claimed advantages over current state-of-the-art SCC characterization procedures.

The breaking load method utilizes data from tension tests performed on replicate groups of smooth specimens after various lengths of exposure to static stress and corrosive environment. The breaking loads from the tension test are converted to "apparent" tensile strength values which can then be compared against tensile properties of the original material (no exposure). Analyzed in its simplest form, the breaking load test senses SCC damage as a loss in specimen load carrying ability. In general, the larger the strength decrease, the greater the degree of SCC damage in the specimen. By comparing results of various specimens, simultaneously exposed with and without applied static

stress, it is possible to separate the SCC response from that attributed to general or localized corrosion, thus avoiding potential misunderstanding in the test interpretation. Guidelines developed to maximize sensitivity for discriminating levels of SCC performance under the breaking load approach are given. It is shown, for example, that "minute" amounts of crack-like damage can be detected readily when the specimen cross section is small, and that there is an optimum interval of exposure where accurate test interpretation can be assured.

Analysis of breaking load data by extreme-value statistics enables calculation of survival probabilities and a statistically-defined threshold stress applicable to the particular sample of material and test conditions of interest. The SCC performance ratings provided under this smooth specimen testing approach are more discriminating than those obtained from traditional time-to-failure data. Moreover, the breaking load characterization requires substantially fewer specimens and shorter exposure times than conventional procedures for the same level of confidence.

A new elastic-plastic fracture mechanics model is given for quantifying damage in the stress corroded tension specimens by an "effective flaw size" calculated directly from measured breaking stress values and the material strength and fracture toughness properties. The effective flaw, in this case, corresponds to the weakest link in the specimen at the time of failure, and the

dimension most descriptive of the calculated flaw size is the maximum depth of SCC penetration from the specimen surface. Predicted combinations of breaking strengths and flaw depths are shown to agree very well with actual measurements made on 0.125 in. and 0.225 in. diameter tensile specimens after "small" flaws were introduced either by fatigue or SCC. These comparisons were made on six variations of high strength 7X75 plate alloys covering a range of strength and toughness combinations typically required of aluminum aerospace materials. A significant outcome of the above observations is that SCC characterization can be extended to shallow and more natural flaws, while preserving many of the advantages of traditional fracture mechanics theory applied to specimens containing deep cracks. For example, the statistical progression of crack-like damage within a material can be followed with time by removing samples for tension tests after selected intervals of exposure. Thus, materials can be compared on the basis of either their probabilities of initiating and propagating stress corrosion flaws to an arbitrary depth in a given exposure period or by their respective rates of SCC propagation, both being meaningful engineering parameters. A second advantage to using flaw depth, or rate of growth, as parameters to rate SCC performance is that the potential biases of alloy strength and toughness and of specimen size are removed. In contrast, breaking strength or lifetime under exposure is dependent on the above mechanical factors.

This investigation includes results on: (a) extensive SCC characterizations on three temper variants of 7075 alloy plate by the breaking load method and by conventional test procedures using statically loaded smooth tension specimens and fracture mechanics (DCB, WOL) crack growth specimens; and (b) somewhat more limited breaking load-SCC test results on advanced high strength powder metallurgy (P/M) alloys. Based on the findings previously outlined, significant advantages promised by the breaking load method can be stated as follows:

- Provides a numerical measure of SCC damage that is amenable to quantitative analysis by statistical and fracture mechanics procedures.
- Significantly more discriminating capability than pass-fail tests for rating performance of materials with improved SCC resistance, without requiring a prohibitive number of replicate tests.
- Capable of determining specimen survival probabilities without depending on actual failures during exposure, and the calculation of a statistical threshold stress for specified test conditions.
- The specimen breaking strength can be converted to an effective flaw size through an elastic-plastic fracture mechanics model, which takes into account the strength and fracture toughness properties of the alloy under test. The effective flaw provides an estimate of the maximum depth of SCC penetration developed by the exposure.

- A single test procedure is made available for characterizing SCC in the following quantitative terms: probability of initiation and growth of SCC to an arbitrary flaw depth, and a SCC growth rate that is correlatable to the plateau or average crack velocity measured in traditional precracked specimen (DCB or WOL type) tests.
- The advantages mentioned above can be realized in substantially shorter exposure periods to the 3.5% NaCl alternate immersion test than presently specified in ASTM Standard G47.
- Offers an opportunity for improved clarification of SCC mechanisms.
- Capability of the method to define effective flaw size distributions and their variation with time has engineering potential. These parameters can be related to design and material selection criteria having the objectives of improving life-cycle economics of a part, structure, or entire aircraft fleet.

In summary, the SCC breaking load approach represents a significant new tool that is available for measurement of SCC phenomena. This new method brings together the disciplines of statistics and fracture mechanics (LEFM and EPFM), and it provides an evaluation technique having the advantages of shorter test times, fewer specimens, high SCC measurement precision and completely quantitative descriptors of SCC initiation and crack growth. Conceptual extension of the breaking load approach seems

well suited for future SCC examinations relating to such areas as life prediction, short cracks, damage tolerance, and durability applications. Finally, the potential exists for extending the breaking load concept to characterization of other types of degrading phenomena (such as fatigue, corrosion fatigue, fretting, wear, and creep) which promote the development and growth of crack-like flaws within a material.

VIII. RECOMMENDATIONS

A. Recommended Methodology for SCC Characterization of High Strength Aluminum Alloys

The following recommendations are based on the literature survey performed in Phase I, as summarized in Section II of the present report, and on the results of experimental work performed in Phase II of the contract.

1. SCC Tests for Alloy Selection and Design

Proper characterization of high-strength aluminum alloy mill products requires evaluation of both the probability of SCC initiation* under given loading and environmental conditions and the rate of ensuing subcritical crack growth. The breaking load method of testing small sized, smooth, tension specimens described in this report is recommended for further trial and adoption for these purposes. Unfortunately, the current specimen design cannot be used for short transverse tests of section thicknesses less than 1.5 inches. When tension specimens cannot be used, then C-rings (ASTM G38) (10) or tuning forks and DCB specimens (52, 53) are recommended. If there is need for a threshold stress intensity factor, K_{th} , a K-increasing type of test with WOL or DCB

* Provisionally, initiation can be defined to a predetermined flaw size (depth of penetration).

specimens may be used. The recommended environmental exposure is 3.5% NaCl solution by alternate immersion (ASTM G44 (10)) for smooth specimen tests or by dropwise application for precracked specimens, as was done in this investigation.

2. Screening Tests for Alloy Development

The same considerations given in the preceding paragraph also apply for alloy development tests. When, for the first time, a new class of material is to be examined by the breaking load method, it is advisable to conduct screening tests at various exposure stresses and times of exposure to determine optimum testing conditions. It is also advisable to consider use of control specimens exposed at zero stress and examination of the specimen fractures to respectively distinguish whether SCC occurs primarily as fissures or pits, and whether flaws or other metallographic features in the metal contribute to degradation of specimen strength.

B. Future Work - Breaking Load Test Approach

The current investigation shows the breaking-load test approach to be a promising new tool, capable of providing more precise and quantitative descriptors of material resistance to SCC in shorter times and with fewer specimens than is currently attainable with traditional test methods. Recognizing these advantages, this section proposes areas of further work related to the advancement and use of the method. Meeting these objectives could be accelerated by encouraging outside involvement in this

activity through organizations such as ASTM (notably, subcommittees G01.06 and E24.04) and NACE. Future work suggestions are outlined below in the following general categories: (1) additional verification, (2) test/evaluation procedures, (3) fundamental understanding (mechanisms), and (4) applications.

1. Additional Verification

- a. Determine the applicability of the breaking load method to other aluminum alloys and tempers where SCC is important. Gain more quantitative understanding of how SCC resistance is affected by alloy type and by strength-toughness property trade-offs.
- b. Determine whether the breaking load method will significantly decrease or eliminate run to run and interlaboratory variability in 3.5% NaCl alternate immersion tests. Currently, such variability is a serious constraint in the evaluation of aluminum alloys and tempers having intermediate resistance to SCC.
- c. Correlate results of accelerated breaking load tests to long exposure data obtained in service environments.
- d. Determine the applicability of the breaking load approach to other alloy systems (e.g., steel, titanium, ...)

and environments. Identify what elements are common to the characterization of SCC by the breaking load method, regardless of alloy type or environment.

2. Test/Evaluation Methods

a. Specimen Configuration and Loading Arrangements

- Perform stress analysis of the current stressing frame (Figure 13). Use these results in combination with the load versus deflection (compliance) relationship developed for flawed tension specimens to assess variability of the exposure stress with depth of SCC penetration. Evaluate the respective influences of specimen configuration and load frame stiffness on the above, and how the breaking load test response is affected by alloy strength and toughness.
- Examine the influence of elastic modulus on specimen loading mechanics, and determine whether this influence is important to comparative breaking load studies on traditional aluminum alloys vs. new aluminum lithium and metal matrix composite materials showing 10-50% modulus improvement.
- Study the feasibility of a fixed (or dead weight) loading arrangement as an improved alternative to the current stressing frame.

- Establish a breaking load specimen and related procedures for examining short transverse behavior in product less than 1.5 in. thick.

b. Test Procedures

- Establish test procedure guidelines including requirements for optimum exposure conditions. Determine sensitivity of these recommendations to changes in alloy or environment.
- Establish the influence of load removal at the end of the exposure test, and the effect of time delay between exposure and the tension test. Determine if it is acceptable to store exposed specimens for later tension testing when convenient. In the current program, exposed specimens were tension tested within one hour after removal from the environment.

c. Analysis Methods

- Statistical Procedures:
 - Though extreme-value analysis is known to be applicable to data from conventional tension tests (unexposed), it needs to be proven that the same statistical assumptions apply for exposed (or flawed) specimen breaking load behaviors. Appropriateness of the assumed extreme-value distribution for exposed specimen breaking strengths should be verified by using larger numbers of replicate specimens (at selected exposure conditions) than was possible within the current investigation scope.

- Determine whether there is a more statistically satisfying way to incorporate SCC failures into analysis of breaking load data.
- Define a more reliable procedure for estimating the statistical threshold.
- Fracture Mechanics and Effective Flaw Size Concepts:
 - Derive rigorous elastic-plastic crack driving force and compliance equations for describing behavior of flawed specimen configurations of interest.
 - Test the hypothesis that probable lifetime for growth of "small" SCC flaws to a given size can be estimated from the probabilistic crack growth rate relationship $[(da/dt)_{eff}]$ vs. crack driving force. Show that crack growth data developed from one test configuration can be applied to predict behavior of another tested in the same environment (e.g., tension vs. bending, fixed load vs. fixed displacement, etc.).

3. Fundamental Understanding (Mechanisms)

- a. Using special metallurgical and specimen preparation techniques, examine the condition of exposed specimens prior to the tension test; check for evidence of damage and compare to the post fracture condition. Assess whether SCC flaw dimensions before and after the tension test are comparable.
- b. Make use of high precision load-deflection measurements to study the possibility of localized strain hardening or slow stable tearing during the tension test. Examine possible alternative descriptors of performance, such as total energy to fracture (area under the load-deflection curve). Consider, also, the use of load-deflection-time

data for studying SCC process kinetics during the exposure portion of the test.

- c. Perform breaking load tests to more sensitively study the following factors which may influence SCC.
 - Effects of alloy composition and microstructure.
 - Electrochemical and environmental factors.
 - Hydrogen-assisted cracking or hydrogen hardening, the evidence of which can be explored by studying effects of outgassing treatments.

4. Applications

- a. Expand the breaking load data base on established and advanced materials. Define capability claims for these materials in terms of breaking load results.
- b. Establish a link between probability of initiation and growth of SCC determined from laboratory coupons and SCC behavior of actual parts. Develop probabilistic life assessment models for use in scheduling inspection, maintenance and retirement of parts in service.
- c. Extend concepts of the breaking load approach to examinations of environment assisted crack nucleation and growth under other forms of damage such as fatigue, corrosion fatigue, elevated temperature fatigue, creep, fretting, wear, etc.

IX. REFERENCES

1. D. O. Sprowls and E. H. Spuhler, "Avoiding Stress-Corrosion Cracking in High Strength Aluminum Alloy Structures," Alcoa Green Letter 188 (Rev. 1982-01), Published by Aluminum Company of America, Alcoa Technical Center, Alcoa Center, PA.
2. M. O. Speidel, "Current Understanding of Stress-Corrosion Crack Growth in Aluminum Alloys," The Theory of Stress Corrosion Cracking in Alloys, (ed. J. C. Scully), NATO Scientific Affairs Division, Brussels, 1971, pp. 289-344.
3. A. W. Thompson, "Current Status of the Role of Hydrogen in Stress-Corrosion Cracking," Materials Science and Engineering, Vol. 43, 1980, pp. 41-46.
4. R. B. Mears, R. H. Brown and E. H. Dix, Jr., "A Generalized Theory of Stress-Corrosion of Alloys," Symposium on Stress-Corrosion Cracking of Metals, published jointly by ASTM and AIME, 1945, pp. 323-339.
5. D. O. Sprowls, "A Study of Environmental Characterization of Conventional and Advanced Aluminum Alloys for Selection and Design," Phase I - Literature Review, NASA CR-172387, August 31, 1984.
6. G. M. Scamans, "Discontinuous Propagation of Stress-Corrosion Cracks in Al-Zn-Mg Alloys," Scripta Metallurgica, Vol. 13, 1979, pp. 245-250.
7. D. O. Sprowls, "The Stress Corrosion of Aluminum Alloys," paper presented at an international conference on Control and Exploitation of the Corrosion of Aluminum Alloys, held at Cranfield Institute of Technology, Bedfordshire, England, April 5-8, 1983.
8. E. H. Dix, Jr., "Symposium on Stress-Corrosion Cracking, Introduction," Symposium on Stress-Corrosion Cracking of Metals, published jointly by ASTM and AIME, 1945, pp. 1-5.
9. E. H. Dix, Jr., "Aluminum-Zinc-Magnesium Alloys, Their Development and Commercial Productions," Trans. ASM, Vol. 42, 1950, pp. 1057-1127.
10. 1983 Annual Book of ASTM Standards, Section 3, Vol. 03.02, American Society for Testing and Materials, Philadelphia, PA.
11. R. N. Parkins, F. Mazza, J. J. Royuela and J. C. Scully, "Report Prepared for the European Federation of Corrosion Working Party on Stress Corrosion Test Methods," British Corrosion Journal, Vol. 7, July 1972, pp. 154-167.

12. H. Bohni and H. H. Uhlig, "Environmental Factors Affecting the Critical Pitting Potential of Aluminum," Journal of the Electrochemical Society, Vol. 116, Part II, 1969, pp. 906-910.
13. A. H. Le, B. F. Brown, and R. T. Foley, "The Chemical Nature of Aluminum Corrosion: IV. Some Anion Effects on SCC of AA 7075-T651," Corrosion, Vol. 36, No. 12, December 1980, pp. 673-679.
14. D. O. Sprowls, J. D. Walsh and M. B. Shumaker, in Localized Corrosion-Cause of Metal Failure, ASTM STP 516, American Society for Testing and Materials, 1972, p. 38.
15. B. W. Lifka, "SCC Resistant Aluminum Alloy 7075-T73 Performance in Various Environments," Aluminium, Vol. 53, No. 12, 1977, pp. 750-752.
16. M. O. Speidel and M. V. Hyatt, "Stress-Corrosion Cracking of High Strength Aluminum Alloys," Advances in Corrosion Science and Technology, Vol. 2 (edited by Mars G. Fontana and Roger W. Staehle), Plenum Press, New York, NY, 1972, pp. 115-335.
17. ASTM E399-83, "Standard Test Method for Plane-Strain Fracture Toughness of Metallic Materials," 1983 Annual Book of ASTM Standards, Section 3, Vol. 03.01, 1983, pp. 518-553.
18. ASTM E647-83, "Standard Test Method for Constant-Load-Amplitude Fatigue Crack Growth Rates Above 10^{-8} m/cycle," 1983 Annual Book of ASTM Standards, Section 3, Vol. 03.01, 1983, pp. 710-730.
19. MIL-A-83444, United States Air Force Military Specification on Airplane Damage Tolerance Requirements, July 2, 1974.
20. J. G. Kaufman, "Stress Corrosion--Tradition vs. Fractured Mechanics," Guest editorial, Corrosion, Vol. 35, No. 4, April 1979, p. i.
21. S. J. Hudak, "Small Crack Behavior and the Prediction of Fatigue Life," Journal of Engineering Materials and Technology, Transactions ASME, Ser. H, Vol. 103, 1981, pp. 26-35.
22. B. N. Leis, M. F. Kanninen, A. T. Hopper, J. Ahmad, and D. Broek, "A Critical Review of the Short Crack Fatigue Problem in Fatigue" AFWAL-TR-83-4019, Air Force Wright Aeronautical Laboratories, Wright-Patterson Air Force Base, Ohio, January 1983.
23. R. O. Ritchie and S. Suresh, "Mechanics and Physics of the Growth of Small Cracks" in Behavior of Short Cracks in Airframe Components, AGARD Conference Proceedings No. 328, April 1983.

24. H. Kitagawa and S. Takahashi, "Applicability of Fracture Mechanics to Very Small Cracks or Cracks in the Early Stage," in Proceedings Second International Conference on Mechanical Behavior of Materials, 1979, pp. 627-631.
25. K. Tanaka, Y. Nakai and M. Yamashita, "Fatigue Growth Threshold of Small Cracks," International Journal of Fracture, Vol. 17, 1981, pp. 519-533.
26. J. W. Hutchinson, "Singular Behavior at the End of a Tensile Crack in a Hardening Material," Journal of Mechanics and Physics of Solids, Vol. 16, 1968, pp. 1-12.
27. J. R. Rice and G. R. Rosengren, "Plane Strain Deformation Near a Crack Tip in a Power Hardening Material," Journal of Mechanics and Physics of Solids, Vol. 16, 1968, pp. 13-31.
28. P. C. Paris, "Fracture Mechanics in the Elastic-Plastic Regime," Flaw Growth and Fracture, ASTM STP 631, American Society for Testing and Materials, 1977, pp. 3-27.
29. N. E. Dowling, "Crack Growth During Low Cycle Fatigue of Smooth Axial Specimens," in Cyclic Stress-Strain and Plastic Deformation Aspects of Fatigue Crack Growth, ASTM STP 637, American Society of Testing and Materials, 1977, pp. 97-121.
30. G. G. Trantina and H. G. DeLorenzi, "Elastic-Plastic Fracture Mechanics of Small Cracks," AMMRC-MS-82-4, Proceedings of the Army Symposium on Solid Mechanics Problems in Systems Design, AMMRC, Watertown, MA, September 1982, pp. 203-214.
31. F. A. Champion, "The Assessment of the Susceptibility of Aluminum Alloys to Stress Corrosion," Symposium on Stress Corrosion Cracking of Metals (1944), published jointly by ASTM and AIME, 1945, p. 358.
32. E. L. Jones, "Stress Corrosion of Aluminum-Magnesium Alloys. I. The Effect of Tensile Stress on the Corrosion of Al-7% Mg and Al-5% Mg Alloys," Journal of Applied Chemistry, Vol. 4, 1954, pp. 1-7.
33. A. Prati, "The Anodic Test as a Method of Controlling the Stress Corrosion Susceptibility of Al-Zn-Mg Alloys," Alluminio E. Nuova Metallurgia, Vol. 39, No. 8, 1970, pp. 407-412.
34. B. W. Lifka, D. O. Sprowls and R. A. Kelsey, "Investigation of Smooth Specimen SCC Test Procedures, Variations in Environment, Specimen Size, Stressing Frame, and Stress State," NASA CR-120752, May 12, 1975.

35. D. O. Sprowls, T. J. Summerson, G. M. Ugiansky, S. G. Epstein, and H. L. Craig, "Evaluation of a Proposed Standard Method of Testing for Susceptibility to SCC of High Strength 7XXX Series Aluminum Alloy Products," Stress Corrosion-New Approaches, ASTM STP 610, American Society for Testing and Materials, 1976, pp. 3-31.
36. ASTM B557-81, "Standard Methods of Tension Testing Wrought and Cast Aluminum and Magnesium-Alloy Products," 1983 Annual Book of ASTM Standards, Section 3, Vol. 03.01, 1983, pp. 64-80.
37. ASTM E646-78, "Standard Method of Test for Tensile Strain-Hardening Exponents (n-values) of Metallic Sheet Materials," 1983 Annual Book of ASTM Standards, Section 3, Vol. 03.01, 1983, pp. 700-709.
38. A. A. Griffith, "The Phenomena of Rupture and Flow in Solids," *Phil. Trans. Roy. Soc.*, Vol. 221A, 1920, p. 163.
39. A. A. Griffith, "The Theory of Rupture," *First International Congress of Applied Mechanics*, Delft, 1924, p. 55.
40. J. C. Fisher and J. H. Hollomon, "A Statistical Theory of Fracture," *Tech. Pub. No. 2218, Metals Technology, AIME*, Vol. 14, 1947, p. 5.
41. B. Epstein, "Statistical Aspects of Fracture Problems," *Journal of Applied Physics*, Vol. 19, 1948, p. 140.
42. B. Epstein, "Application of the Theory of Extreme Values in Fracture Problems," *Journal of American Statistics Association*, Vol. 43, 1948, p. 403.
43. A. M. Freudenthal, "The Statistical Aspects of Fatigue of Materials," *Proc. Roy. Soc.*, Vol. A187, 1946, p. 416.
44. E. J. Gumbel, "Les Valeurs Extremes des Distributions Statistiques," *Ann. Inst. Henri Poincare*, Vol. 4, 1935, p. 115.
45. E. J. Gumbel, "Statistische Theorie de Ermudungerscheinungen bei Metallen," *Mitt. Fur Mat., Stat.*, Vol. 8, 1956, p. 97.
46. E. J. Gumbel, Statistical Theory of Extreme Values and Some Practical Applications, U. S. Dept. of Commerce, Applied Mathematics Series 33, 1954.
47. E. J. Gumbel, Statistics of Extremes, Columbia University Press, New York, 1958.
48. R. B. Mears and R. H. Brown, *Ind. Eng. Chem.*, Vol. 29, No. 10, 1937, p. 1087.

49. P. M. Aziz, "Application of the Statistical Theory of Extreme Values to the Analysis of Maximum Pit Depth Data for Aluminum," *Corrosion*, Vol. 12, 1956, pp. 495t-506t.
50. R. Parsons, Statistical Analysis; A Decision-Making Approach, 2nd Edition, 1978, Harper & Row Publishers, p. 240.
51. M. V. Hyatt, "Use of Precracked Specimens in Stress Corrosion Testing of High Strength Aluminum Alloys," *Corrosion*, Vol. 26, No. 11, November 1970, pp. 487-503.
52. H. R. Smith and D. E. Piper, "Stress Corrosion Testing with Precracked Specimens," Chapter 2 in Stress-Corrosion Cracking in High Strength Steels and in Titanium and Aluminum Alloys (B. F. Brown, ed.), Naval Research Laboratories, Washington, DC, 1972.
53. D. O. Sprowls, M. B. Shumaker, J. D. Walsh, and J. W. Coursen, "Evaluation of Stress-Corrosion Cracking Susceptibility Using Fracture Mechanics Techniques," NASA CR-124469, May 31, 1973.
54. J. G. Kaufman, J. W. Coursen, and D. O. Sprowls, "An Automated Method for Evaluating Resistance to Stress-Corrosion Cracking with Ring-Loaded Precracked Specimens," in Stress-Corrosion-New Approaches, ASTM STP 610, American Society for Testing and Materials, 1976, pp. 94-107.
55. J. C. Newman, Jr., Analysis of WOL Stress Corrosion Specimens, Section 2.6, page 11 of Instructions for Round Robin Test Program on Stress-Corrosion Cracking of 7075 Aluminum Alloy Plate, February 11, 1982 (Rev. Nov. 23, 1982).
56. J. R. Rice, "The Mechanics of Crack Tip Deformation and Extension by Fatigue," Fatigue Crack Propagation, ASTM STP 415, American Society for Testing and Materials, 1967, pp. 247-311.
57. G. G. Trantina, H. G. DeLorenzi, W. W. Wilkening, "Three Dimensional Elastic-Plastic Finite Element Analysis of Small Surface Cracks," *Engineering Fracture Mechanics*, Vol. 18, No. 5, 1983, pp. 925-938.
58. D. M. Parks and C. S. White, "Elastic-Plastic Line-Spring Finite Elements for Surface-Cracked Plates and Shells," *Journal of Pressure Vessel Technology*, Vol. 104, Nov. 1982, pp. 287-292.
59. J. C. Newman, Jr., "A Review and Assessment of the Stress-Intensity Factors for Surface Cracks," Part Through Crack Fatigue Life Prediction, ASTM STP 687, American Society for Testing and Materials, 1979, pp. 16-42.

60. A. Athanassiadis, J. M. Boissenot, P. Brevet, D. Francois, and A. Raharinaivo, "Linear Elastic Fracture Mechanics Computations of Cracked Cylindrical Tensioned Bodies," *International Journal of Fracture*, Vol. 17, 1981, pp. 553-566.
61. M. A. Astiz, "Estudid de la Estabilidad de una Fisura Superficial en un Alambre de Acero Alta Resistencia," Tesis defendia en la Escuela T. S. de Ingenieros de Caminos, Canales y Puertos, Universidad Politecnica de Madrid, 1976.
62. R. P. Gangloff, "Quantitative Measurements of the Growth Kinetics of Small Fatigue Cracks in 10 Ni Steel," Fatigue Crack Growth Measurement and Data Analysis, ASTM STP 738, American Society for Testing and Materials, 1981, pp. 120-138.
63. O. E. K. Daoud, D. J. Cartwright, and M. Carney, "Strain-Energy Release Rate for a Single-Edge-Cracked Circular Bar in Tension," *Journal of Strain Analysis*, Vol. 13, No. 2, 1978, pp. 83-89.
64. P. C. Paris and G. C. Sih, "Stress Analysis of Cracks," Fracture Toughness Testing and Its Applications, ASTM STP 381, American Society for Testing and Materials, 1965, pp. 30-83.
65. D. O. Harris, "Stress Intensity Factors for Hollow Circumferentially Notched Round Bars," *Journal of Basic Engineering*, Vol. 89, 1967, p. 49.
66. J. G. Kaufmann, "Design of Aluminum Alloys for High Toughness and High Fatigue Strength," Specialists Meeting on Alloy Design for Fatigue and Fracture Resistance, AGARD Conference Proceedings No. 185, Brussels, Belgium, 1975.
67. R. J. Bucci, "Selecting Aluminum Alloys to Resist Failure by Fracture Mechanisms," *Engineering Fracture Mechanics*, Vol. 12, 1979, pp. 407-441.
68. MIL-HDBK-5C, "Metallic Materials and Elements for Aerospace Vehicle Structures," Vol. I, December 1979.
69. D. O. Sprowls and J. D. Walsh, "Evaluating Stress-Corrosion Crack Propagation Rates in High Strength Aluminum Alloys with Bolt Loaded Precracked Double Cantilever Beam Specimens," in Stress Corrosion-New Approaches, ASTM STP 610, American Society for Testing and Materials, 1976, pp. 143-156.
70. C. Micheletti and M. Buratti, "New Testing Methods for the Evaluation of the Stress-Corrosion Behavior of High-Strength Aluminum Alloys by the Use of Precracked Specimens," Symposium Proceedings, Aluminum Alloys in the Aircraft Industry, Turin, Italy, 1976 October 1-2, pp. 149-159.

71. B. W. Lifka and D. O. Sprowls, "Significance of Intergranular Corrosion of High-Strength Aluminum Alloy Products," Localized Corrosion-Cause of Metal Failure, ASTM STP 516, American Society for Testing and Materials, 1972, pp. 120-144.
72. C. P. Hirth, "Effects of Hydrogen on the Properties of Iron and Steel," Metallurgical Transactions, Vol. 11A, 1980, pp. 861-890.
73. W. R. Wearmouth, G. P. Dean and R. N. Parkins, "Role of Stress in the Stress-Corrosion Cracking of a Mg-Al Alloy," Corrosion, Vol. 29, No. 6, 1973, pp. 251-258.
74. N. E. Frost and D. S. Dugdale, "Fatigue Tests on Notched Mild Steel Plates with Measurements of Fatigue Cracks," Journal of Mechanics and Physics of Solids, Vol. 5, 1957, pp. 182-192.
75. M. S. Hunter and W. G. Fricke, Jr., "Fatigue Crack Propagation in Aluminum Alloys," in Proceedings of the American Society for Testing and Materials, Vol. 56, 1956, pp. 1038-1050.
76. M. S. Hunter and W. G. Fricke, Jr., "Cracking of Notch Fatigue Specimens in Proceedings of the American Society for Testing and Materials, Vol. 57, 1957, pp. 643-654.
77. MIL-STD-1530A, "Aircraft Structural Integrity Program," United States Air Force, December 1975.
78. MIL-A-8866B, "Airplane Strength and Rigidity Reliability Requirements, Repeated Loads and Fatigue," United States Air Force, August 1975.
79. MIL-A-8867B, "Airplane Structural Ground Test," United States Air Force, January 1975.
80. S. D. Manning and V. D. Smith, "Economic Life Criteria for Metallic Airframes," Proceedings 21st AIAA Structural Dynamics and Materials Conference, Part 1, 1980, pp. 504-511.
81. J. L. Rudd, J. N. Yang, S. D. Manning, and B. G. W. Yee, "Probabalistic Fracture Mechanics Analysis Methods for Structural Durability," Behavior of Short Cracks in Airframe Components, AGARD Conference Proceedings No. 328, April 1983.
82. P. J. Noronna, S. P. Henslee, D. E. Gordon, Z. R. Wolanski, and B. G. W. Yee, "Fastener Hole Quality," AFFDL-TR-78-206, Volumes 1 and 2, U. S. Air Force Flight Dynamics Laboratory, Wright-Patterson Air Force Base, Ohio, December 1978.

83. J. M. Potter, "Advances in Fastener Hole Quality Through the Application of Solid Mechanics," in Proceedings of the Army Symposium on Solid Mechanics, 1978-Case Studies on Structural Reliability, AMMRC-MS-78-3, Army Materials and Mechanics Research Center, Watertown, MA, September 1978.
84. J. M. Potter and B. G. W. Yee, "Use of Small Crack Data to Bring About and Quantify Improvements to Aircraft Structural Integrity," Behavior of Short Cracks in Airframe Components, AGARD Conference Proceedings No. 328, April 1983.
85. J. N. Yang and R. C. Donath, "Statistics of Crack Growth of a Superalloy under Sustained Load," AFWAL-TR-82-4102, U. S. Air Force Wright Aeronautical Laboratories, Wright-Patterson Air Force Base, Ohio, December 1982.
86. C. G. Annis, J. S. Cargill, J. A. Harris, Jr., and M. C. Van Wanderham, "Engine Component Retirement-for-Cause: A Non-destructive Evaluation (NDE) and Fracture Mechanics-Based Maintenance Concept" Journal of Metals, July 1981, pp. 24-27.
87. M. E. Fine and R. O. Ritchie, "Fatigue Crack Initiation and Near-Threshold Crack Growth," Fatigue and Microstructure, American Society for Metals, 1979, pp. 245-278.
88. S. Hirose and M. E. Fine, "Fatigue Crack Initiation and Microcrack Propagation in X7091 Type Aluminum P/M Alloys," Metallurgical Transactions, Vol. 14A, June 1983, p. 1189.
89. R. G. Mitchell, "An Airlines View of Aircraft Corrosion Problems," Corrosion Prevention and Control, June 1981, pp. 11-17.
90. R. P. Reed, J. H. Smith, and B. W. Christ, The Economic Effects of Fracture in the United States, Special Publication 647-1, U. S. Department of Commerce, National Bureau of Standards, March 1983.
91. J. J. Duga, W. H. Fisher, R. W. Buxbaum, A. R. Rosenfield, A. R. Buhr, E. J. Honton, and S. C. McMillan, The Economic Effects of Fracture in the United States, Special Publication 647-2, U. S. Department of Commerce, National Bureau of Standards, March 1983.

ORIGINAL PAGE IS
OF POOR QUALITY

TABLE I
RESISTANCE TO STRESS-CORRUSSION RATINGS⁽¹⁾ FOR
HIGH-STRENGTH ALUMINUM ALLOY PRODUCTS
ASTM G 64-80(REF.10)

Alloy and Temper ⁽²⁾	Test Direction ⁽³⁾	Rolled Plate	Rod and Bar ⁽⁴⁾	Extruded Shapes	Forgings
7075-T6	L LT ST	A B ⁽⁵⁾ D	A D D	A B ⁽⁵⁾ D	A B ⁽⁵⁾ D
7075-T73	L LT ST	A A A	A A A	A A A	A A A
7075-T76	L LT ST	A A C	(6) (6) (6)	A A C	(6) (6) (6)

NOTES:

- (1) The interpretation of the ratings is as follows:

Rating	Interpretation
A	Very high. No record of service problems and SCC not anticipated in general applications.
B	High. No record of service problems and SCC not anticipated at stresses of the magnitude caused by solution heat treatment. Precautions must be taken to avoid high sustained tensile stress exceeding 50 percent of the minimum specified yield strength produced by any combination of sources including heat treatment straightening, forming, fit-up, and sustained service loads.
C	Intermediate. SCC not anticipated if the total sustained tensile stress is less than 25 percent of the minimum specified yield strength. This rating is designated for the short transverse direction in improved products used primarily for high resistance to exfoliation corrosion in relatively thin structures where appreciable short transverse stresses are unlikely.
D	Low. SCC failures have occurred in service or would be anticipated if there is any sustained tensile stress in the designated test direction. This rating currently is designated only for the short transverse direction in certain materials.

Caution - The stress levels mentioned above are test dependent, not to be interpreted as "threshold" stresses, and are not recommended for design.

- (2) The ratings apply to standard mill products in the types of tempers indicated, including stress-relieved tempers, and could be invalidated in some cases by application of nonstandard thermal treatments or mechanical deformation at room temperature by the user.
- (3) Test direction refers to orientation of the stressing direction relative to the directional grain structure typical of wrought materials, which in the case of extrusions and forgings may not be predictable from the geometrical cross section of the product.
- L - Longitudinal: parallel to direction of principal metal extension during manufacture of the product.
- LT - Long Transverse: perpendicular to direction of principal metal extension. In products whose grain structure clearly shows directionality (width-to-thickness ratio greater than two) it is that perpendicular direction parallel to the major grain dimension.
- ST - Short Transverse: perpendicular to direction of principal metal extension and parallel to minor dimension of grains in products with significant grain directionality.
- (4) Sections with width-to-thickness ratio equal to or less than two, for which there is no distinction between LT and ST.
- (5) Rating is one class lower for thicker sections: extrusions, 25 mm (1 in.) and over; plate and forgings 40 mm (1.5 in.) and over.
- (6) Rating not established because the product is not offered commercially.

TABLE II

COMPOSITION AND MECHANICAL PROPERTIES OF 2.5 IN. THICK ALUMINUM ALLOY
7075-T651 PLATE USED AS THE BASIS FOR THE SCC TESTING PROGRAM

Chemical Composition (Analysis of Remelted Sample of Plate)

0.11% Si, 0.26% Fe, 1.57% Cu, 0.05% Mn, 2.39% Mg, 0.19% Cr, 0.00% Ni, 5.80% Zn, 0.05% Ti

Mechanical Properties

Long Transverse

Tensile Strength, ksi
Yield Strength, 0.2%, ksi
Elongation in 1" (4D), %
Reduction of Area, %

78.3
67.6
11.8
18

Samples for SCC Tests

<u>Sample No.</u>	<u>Plate Temper</u>	<u>Condition</u>
574619	T651	Commercial T651, as-received from plant. Electrical conductivity = 31.9 %IACS.
550915	T7X1*	Plant 7075-T651 heated at 335°F to electrical conductivity of 37.0% IACS.
547620	T7X2*	Plant 7075-T651 heated at 335°F to electrical conductivity of 37.8% IACS.

* Special samples overaged to produce improved resistance to SCC; not representative of any standard tempers. Higher resistance to SCC is associated with higher % electrical conductivity.

TABLE III

OUTDOOR SCC TESTS OF SHORT TRANSVERSE SPECIMENS OF 7075-T651 PLATE (1,2)

Exposure Stress (ksi)	F/N ⁽³⁾	Time to Failure, Days
<u>Seacost Atmosphere at Point Judith, R.I.</u>		
32	9/9	7, 7, 7, 7, 7, 7, 7, 15, 15
22	9/9	7, 7, 7, 15, 15, 37, 37, 78
13	9/9	7, 15, 15, 37, 37, 37, 54, 54,
<u>Industrial Seacoast Atmosphere at Vernon (Los Angeles), CA</u>		
32	9/9	162, 162, 163, 197, 200, 206, 209, 220, 313
22	5/9	229, 267, 416, 472, 474; 4 survivors at 2245 days
13	0/9	9 survivors at 2245 days
<u>Mild Industrial Inland Atmosphere at Alcoa Center, PA</u>		
32	7/9	728, 881, 889, 889, 959, 1324, 1537; 2 survivors at 2241 days
22	3/9	881, 889, 959; 6 survivors at 2241 days
13	0/9	9 survivors at 2241 days
<u>3.5% NaCl Alternate Immersion ASTM G44 (Ref. 10)</u>		
22	14/15	14 at 7 days; 1 survivor at 84 days
13	8/15	7, 7, 37, 45, 67, 73, 77, 84; 7 survivors at 84 days

- NOTES: (1) Davenport production plate 2.5 in. thick (Alcoa Sample No. 475333).
 (2) Test specimens 0.125 in. diameter x 2 in. long stressed in frames shown in Figure 13.
 (3) Failure ratio: number of failures/number of specimens exposed.

TABLE IV

BREAKING LOAD TEST PROGRAM FOR 7075 ALLOY PLATE IN THREE TEMPER

Smooth Tension Specimens Orientation	Diameter (in.)	Exposure Stress (ksi)	Scheduled Exposure Periods in Days (1)			Total Specimens
			T651	T7X1	T7X2	
Short Transverse	0.125	0	0,2,4,6,9	0,2,4,6,9	0,2,4,6,9	75
	0.125	10	2,4,6,9,*	--	--	25
	0.125	20	2,4,6,9	2,4,6,9,*	2,4,6,9	65
	0.125	30	2,4,6,9	2,4,6,9	2,4,6,9,*	65
	0.125	40	--	2,4,6,9	2,4,6,9,*	45
Short Transverse	0.225	0	--	0,2,4,6,9,12	--	30
	0.225	20	--	2,4,6,9,12,*	--	30
	0.225	30	--	2,4,6,9,12,*	--	30
	0.225	40	--	2,4,6,9,12,*	--	30
Long Transverse	0.225	0	0,2,4,8,15	--	--	25
	0.225	30	2,4,8,15,*	--	--	25
	0.225	40	2,4,8,15,*	--	--	25
						470

ORIGINAL PAGE IS
OF POOR QUALITY

- NOTES: (1) Exposed to 3.5% NaCl alternate immersion (ASTM G44). Specimens were exposed in sets of 5 for each period.
- (2) * One set of 5 replicate specimens exposed until failure, or terminated at 60 days.

TABLE V

SHORT TRANSVERSE TENSILE AND FRACTURE TOUGHNESS (K_{IC})
PROPERTIES OF 7X75-TYPE ALLOYS (AVERAGE OF DUPLICATE TESTS)

Alloy	Temper	Plate (a) Thickness (in.)	Alcoa Sample No.	QUTS (b) (ksi)	QYS (b) 0.2% Offset (ksi)	Elong. (b) In 4D (%)	Strain Hardening Coefficients K (ksi)	n	K_{IC} (ksi $\sqrt{in.}$) (d)
7075	T651	2.5	547619-2	76.8	63.8	6.0	102	0.070	19.3
7075	T7X1	2.5	550915	70.6	62.0	3.5	92.2	0.058	19.4
7075	T7X2	2.5	547620-2	69.4	60.4	3.5	91.8	0.062	20.2
7475	T651	3.0	518351	77.2	60.6	9.3	104	0.078	34.9
7475	T7651	3.0	518358	72.2	61.5	6.0	98	0.077	34.7
7475	T7351	3.0	518365	70.9	58.0	9.3	97	0.083	36.3

NOTES:

- (a) All test specimens removed from the center plate thickness.
- (b) Tensile properties determined in accordance with ASTM method E646-78, using standard 0.25 in. diameter tapered seat specimens with mounted extensometer of 1 in. gauge length.
- (c) Procedures for determining strain hardening coefficients in accordance with ASTM Method E646-78, using standard 0.25 and 0.125 in. tapered seat specimens with mounted extensometer of 1 in. and 0.5 in. gauge lengths, respectively, for the three temper variants of alloys 7075 and 7475.
- (d) Fracture toughness tests made in accordance to ASTM method E399-83, using 1 in. thickness standard compact specimens.

TABLE VI

SUMMARY OF BREAKING LOAD SPECIMEN FAILURES OF 7075 ALLOY SPECIMENS INCURRED DURING EXPOSURE TO 3.5% NaCl SOLUTION BY ALTERNATE IMMERSION PER ASTM G44

Plate Temper	Test Orientation	Specimen Diameter-(in.)	Exposure Stress-(ksi)	Scheduled Exposure Time-(Days)	Number of Failures	Time to Failure-(Days)
T651	Short Trans.	0.125	20	6	4	5,5,5,6
T651	Short Trans.	0.125	20	9	4	5,5,5,5
T651	Short Trans.	0.125	30	4	5	3,3,3,3,4
T651	Short Trans.	0.125	30	6	5	3,3,3,3,6
T651	Short Trans.	0.125	30	9	5	3,3,3,3,3
T7X1	Short Trans.	0.125	40	6	1	5
T7X1	Short Trans.	0.125	40	9	1	4
T7X1	Short Trans.	0.225	30	60	1	37
T7X1	Short Trans.	0.225	40	9	1	7
T7X1	Short Trans.	0.225	40	60	3	12,15,37

NOTES: (1) Specimens were exposed in sets of five (See Table IV); except for T7X1, 0.225 in. dia. specimens at 40 ksi, 60 days which was exposed in set of four.
 (2) Results of breaking load tests of the surviving specimens are given in Tables 1, 4, and 10 of Appendix C.

TABLE VII

99% SURVIVAL STRESS⁽¹⁾ AND STATISTICAL THRESHOLD STRESS⁽²⁾ VALUES CALCULATED FROM
BREAKING LOAD TESTS OF THREE TEMPER VARIANTS OF 2.5 IN. THICK 7075 ALLOY PLATE
EXPOSED TO 3.5% NaCl SOLUTION BY ALTERNATE IMMERSION (ASTM G44).

Plate Temper	Test Orientation	Specimen Diameter-(in.)	Averaged 99% Survival Stress-(ksi)(3)				Statistical Threshold Stress-(ksi)(4)
			Exposure Period (days)	Exposure Stress			
			20 ksi	30 ksi	40 ksi		
T651	Long Trans.	0.225	4 & 8	--	72	70	55
T651	Short Trans.	0.125	4, 6 & 9	0	0	0	17
T7X1	Short Trans.	0.125	4, 6 & 9	61	44	12	31
T7X1	Short Trans.	0.225	4, 6 & 9	54	44	30	31
T7X2	Short Trans.	0.125	4, 6 & 9	66	67	64	54

NOTES: (1) The 99% survival stress is described in Section III.D.2.b.

(2) 95% confidence of a probability of failure of 1% or less.

(3) 99% survival stress values (point estimates; Ref. Appendix C Tables 3, 6, 9, 12 and 15) averaged for the indicated exposure periods at each exposure stress.

(4) Ref. Table B2 Appendix B.

TABLE VIII

GRAPHICAL DEVELOPMENT OF STRESS CORROSION CRACK GROWTH RATE CURVES
FROM DCB SPECIMENS OF 7075 ALLOY PLATE

Plate Temper	Specimen No.	Hours		Crack-(in.)		K	da/dt
		Total	Interval	Length	Growth	(ksi/in.)	(in./hr.)
T651	1	0	0	1.182	0	17.6	0
		504	504	1.392	0.210	13.7	4.2×10^{-4}
		672	168	1.398	0.006	13.6	3.6×10^{-4}
		1248	576	1.655	0.257	10.4	4.5×10^{-4}
		1848	600	1.793	0.138	9.1	2.4×10^{-4}
T651	2	0	0	1.125	0	16.5	0
		552	552	1.400	0.275	11.8	5.0×10^{-4}
		936	384	1.491	0.091	10.7	2.4×10^{-4}
		1248	312	1.667	0.176	8.9	5.6×10^{-4}
		1848	600	1.835	0.168	7.6	2.8×10^{-4}
T7X1	1	0	0	1.225	0	19.2	0
		336	336	1.255	0.030	18.5	8.9×10^{-5}
		1104	768	1.271	0.016	18.2	2.1×10^{-6}
		1848	744	1.278	0.007	18.0	9.4×10^{-6}
T7X1	2	0	0	1.158	0	19.2	0
		552	552	1.171	0.013	18.9	2.4×10^{-5}
		1248	696	1.269	0.098	16.7	1.4×10^{-5}
		1848	600	1.303	0.034	16.0	5.7×10^{-5}
T7X2	1	0	0	1.146	0	19.2	0
		96	96	1.160	0.014	18.9	1.5×10^{-6}
		1848	1752	1.169	0.009	18.6	2.3×10^{-6}
T7X2	2	0	0	1.096	0	23.2	0
		168	168	1.120	0.024	22.4	1.4×10^{-4}
		936	768	1.131	0.011	22.1	1.4×10^{-5}
		1104	168	1.155	0.024	21.4	1.4×10^{-4}
		1848	744	1.167	0.012	21.1	1.6×10^{-5}

NOTES: (1) See Tables 1-6 in Appendix D for the basic data.

TABLE IX

RESULTS OF SCC TESTS ON FATIGUE PRECRACKED WOL SPECIMENS (a) OF 7075 ALLOY PLATE
3.5% NaCl SOLUTION ADDED DROPWISE 3 TIMES/DAY

Plate Temper	K_{Ic} (ksi $\sqrt{in.}$)	Specimen Number	$K - (K_{Ic}/\sqrt{in.})$ Start Finish	Hours Exposure	Crack Growth, (in.)	Estimated Threshold, K_{th} ksi/in. $\frac{K_{th}}{\%K_{Ic}}$
T651	19.3	SL-1	9.4 15.9	1580	0.606	5 26
		SL-2	6.9 8.5	2090	0.259	
		SL-3	4.0 4.0	1340	0	
		SL-3	7.9 9.3	650	0.272	
T7X1	19.4	SL-3	14.0 14.4	2330	0.030(c)	13 67 16(b) 82
		SL-2	9.4 9.4	1580	0	
		SL-1	6.7 6.8	1340	0	
T7X2	20.2	SL-3	18.8 18.6	1580	0.005	19 94 18(b) 89
		SL-2	15.4 15.0	2330	0	
		SL-1	14.9 14.8	1580	0	

NOTES: (a) Ring loaded. K-increasing test.

(b) Estimated from bolt loaded DCB, K-decreasing test.

(c) Crack growth determined by post-test examination of the fracture.

TABLE X

FLAW SIZE MEASUREMENTS FROM BREAKING LOAD SPECIMENS ORIENTED IN SHORT TRANSVERSE DIRECTION
AND EXPOSED TO 3.5 PERCENT SODIUM CHLORIDE BY ALTERNATE IMMERSION

Alloy	Temper	Alcoa Sample Number	Specimen Diameter (in.)	Specimen Number	Gross Fracture Stress (ksi)	Exposure Stress (ksi)	Exposure Time (Days)	Deepest Penetration a_{max} (in.)	Flawed Area Fraction A_c/A_o	Equiv. Annular Flaw Depth a_e (in.)	Single or Annular Flaw
7075	T651	547619-2	0.125	7	76.3	0	2	0.0031	0	0	--
				9	71.7	0	2	0.0075	0.09	0.0029	Annular
				21	69.0	0	9	0.0168	0.19	0.0063	Annular
				24	67.4	0	9	0.0089	0.15	0.0049	Annular
				52	72.2	20	2	0.0088	0.06	0.0019	Annular
				53	62.1	20	2	0.0183	0.13	0.0043	Annular
				57	61.3	20	4	0.0265	0.36	0.0125	Annular
				60	35.0	20	4	0.0515	0.41	0.0145	Single
				61	58.9	20	6	0.0199	0.32	0.0110	Annular
				66	60.5	20	9	0.0159	0.28	0.0095	Annular
				71	68.0	30	2	0.0143	0.14	0.0045	Annular
				72	53.9	30	2	0.0248	0.32	0.0110	Annular
				73	68.6	40	2	0.0105	0.02	0.0006	Single
				75	59.7	40	2	0.0181	0.10	0.0033	Single
7075	T7X1	550915	0.125	79	58.1	40	4	0.0156	0.17	0.0055	Annular
				80	49.9	40	4	0.0268	0.19	0.0063	Single
				83	61.4	40	6	0.0110	0.18	0.0059	Annular
				84	45.2	40	6	0.0329	0.30	0.0103	Single
				87	59.2	40	9	0.0216	0.17	0.0055	Annular
				88	47.5	40	9	0.0259	0.27	0.0091	Single
				194	69.4	40	2	0.0137	0.01	0.0005	Single
				196	70.9	40	2	0	0	0	--
				208	63.1	40	9	0.0236	0.10	0.0059	Annular
				218	47.0	40	9	0.0380	0.16	0.0095	Single
				213	63.9	40	12	0.0135	0.07	0.0041	Annular
				214	67.8	40	12	0.0128	0.07	0.0041	Annular
				6	70.3	0	2	0.0046	0.01	0.0003	Single
				7	69.3	0	2	0.0048	<0.01	<0.0003	Single
7075	T7X2	547620-2	0.125	21	65.8	0	9	0.0106	0.07	0.0023	Annular
				24	67.6	0	9	0.0100	0.05	0.0016	Annular
				78	71.3	40	2	0	0	0	--
				79	70.4	40	2	0	0	0	--
				92	68.9	40	9	0.0089	0.05	0.0016	Annular
				94	66.5	40	9	0.0088	0.03	0.0025	Annular

TABLE XI

RESULTS OF BREAKING LOAD EXPERIMENTS ON FATIGUE PRECRACKED, SHORT-TRANSVERSE,
0.125-INCH DIAMETER TENSILE BARS OF ALUMINUM 7X75 PLATE ALLOYS

Alloy and Temper	Plate Thickness, (in.)	Alcoa Sample Number	Specimen Number	Breaking Load (lbs.)	Gross Fracture Stress (ksi)	Size and Shape of Fatigue Crack (a)(b)				
						a (in.)	$\frac{a}{b}$ (radius) (in.)	$\frac{c}{a}$ (in.)	$\frac{a}{D}$ (in.)	$\frac{a}{S}$ (in.)
7075-T651	2.50	547619-2	ST91	917	74.7	0.0062 (c)	--	--	0.0496	0
			ST92	789	64.3	0.0224	0.434	0.0271	0.0272	0.827
			ST93	632	51.5	0.0369	0.658	0.0411	0.0409	0.897
			ST94	703	57.3	0.0309	0.501	0.0313	0.0310	0.987
			ST95	774 (d)	63.1	0.0210	0.526	0.0329	0.0343	0.637
			ST96	450 (d)	36.7 (d)	0.0489	0.966	0.0604	0.0617	0.613
			ST97	590	48.1 (d)(e)	0.0392	0.661	0.0413	0.0408	0.809
			ST98	>500 (d)(e)	>40.7 (d)(e)	(e)	0.992	0.0620	0.0593	0.948
			ST99	480 (d)	39.1 (d)	0.0601 (f)	0.992	0.0620	0.0593	(e) (f)
			ST100	784	63.9	0.0231	0.459	0.0287	0.0288	1.014 (f)
7475-T651	3.00	518351	ST10A	400 (d)	32.6 (d)	0.0630	1.369	0.0856	0.1010	0.805
			ST98	890	72.5	0.0167	0.330	0.0206	0.0206	0.736
			ST12C	771	62.8	0.0377	0.723	0.0452	0.0454	0.809
			ST11D	800	65.2	0.0313	0.524	0.0327	0.0325	0.834
			ST8E	685	55.8	0.0385	0.744	0.0465	0.0469	0.957
			ST9F	759	61.8	0.0367	0.664	0.0415	0.0412	0.827
			ST12A	400 (d)	32.6 (d)	0.0667	1.244	0.0778	0.0767	0.885
7475-T7651	3.00	518358	ST7B	686	55.9	0.0401	0.769	0.0481	0.0483	0.858
			ST8C	764 (d)	62.3 (d)	0.0272	0.563	0.0352	0.0356	0.835
			ST11D	400 (d)	32.6 (d)	0.0531	1.053	0.0658	0.0647	0.773
			ST10E	714	58.2	0.0324	0.582	0.0364	0.0363	0.803
			ST9F	742	60.5	0.0320	0.631	0.0395	0.0398	0.891
			ST36	734	59.8	0.0319	0.545	0.0341	0.0338	0.811
			ST7A	450 (d)	36.7 (d)	0.0613	1.175	0.0734	0.0741	0.936
7475-T7351	3.00	513365	ST8B	697	56.8	0.0368	0.735	0.0459	0.0467	0.835
			ST9C	869	70.8	0.0058	0.433	0.0271	0.0271	0.802
			ST11D	630	51.3	0.0480	0.755	0.0472	0.0458	0.213
			ST10E	760	62.0	0.0351	0.539	0.0337	0.0332	1.017
			ST12F	382	31.1	0.0631	1.173	0.0733	0.0724	1.042
										0.861

NOTES: (a) Estimated elliptical flaw sizes determined from SEM photos of specimen fracture surfaces.
(b) Refer to Fig. 22a for flaw geometry nomenclature.

(c) No detectable crack growth, assume chord crack of depth equal to the original starter notch.

(d) Failure occurred during fatigue loading, breaking load assumed equal to maximum cyclic load.

(e) Failed at the specimen shoulder.

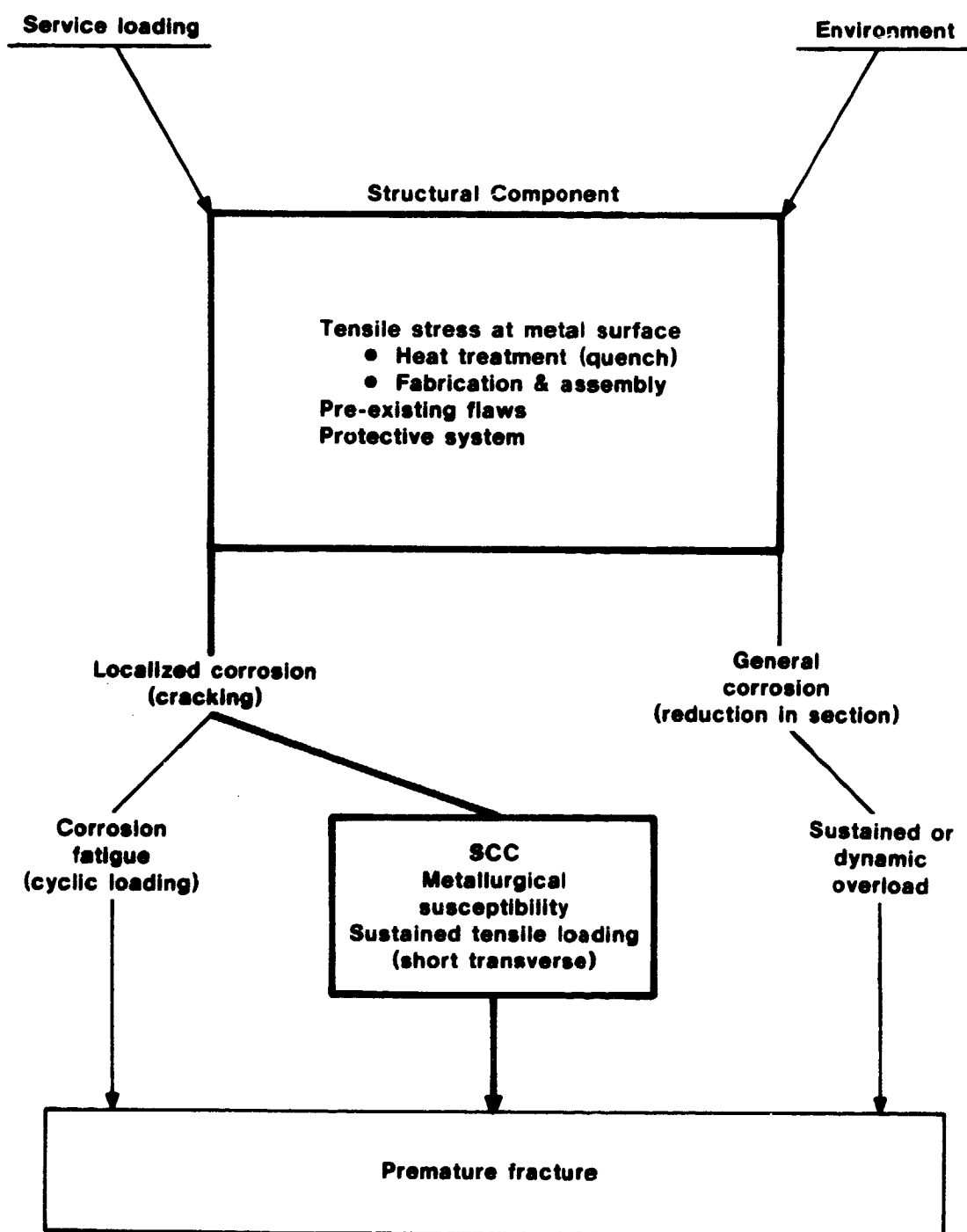
(f) Irregular shape part through crack at failure.

TABLE XII

SCC COMPARISONS OF THREE TEMPER VARIANTS OF 7075 ALLOY PLATE BY DIFFERENT
ACCELERATED SCC TEST METHODS - SHORT TRANSVERSE STRESS

Measure of SCC Susceptibility	Plate Temper	
	T651	T7X1
Original Mechanical Properties		
Tensile Strength, ksi	74.4	70.1
Yield Strength, 0.2% Offset, ksi	61.7	59.5
Fracture Toughness (S-L), K_{Ic} , ksi $\sqrt{in.}$	19.3	19.4
Smooth 0.125 In. Tension Specimens Exposed to 3.5% NaCl Alternate Immersion Test (ASTM G44)		
Breaking Load Test Method		
Statistical Threshold Stress - 99% Survival, 95% Confidence, ksi (%YS)	17(27)	31(50)
Probability of Survival at Exposure Stress of 30 ksi, 6 Days Exposure, %	0	100
99% Survival Stress at Exposure Stress of 40 ksi, 6 Days Exposure, %	0	71
99% Survival Stress at Exposure Stress of 3 ksi, 6 Days Exposure, ksi (%YS)	0	53(85)
99% Survival Stress at Exposure Stress of 40 ksi, 6 Days Exposure, ksi (%YS)	0	64(107)
Calculated Mean SCC Flaw Depth Stress of 0 ksi, 6 Days Exposure, in.	.016	.009
Calculated Mean SCC Flaw Depth Stress of 20 ksi, 6 Days Exposure, in.	$\geq .056$.013
Calculated Mean SCC Flaw Depth Stress of 30 ksi, 6 Days Exposure, in.	$\geq .052(a_c)$.018
Calculated Mean SCC Flaw Depth Stress of 40 ksi, 6 Days Exposure, in.	$\geq .043(a_{cr})$.029
99% Penetration Limit at Exposure Stress of 20 ksi, 6 Days Exposure, in.	$\geq .070$.019
99% Penetration Limit at Exposure Stress of 30 ksi, 6 Days Exposure, in.	∞	.028
99% Penetration Limit at Exposure Stress of 40 ksi, 6 Days Exposure, in.	∞	.015
Average SCC Growth Rate (2-4-6 days) Stress of 20 ksi, in./hr.	3.8×10^{-4}	6.3×10^{-5}
Average SCC Growth Rate (2-4-6 days) Stress of 30 ksi, in./hr.	5.4×10^{-4}	6.9×10^{-5}
Average SCC Growth Rate (2-4-6 days) Stress of 40 ksi, in./hr.	--	1.5×10^{-4}
Traditional Pass-Fail Analysis - 6 Days Exposure Period		
Probability of Survival, Cum., at Exposure Stress of 30 ksi, %	0	100
Probability of Survival, Cum., at Exposure Stress of 40 ksi, %	--	80
Probability of Survival, Binomial Dist., 95% Conf. Limits 30 ksi, %	0-31	74-100
Probability of Survival, Binomial Dist., 95% Conf. Limits 40 ksi, %	--	44-93
Estimated Threshold Stress, ksi, 20 Days Exposure per ASTM G47	$20 > a_{th} > 10$	$40 > a_{th} > 30$
Fracture Mechanics Specimens - 3.5% NaCl added Dropwise to Precrack		
WOL Specimens (S-L), Fatigue Precracked, Ring Loaded		
Estimated K_{Isc} , ksi $\sqrt{in.}$ (% K_{Ic})	5(26)	13(67)
UCB Specimens (S-L), Tension Pop-In, Bolt Loaded		
Estimated K_{th} , ksi $\sqrt{in.}$ (% K_{Ic})	--	16(82)
Estimated Plateau Velocity, in./hr.	4.5×10^{-4}	1.1×10^{-4}
Average Initial Velocity (0-1000 hr.), in./hr.	4.0×10^{-4}	5.6×10^{-5}
(a_{cr}) Corresponds to the critical flaw depth estimated by the wide range EPFM solution (equation (8)) when the exposure stress is equated to the breaking strength.		

ORIGINAL PAGE IS
OF POOR QUALITY

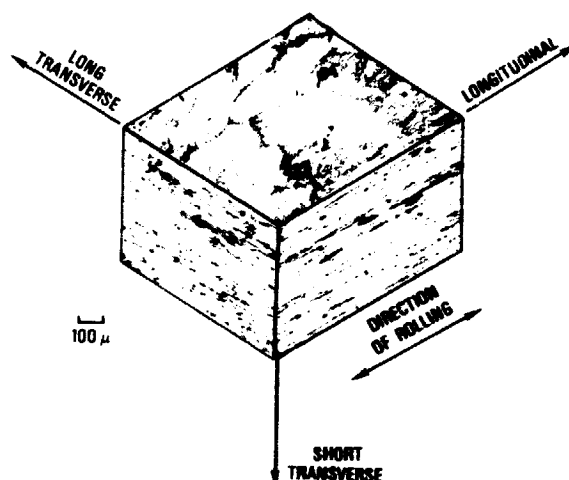


SCC is one of the processes that can result from interaction of tensile stress and the environment with the surface of a structural component.

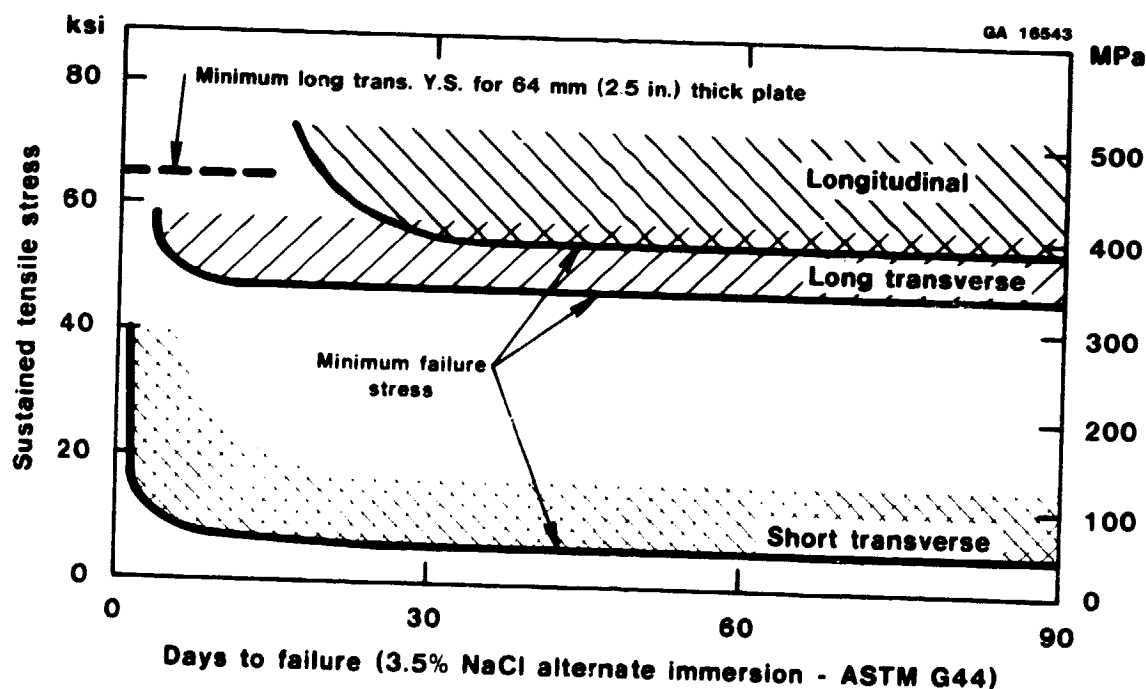
Causes of Premature Fracture Influenced by Corrosion of a Structural Component.

Figure 1

ORIGINAL PAGE IS
OF POOR QUALITY



Directional Grain Structure of 7075-T651 Hot Rolled Plate

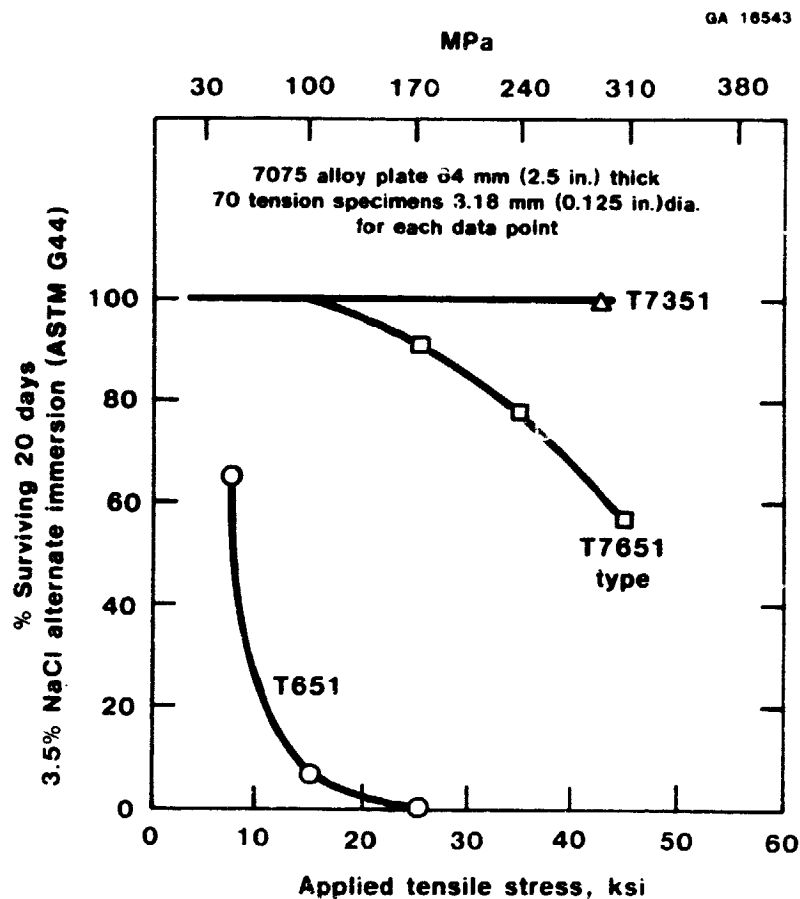


Tests were made on 3.18 mm (0.125 in.) diameter tension specimens machined from the mid-plane of 7075-T651 plates of various thicknesses. The solid line, lower bound defines the SCC performance of test specimens with different orientation to the grain structure. Note the relatively low stress levels at which short transverse specimens failed compared to the long transverse and longitudinal specimens (Ref. 1).

Effects of the Magnitude of Sustained Tensile Stress and Its Orientation Relative to the Grain Structure on the SCC Resistance of a Metallurgically Susceptible Material

Figure 2

ORIGINAL FILED IN
OF POOR QUALITY

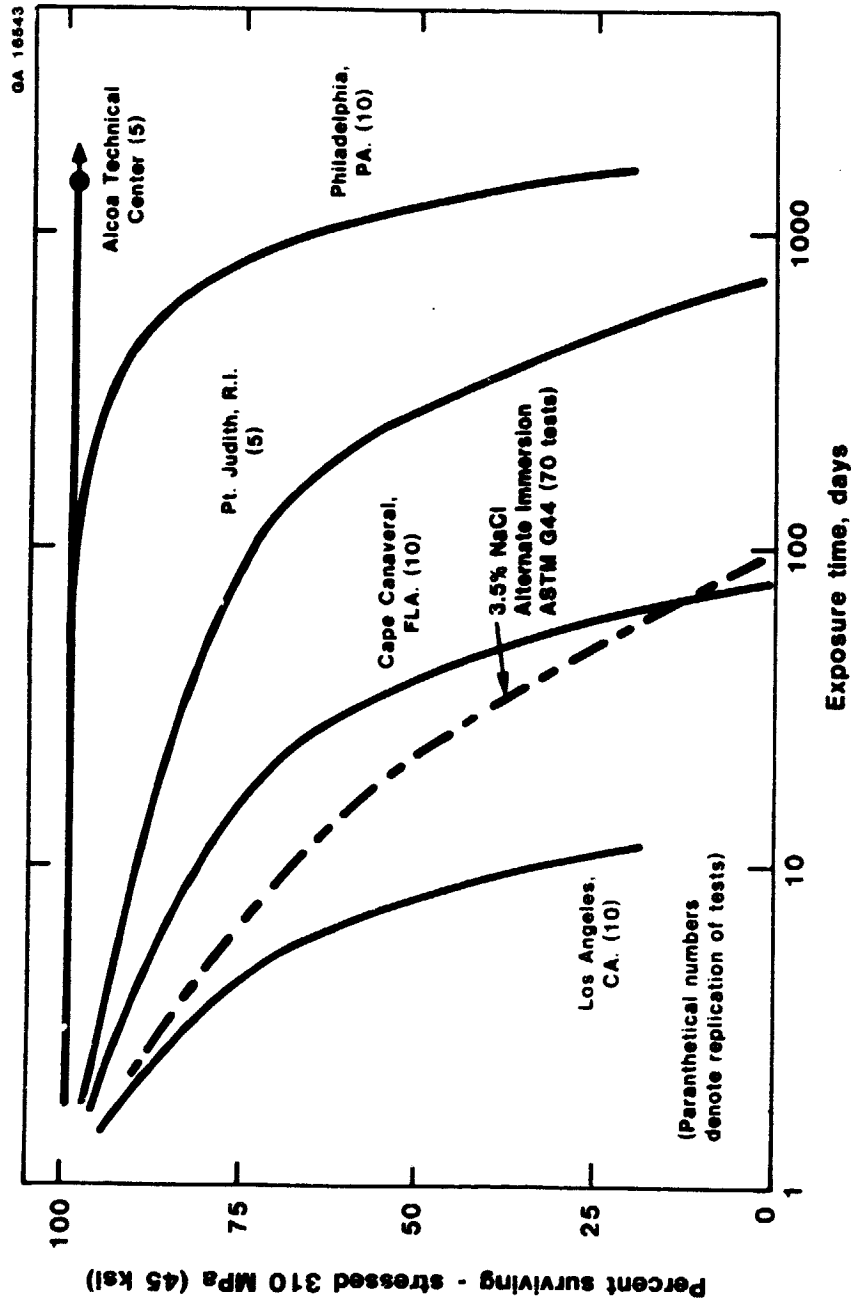


The metallurgical susceptibility to SCC is significantly less for the T7351 and T7651-type tempers. Their improved performance compared to the T651 is indicated by the higher percent survival curves shown as a function of stress (Ref. 1).

**Effect of Temper on SCC Performance of Alloy 7075 Plate Stressed
in the Critical Short Transverse Direction.**

Figure 3

ORIGINAL FILED
OF POOR QUALITY



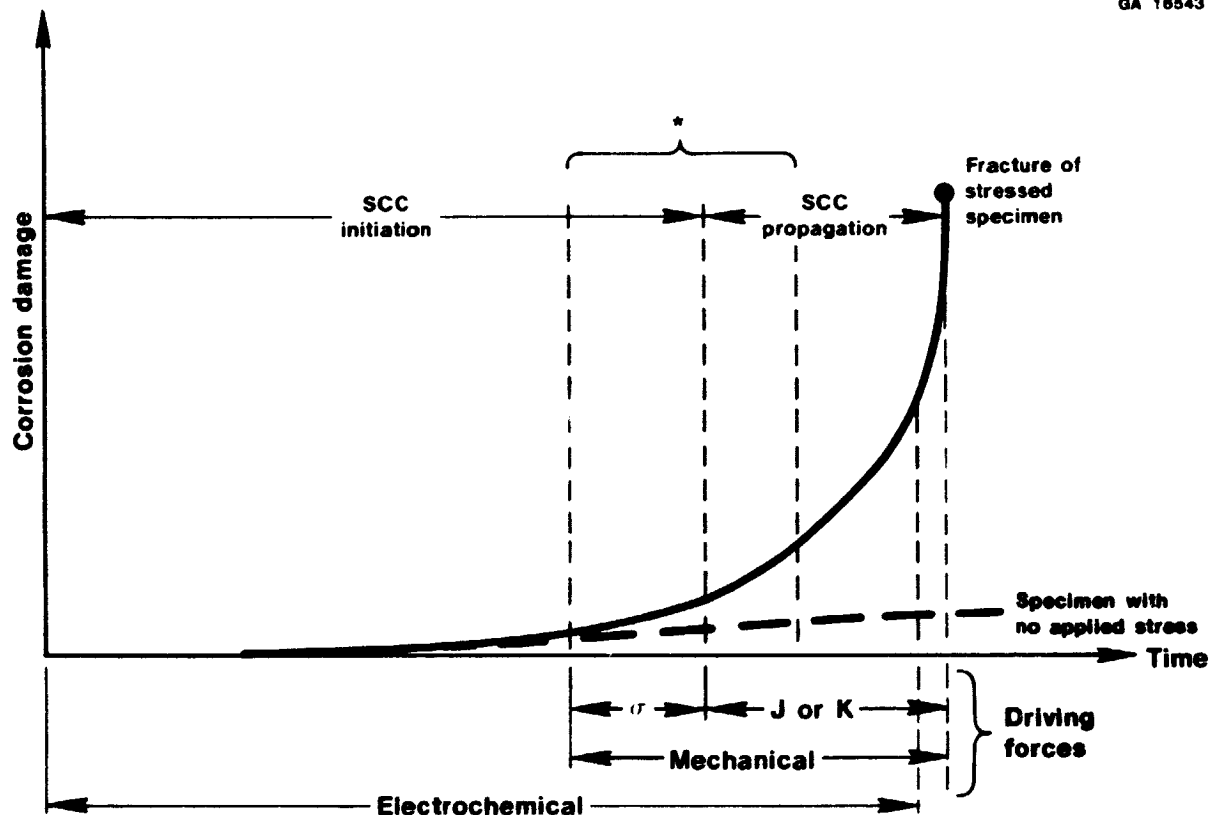
Tests were made on short transverse 3.18 mm (0.125 in.) diameter tension specimens from the same lot of 7075-T7651 type plate included in Figure 3.

Effect of Variations in Geographic Atmospheric Environment on the Probability and Time to Failure by SCC of a Material with an Intermediate Susceptibility

Figure 4

ORIGINAL PAGE
OF POOR QUALITY

GA 16543

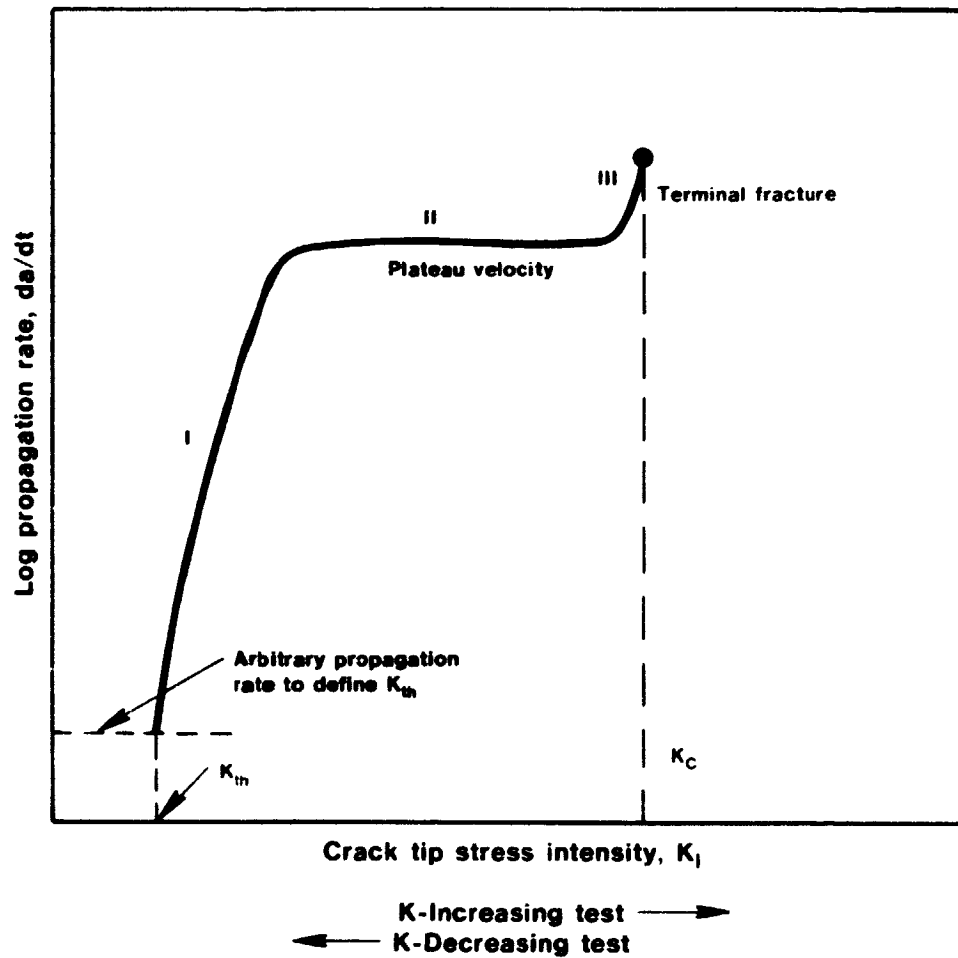


*Transition of driving force from dominance by electrochemical factors to chiefly mechanical factors. Precise separation of "initiation" and "propagation" stages is experimentally difficult. Stimulation of cracking by atomic hydrogen may also become involved in this transition region.

**The Relative Influences of Electrochemical and Mechanical Factors
in the Corrosion and SCC Damage to a Susceptible Material
Figure 5**

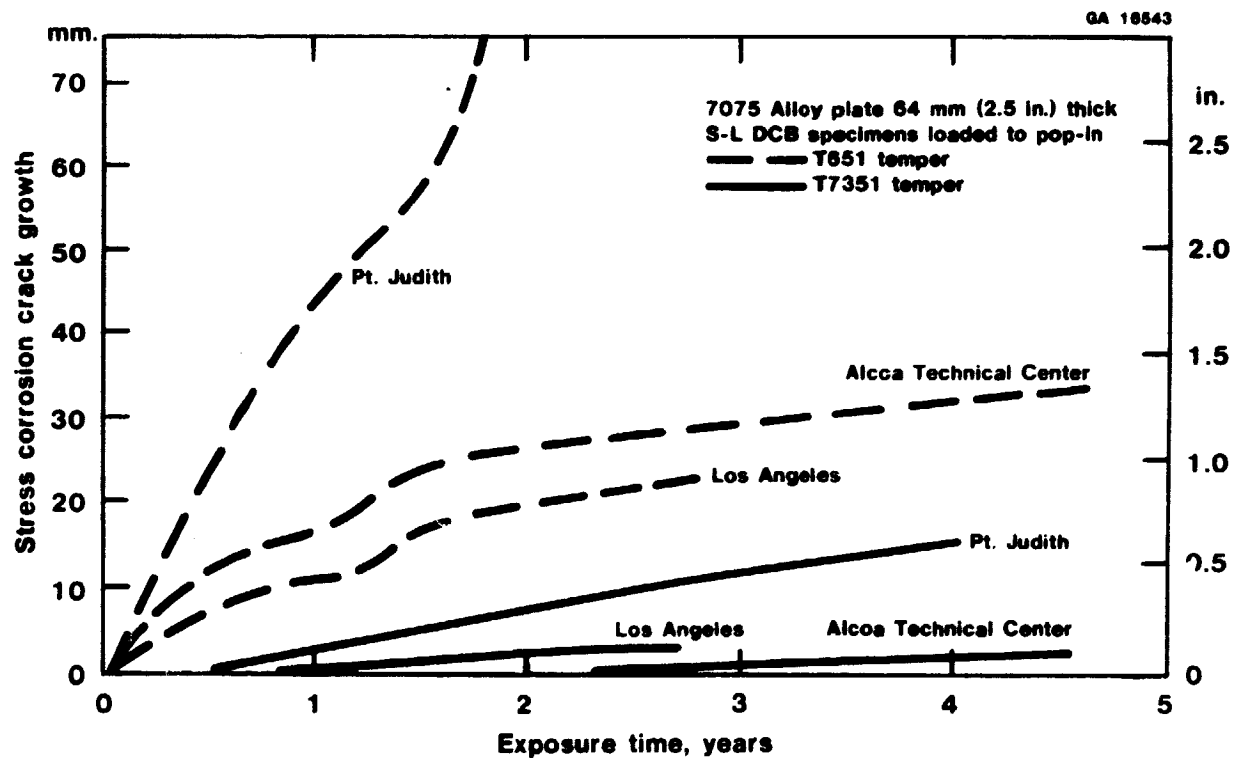
ORIGINAL PAGE IS
OF POOR QUALITY

QA 18843



Application of Linear Elastic Fracture Mechanics (LEFM)
to the Propagation of SCC
Figure 6

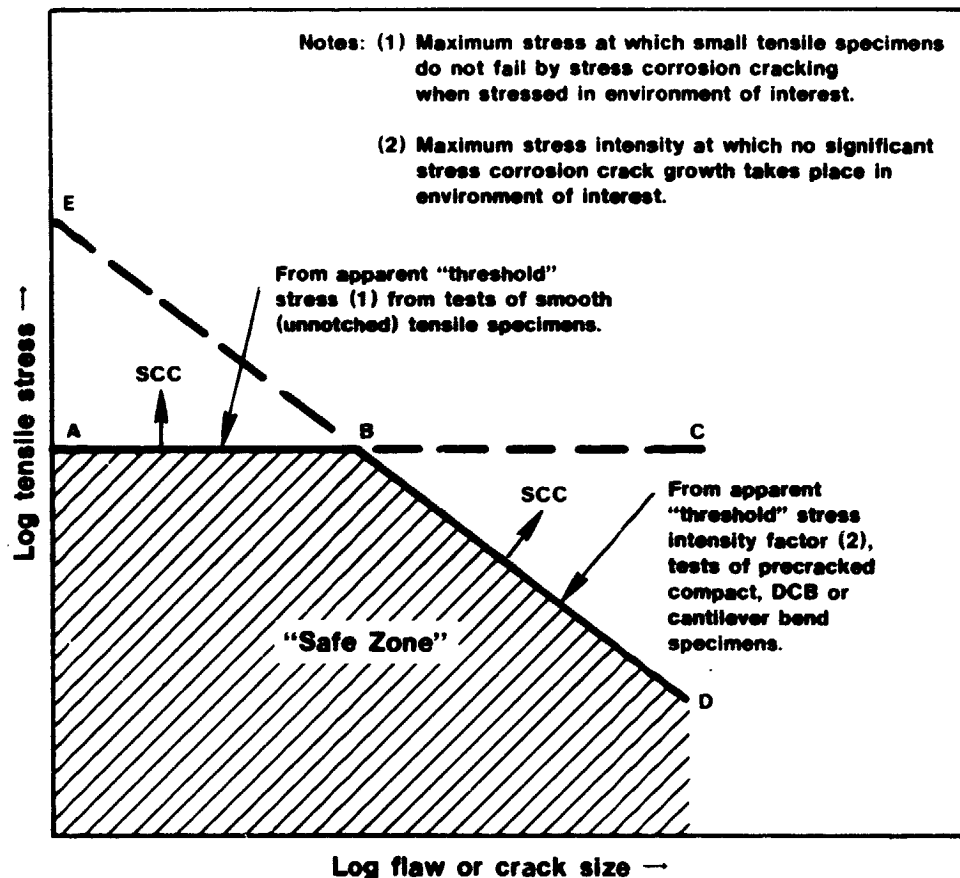
ORIGINAL PAGE
OF POOR QUALITY



Comparison of SCC Growth in 7075 Alloy Plate for Various
Geographical Locations within the Continental United States
Figure 7

ORIGINAL PAGE
OF POOR QUALITY

QA 16543



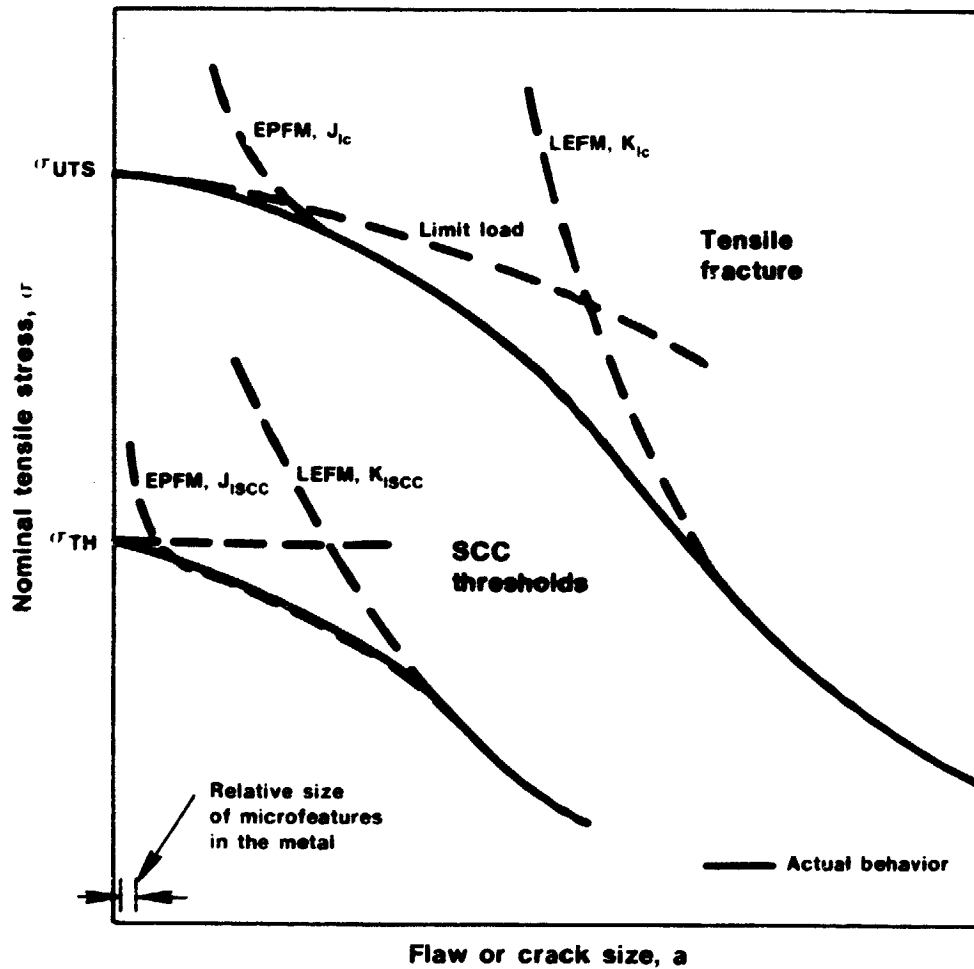
This diagram shows how the exclusive use of either one of the test methods could yield non-conservative conclusions. Consideration of a "safe zone" requires careful interpretation of the specific test conditions.

Schematic Diagram of a Concept for Combining Stress Corrosion Thresholds Obtained on Smooth and LEFM Specimens to Give a Conservative Assessment of Materials

Figure 8

ORIGINAL PAGE 17
OF POOR QUALITY

GA 10543

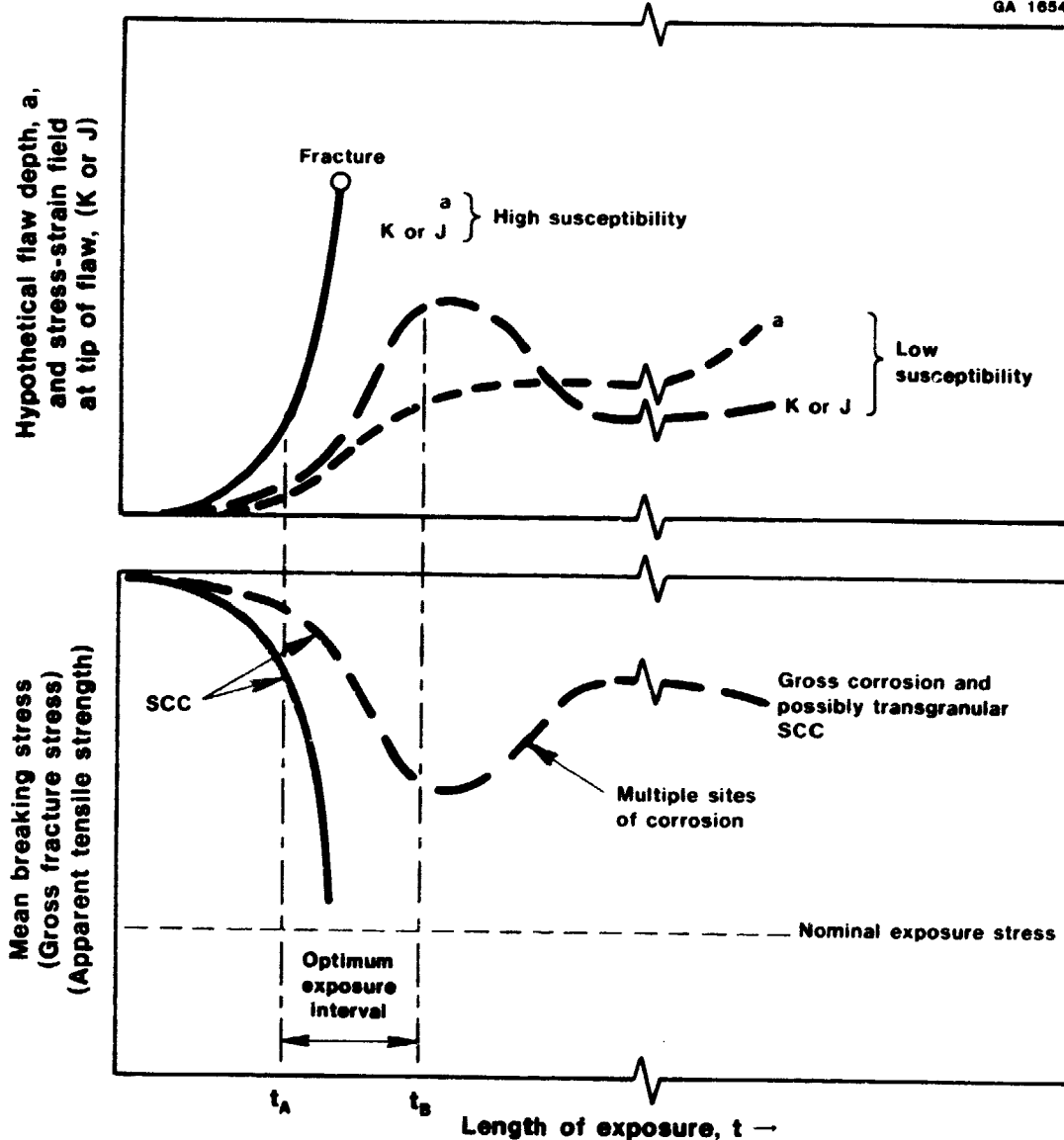


Proposed Linear-Elastic and Elastic-Plastic Models for Describing Critical Combinations of Stress and Flaw Size at SCC Thresholds and at the Onset of Rapid Tensile Fracture.

Figure 9

ORIGINAL PAGE
OF POOR QUALITY

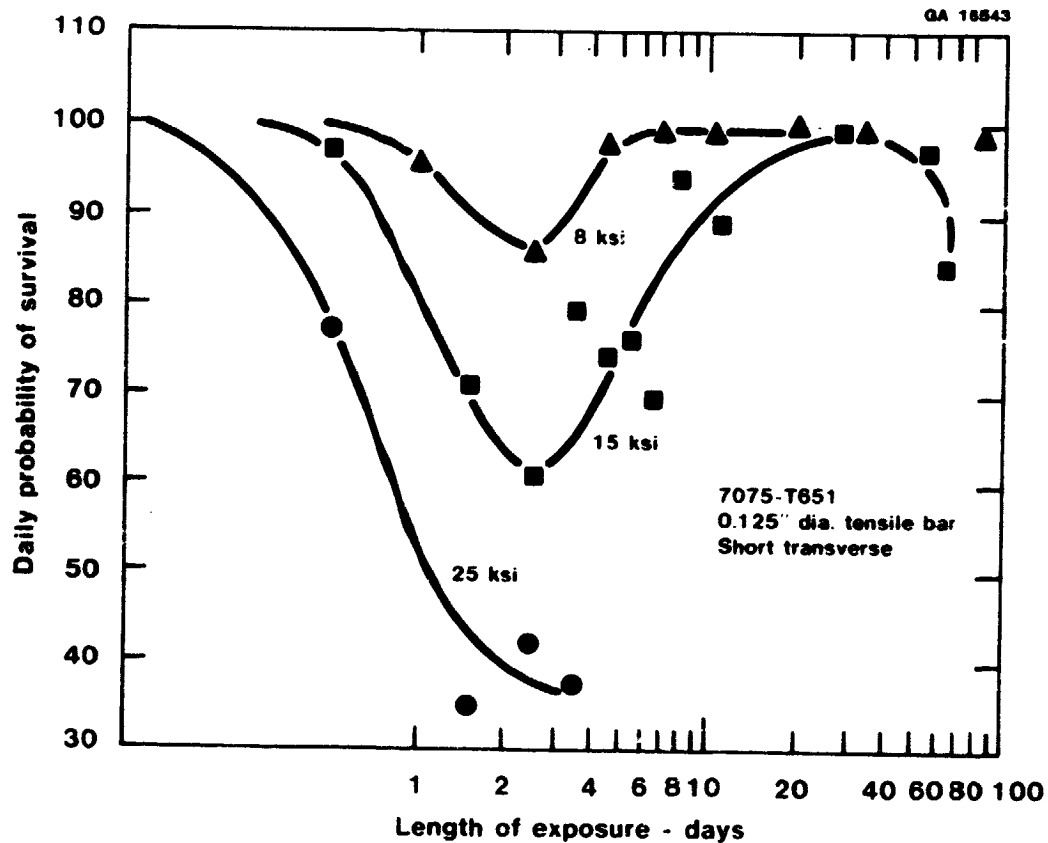
GA 16543



Schematic Representation Showing the Effect of Stress Corrosion Crack Growth and the Concurrent Crack Tip Stress and Strain Field Intensity (i.e., K or J) on Specimen Breaking Stress After Exposure to Environment Under Sustained Stress

Figure 10

ORIGINAL SOURCE
OF POOR QUALITY



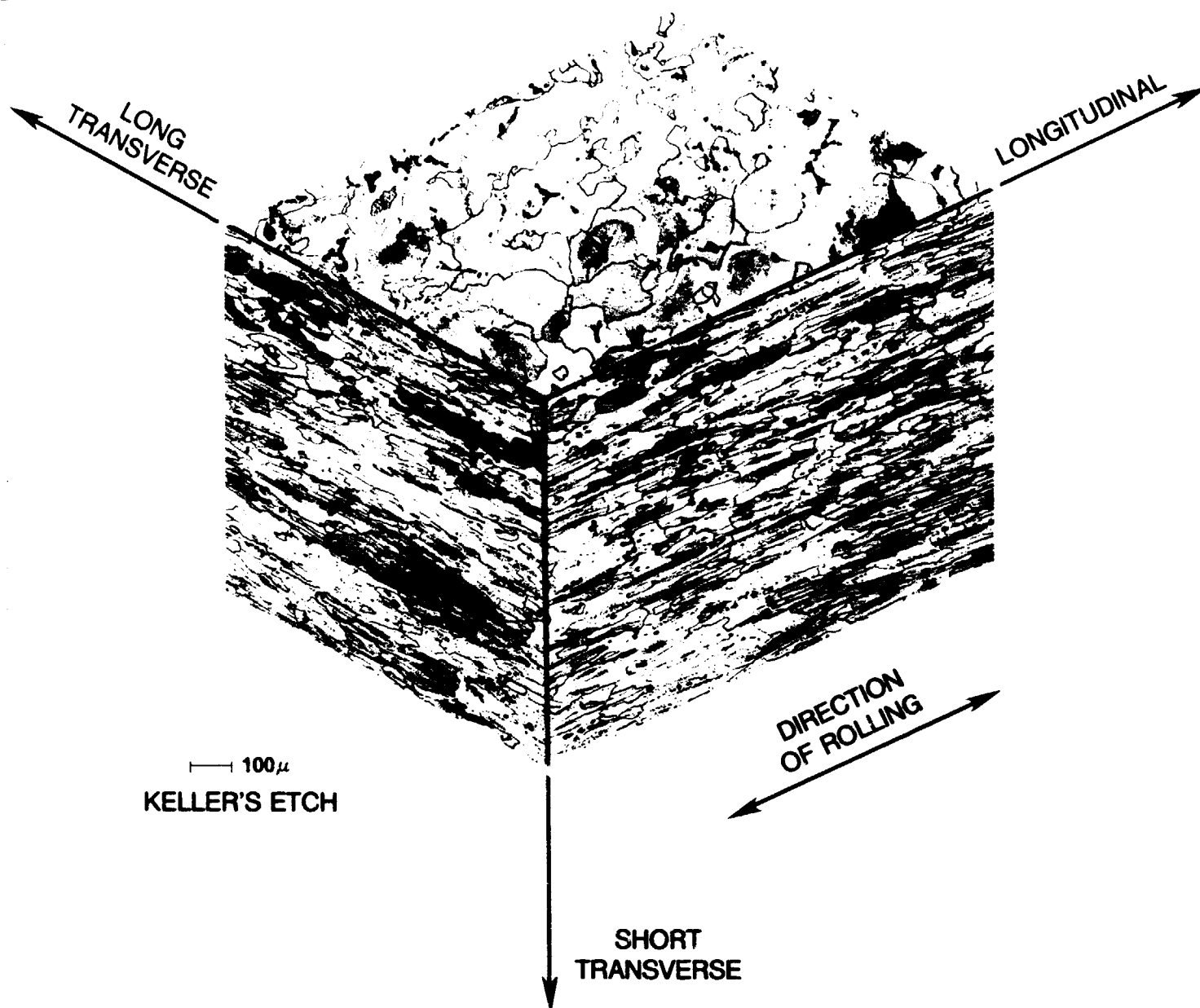
3.5% NaCl alternate immersion (ASTM G44)

This plot of data from Ref. 35 illustrates an increased daily probability of survival if the test specimen does not fail during the early part of exposure to aggressive environmental conditions.

Effect of Applied Stress and Length of Exposure on Daily Probability of Survival of Alloy 7075-T651.

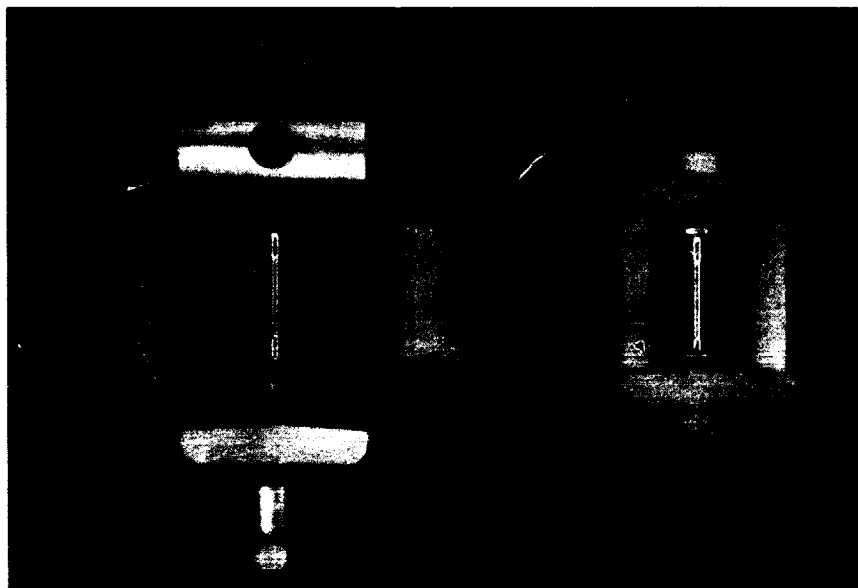
Figure 11

ORIGINAL PAGE IS
OF POOR QUALITY

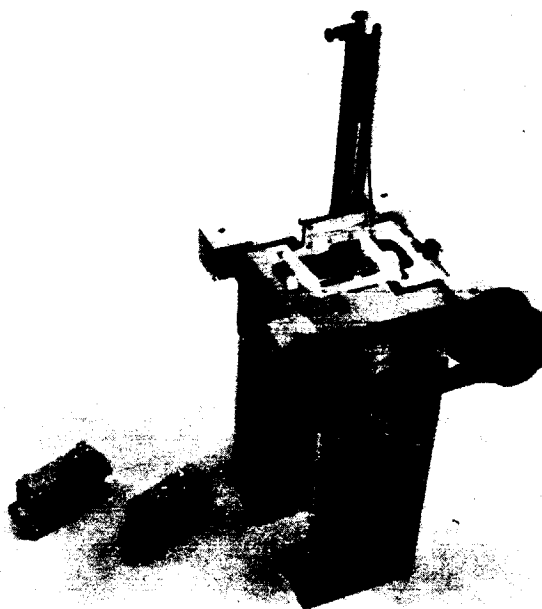


Grain Structure at Mid-Plane of 2.5 in. Thick Plate of 7075-T651
Figure 12

QA 16543



(a) Exploded view (left) showing the 1/8 in. diameter tension specimen and the various parts of the stressing frame. The final stressed assembly (right).

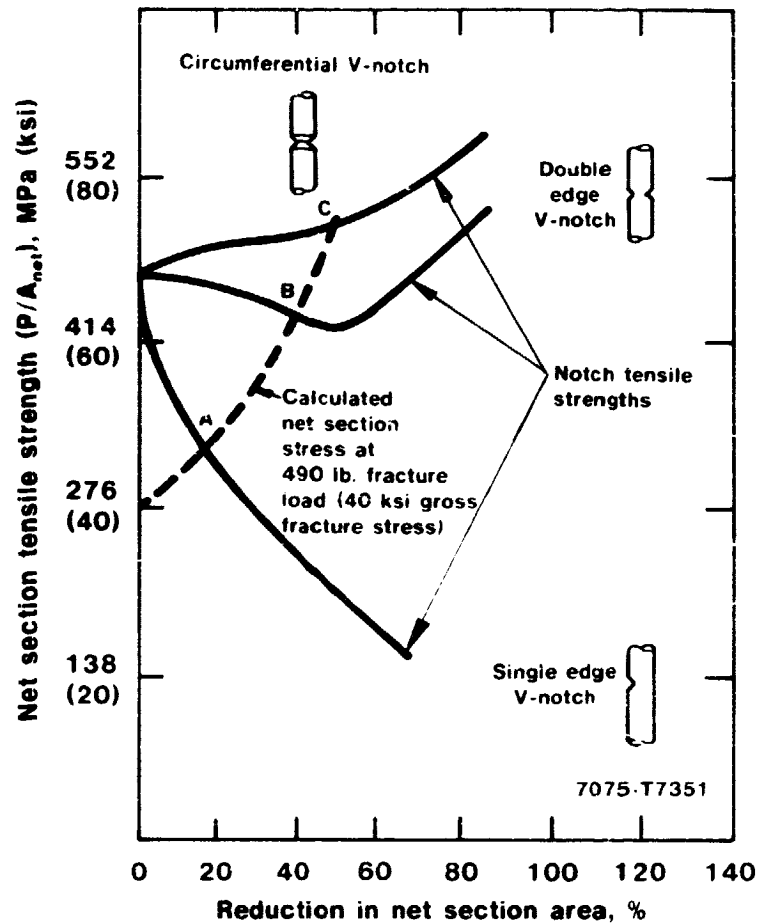


(b) Synchronous loading device used to stress specimens. The specimen is loaded to a prescribed strain value determined from a clip-on gage. The applied stress is given by the product of the strain and the material elastic modulus. A stressed assembly and one assembled finger-tight ready for stressing are shown.

Alcoa Stress Corrosion Testing Frame and Specimen Loading Device
Figure 13

ORIGINAL DOCUMENT
OF POOR QUALITY

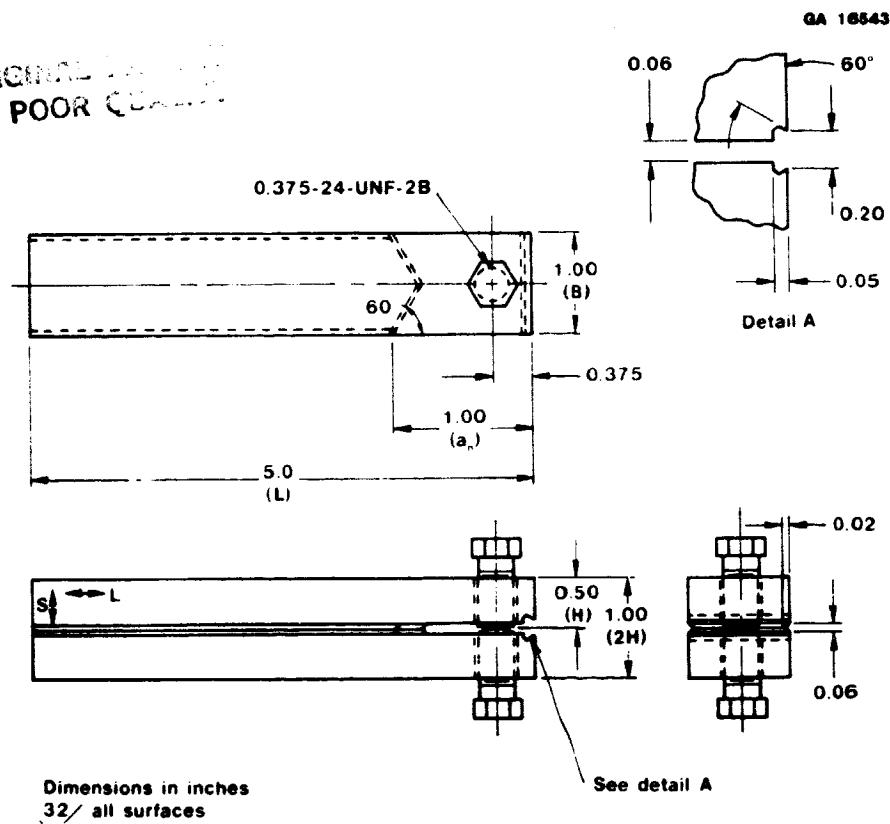
GA 16543



Results of Notch Tensile Tests on Three Flaw Configurations in 0.125 inch Diameter 7075-T7351 Specimens Showing that the Net Section Stress is Notch Configuration Dependent.

Figure 14

ORIGINAL
OF POOR QUALITY



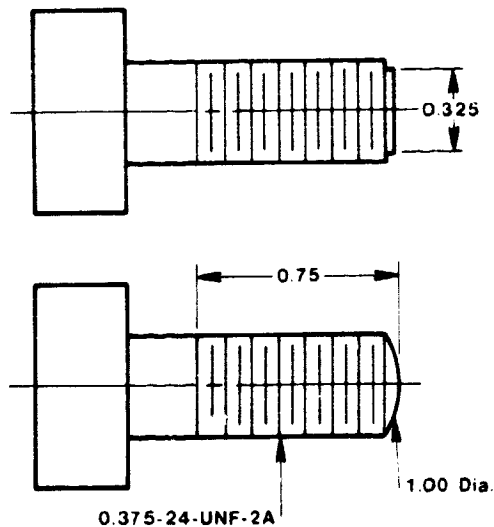
(a) Detailed Machine Drawing for Face Grooved DCB Specimen

Note 1 All dimensions in inches.
Tolerances not specified
0.005.

Note 2 Suggested material:
Austenitic stainless steel,
80,000 psi yield 125,000 psi
ultimate or:
410 stainless steel, heat
treat to Rc 38-43.
Commercial stainless steel
socket head cap screws are
satisfactory.

Note 3 Bolt head design optional.

Note 4 Use one rounded end and
one flat end bolt for
loading each specimen.

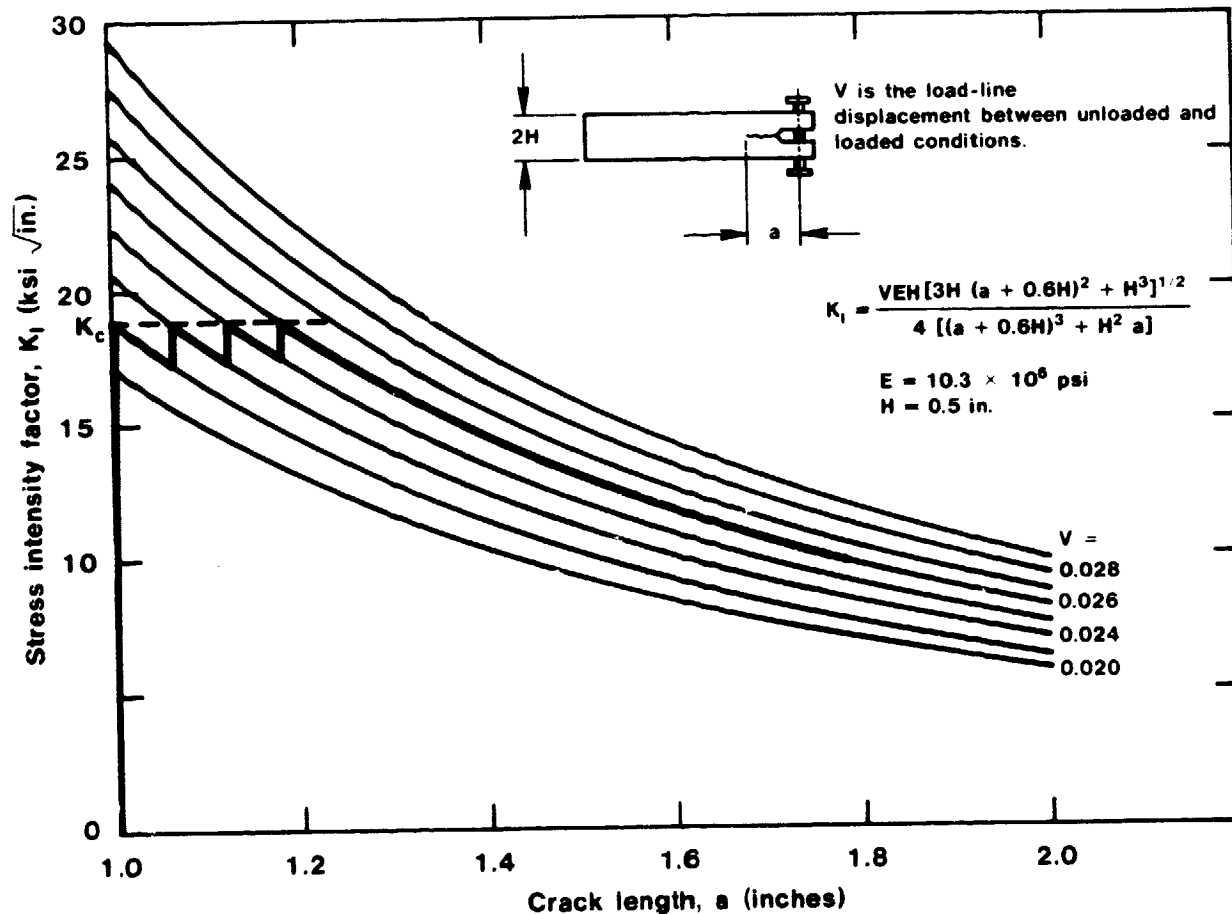


(b) Machine Drawing for DCB Specimen Loading Bolts

Face Grooved Double Catelever Beam (DCB) Specimen
Figure 15

ORIGINAL
OF POOR QUALITY

GA 16543



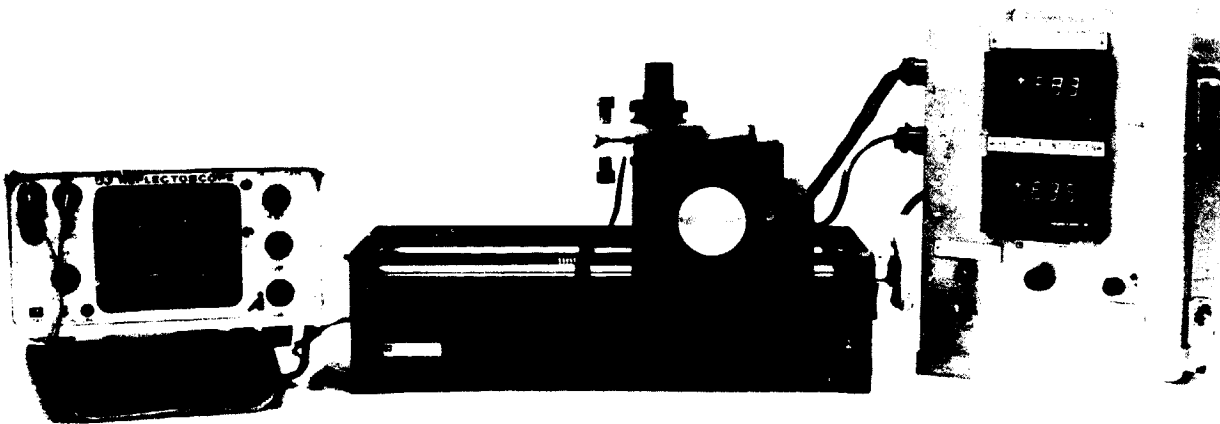
In a fixed displacement loaded DCB specimen, the stress intensity factor, K_I , decreases with crack extension. The highlighted line illustrates how K_I might vary during pop-in crack extension and subsequent environmental crack growth.

Stress Intensity Factor vs. Crack Length for the DCB Specimen, Crack Line Loaded by Constant Displacement.

Figure 16

ORIGINAL P.
OF POOR QUALITY

GA 16543

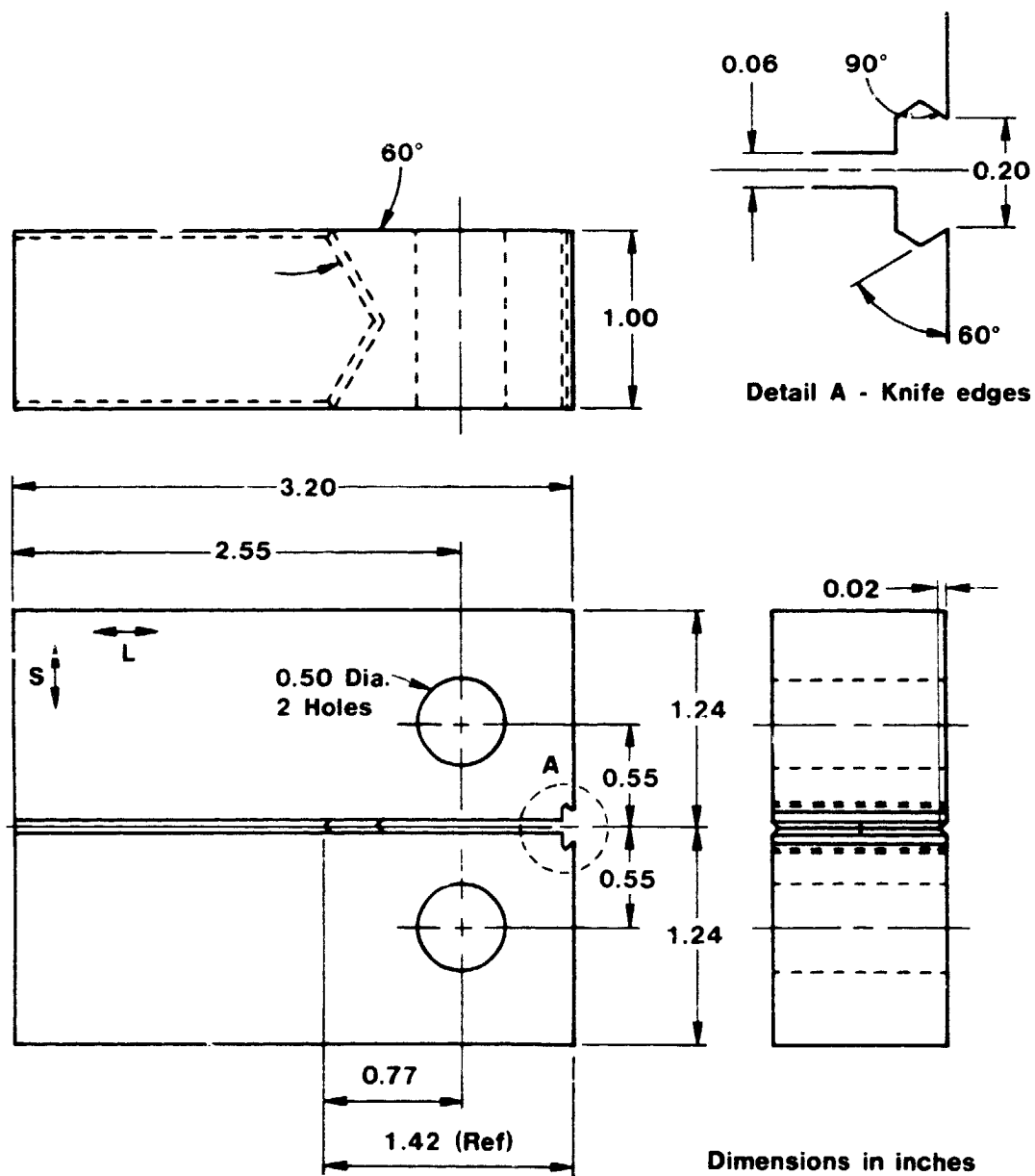


Bolt-loaded specimen is mounted in translation stage at center of picture. Ultrasonic transducer is located just above specimen, and the oscilloscope at left shows peaks indicating the top of specimen (left peak), the crack plane (center peak) and bottom face reflection (third peak). To the right are digital readouts of stage position and peak height for the crack front measurement used to make consistent positioning measurements.

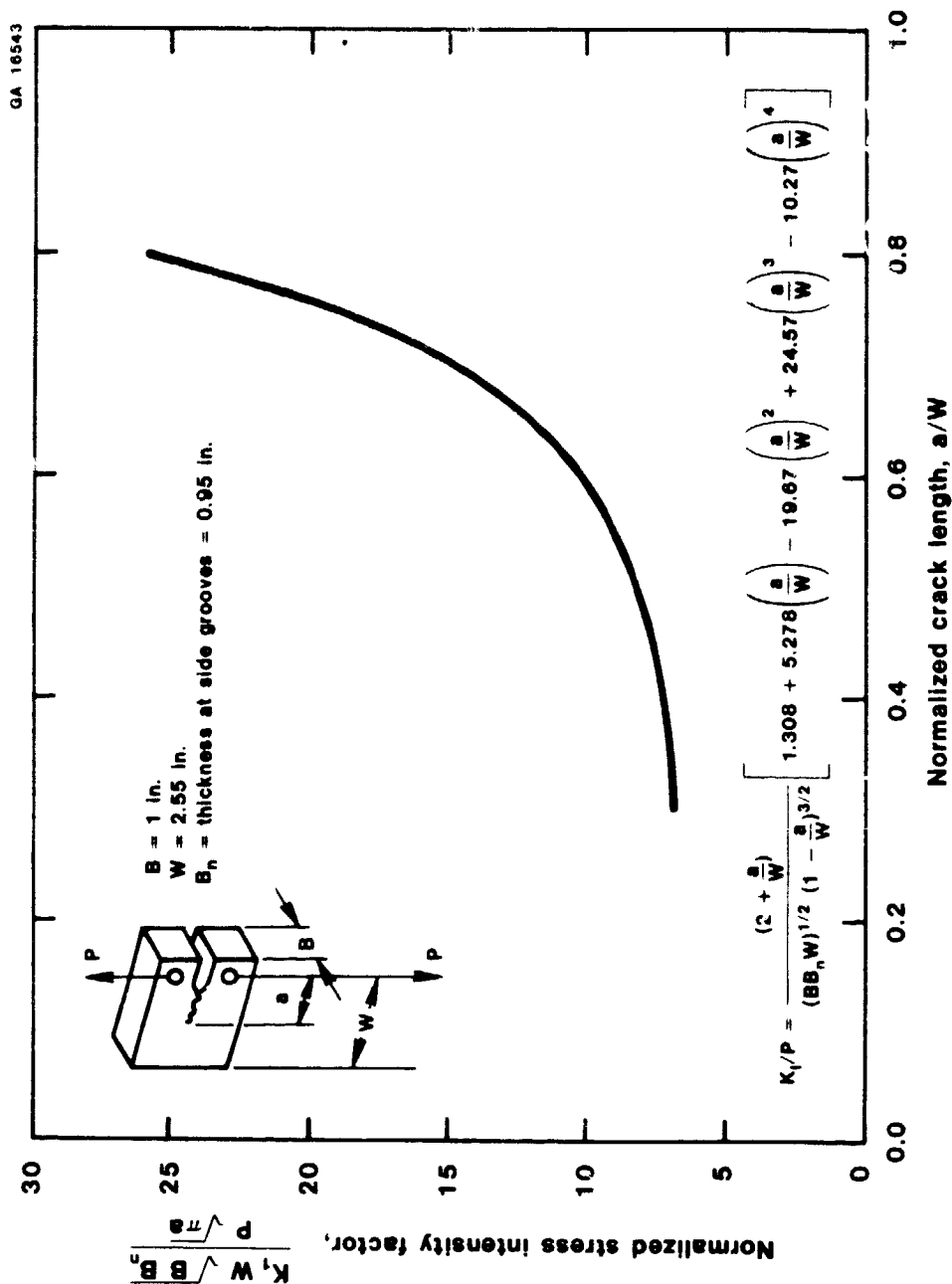
Ultrasonic Crack Measurement System Used for DCB Specimens
Figure 17

C-3

ORIGINAL FILED
OF POOR QUALITY



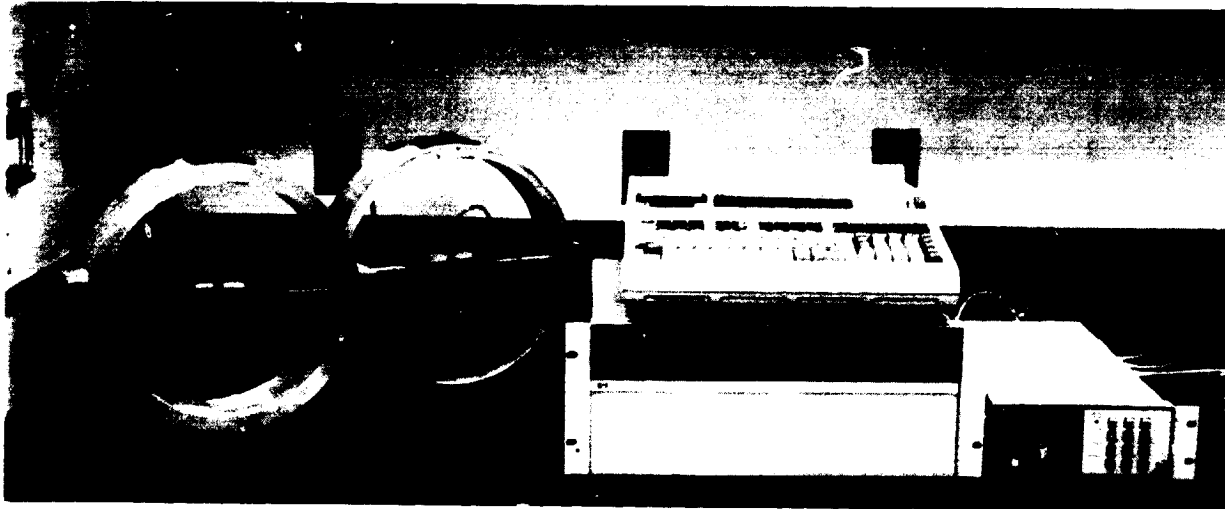
Detailed Geometry of the Pin-Loaded, Modified WOL Specimens
Figure 18



Stress Intensity Factor Solution for the Modified WOL Specimen
 Figure 19

ORIGINAL PAGE IS
OF POOR QUALITY

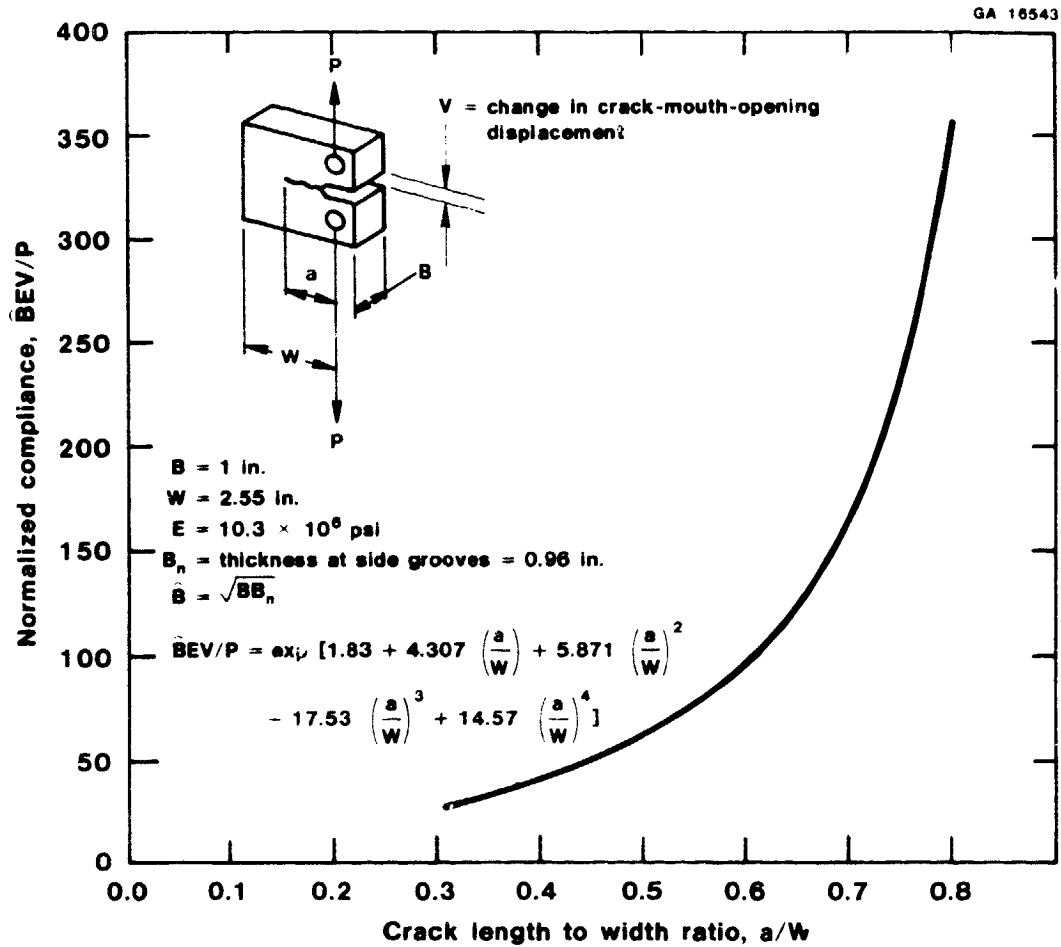
GA 16543



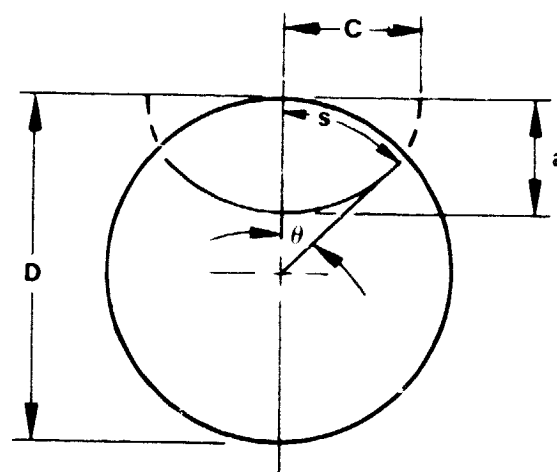
Two loading rings are shown with specimens and clip gages mounted. Box to the left of loading rings contains analog signal conditioning for load and displacement signals. The digital data acquisition system consists of a scanner connected to the analog load and displacement signals, a digital voltmeter, and a portable computer used to read and store data and to control the other instruments.

Ring-Loaded WOL Specimen Test Setup.
Figure 20

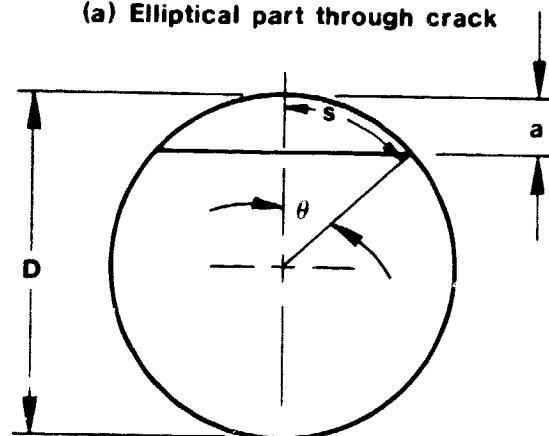
ORIGINAL PAGE IS
OF POOR QUALITY



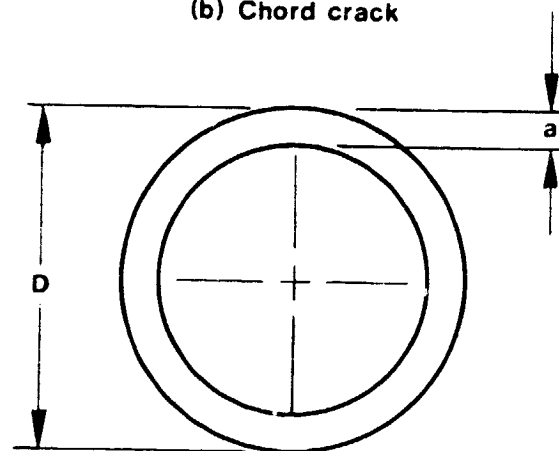
Normalized Compliance Relationship for the Modified WOL Specimen
Figure 21



(a) Elliptical part through crack



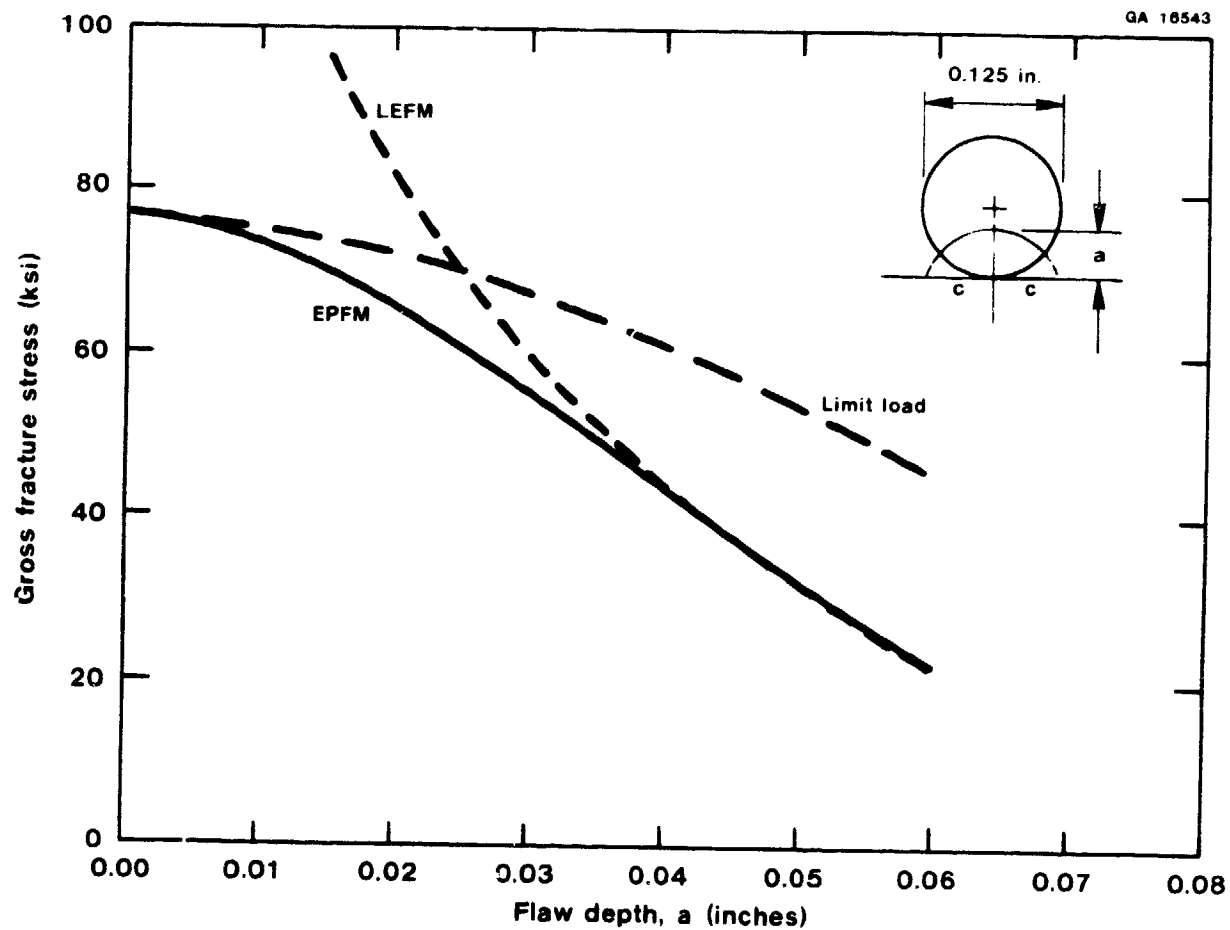
(b) Chord crack



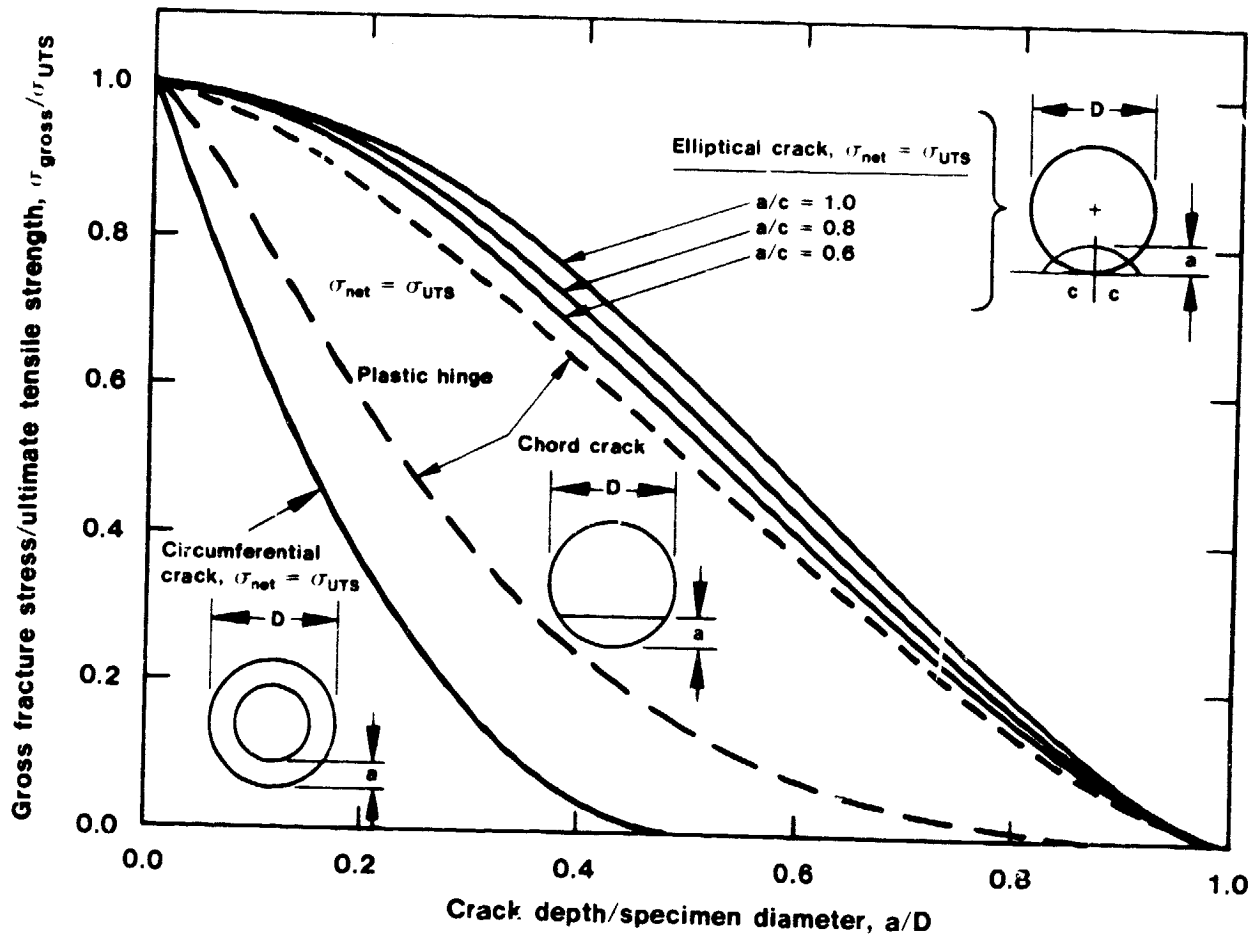
(c) Circumferential crack

Nomenclature for Three Practical Flaw Configurations
within a Cylindrical Tension Specimen
Figure 22

ORIGINAL 1-1-77
OF POOR QUALITY

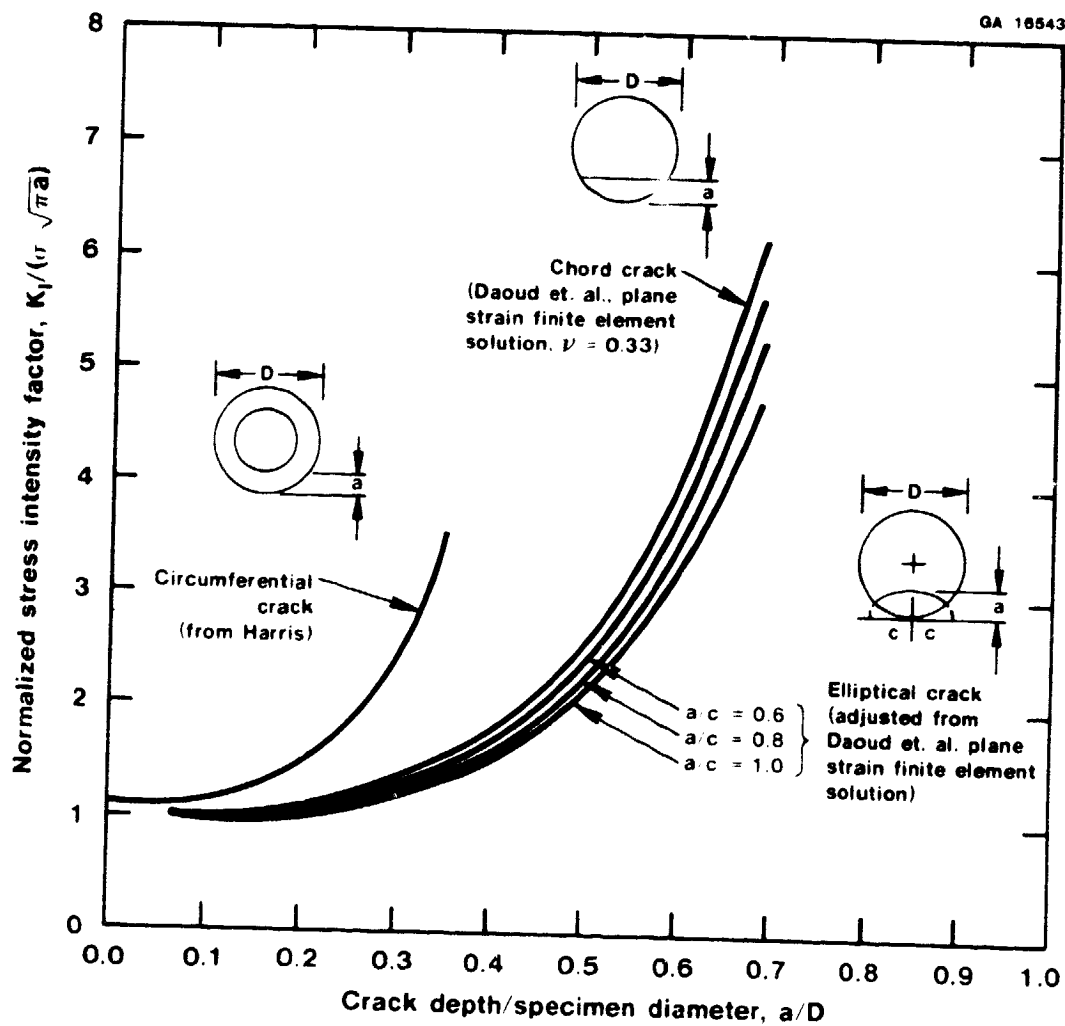


Limit Load, LEFM, and Estimated EPFM (Wide Range) Failure Criteria
for 0.125 in. Diameter, Short Transverse 7075-T651 Tension Specimens
Containing an Elliptical Flaw of Depth a and Aspect Ratio $a/c = 0.8$
Figure 23



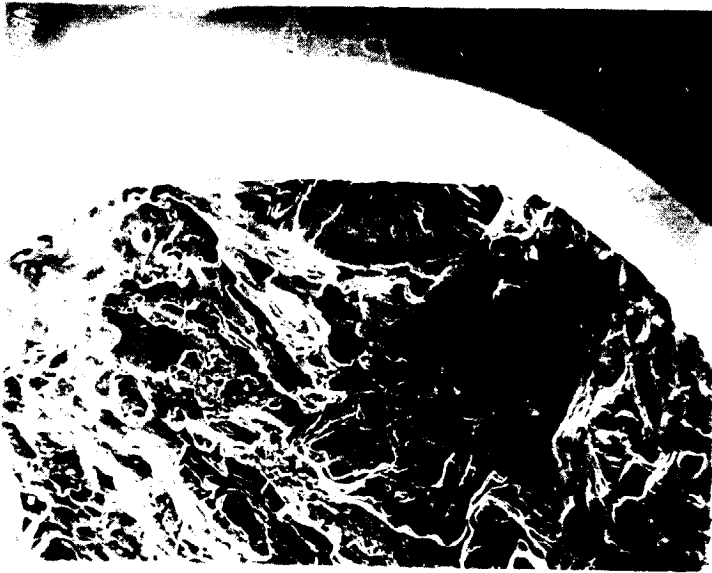
Normalized Limit Solutions for the Axial Loaded Cylindrical Tension Specimen with Various Crack Configurations and Depths.
Figure 24

ORIGINAL PAGE IS
OF POOR QUALITY



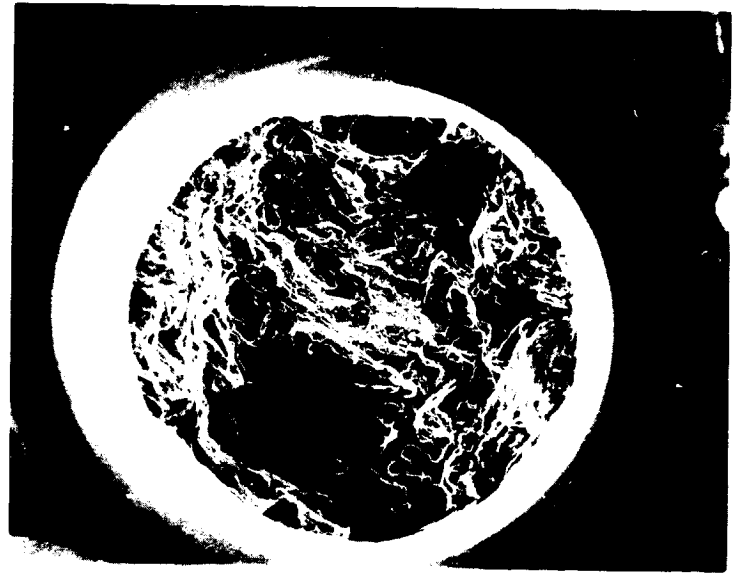
Stress Intensity Factor Solutions for Various Crack Configurations in an
Axial Loaded Cylindrical Tension Specimen.
Figure 25

ORIGINAL PAGE 18
OF POOR QUALITY



0.1 mm

Alloy: 7575-T651 Specimen No. 518351-ST9B

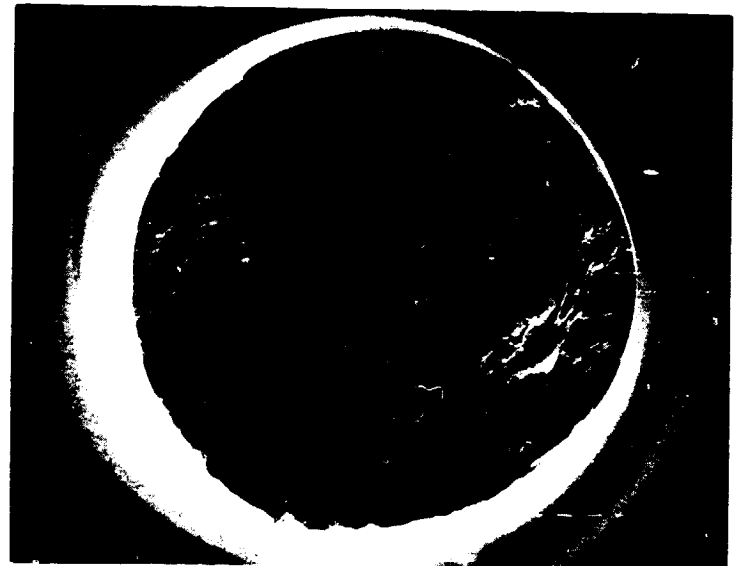


0.5 mm



0.1 mm

Alloy: 7475-T7651 Specimen No. 518358-ST3G

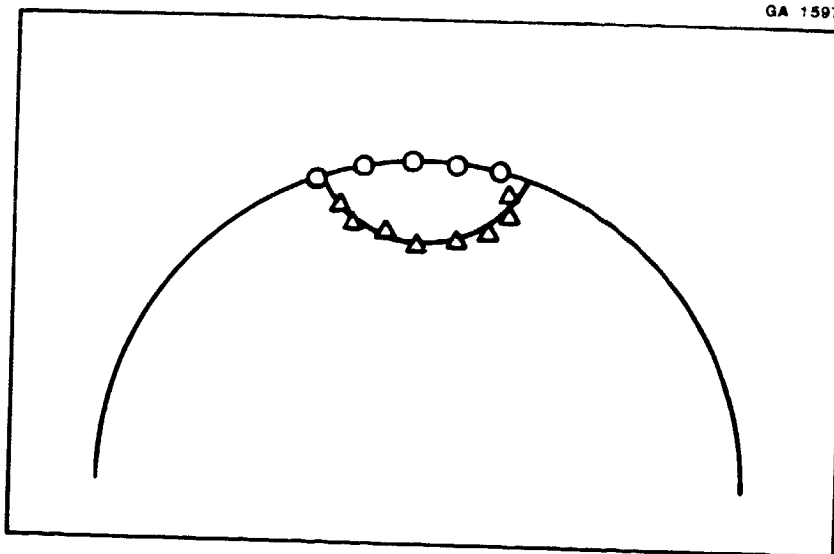


0.5 mm

Typical Fracture Surface Appearance of Chord-Notched and Fatigue
Precracked 0.125 in. Diameter Tension Specimens as Observed Under the
Scanning Electron Microscope
Figure 26

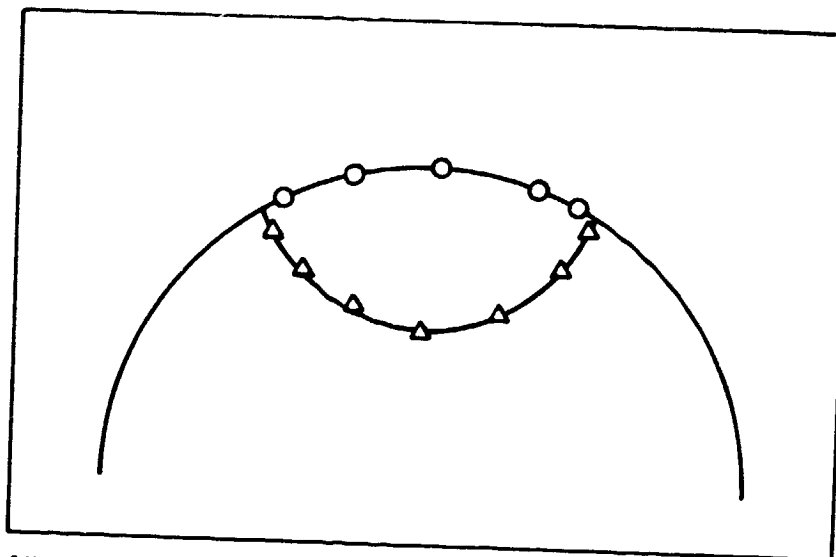
ORIGINAL POLYGRAPH
OF POOR QUALITY

GA 15973



Alloy: 7475-T651

Specimen No. 518351-ST9B

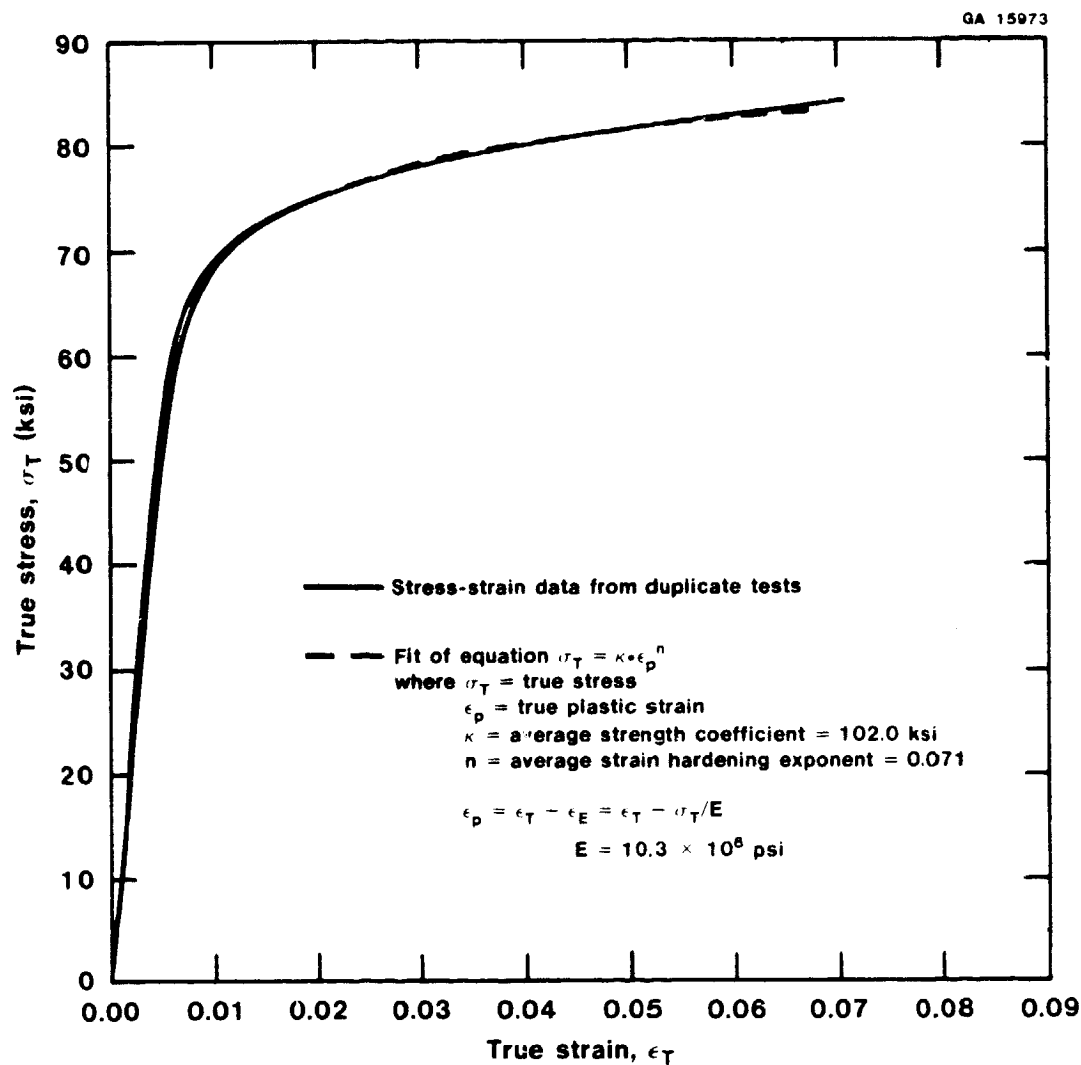


Alloy: 7475-T7651

Specimen No. 518358-ST3G

Typical Curve Fits through Digitized Data from SEM Fractographs
of Fatigue Cracks in 0.125 in. Diameter Tension Specimens
Figure 27

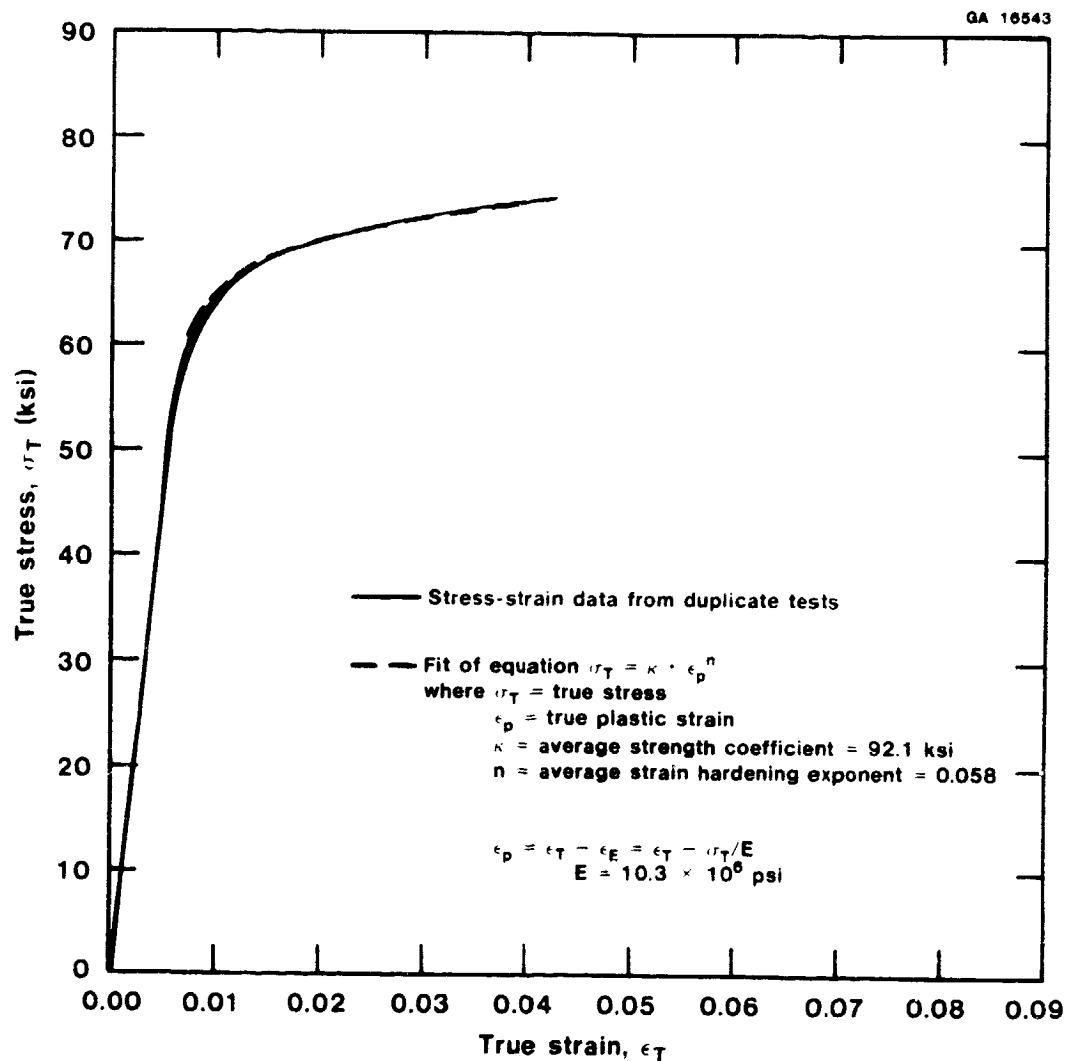
ORIGINAL PAGE 3
OF POOR QUALITY



7075-T651

Comparison of Actual and Fitted Short Transverse True
Stress-True Strain Behavior of 7075 Plate Alloys
Figure 28 (a)

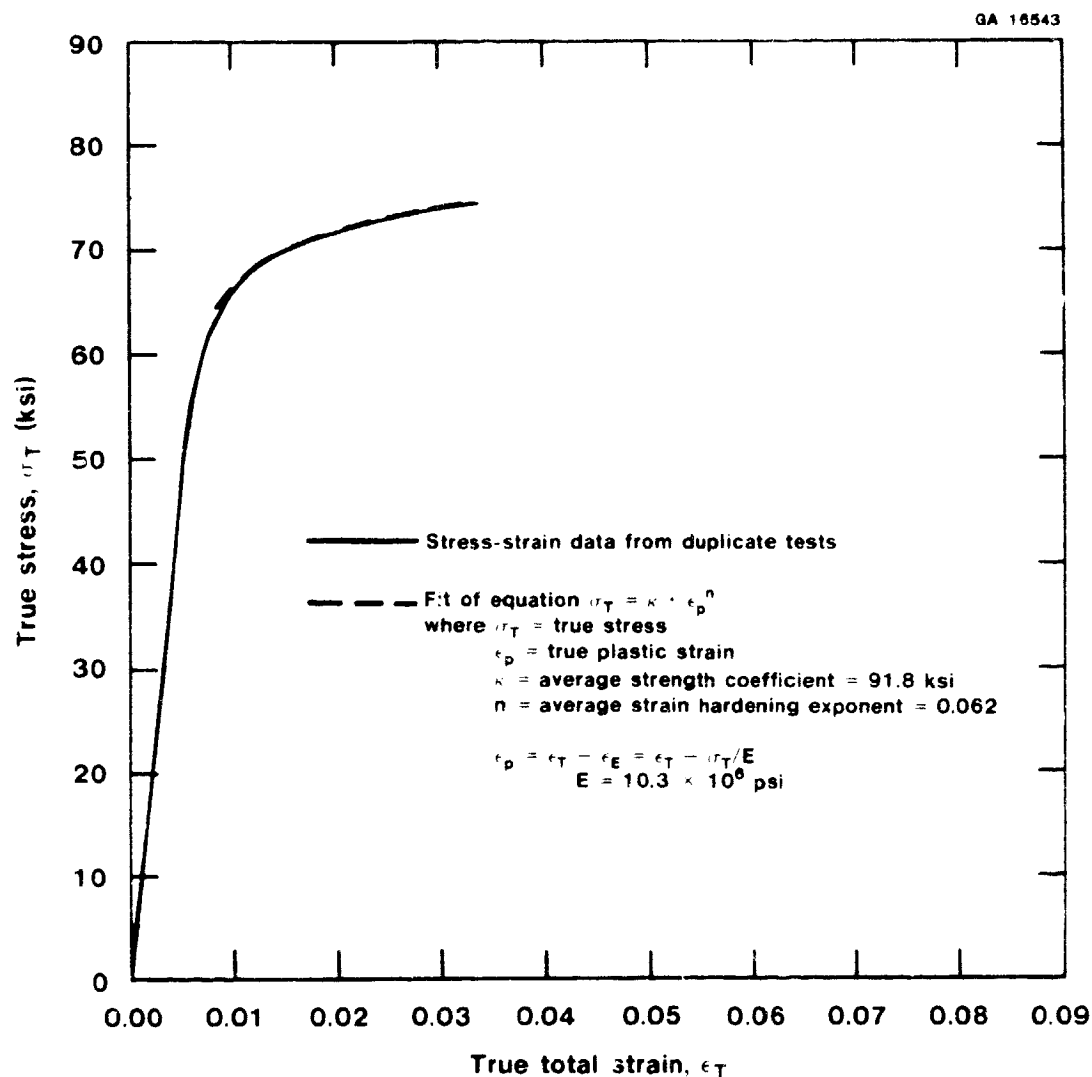
ORIGINAL PAGE IS
OF POOR QUALITY



7075-T7X1

Comparison of Actual and Fitted Short Transverse True Stress-
True Strain Behavior of 7075 Plate Alloys
Figure 28 (b)

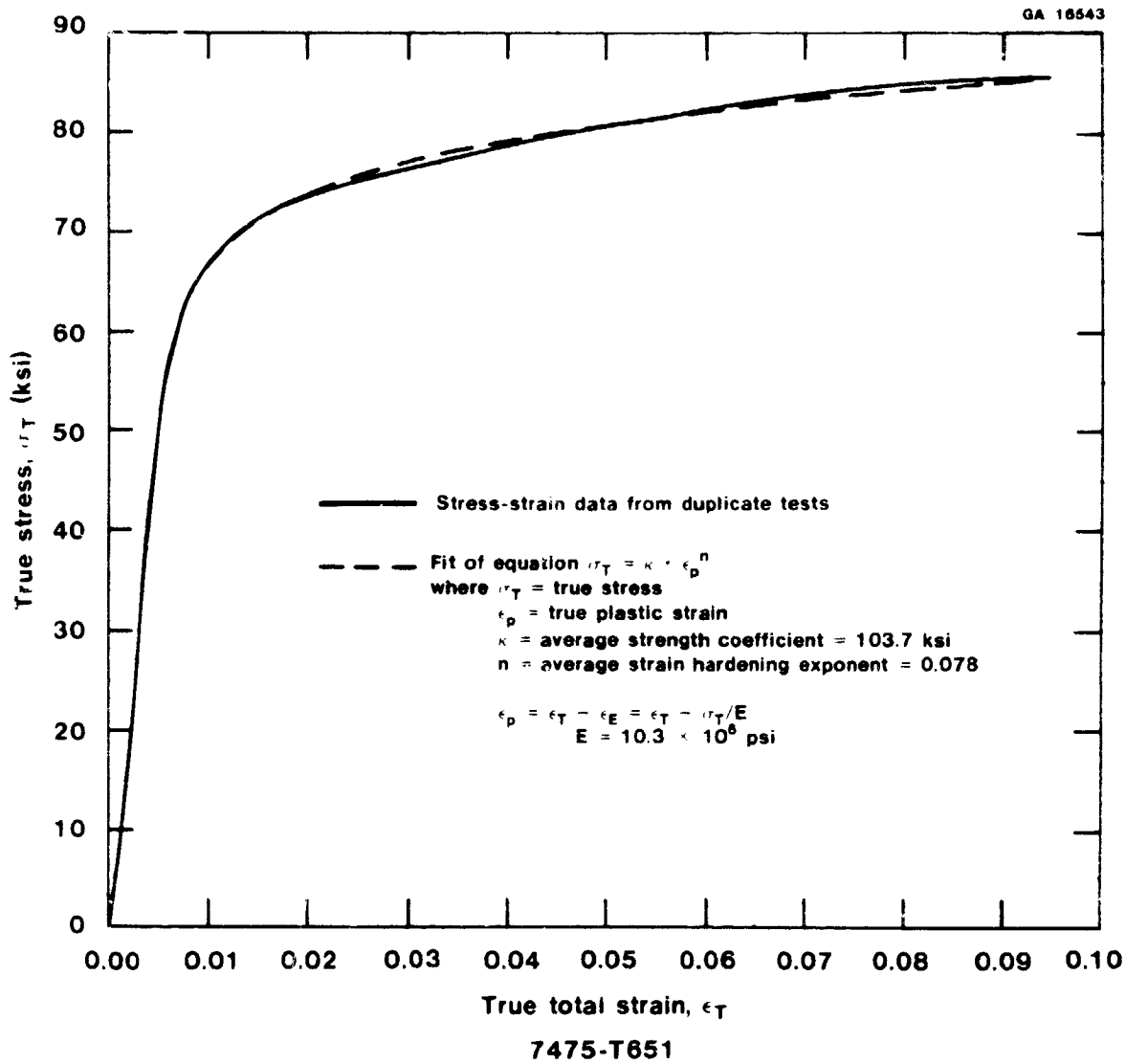
ORIGINAL P...
OF POOR QUALITY



7075-T7X2

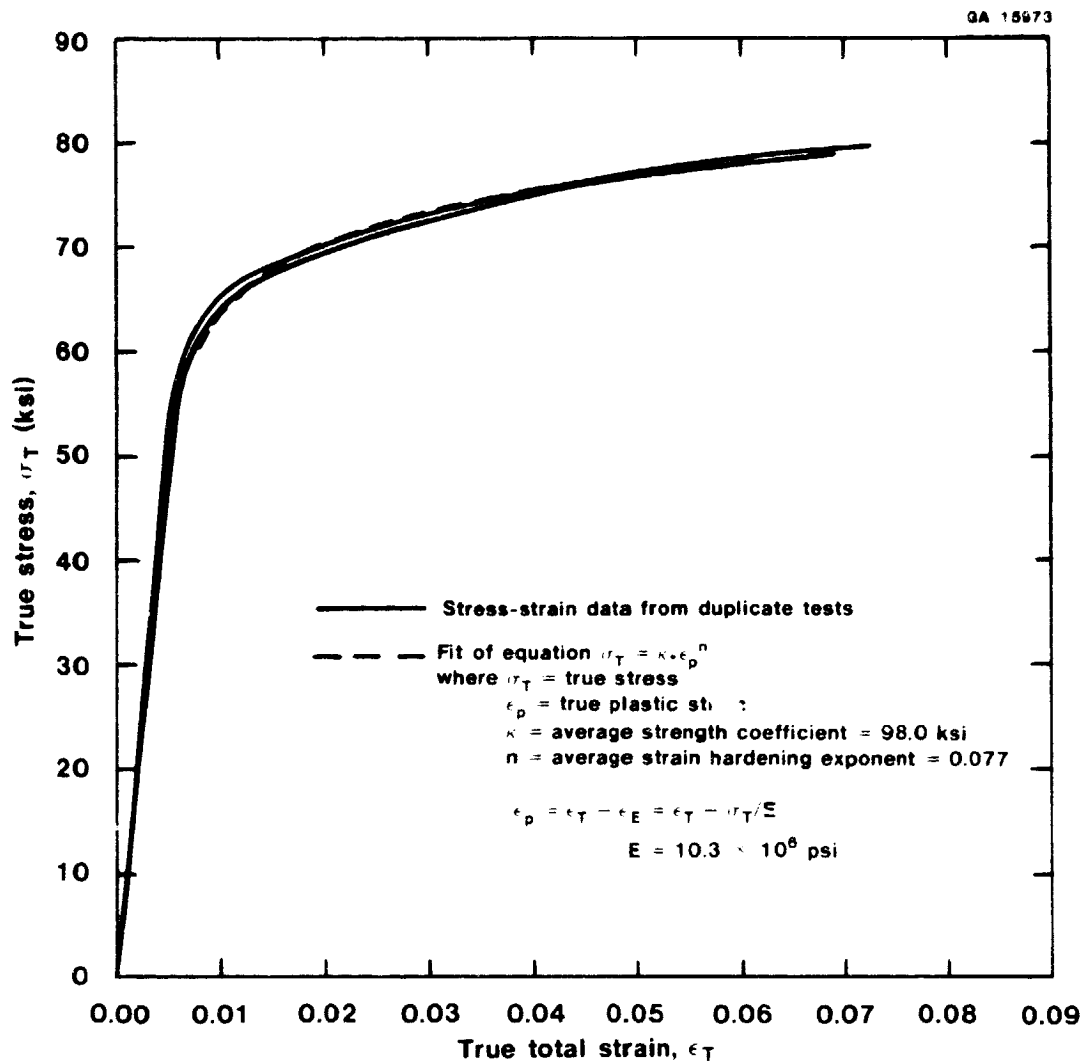
Comparison of Actual and Fitted Short Transverse True Stress-
True Strain Behavior of 7075 Plate Alloys
Figure 28 (c)

ORIGINAL PAGE IS
OF POOR QUALITY



Comparison of Actual and Fitted Short Transverse True Stress-
True Strain Behavior of 7475 Plate Alloys
Figure 29 (a)

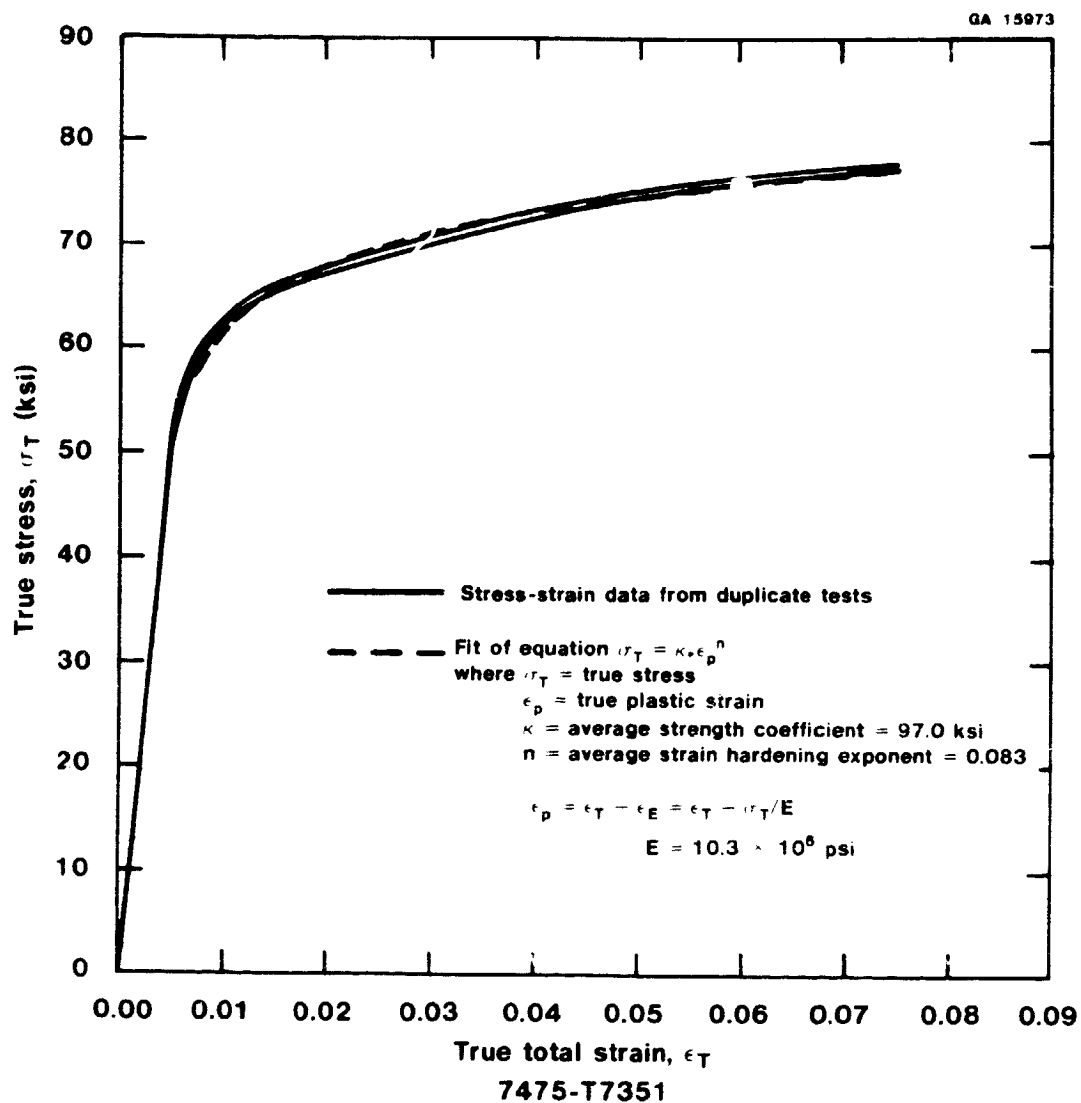
ORIGINAL FILED IN
OF POOR QUALITY



7475-T7651

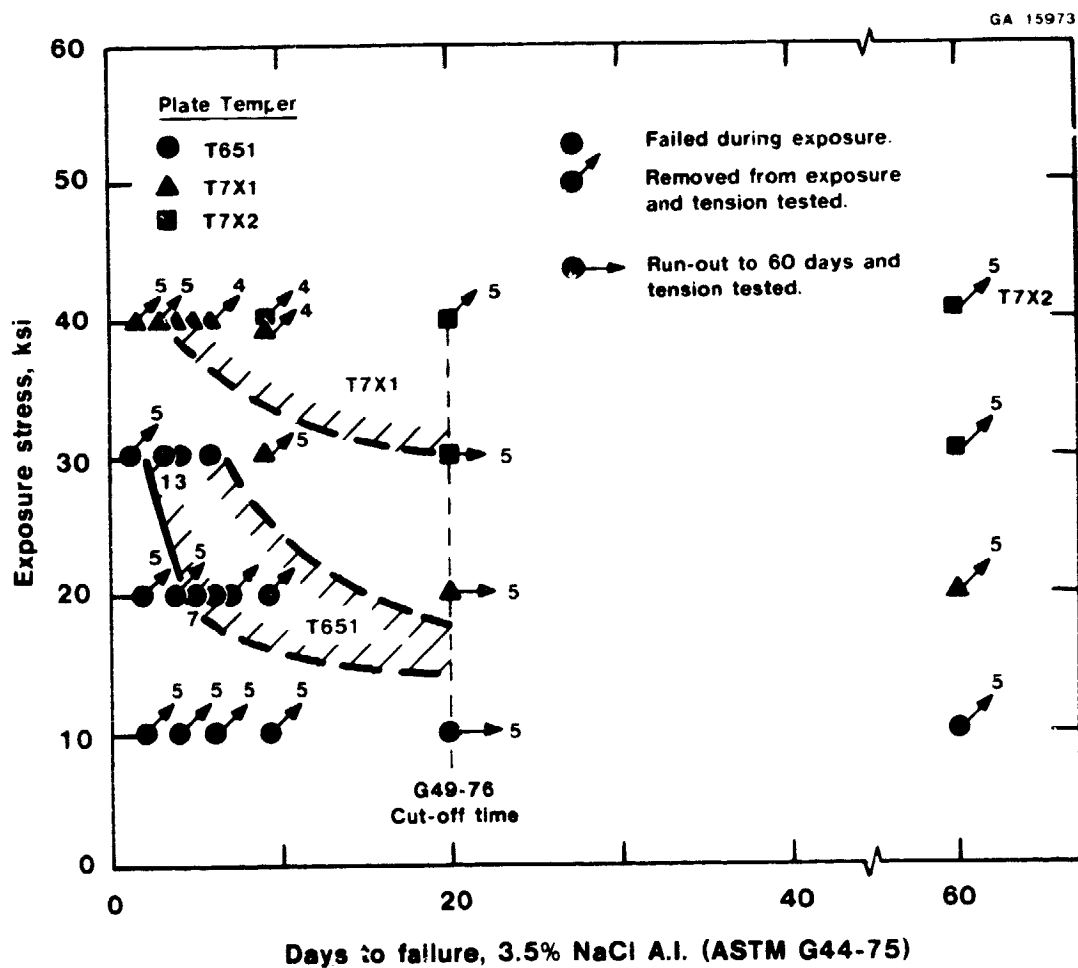
Comparison of Actual and Fitted Short Transverse True Stress-
True Strain Behavior of 7475 Plate Alloys
Figure 29 (b)

ORIGINAL PAGE IS
OF POOR QUALITY



Comparison of Actual and Fitted Short Transverse True Stress-
True Strain Behavior of 7475 Plate Alloys
Figure 29 (c)

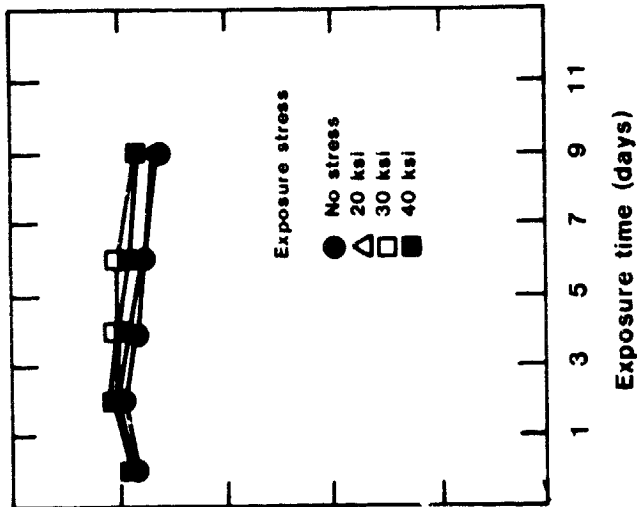
ORIGINAL SOURCE
OF POOR QUALITY



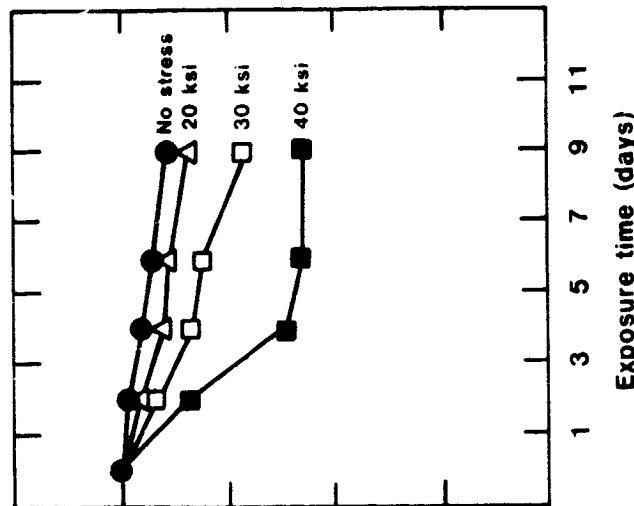
SCC Failure Results of Short Transverse Smooth 0.125" Tension Specimens of 7075 Alloy Plate.

Figure 30

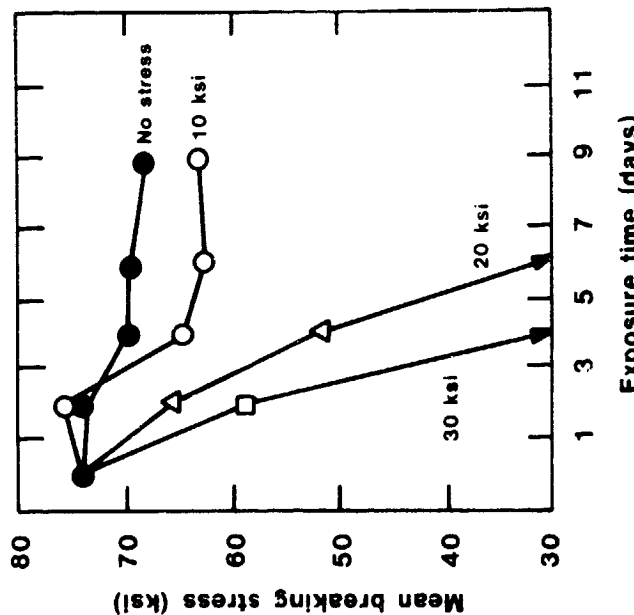
GA 10543

ORIGINAL FILED
OF POOR QUALITY

(c) 7075-T7X2



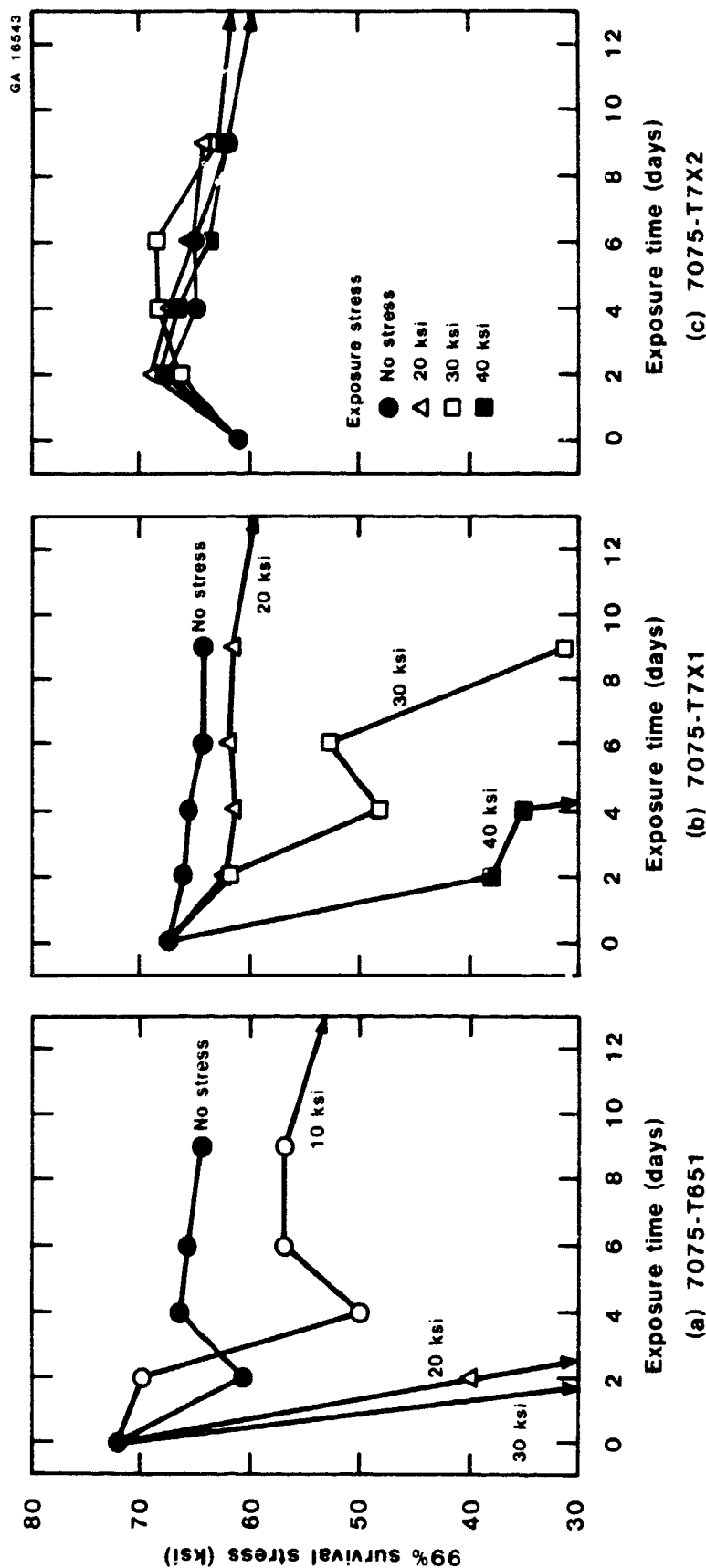
(b) 7075-T7X1



(a) 7075-T651

Mean Breaking Stress vs. Exposure Times for Short Transverse 0.125 in. Diameter Tension Specimens Exposed to 3.5% NaCl Solution by Alternate Immersion (ASTM G44) at Various Exposure Stress Levels. Each Point Represents an Average of Five Specimens Except Where Indicated by Another Number (See Section III.D.2 and Tables 1, 4, and 7 in Appendix C).

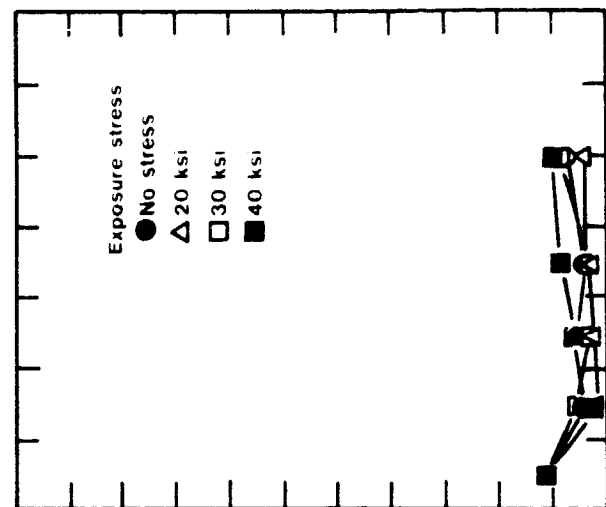
Figure 31



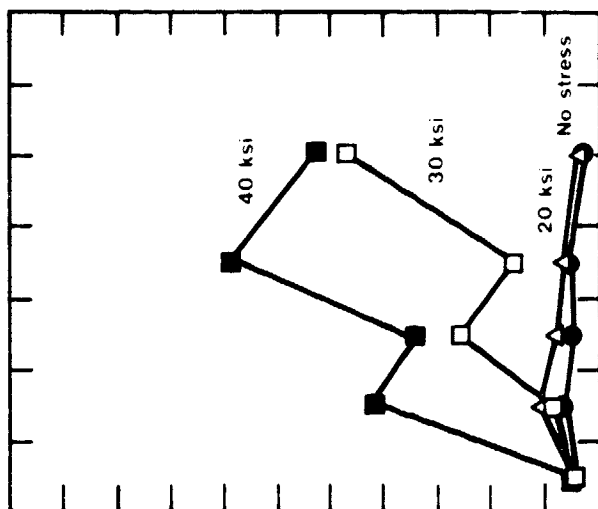
ORIGINAL
OF POOR QUALITY

99% Survival Stress vs. Exposure Time Corresponding to the Mean
Breaking Stresses Shown in Figure 31
(See Tables 3, 6 and 9 in Appendix C)
Figure 32

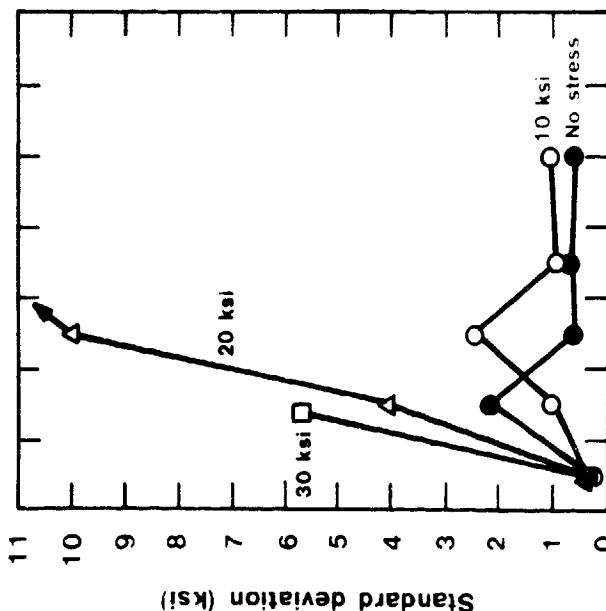
GA 16543



(c) 7075-T7X2



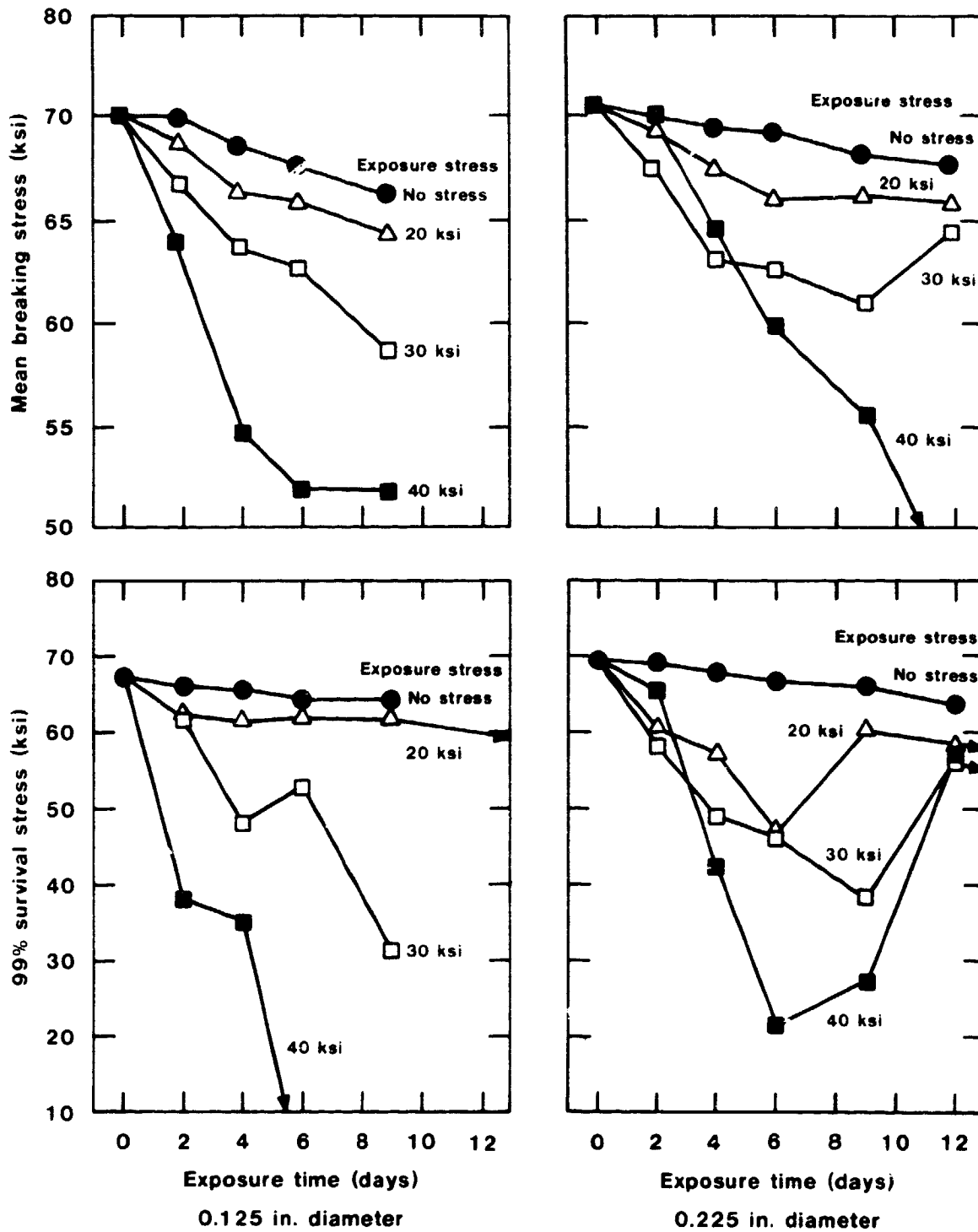
(b) 7075-T7X1



(a) 7075-T651

ORIGINAL PAGE IS
OF POOR QUALITY

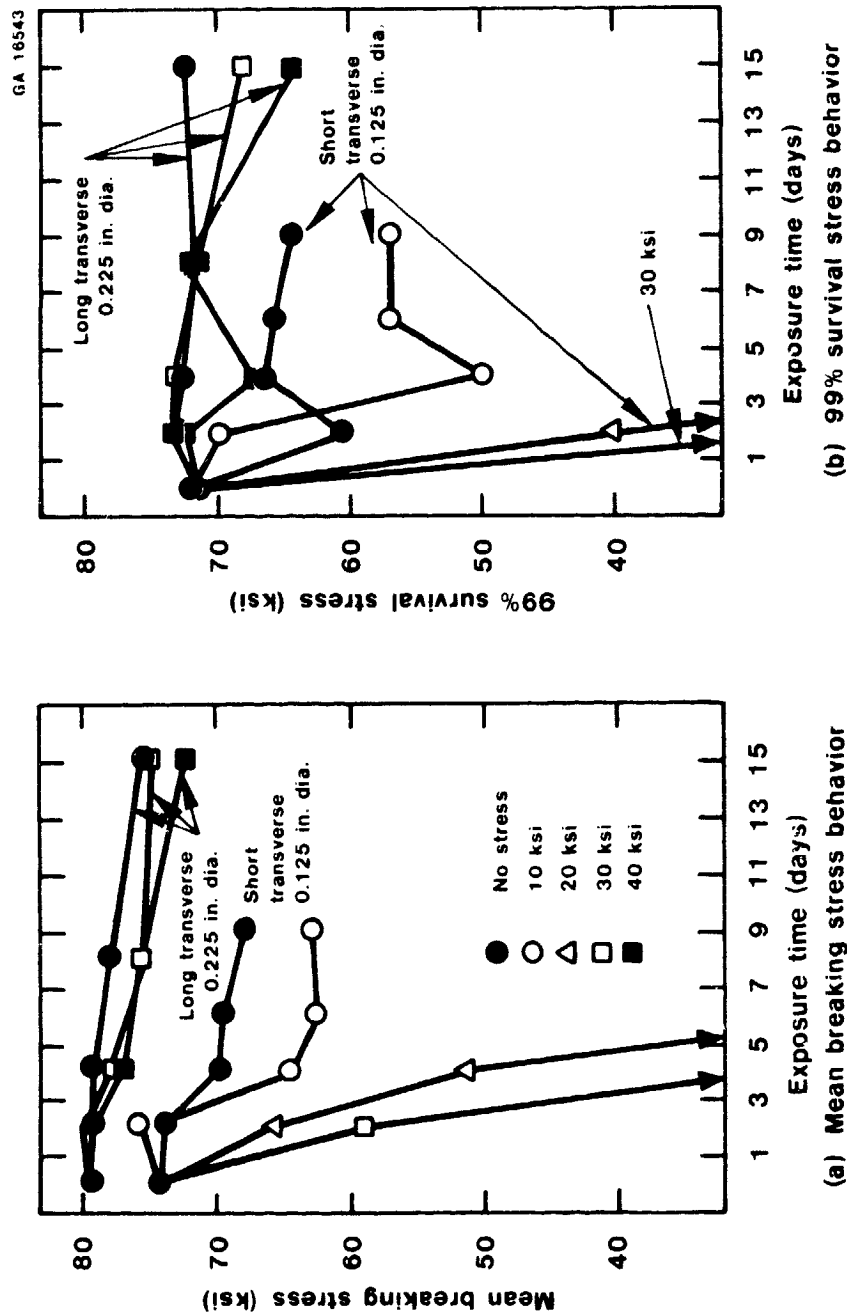
Standard Deviations vs. Exposure Times Corresponding to the Mean
Breaking Stresses Shown in Figure 31
(See Tables 2, 5, and 8 in Appendix C)
Figure 33



Effect of Specimen Diameter on Breaking Stresses in 7075-T7X1 Short Transverse Specimens

Figure 34

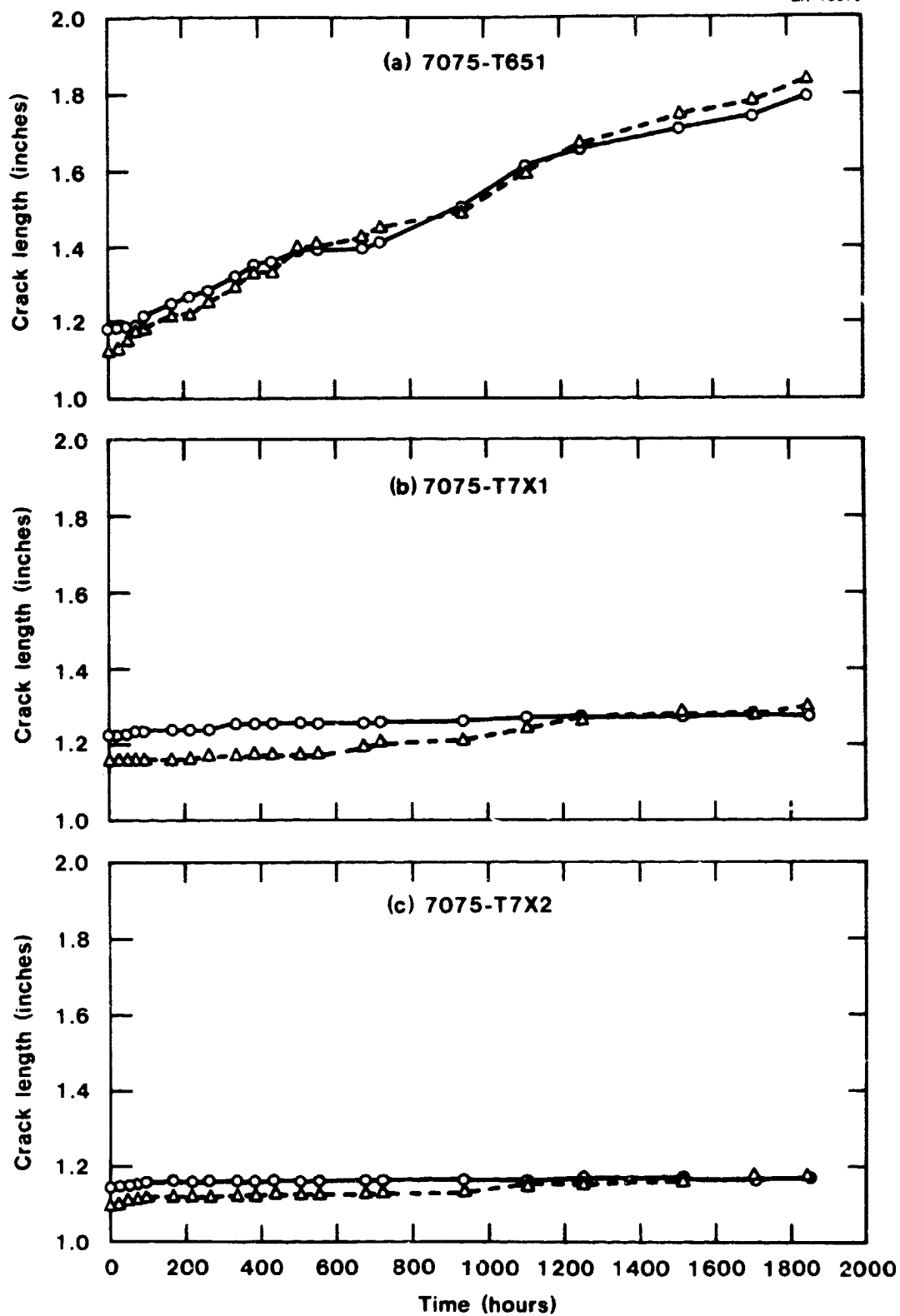
ORIGINAL PAGE IS
OF POOR QUALITY



Effect of Grain Orientation on Breaking Stresses in 7075-T651
Specimens. (See Tables 3 and 15 in Appendix C).
Figure 35

ORIGINAL PHOTOGRAPH
OF POOR QUALITY

GA 15973

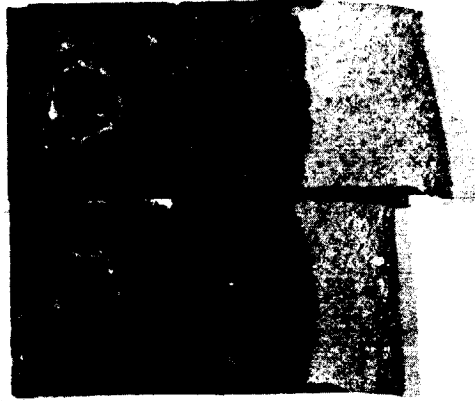


Crack Growth in Bolt-Loaded DCB Specimens Exposed to 3.5% NaCl
Solution Introduced Dropwise into the Crack Three Times a Day
Figure 36

ORIGINAL PAGE IS
OF POOR QUALITY

GA 15973

7075-T7X2
SL1 SL2



7075-T7X1
SL1 SL2



7075-T651
SL1 SL2

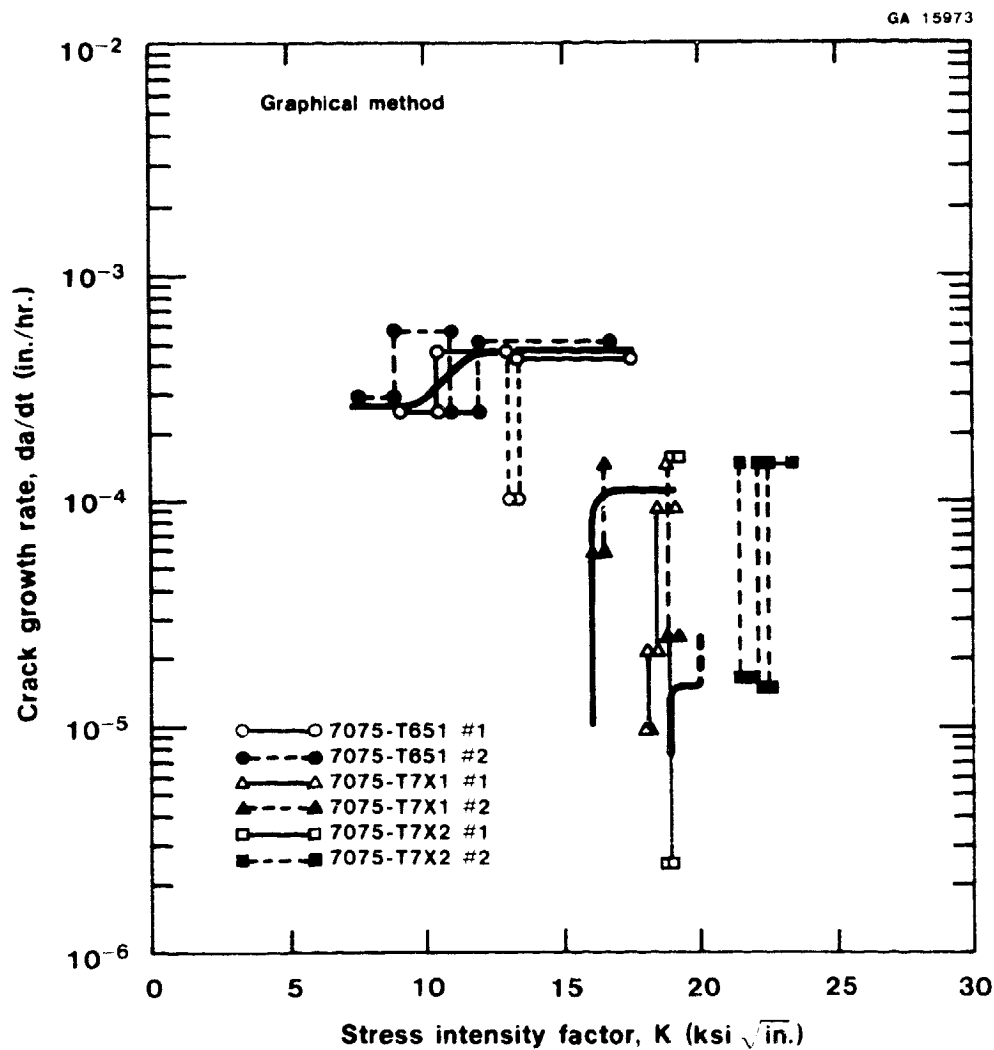


1 in.

Photograph of Fracture Surface Appearance of 7075 DCB Specimens
Exposed to 3.5% NaCl Solution Introduced Dropwise into the Crack
Three Times a Day.

Figure 37

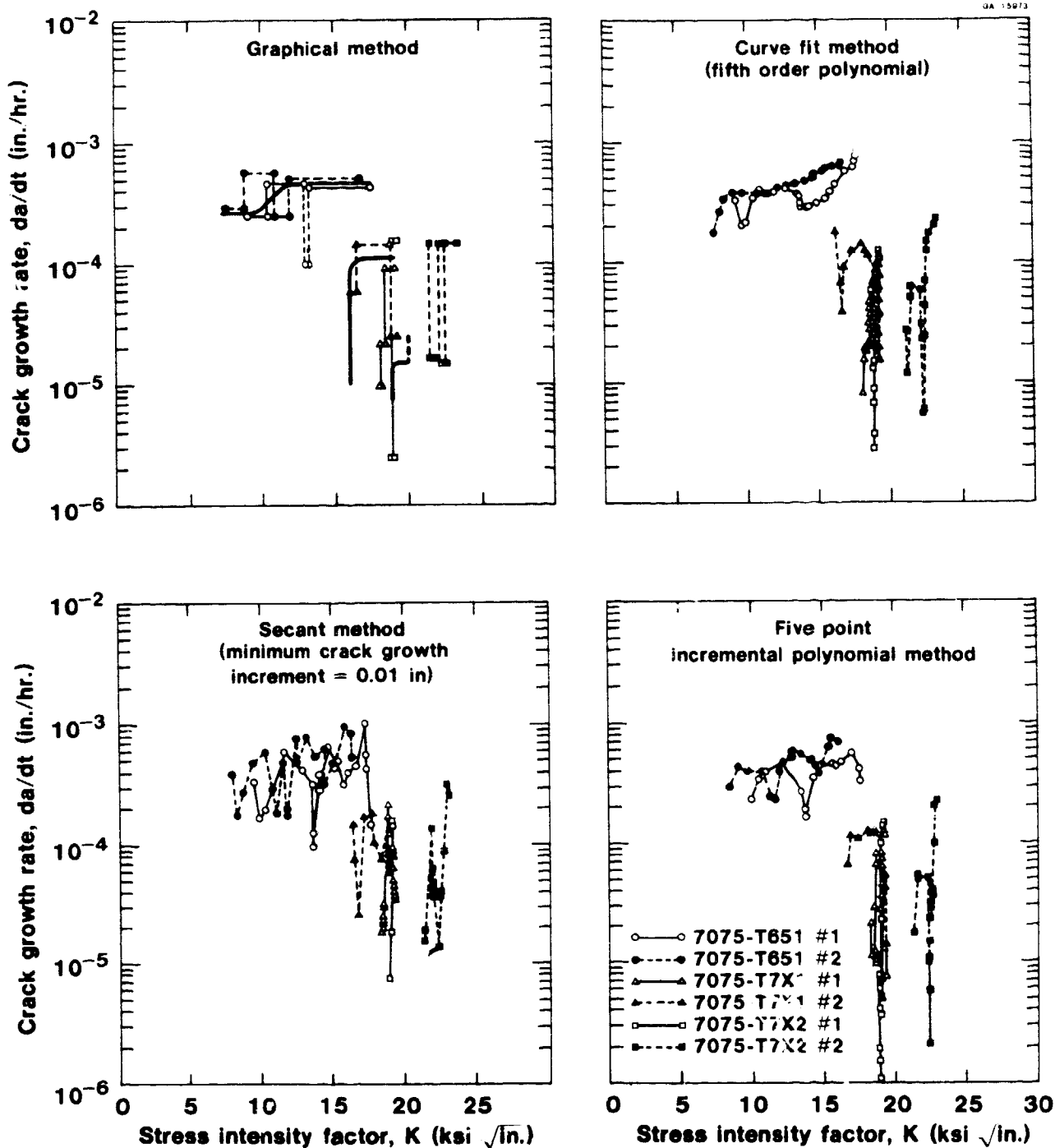
ORIGINAL PAGE IS
OF POOR QUALITY



Graphically Produced Crack Growth Rate Curves from Bolt Loaded DCB
Specimens Exposed to 3.5% NaCl Solution Introduced Dropwise
into the Crack Three Times a Day

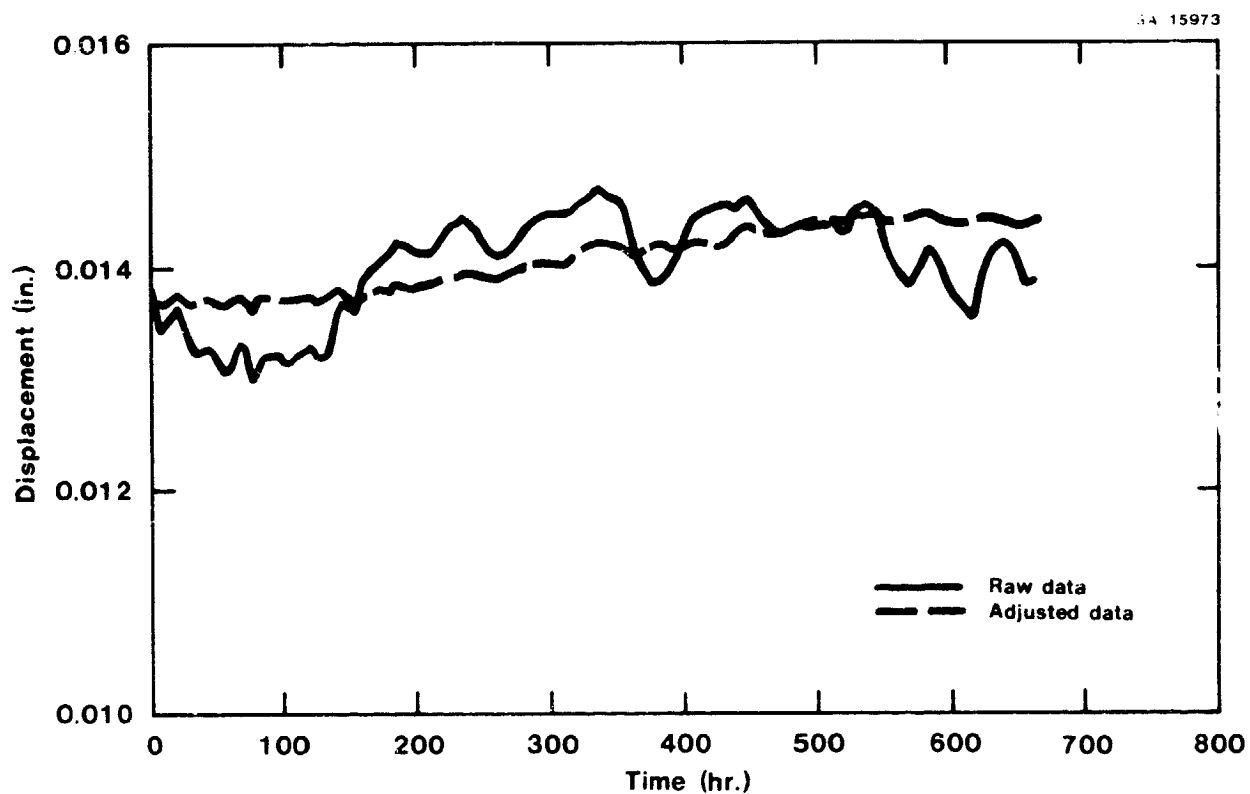
Figure 38

ORIGINAL PAGE
OF POOR QUALITY



Comparison of Crack Growth Rate Curves
Obtained with Various Data Reduction Techniques
Figure 39

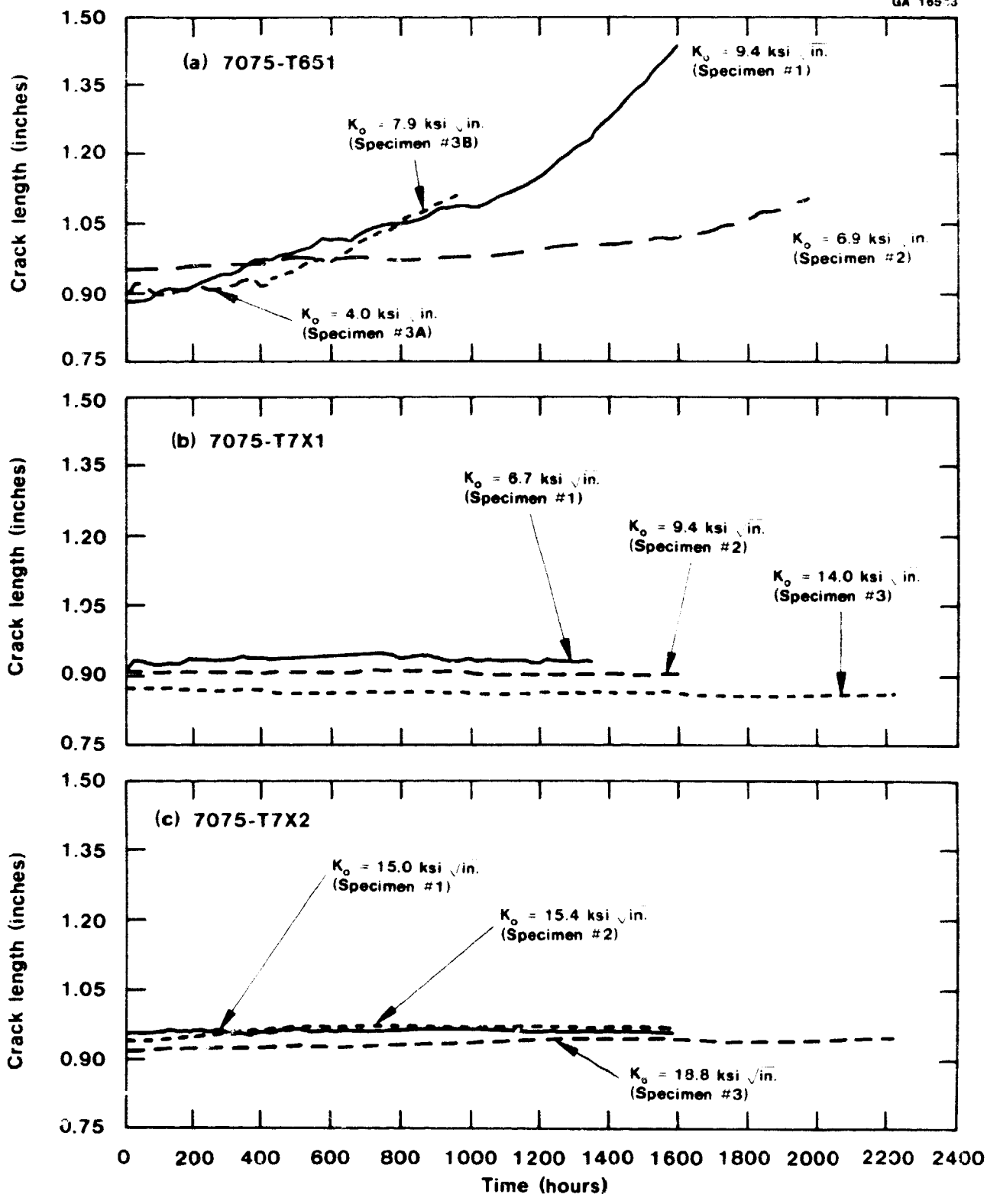
ORIGINAL PAGE IS
OF POOR QUALITY



Raw and Adjusted Crack Mouth Opening Data for Ring-Loaded,
Modified WOL Specimen of 7075-T7X2
Figure 40



GA 165:3



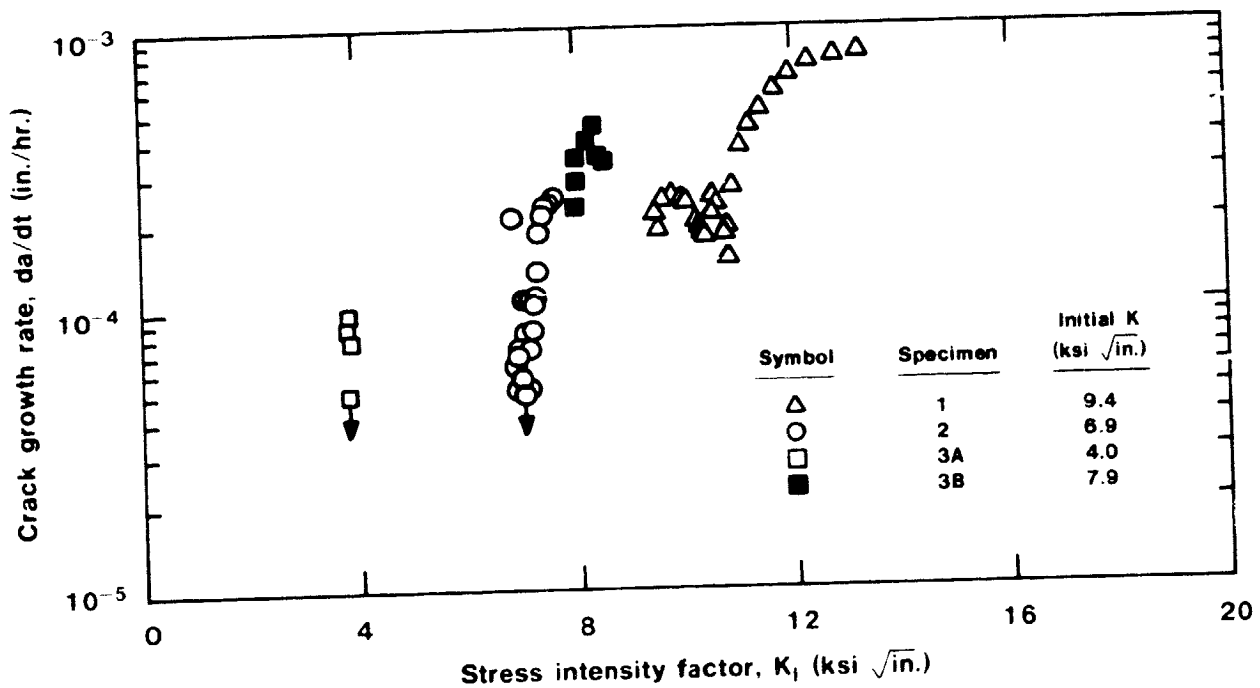
Adjusted Crack Growth Curves from Ring-Loaded WOL Specimens
Exposed to 3.5% NaCl Solution Introduced Dropwise into the Crack
Three Times a Day

Figure 41

ORIGINAL PAGE IS
OF POOR QUALITY

ORIGINAL
OF PHOTOGRAPH

GA 16543



SCC Propagation Rates from Ring-loaded WOL Specimens of 7075-T651 Alloy Exposed to 3.5% NaCl Solution Introduced Dropwise into the Crack Three Times a Day
Figure 42



7075-T7X1 Spec. #SL-2

$K_o = 9.4 \text{ ksi } \sqrt{\text{in.}}$

(Neg. 327597A)



7075-T7X2 Spec. #SL-1

$K_o = 14.9 \text{ ksi } \sqrt{\text{in.}}$

(Neg. 327598A)

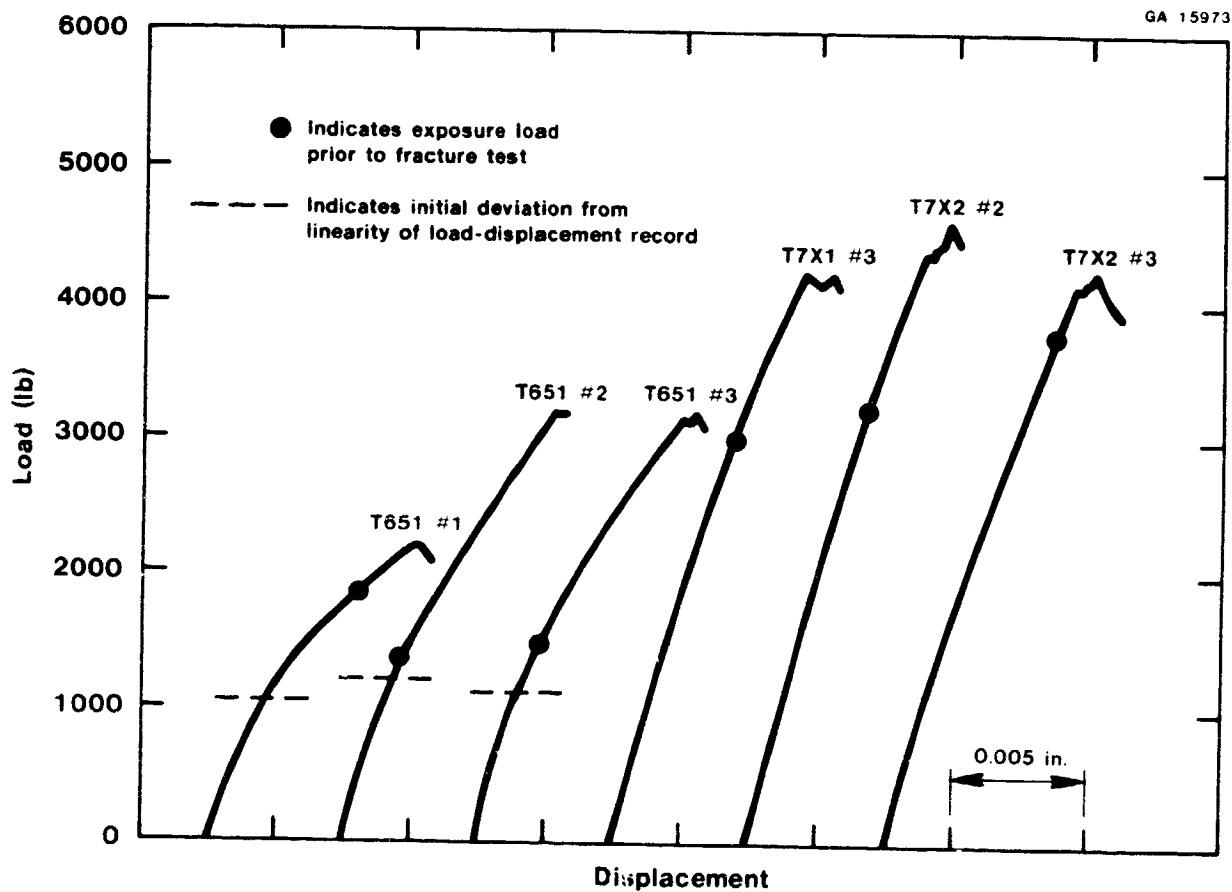
**Photomicrographs of Tips of Fatigue Precracks in WOL Specimens
Exposed 1580 hr. with No Indication of Crack Growth.**

**There is No Evidence of Typical SCC or Severe Corrosion.
It is Questionable Whether the Short Transgranular Branches
at the Crack Tips Occurred During Precracking or Exposure.**

Figure 43

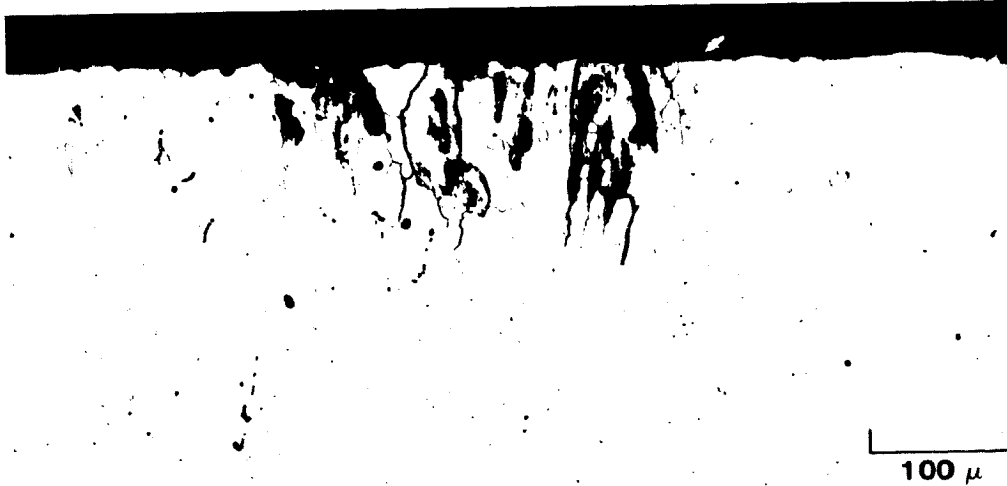
**ORIGINAL PAGE 19
OF POOR QUALITY**

ORIG. FILE
OF P00012

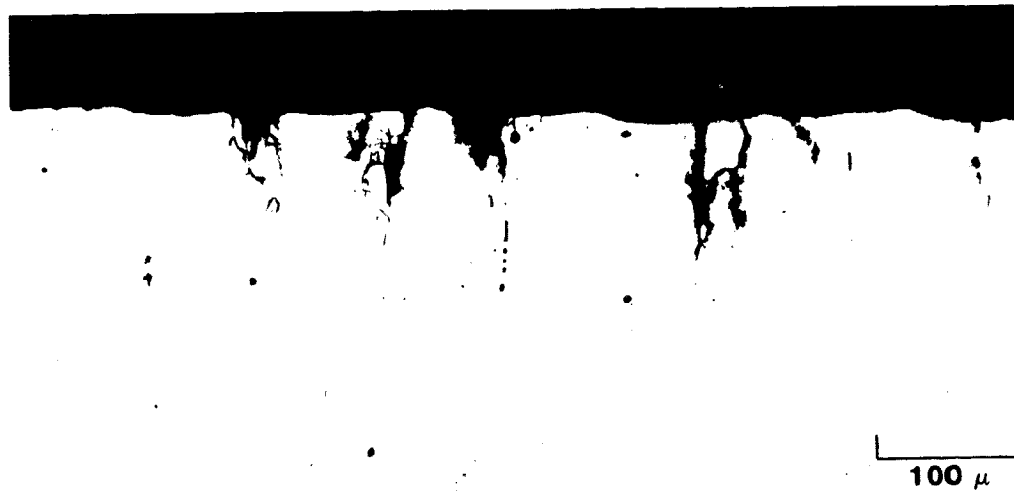


Load-Displacement Records from Fracture Tests of 7075 WOL Specimens
after SCC Tests
Figure 44

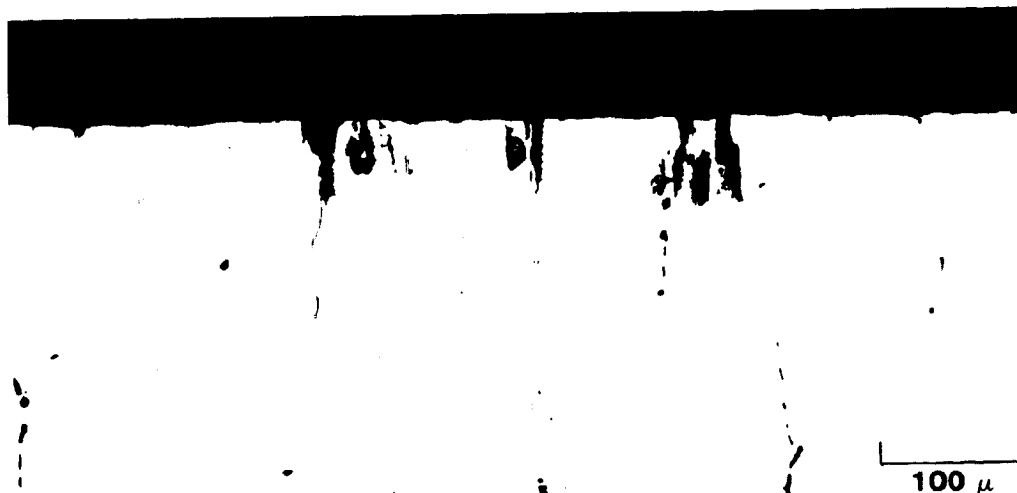
GA 15973



(a)
T651



(b)
T7X1



(c)
T7X2

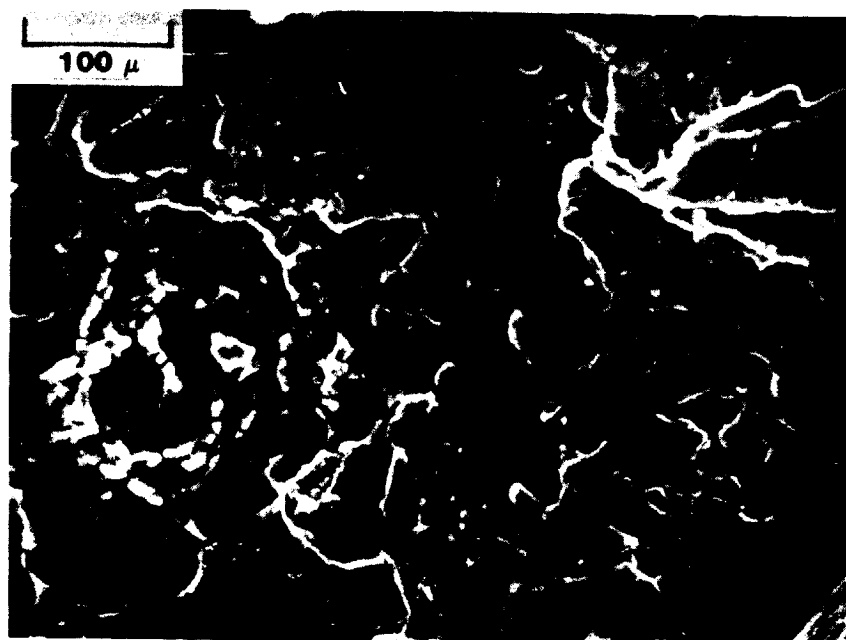
As polished

Longitudinal sections

Typical Forms of Surface Attack in Smooth Tension Specimens of the Three Tempers of 7075 Alloy Plate Exposed 6 Days with No Applied Stress to 3.5% NaCl Alternate Immersion and Then Tension Tested.

Figure 45

ORIGINAL PAGE IS
OF POOR QUALITY



ORIGINAL PHOTOGRAPH
OF POOR QUALITY

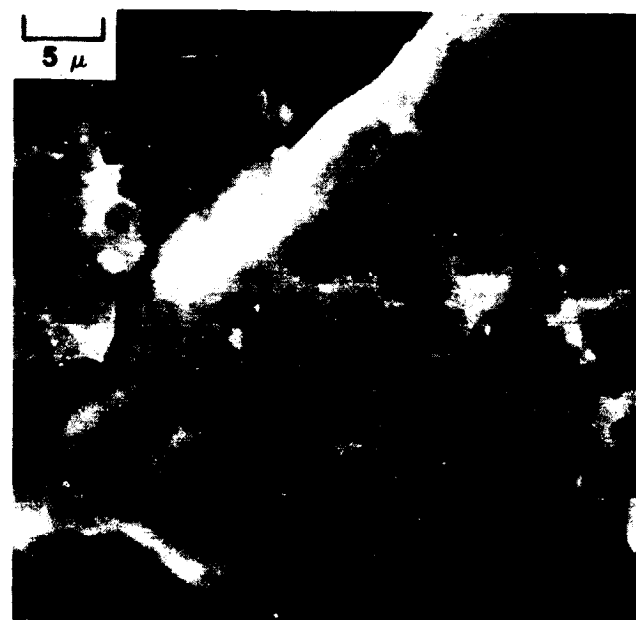
Neg. 5094-7

(a)



Neg. 5094-14

(b)



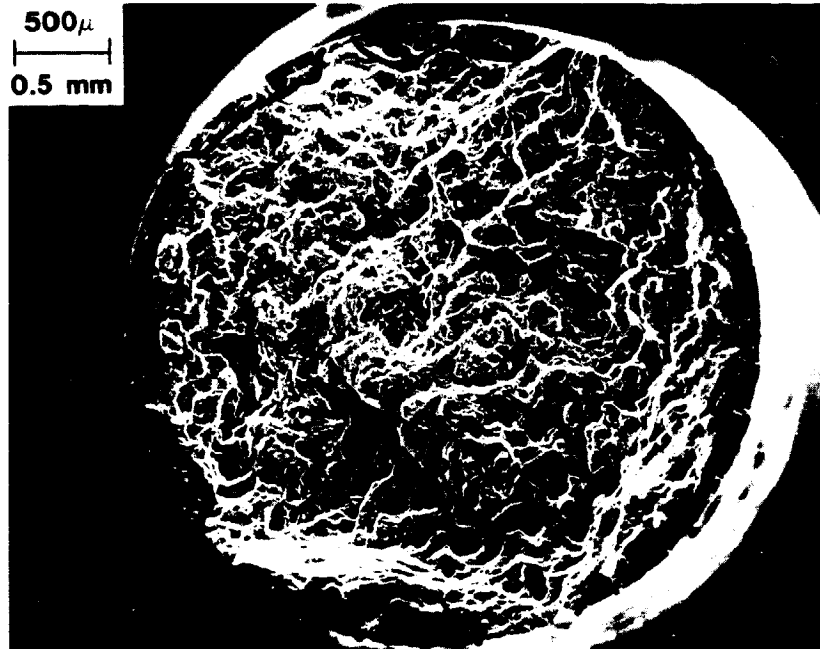
Neg. 5094-13

(c)

- (a) General view of SCC surface near edge of specimen (arrow) showing plateau structure and "mud-cracking" pattern of corrosion deposits.
 (b, c) Higher magnification views near the outer surface (b) and at the deepest penetration of the SCC flaw (c).

Fracture Surface of 7075-T651 Breaking Load Specimen ST67, Which Failed During Alternate Immersion Under 20 ksi Exposure Stress.

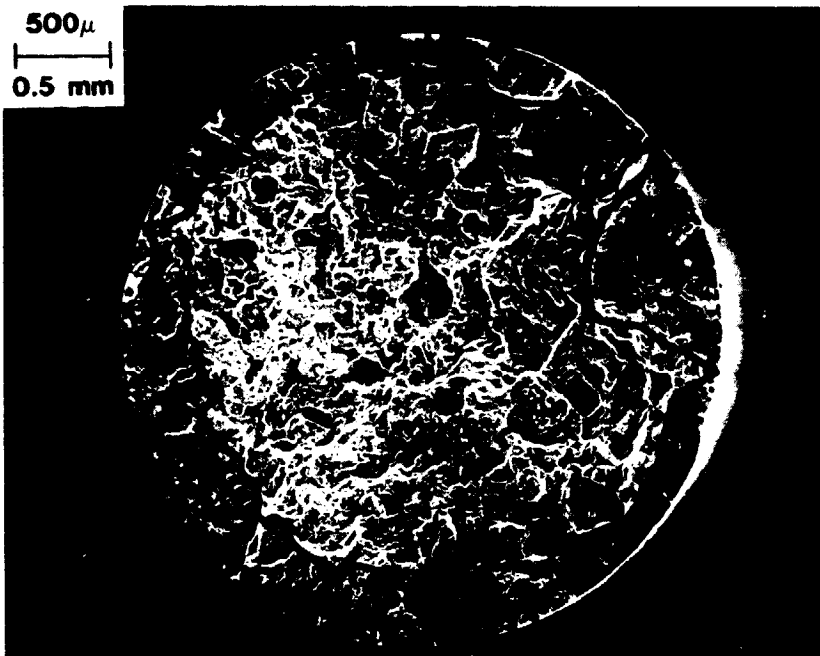
Figure 46



Neg. 5058-3

(a) 7075-T651 0.125 in. diameter specimen ST9.
Exposed 2 days at 0 stress, fracture stress 71.7 ksi.

ORIGINAL PAGE IS
OF POOR QUALITY



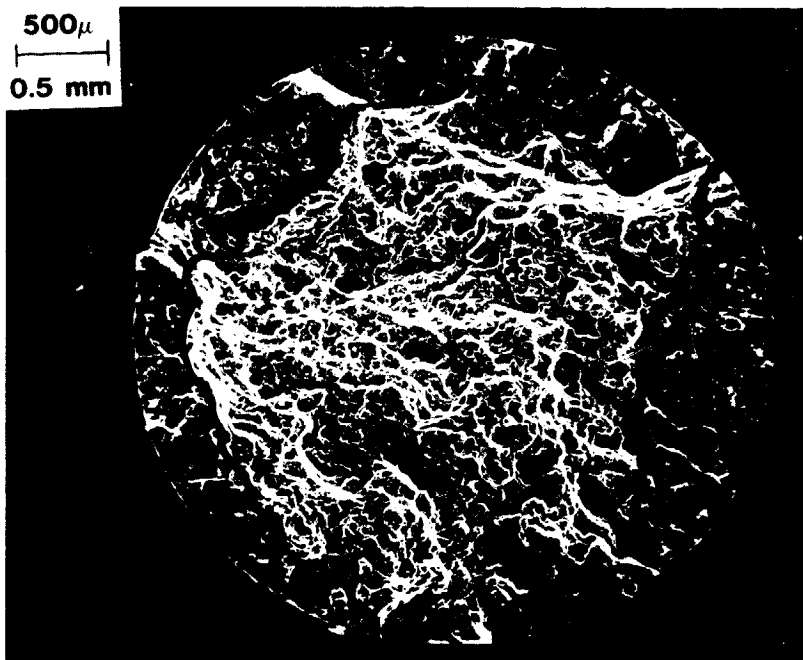
Neg. 5058-8

(b) 7075-T651 0.125 in. diameter specimen ST72.
Exposed 2 days at 30 ksi, fracture stress 53.9 ksi.

Fracture Surface Maps of Several Breaking Load Specimens Illustrating the Range of Flaw Sizes and Shapes Observed ((a)-(h)). The Boundary of Each SCC Flaw has Been Outlined for Clarity.

Figure 47

500 μ
0.5 mm

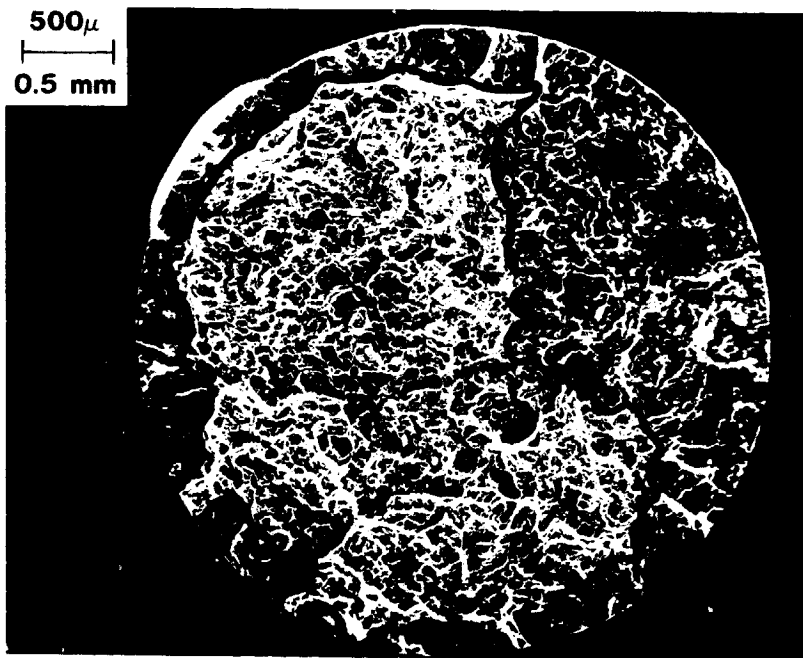


ORIGINAL P. 107
OF POOR QUALITY

Neg. 5078-3

(c) 7075-T651 0.125 in. diameter specimen ST57.
Exposed 4 days at 20 ksi, fracture stress 61.3 ksi.

500 μ
0.5 mm

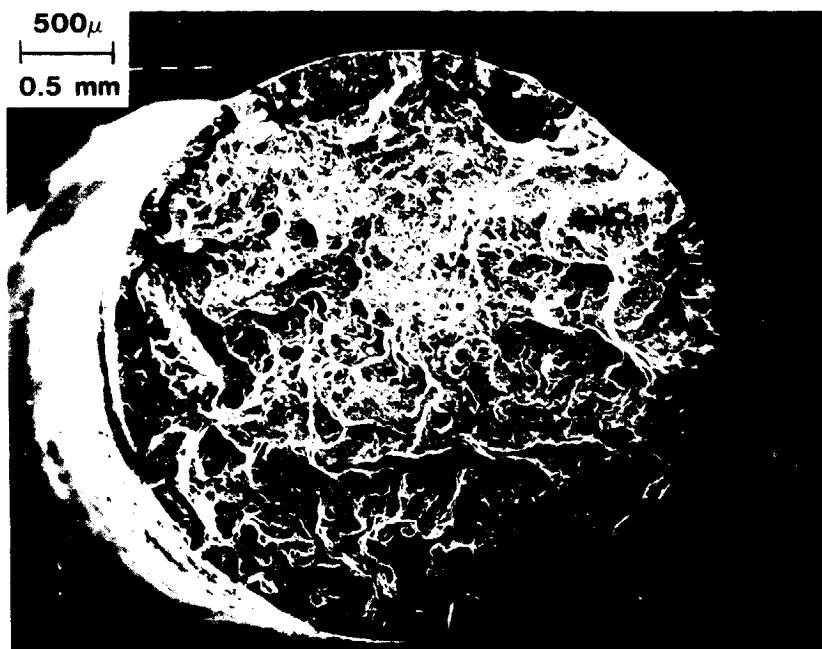


Neg. 5078-4

(d) 7075-T651 0.125 in. diameter specimen ST60.
Exposed 4 days at 20 ksi, fracture stress 35.0 ksi.

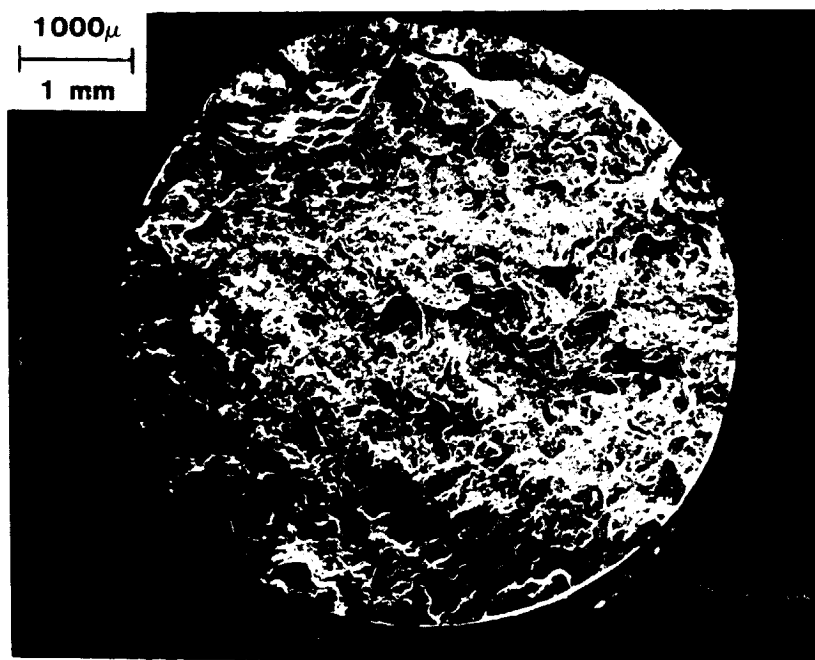
Fracture Surface Maps of Several Breaking Load Specimens Illustrating the Range of Flaw Sizes and Shapes Observed ((a)-(h)). The Boundary of Each SCC Flaw has Been Outlined for Clarity.

Figure 47 (Continued)



Neg. 5058-12

(e) 7075-T7X1 0.125 in. diameter specimen ST87.
Exposed 9 days at 40 ksi, fracture stress 59.2 ksi.

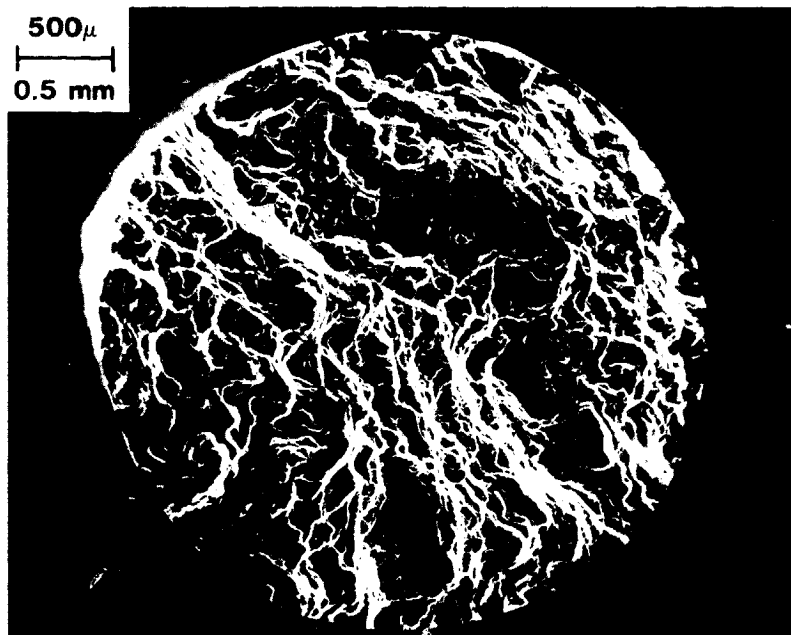


Neg. 5058-18

(f) 7075-T7X1 0.225 in. diameter specimen ST218.
Exposed 9 days at 40 ksi, fracture stress 47.0 ksi.

Fracture Surface Maps of Several Breaking Load Specimens Illustrating the Range of Flaw Sizes and Shapes Observed ((a)-(h)). The Boundary of Each SCC Flaw has Been Outlined for Clarity.

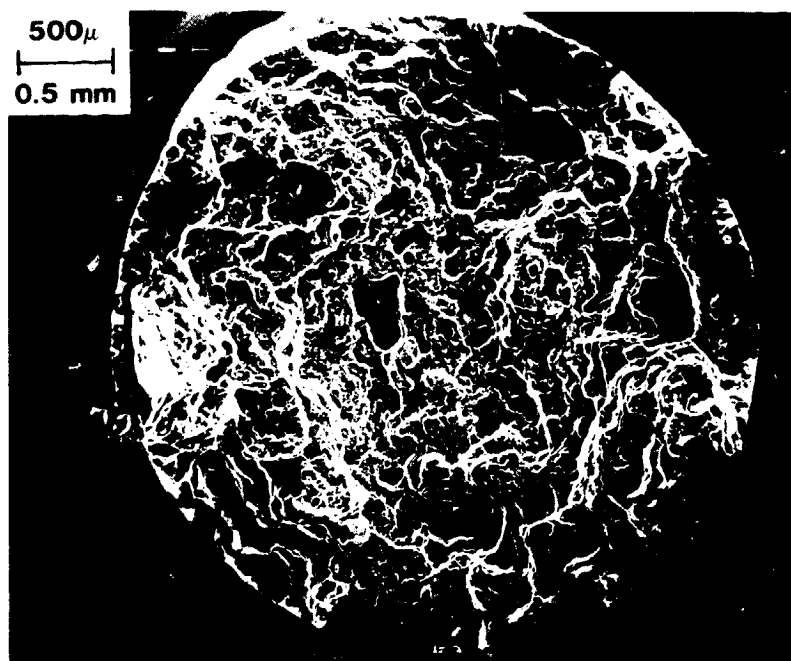
Figure 47 (Continued)



ORIGINAL PAGE IS
OF POOR QUALITY

Neg. 5058-23

- (g) 7075-T7X2 0.125 in. diameter specimen ST6.
Exposed 2 days at 0 ksi, fracture stress 70.3 ksi.



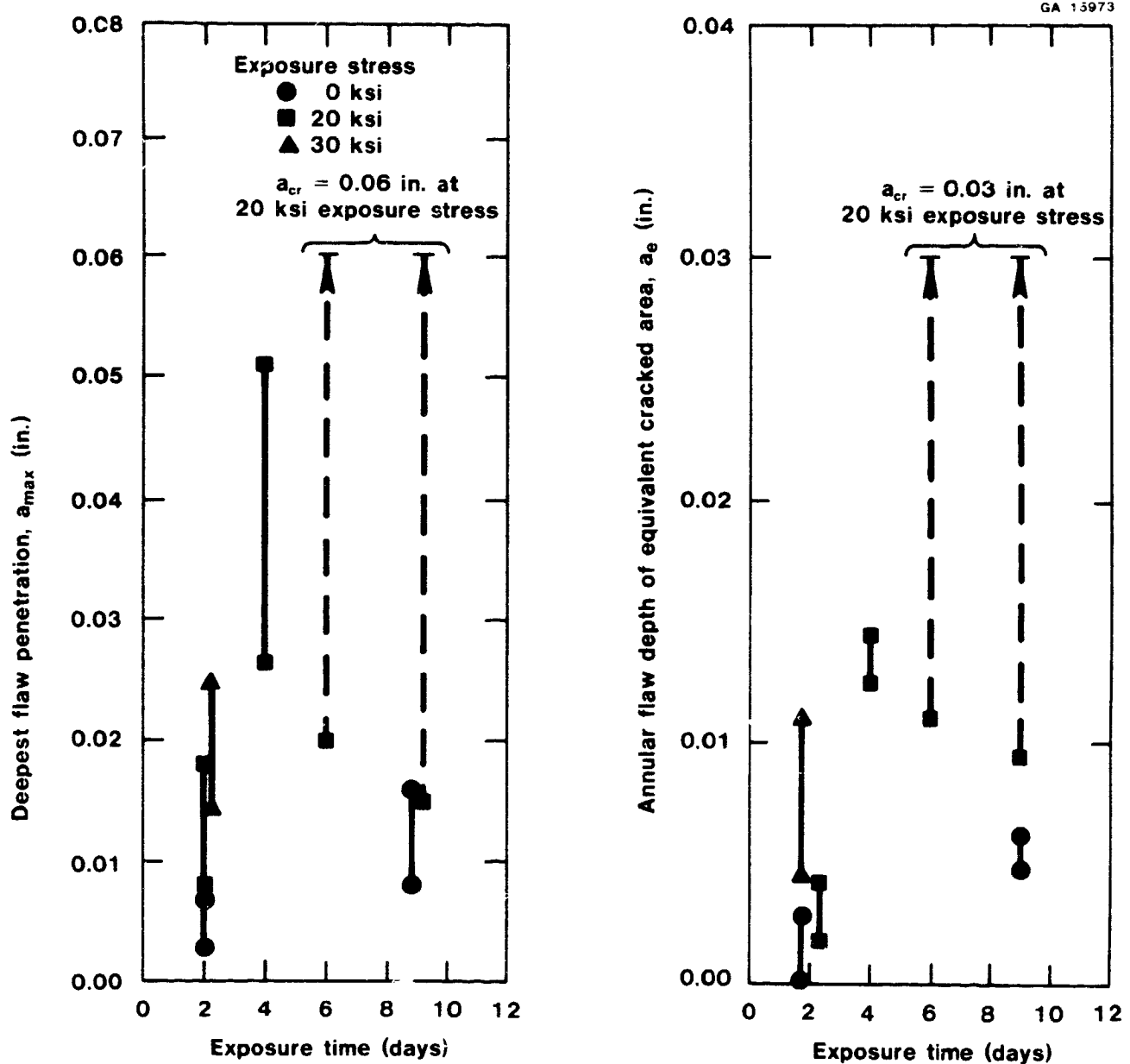
Neg. 5058-31

- (h) 7075-T651 0.125 in. diameter specimen ST94.
Exposed 9 days at 40 ksi, fracture stress 66.5 ksi.

Fracture Surface Maps of Several Breaking Load Specimens Illustrating the Range of Flaw Sizes and Shapes Observed ((a)-(h)). The Boundary of Each SCC Flaw has Been Outlined for Clarity.

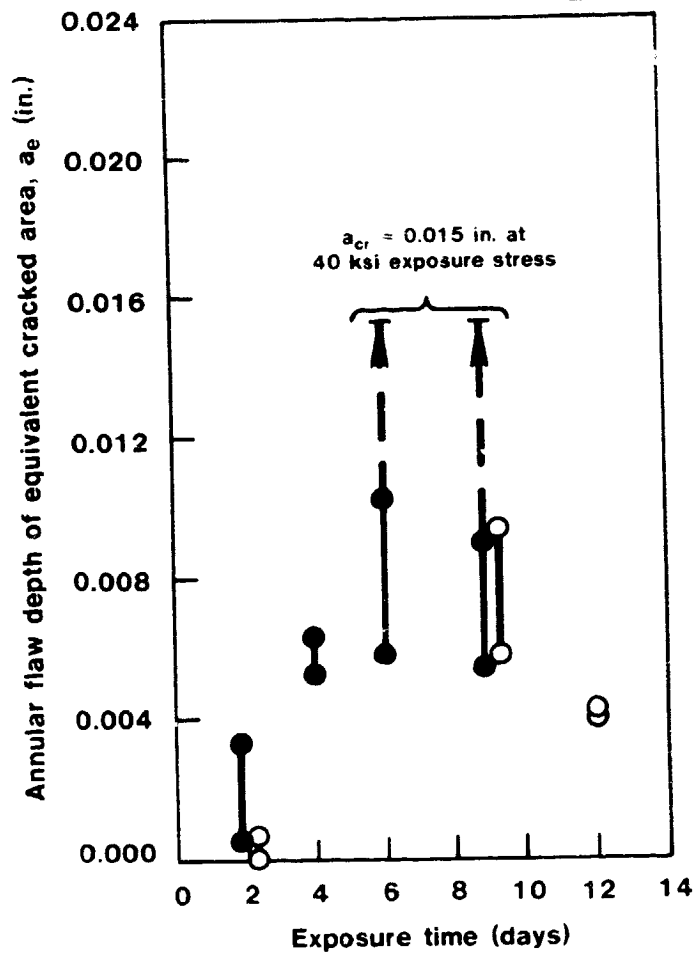
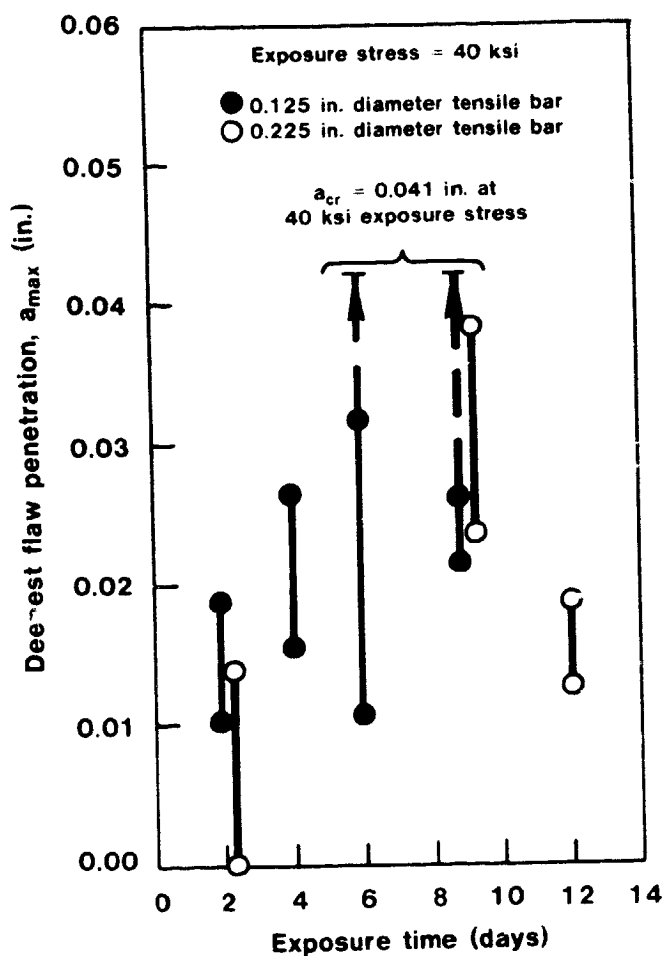
Figure 47 (Continued)

ORIGINAL SIZE
OF POOR QUALITY



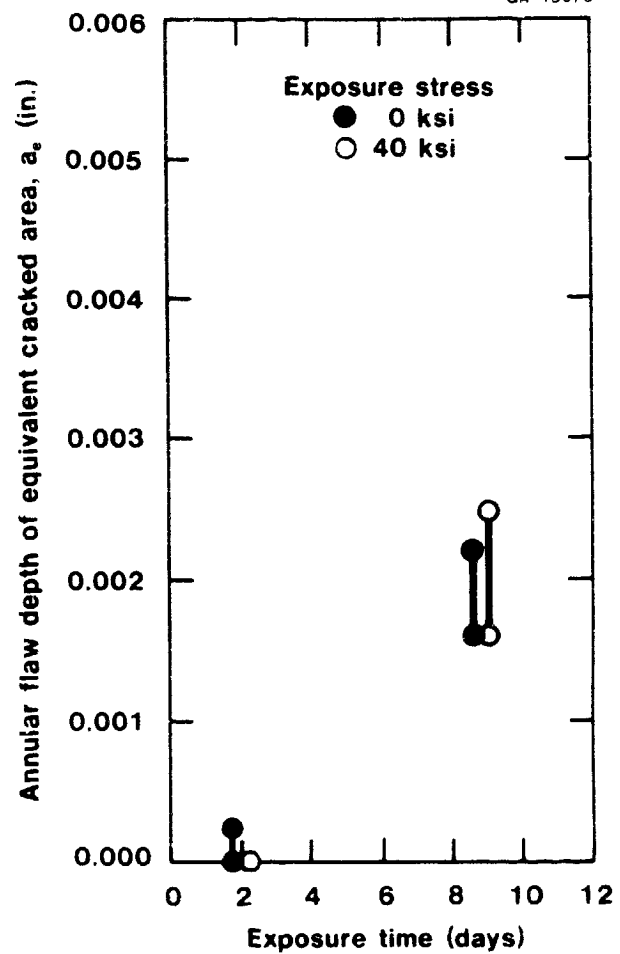
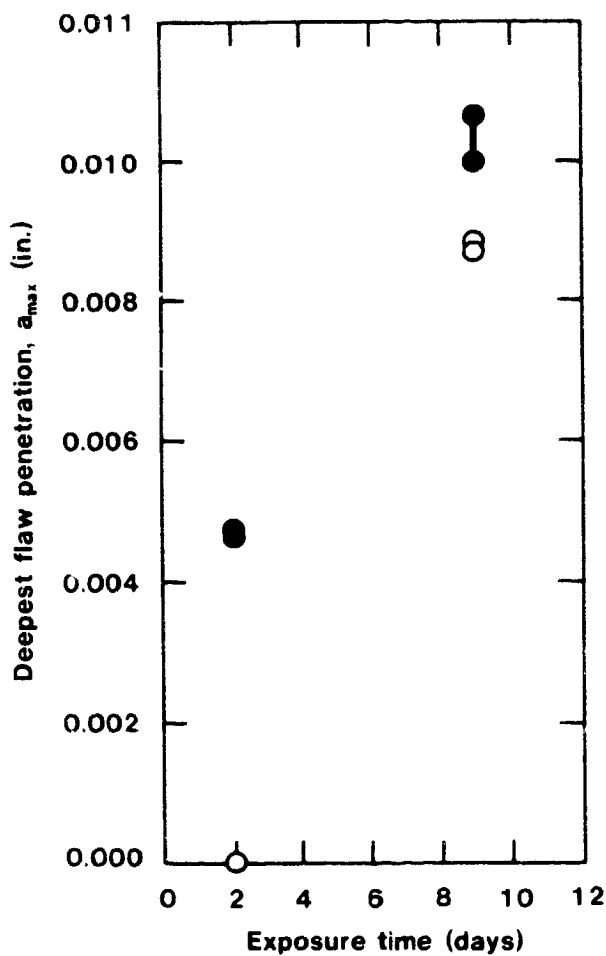
SCC Flaw Sizes Corresponding to Largest and Smallest Breaking Loads Measured in Groups of Five 7075-T651 Alloy 0.125 in. Diameter Tension Specimens Exposed to 3.5 Percent NaCl Solution by Alternate Immersion at Various Levels of Exposure Stress

Figure 48



SCC Flaw Sizes Corresponding to Largest and Smallest Breaking Loads Measured in Groups of Five 7075-T7X1 Alloy 0.125 and 0.225 in. Diameter Tension Specimens Exposed to 3.5 Percent NaCl Solution by Alternate Immersion at 40 ksi Exposure Stress
Figure 49

QUALITY CONTROL
OF POOR QUALITY

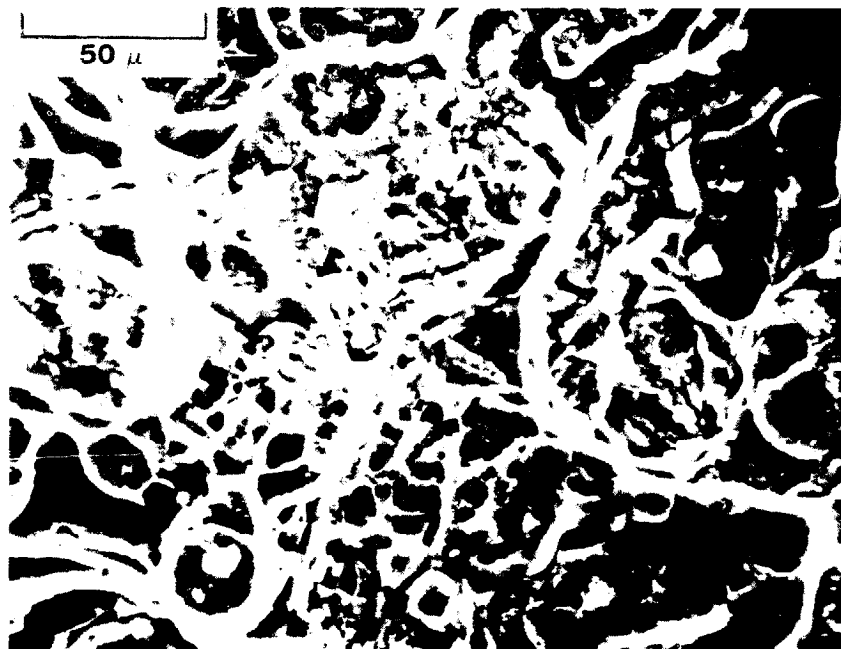


SCC Flaw Sizes Corresponding to Largest and Smallest Breaking Loads Measured in Groups of Five 7075-T7X2 Alloy 0.125 in. Diameter Tension Specimens Exposed to 3.5 Percent NaCl Solution by Alternate Immersion at 0 and 40 ksi Exposure Stress

Figure 50

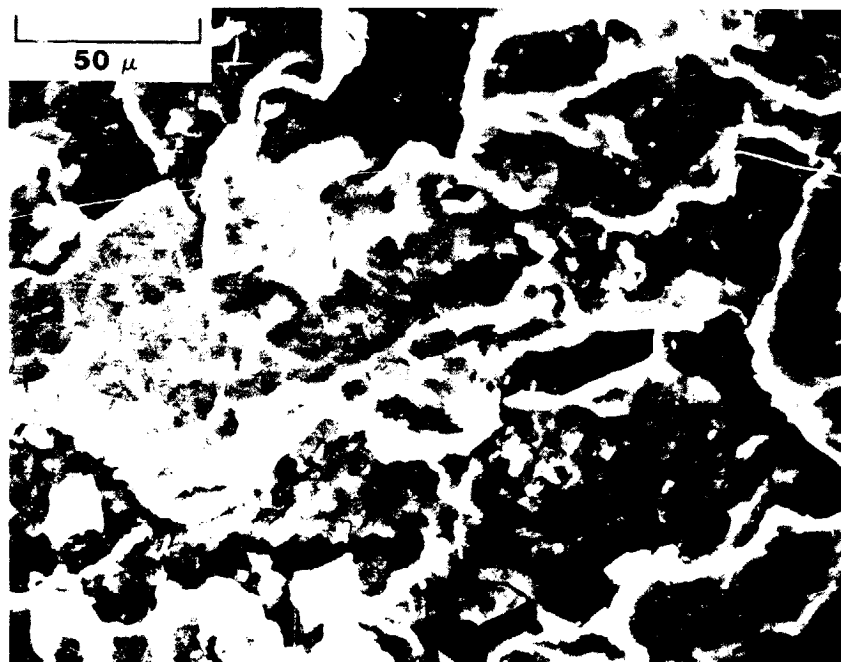
ORIGINAL PAGE
OF POOR QUALITY

GA 15973



Neg. 5012-3

(a)

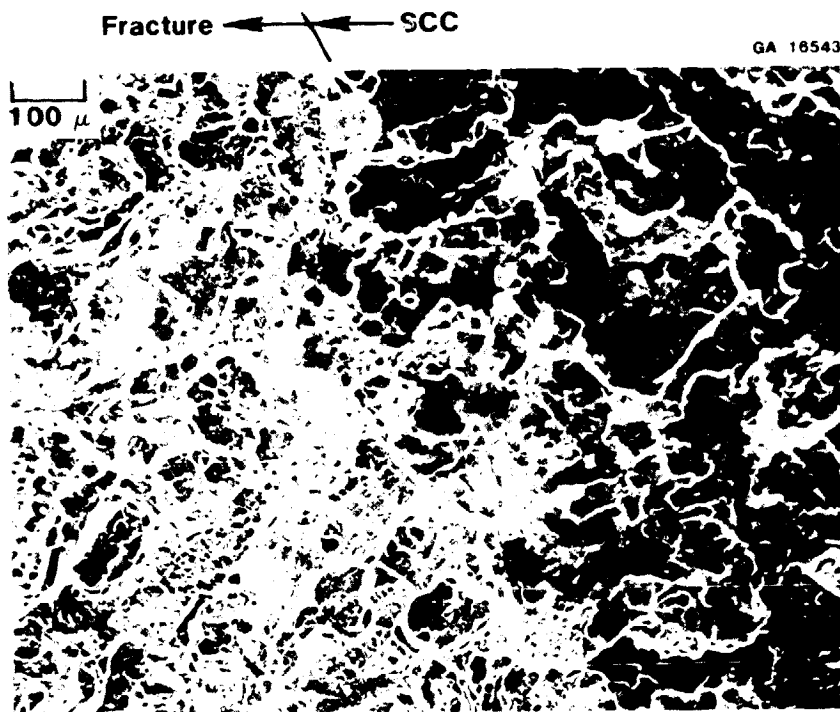


Neg. 5012-6

(b)

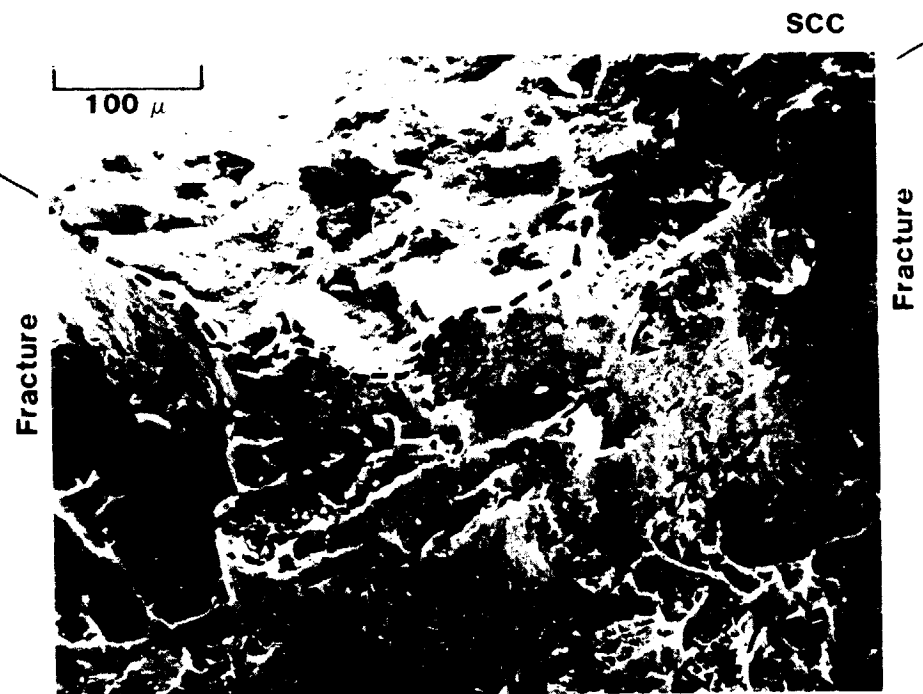
Fracture Surface of Breaking Load Specimen of 7075-T651 (ST63)
Showing: (a) Dimples in Tensile Fracture Region and (b) Plateau Structure
in SCC Region.

Figure 51



Neg. 5012-7

(a)

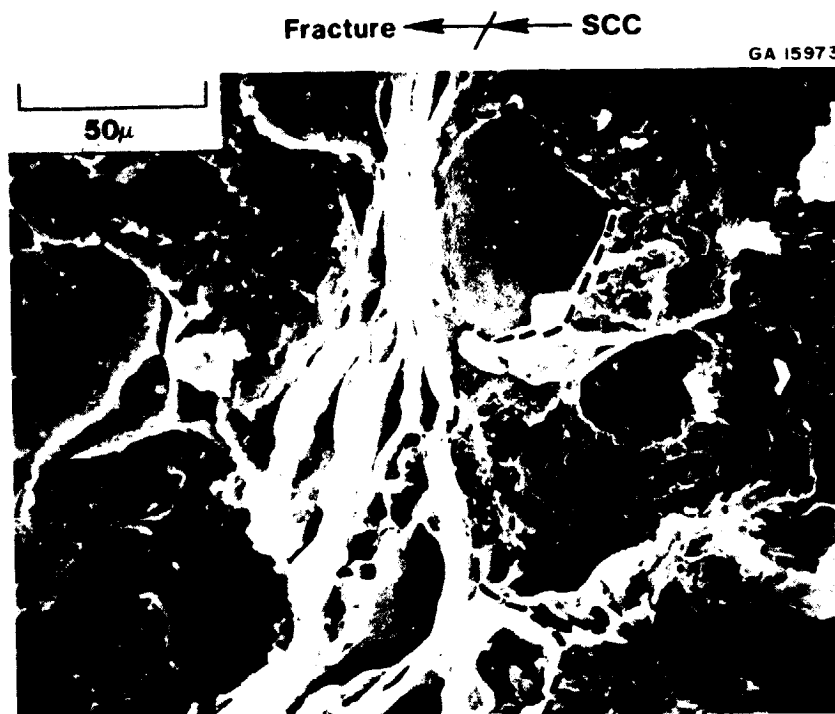


Neg. 5012-37

(b) Shows steep wall separating SCC surface from dimpled tensile fracture regions.

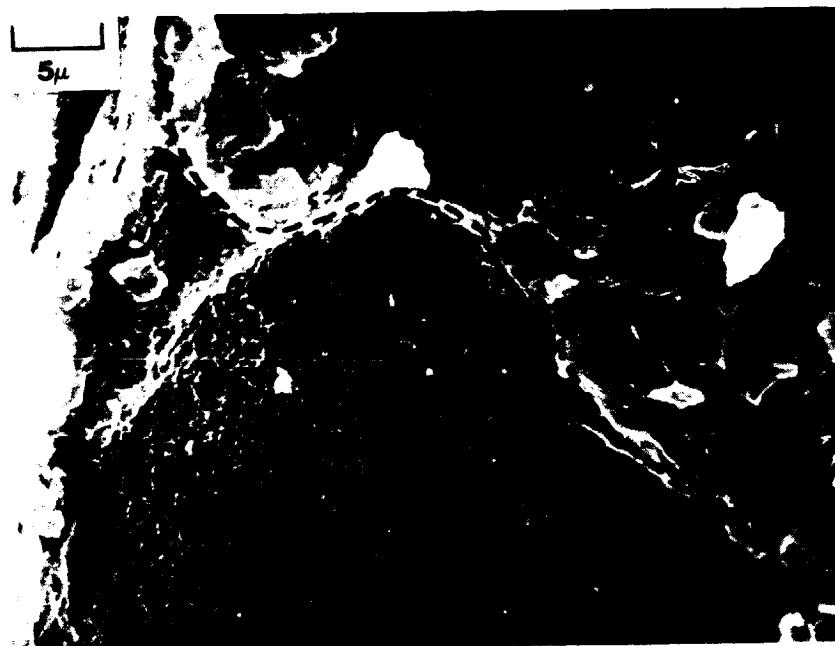
Transition from SCC to Tensile Fracture Surface in Breaking Load
Specimen of 7075-T651 (ST60)

Figure 52



Neg. 5012-55

(a) Shows steep wall separating SCC plateau from dimpled tensile fracture region.

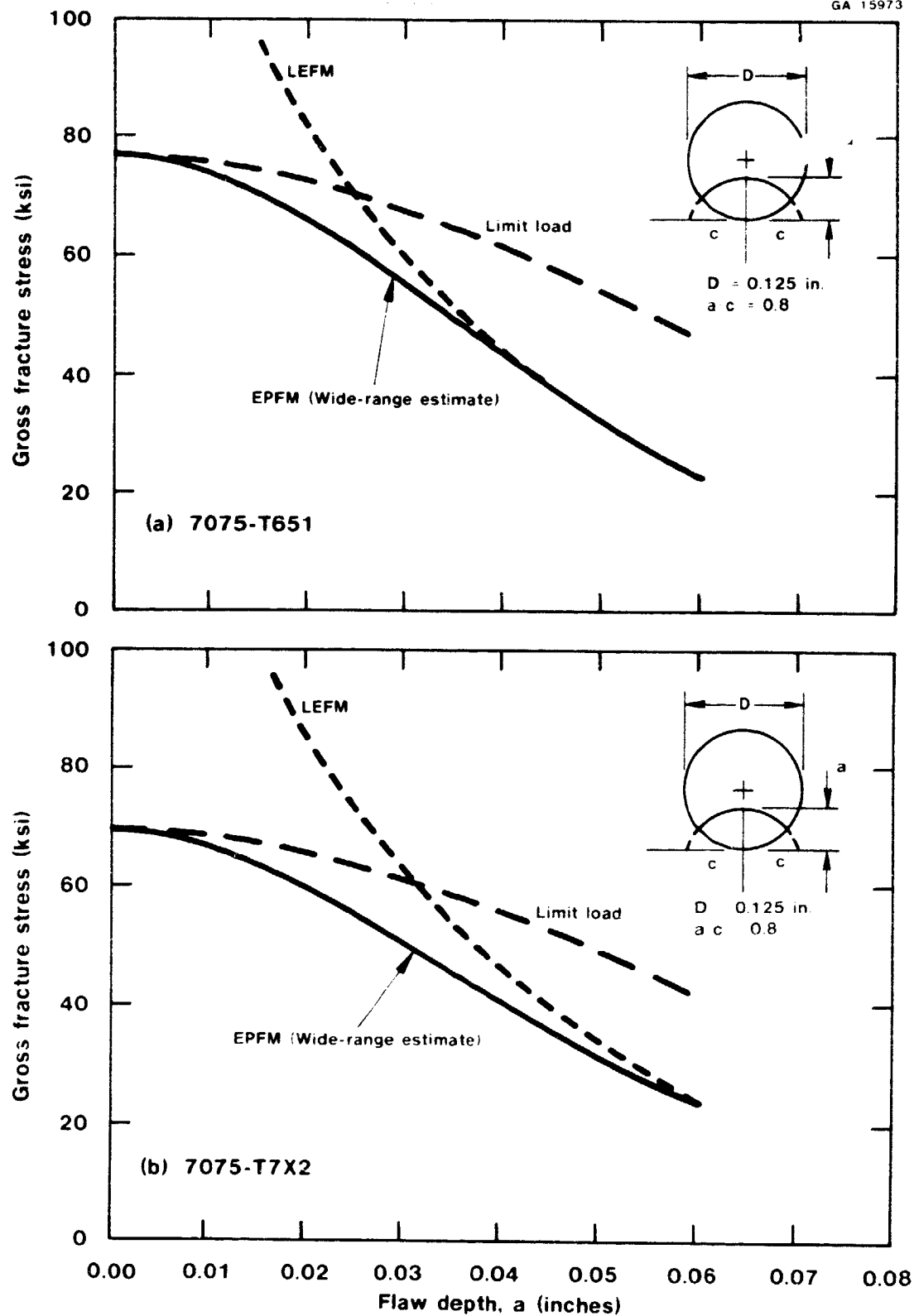


Neg. 5012-58

(b) Enlargement of a portion of the above fractograph showing fine dimples produced during tensile fracture on plateau adjacent to the SCC flaw at right.

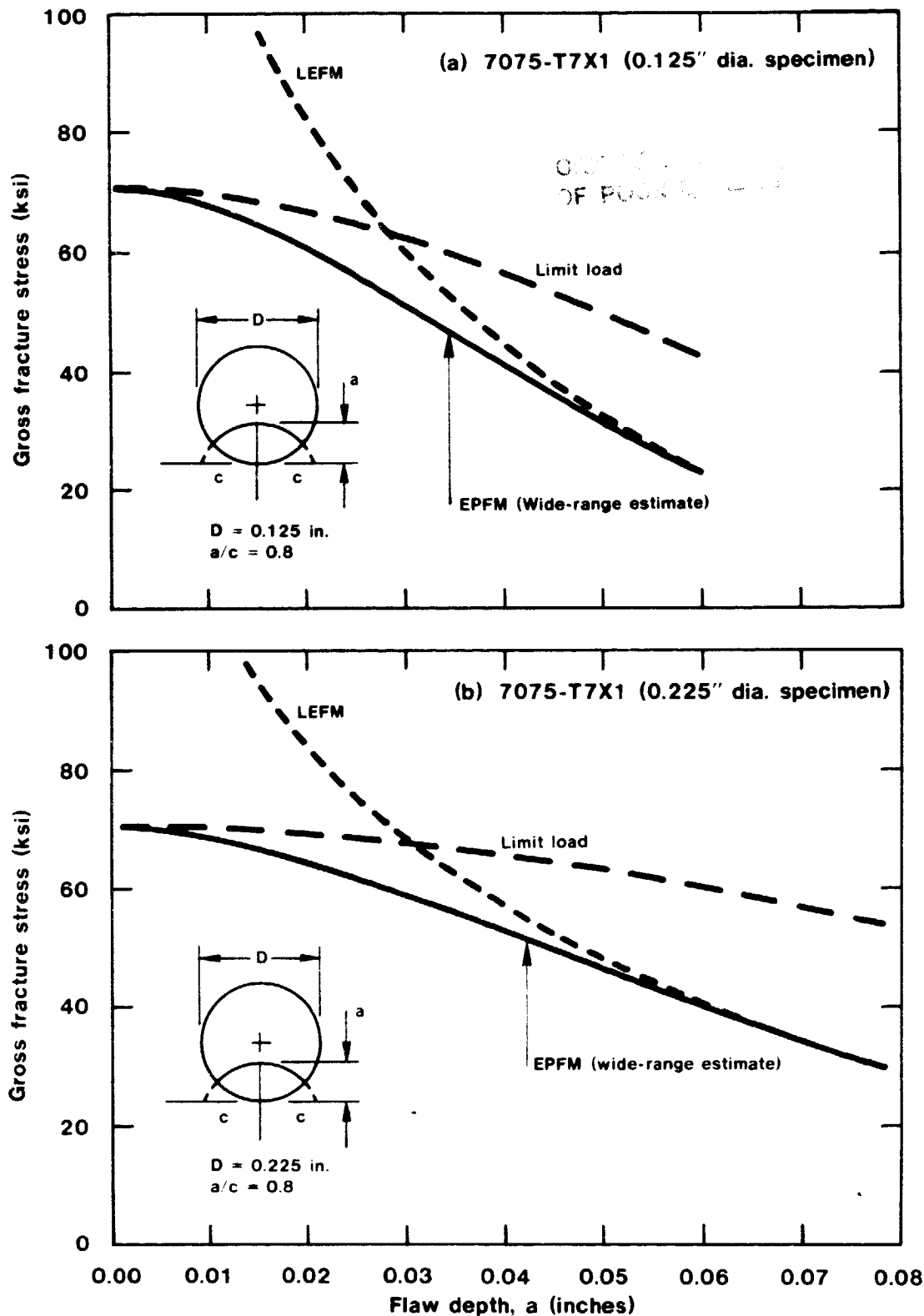
Transition from SCC to Tensile Fracture in Breaking Load Specimen
of 7075-T7X1 (ST80)

Figure 53



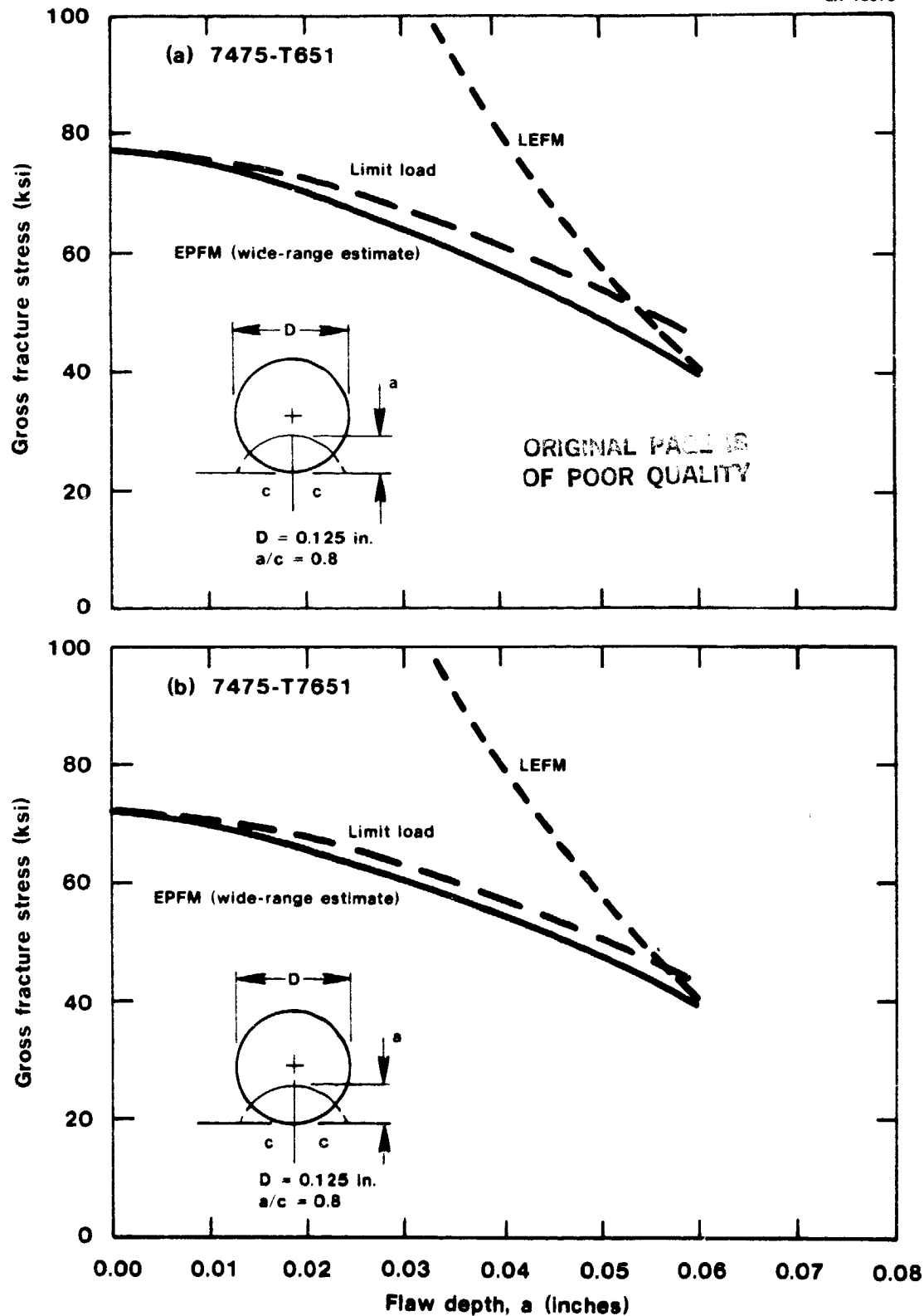
Limit Load, LEFM and Estimated Wide-Range EPFM Failure Criteria for 0.125 in. Diameter, Short Transverse 7075-T651 and 7075-T7X2 Tension Specimens Containing an Elliptical Surface Flaw of Depth a and Aspect Ratio $a/c = 0.8$

Figure 54



Limit Load, LEFM and Estimated Wide-Range EPFM Failure Criteria
for 0.125 and 0.225 in. Diameter, Short Transverse 7075-T7X1
Tension Specimens Containing an Elliptical Surface Flaw of Depth a and
Aspect Ratio $a/c = 0.8$

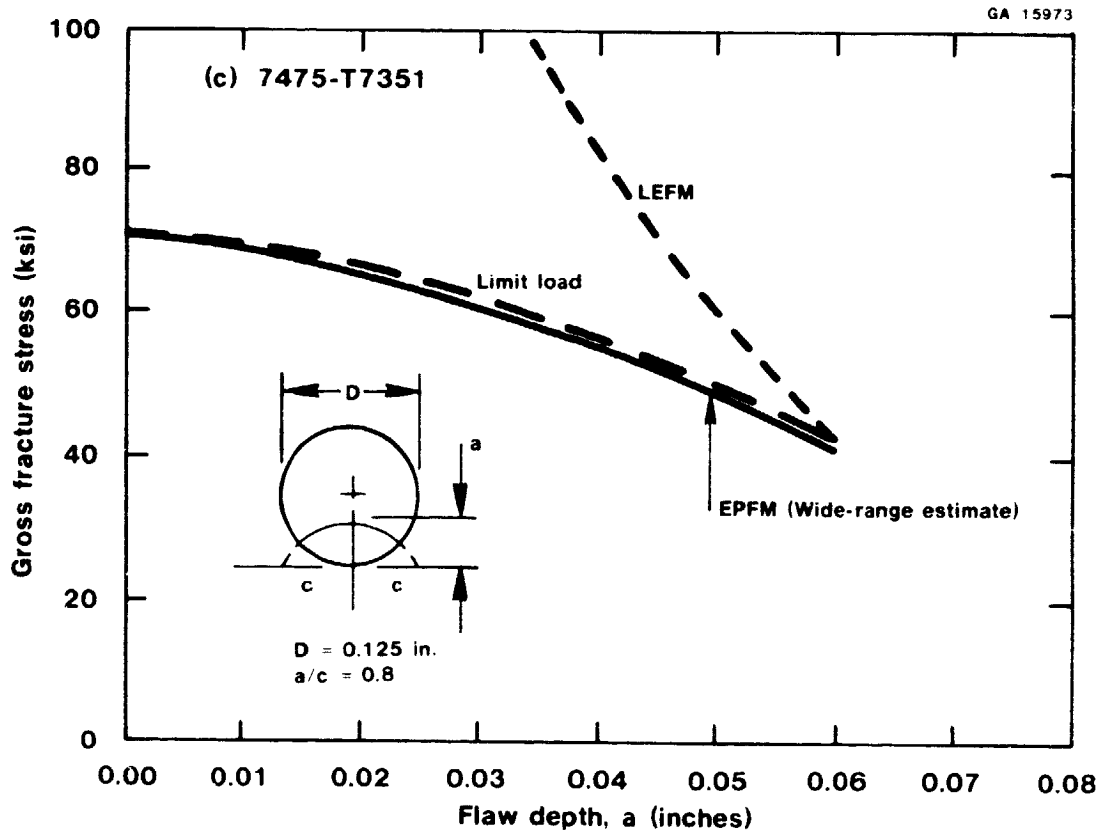
Figure 55



Limit Load, LEFM and Estimated Wide-Range EPFM Failure Criteria for 0.125 in. Diameter, Short Transverse 7475-T651, 7475-T7651 and 7475-T7351 Tension Specimens Containing an Elliptical Surface Crack of Depth a and Aspect Ratio $a/c = 0.8$

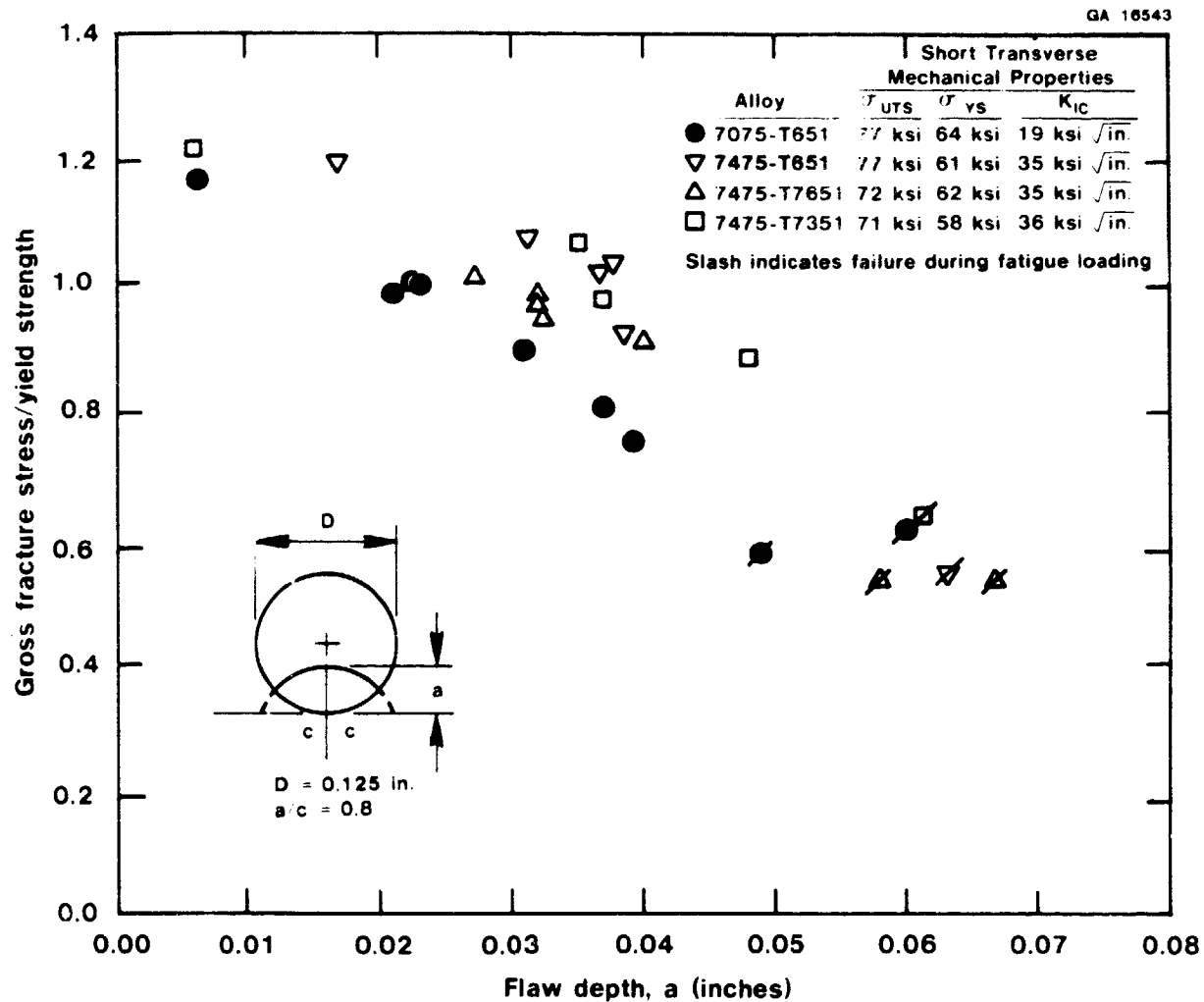
Figure 56

CRACK
OF FL



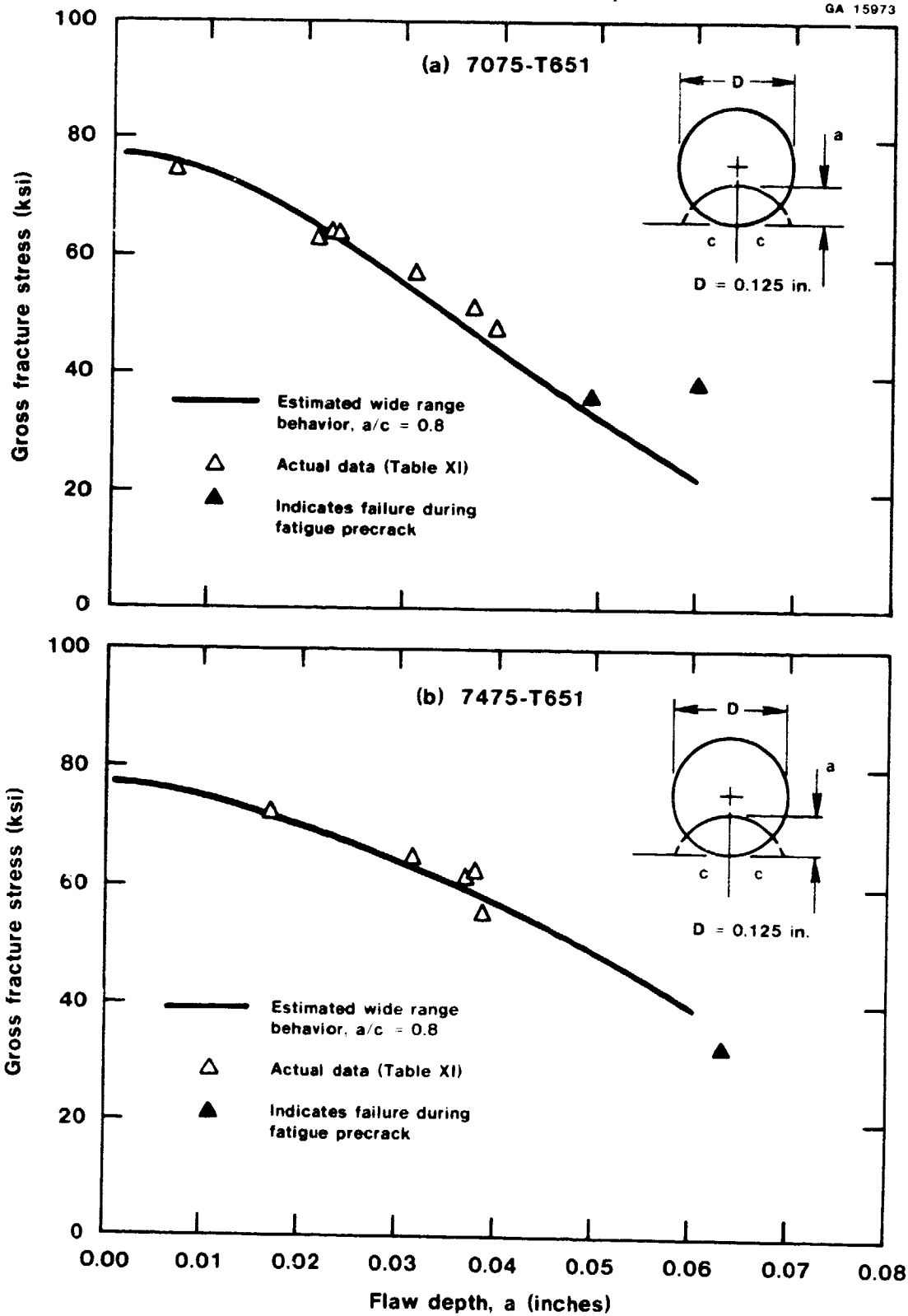
Limit Load, LEFM and Estimated Wide-Range EPFM Failure Criteria
for 0.125 in. Diameter, Short Transverse 7475-T651, 7475-T7651 and
7475-T7351 Tension Specimens Containing an Elliptical Surface Crack
of Depth a and Aspect Ratio $a/c = 0.8$
Figure 56 (Cont.)

ORIGINAL PAGE
OF POOR QUALITY

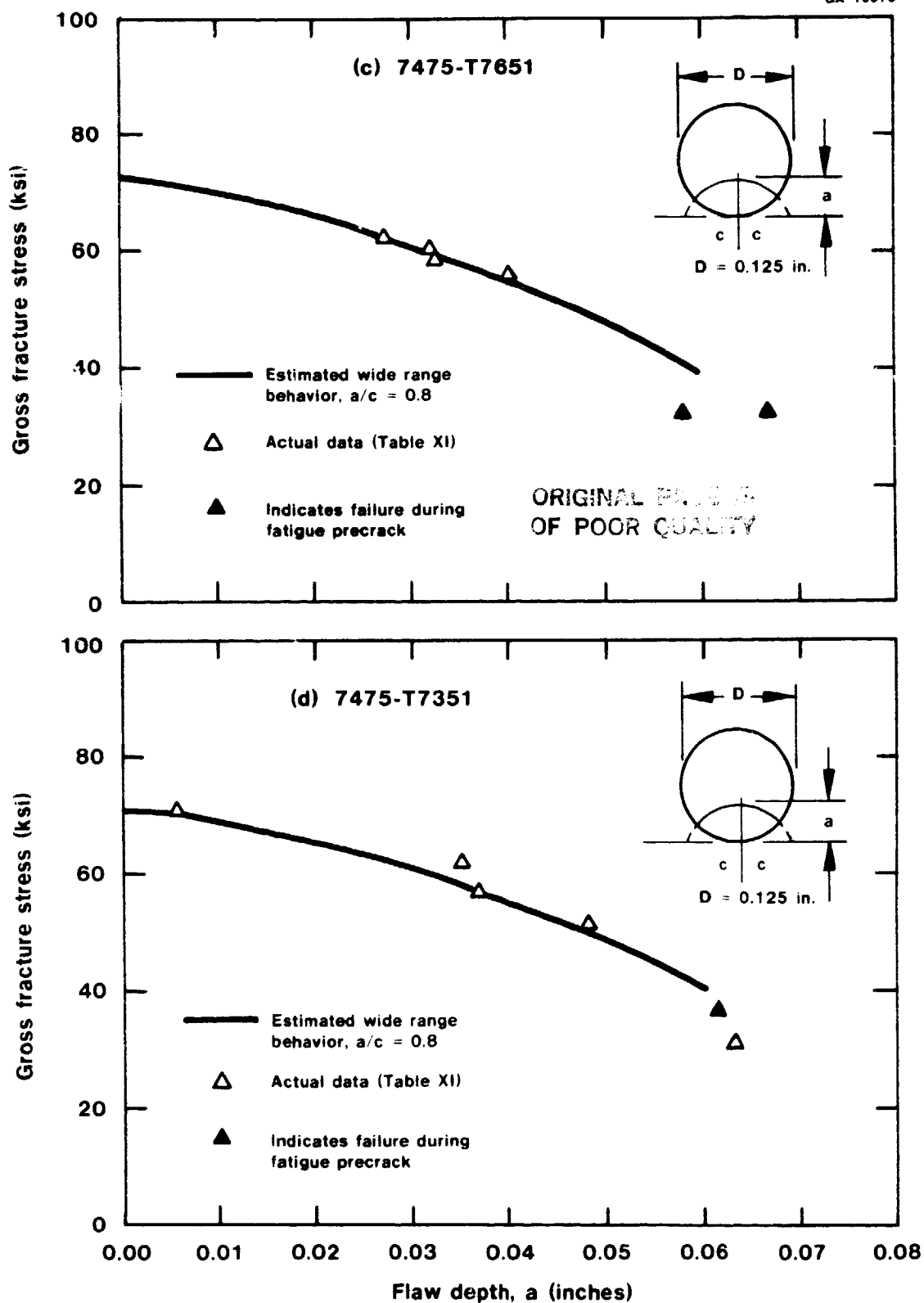


**Comparison of Observed Fracture Stress-Flaw Size Combinations in Fatigue
Precracked Short Transverse 0.125 in. Diameter Tension Specimens
of 7475 and 7075 Plate Alloys.**

Figure 57



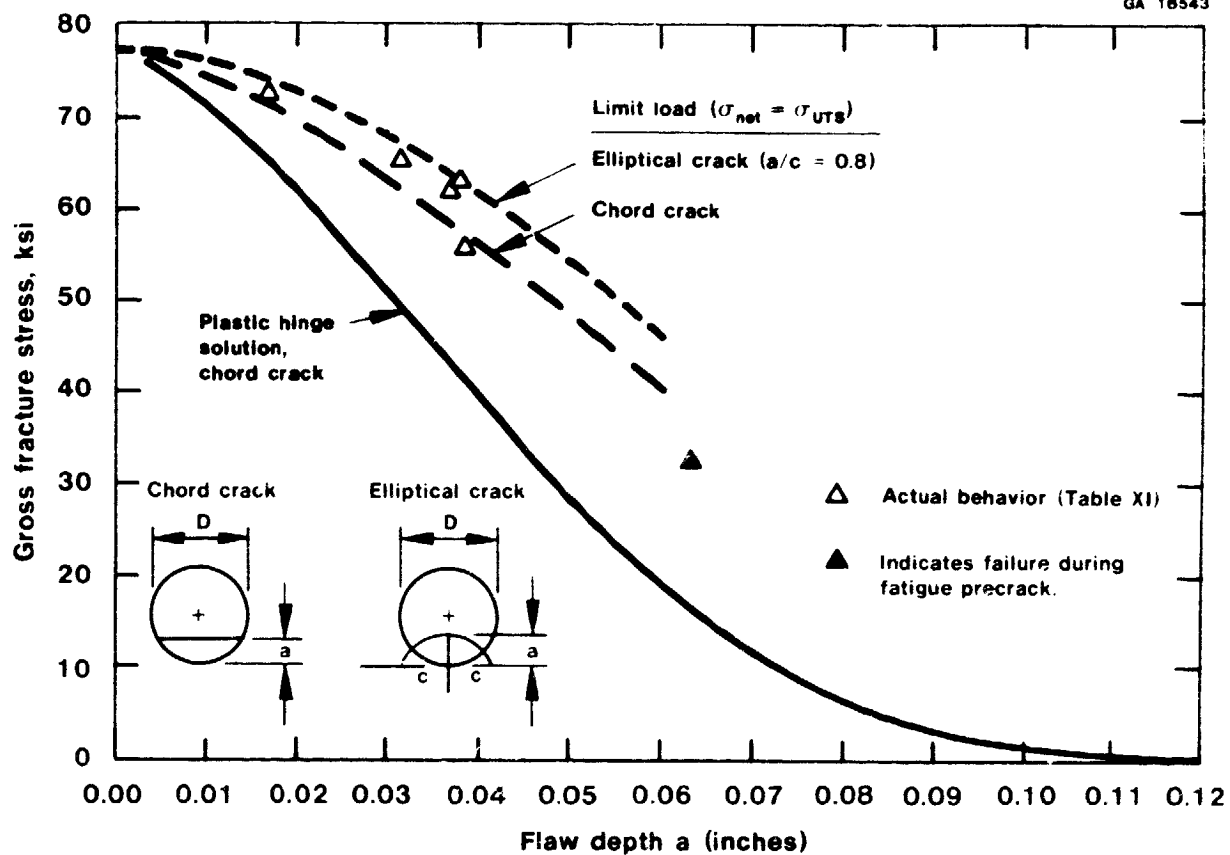
Comparison of Actual and Predicted Fracture Stress-Flaw Size
Combinations in Fatigue Precracked, 0.125 in. Diameter, Short Transverse
Tension Specimens of Commercial 7X75 Plate Alloys
Figure 58



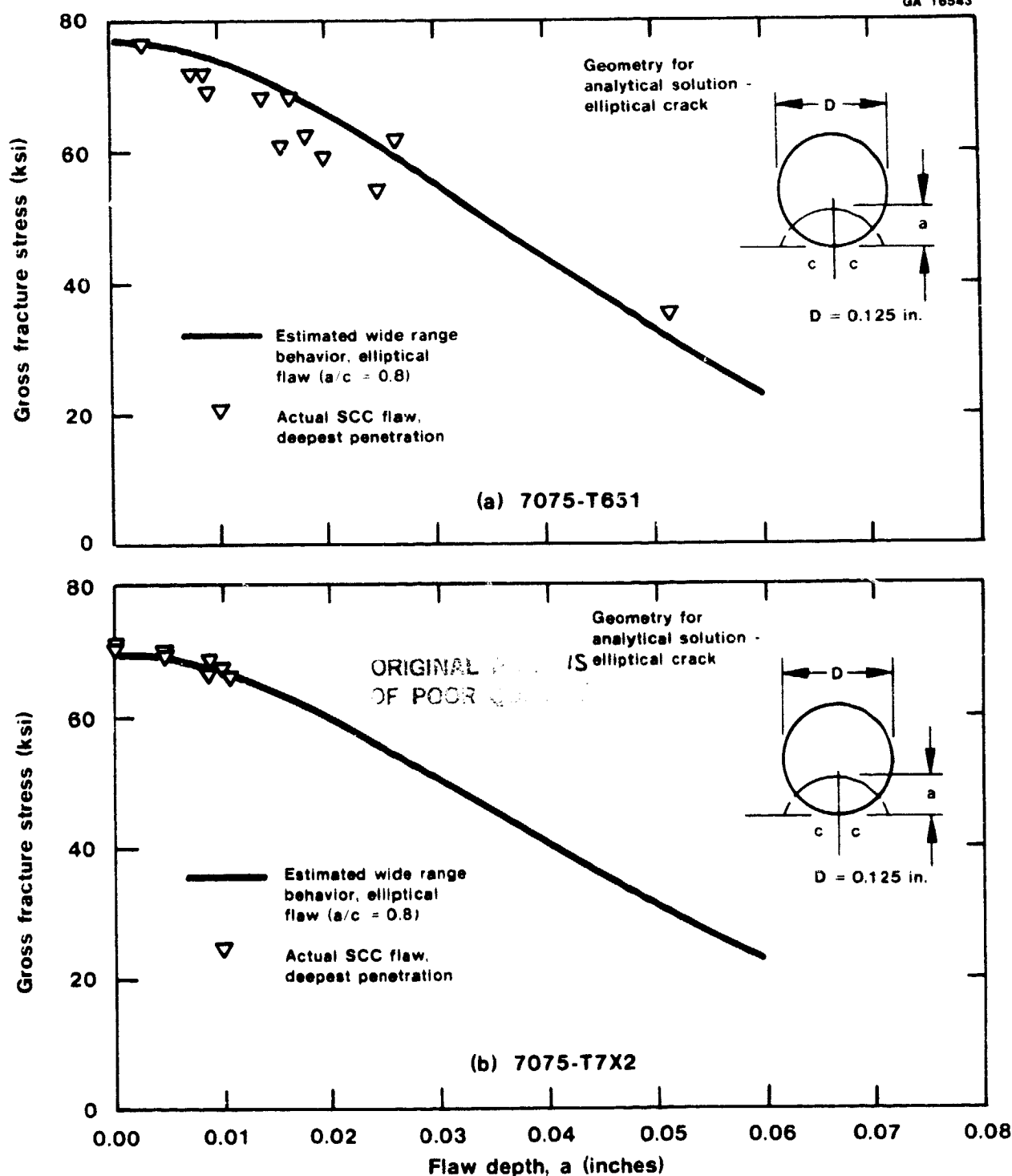
Comparison of Actual and Predicted Fracture Stress-Flaw Size Combinations in Fatigue Precracked, 0.125 in. Diameter, Short Transverse Tension Specimens of Commercial 7X75 Plate Alloys
Figure 58 (Cont.)

ORIGINAL
OF POC...

GA 16543

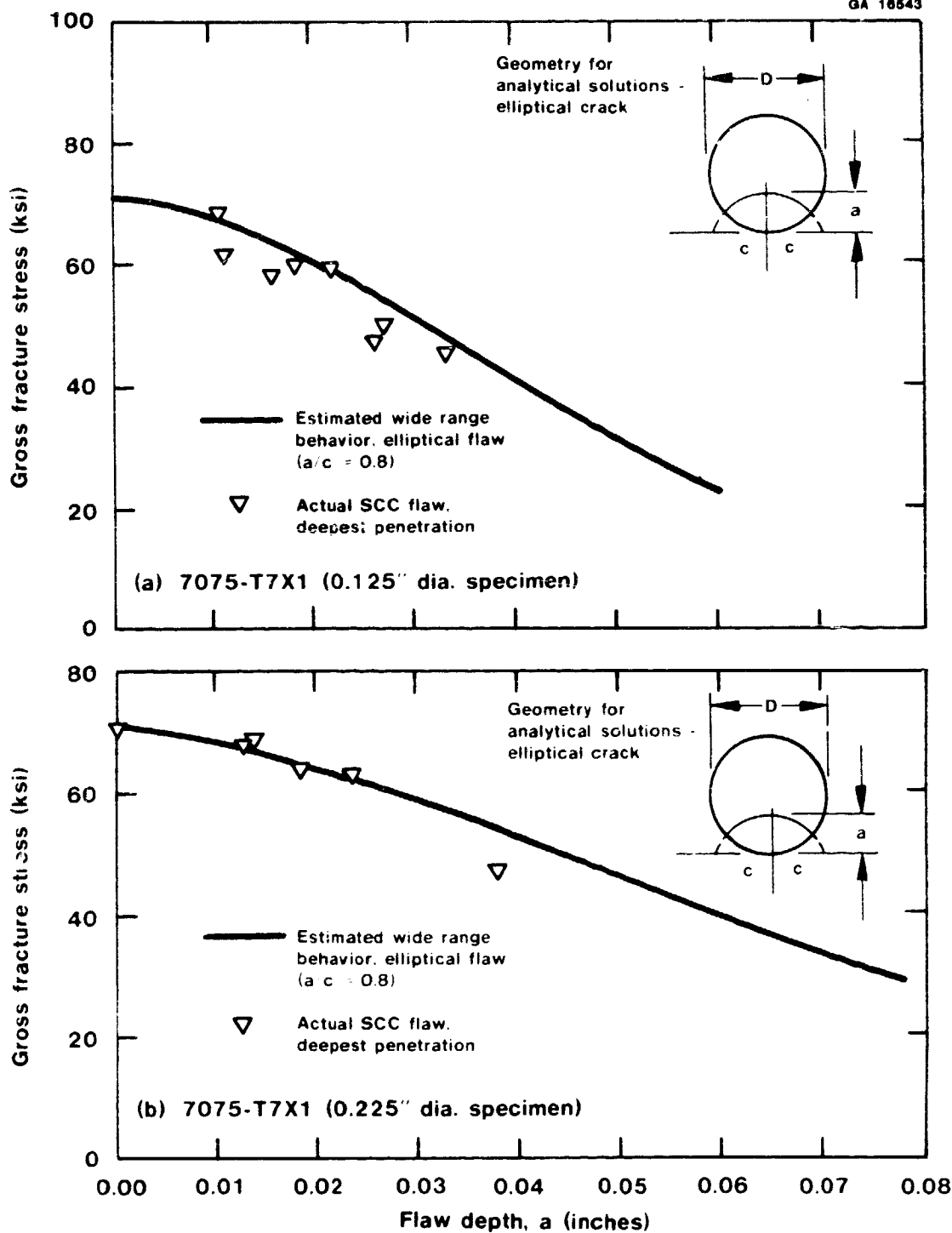


Comparison of Various Plasticity Based Predictions with Actual Fracture Stress-Flaw Size Combinations in 0.125-in. Diameter Fatigue Precracked Tension Specimens of 7475-T651 Alloy
Figure 59



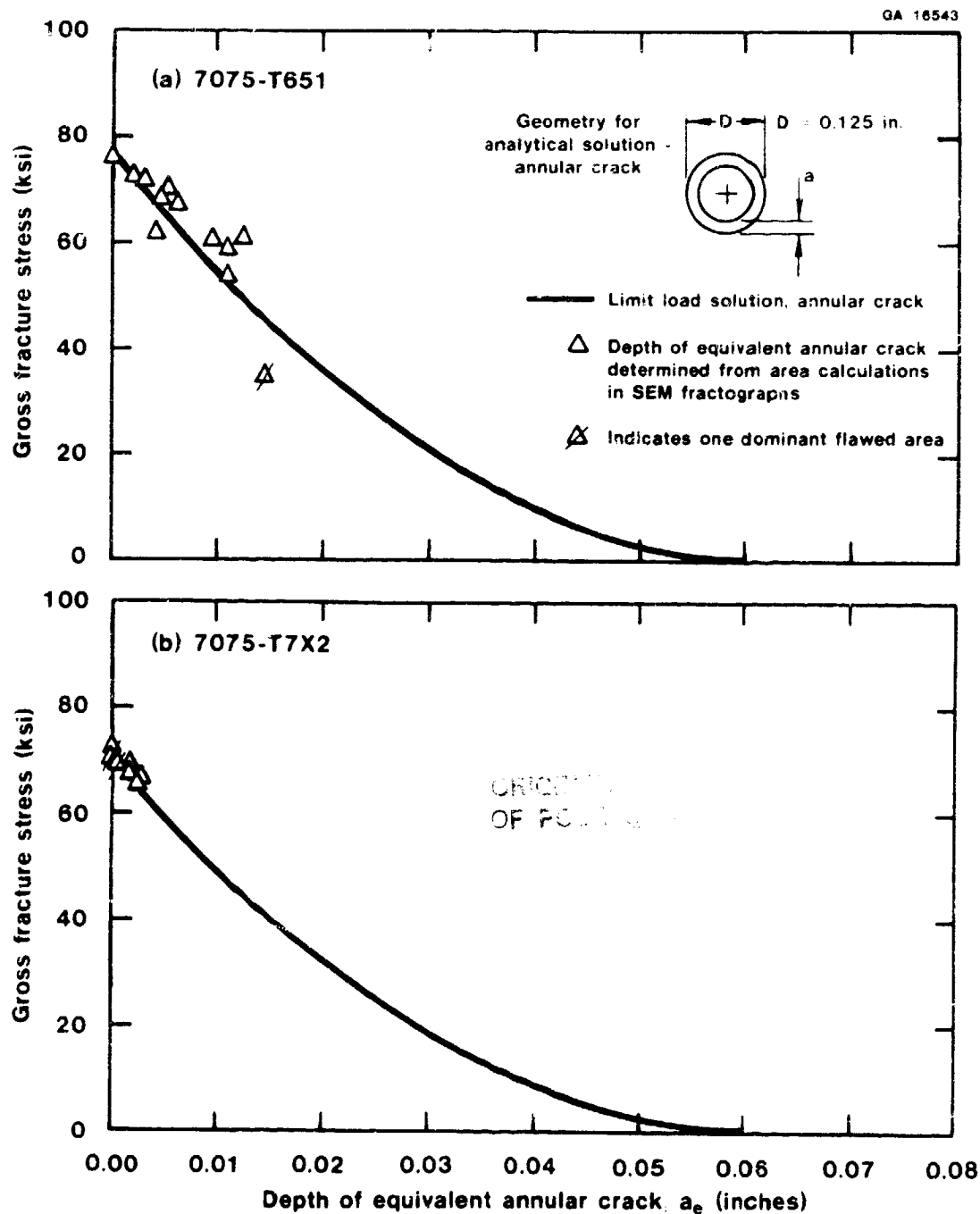
Comparison of Actual and Predicted Fracture Stress vs. Maximum SCC Flaw Depth in Stress Corroded, 0.125 in. Diameter, Short Transverse Tension Specimens of Alloys 7075-T651 and 7075-T7X2

Figure 60

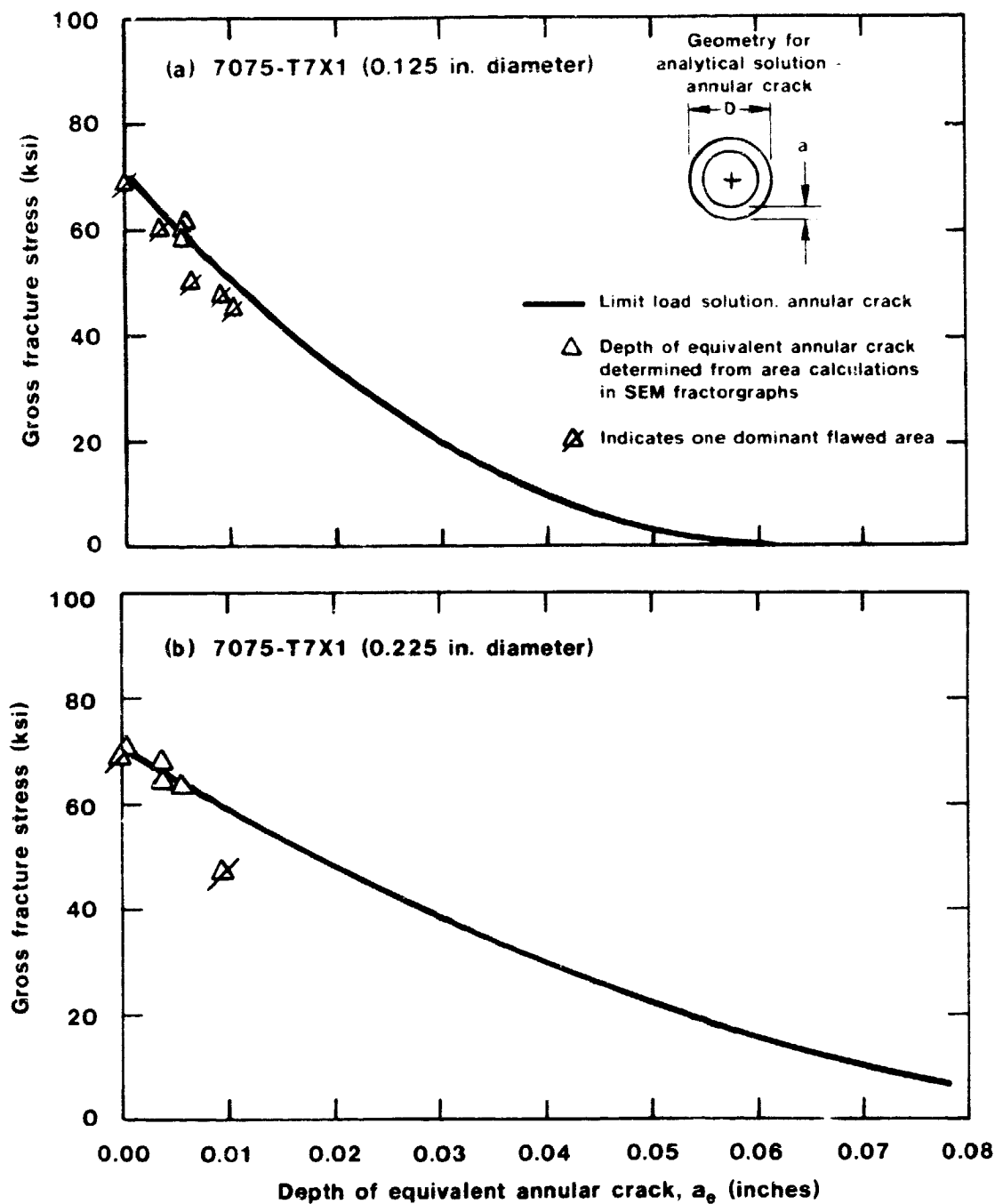


Comparison of Actual and Predicted Fracture Stress vs. Maximum SCC Flaw Depth in Stress Corroded, 0.125 in. and 0.225 in. Diameter, Short Transverse Tension Specimens of Alloy 7075-T7X1

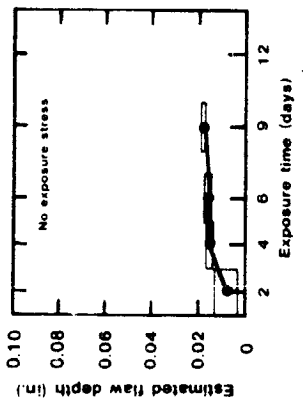
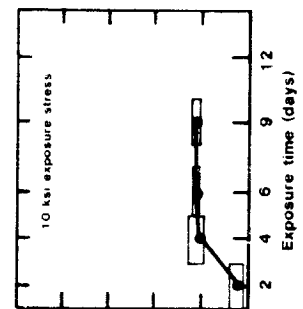
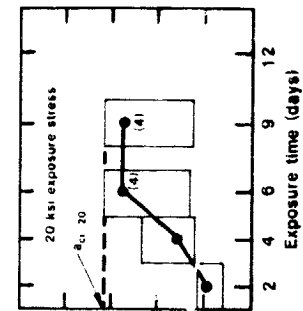
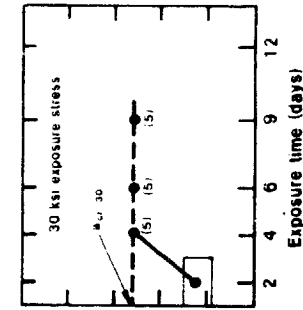
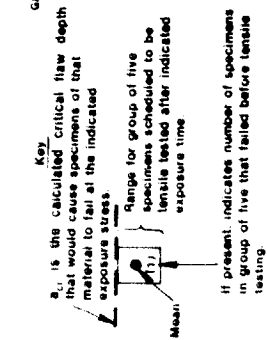
Figure 61



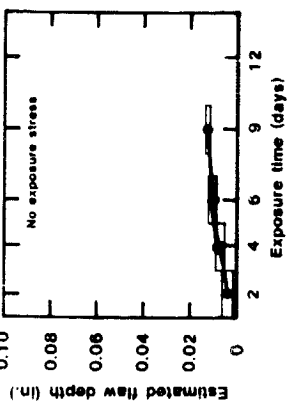
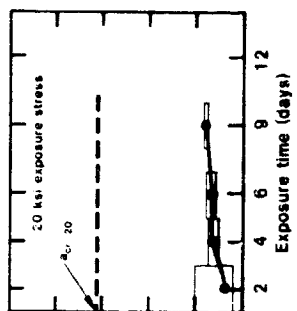
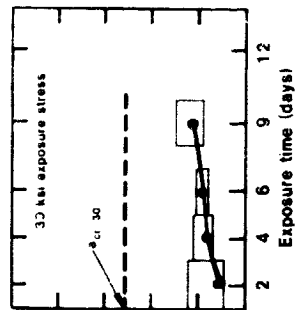
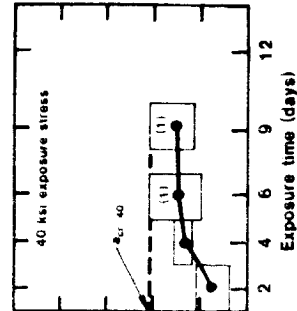
Comparison of Actual and Predicted Fracture Stress vs. Depth of Equivalent Annular Crack in Stress Corroded 0.125-in. Diameter, Short Transverse Tension Specimens of Alloys 7075-T651 and 7075-T7X2
Figure 62



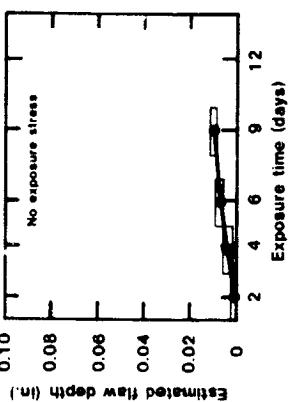
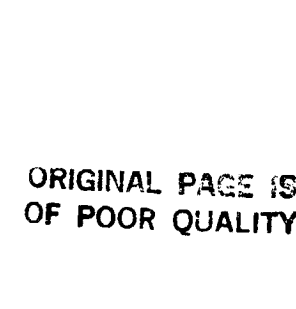
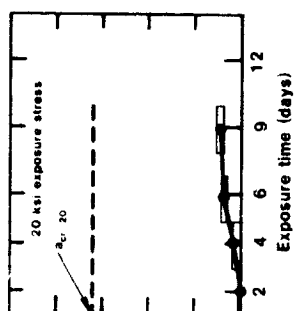
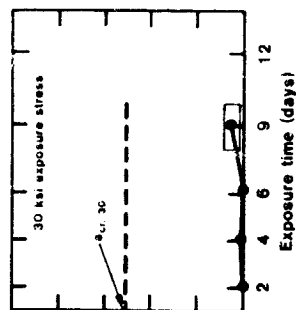
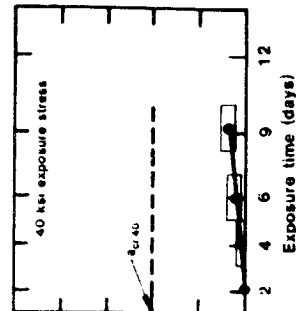
Comparison of Actual and Predicted Fracture Stress vs. Depth of Equivalent Annular Crack in Stress Corroded 0.125 in. and 0.225 in. Diameter, Short Transverse Tension Specimens of Alloy 7075-T7X1
Figure 63



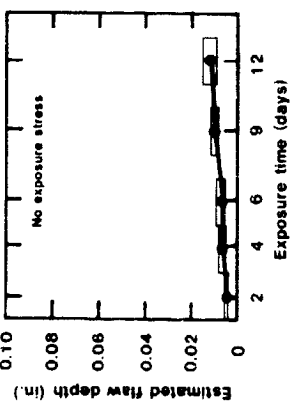
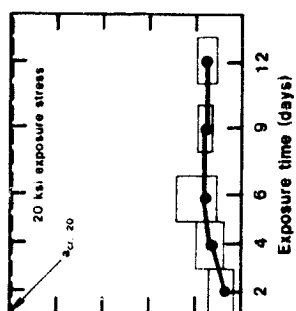
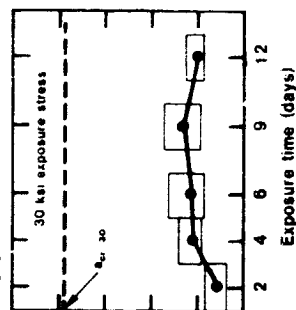
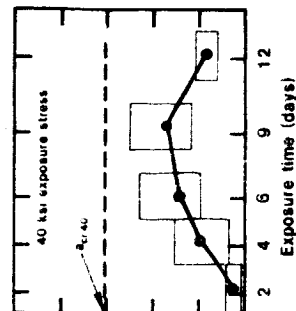
(a) 7075-T651, short transverse 0.125 in. diameter specimens.



(b) 7075-T7X1, short transverse 0.125 in. diameter specimens.



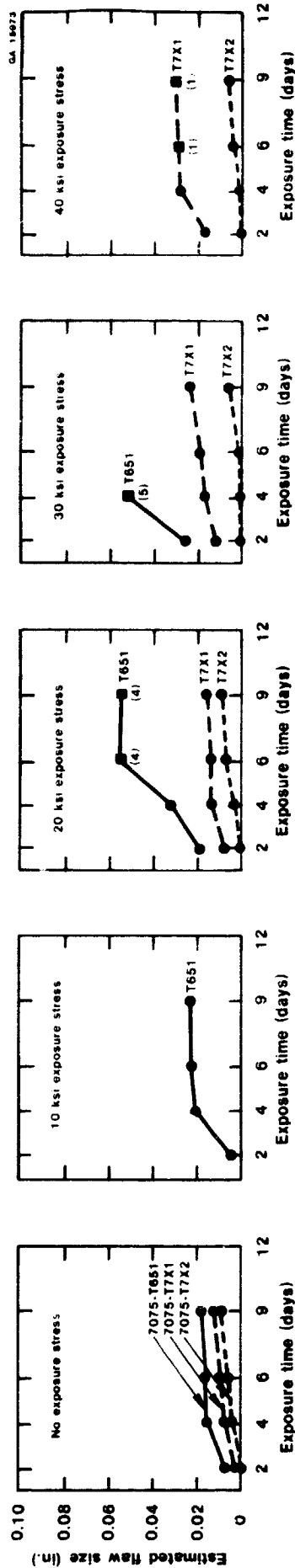
(c) 7075-T7X2, short transverse 0.125 in. diameter specimens.



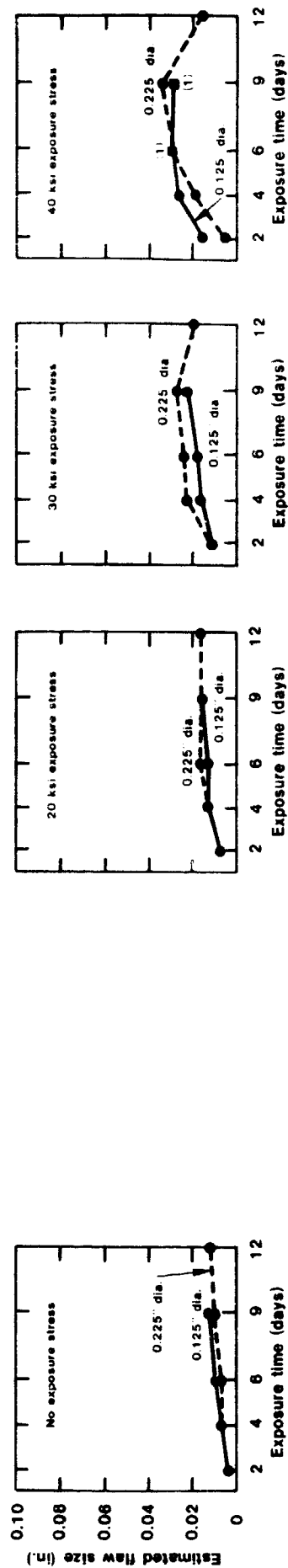
(d) 7075-T7X1, short transverse 0.225 in. diameter specimens.

Estimated SCC Flaw Growth in 7075 Alloy Tension Specimens Calculated from Breaking Load Data and Wide Range EPFM Model. Specimens were Exposed to 3.5% NaCl Solution by Alternate Immersion (ASTM G44) at the Indicated Exposure Stress for Various Times and Then Tensile Tested.

Figure 84



(a) Comparisons of 7075-T651, 7075-T7X1 and 7075-T7X2 short transverse 0.125 in. diameter [See Figure 64 (a), (b), and (c)].



(b) Comparisons of two short transverse specimen diameters (0.125 in. and 0.225 in.) of 7075-T7X1 showing nearly identical flaw growth [See Figure 64 (b) and (d)].

Notes - All data points calculated from a mean of five breaking loads.

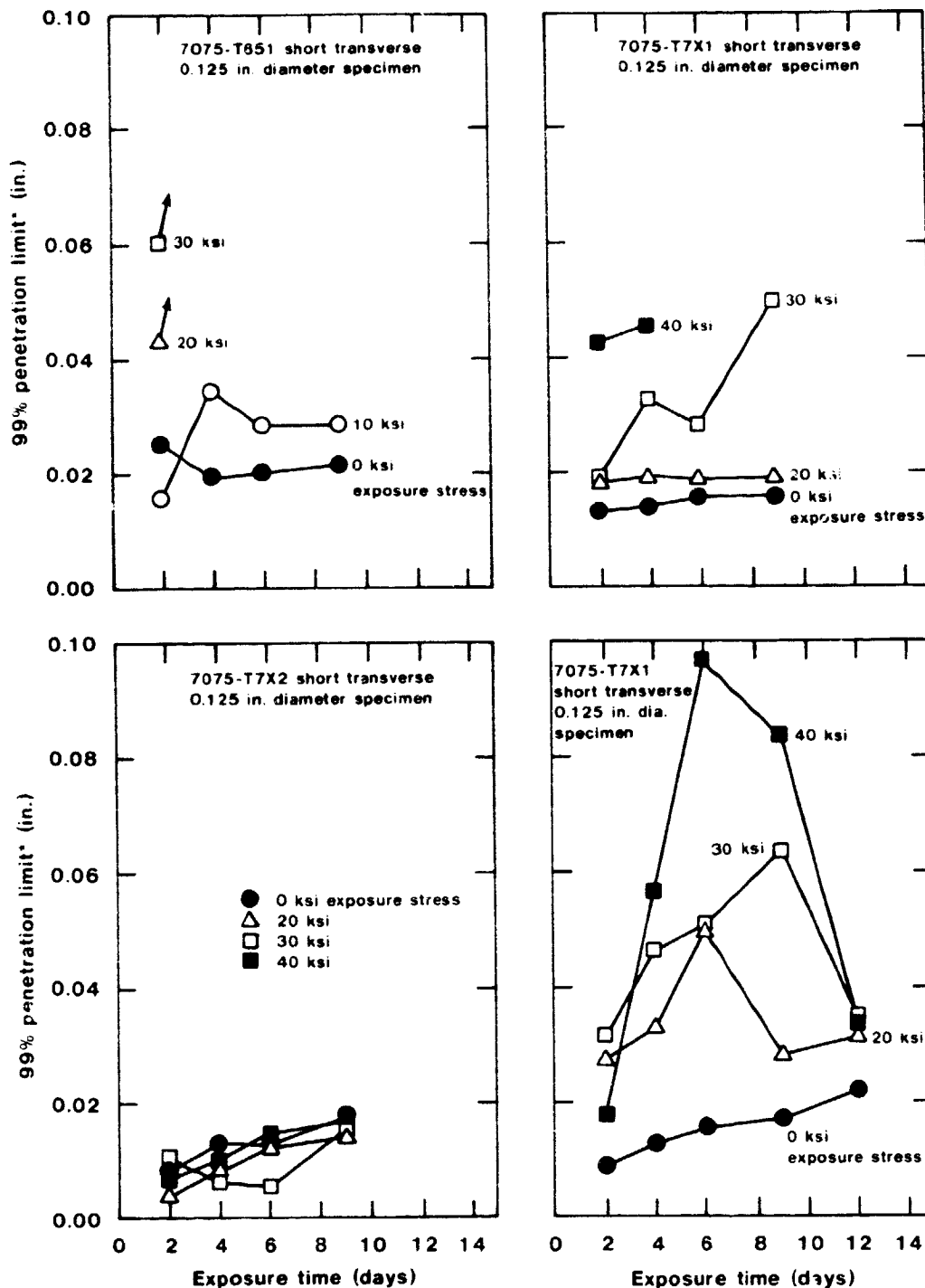
○ - Indicates no failures before tensile testing.

■ - Indicates that the number of failures in parenthesis is included in the mean breaking load.

— - Mean breaking load calculated by using the exposure stress as the breaking strength for failed specimens.

Comparisons of Estimated Mean SCC Flaw Growth in 7075 Alloy Tension Specimens Calculated from Breaking Load Data and Wide Range EPFM Model (See Figure 64).

Figure 65



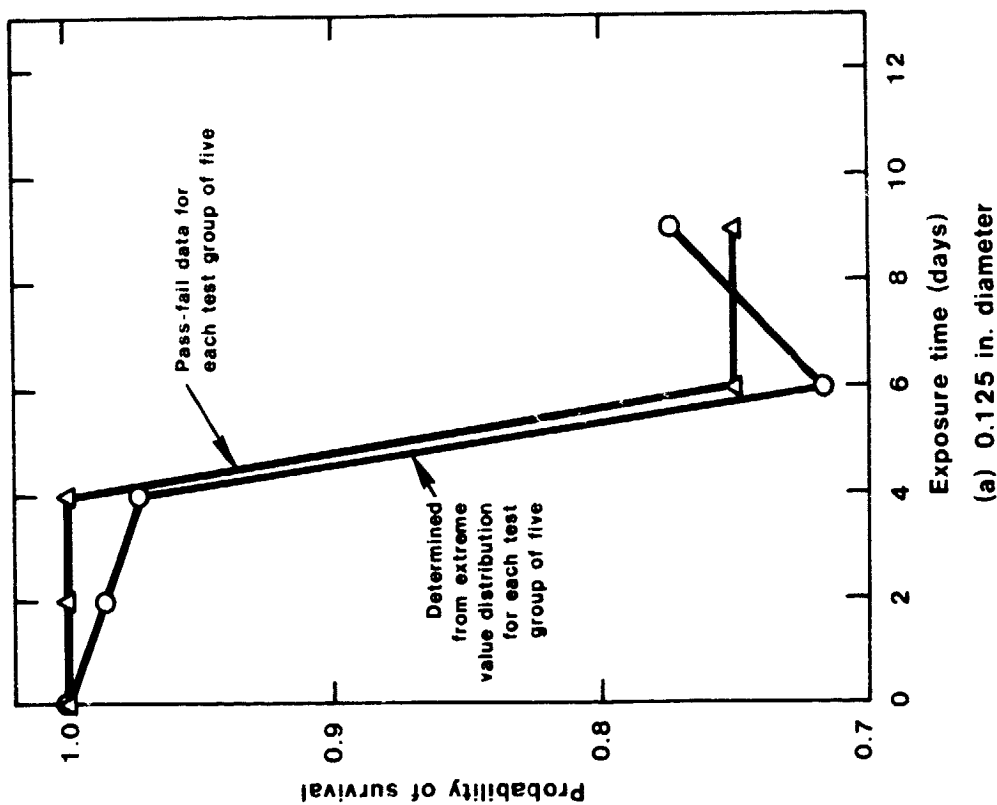
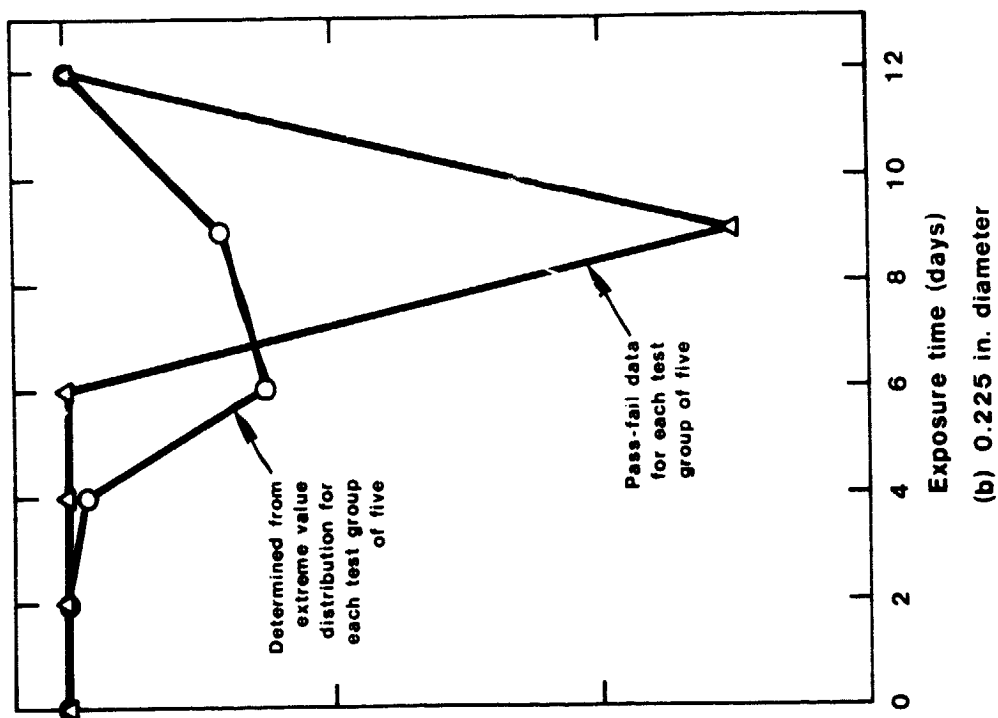
*The 99% penetration limit (a_{99}) is the estimated SCC flaw depth that would not be exceeded in 99% of the specimens, as calculated from the 99% survival stress and the wide range EPFM estimate for flaw size vs. breaking stress.

Short transverse tension specimens were exposed to 3.5% NaCl solution by alternate immersion (ASTM G44) at the indicated exposure stress for various times and then tensile tested.

Calculated 99% Penetration Limits for 0.125 in. Diameter Specimens of 7075-T651, 7075-T7X1, and 7075-T7X2 and for 0.225 in. Diameter Specimens of 7075-T7X1.

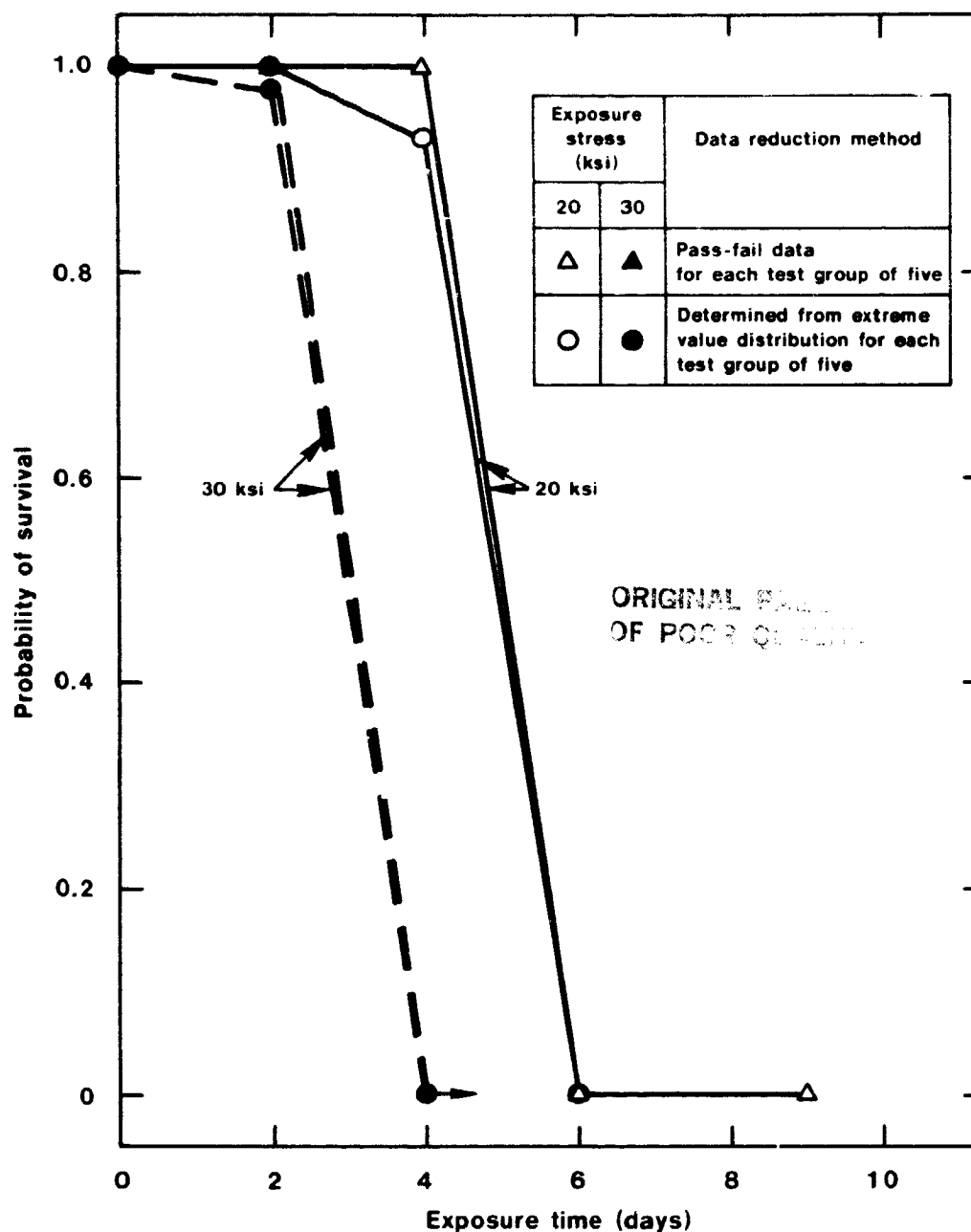
Figure 66

ORIGINAL TEST DATA
OF POOR QUALITY



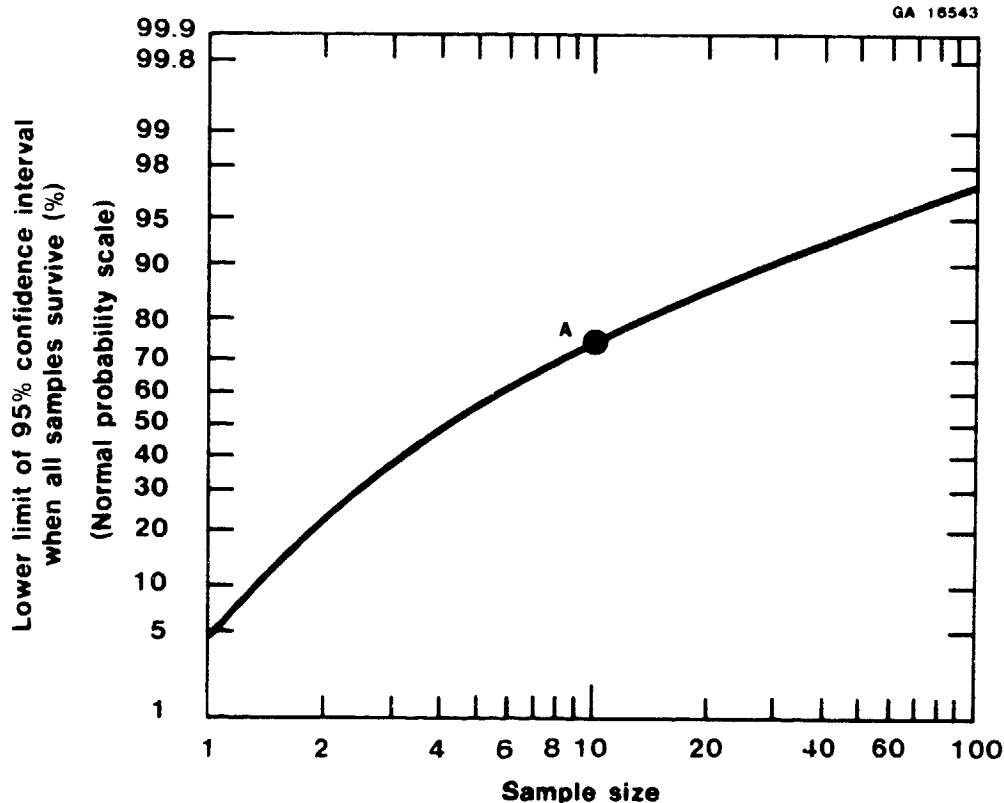
Comparison of Survival Probabilities for Two Specimen Diameters, Calculated from Breaking Load and Traditional Pass-Fail Data for Short Transverse Specimens of 7075-T7X1 Exposed to 3/5% NaCl Alternate Immersion (ASTM G44) at 40 ksi for Various Exposure Times and then Tensile Tested.

Figure 67



Comparison of Probability of Survival Calculated from Breaking Load and Traditional Pass-Fail Data for Short Transverse 0.125 in. Diameter Specimens of 7075-T651 Exposed to 3.5% NaCl Alternate Immersion Test (ASTM G44) at 20 and 30 ksi for Various Exposure Times and Then Tensile Tested.

Figure 68

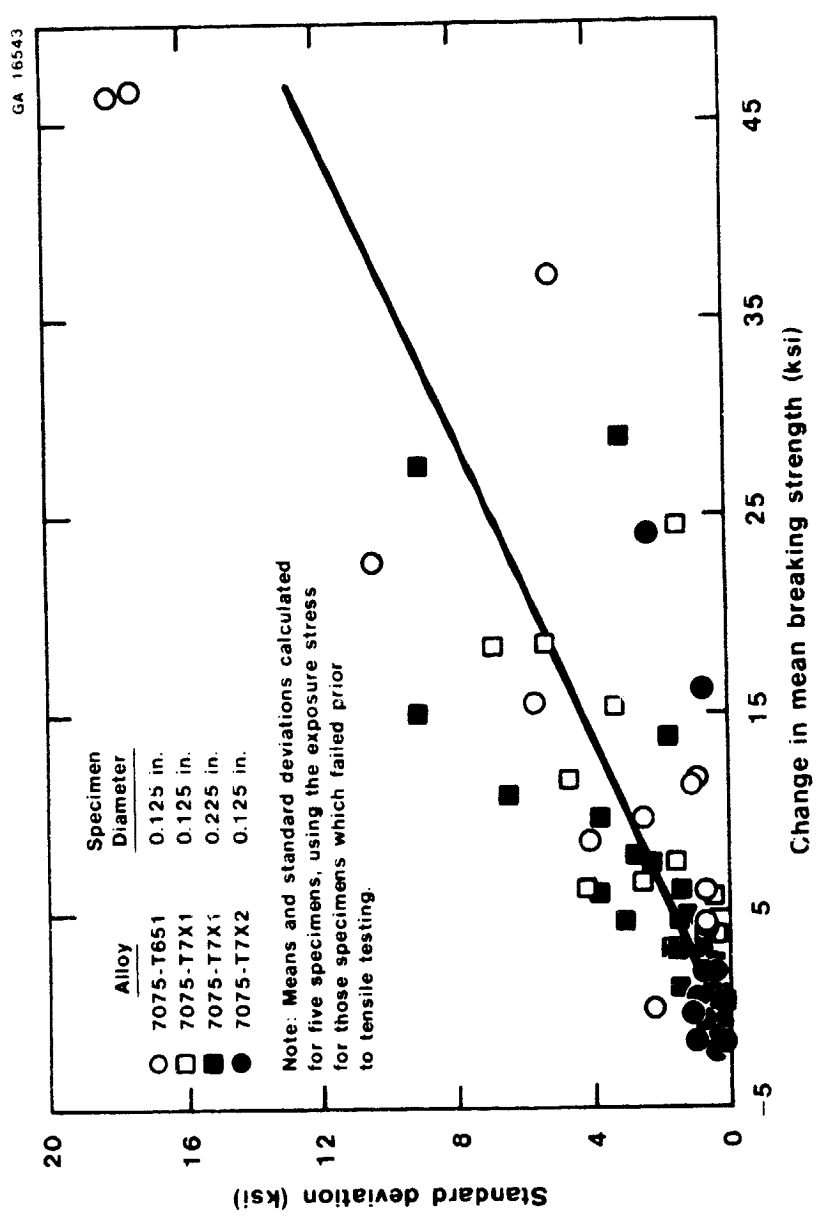


Point A indicates that for a sample size of 10 specimens, all surviving, the true probability of survival lies between 0.75 and 1.0 with 95% confidence. There is a family of similar curves for other estimated survival probabilities (N_s/N_T).

Effect of Sample Size on Lower Limit of 95% Confidence Interval of the Estimated Probability of Survival (P) Using Pass-Fail (Binomial) Data When All Specimens Survive ($P = 1$)

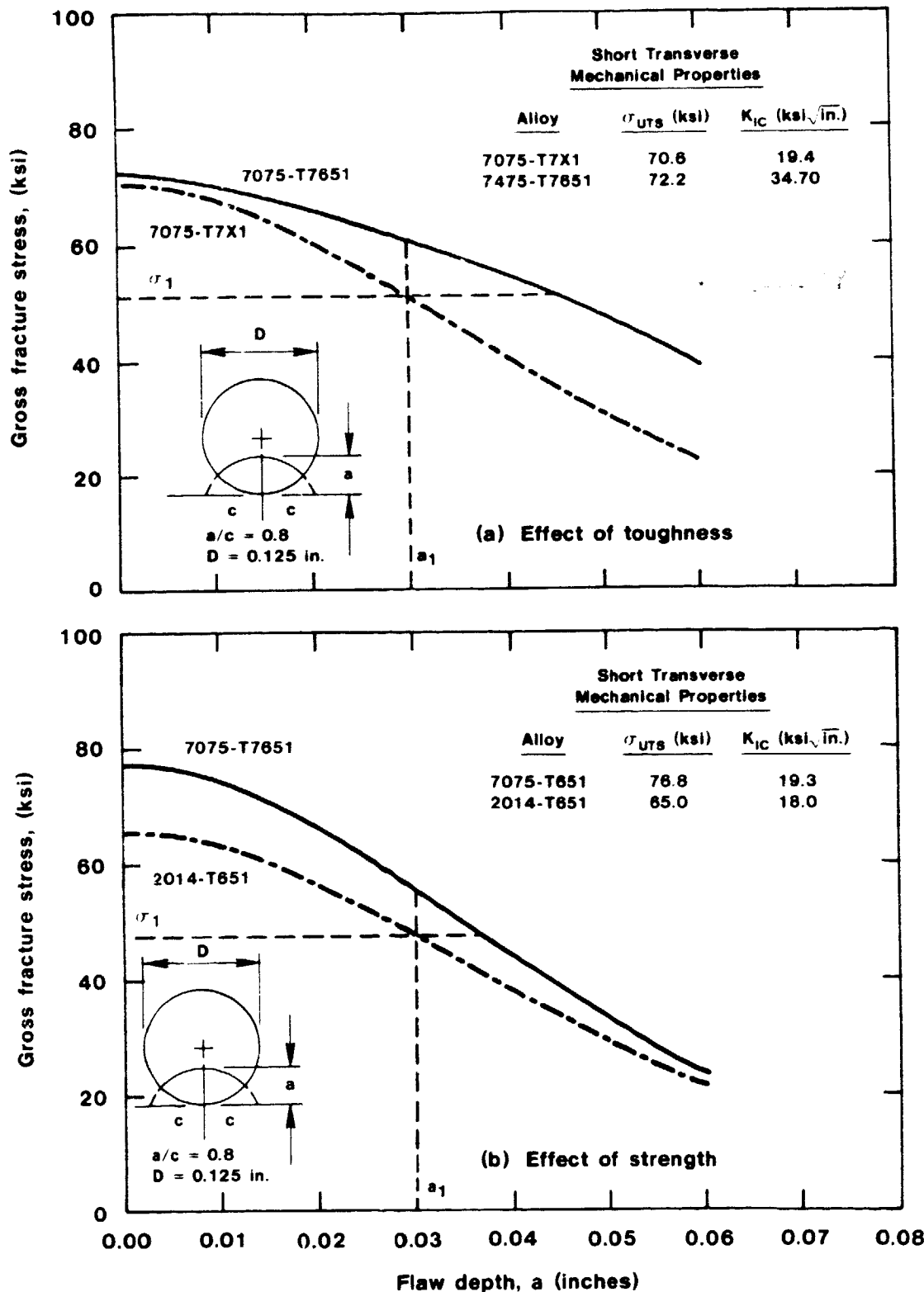
Figure 69

ORIGINAL FILE
OF POCR QUALITY



Summary of Breaking Load Data for Short Transverse Tests of 7075 Alloy Plate Showing the Relationship Between Standard Deviation and Change in Mean Breaking Strength Relative to the Unexposed Data Set for Each Temper.

Figure 70

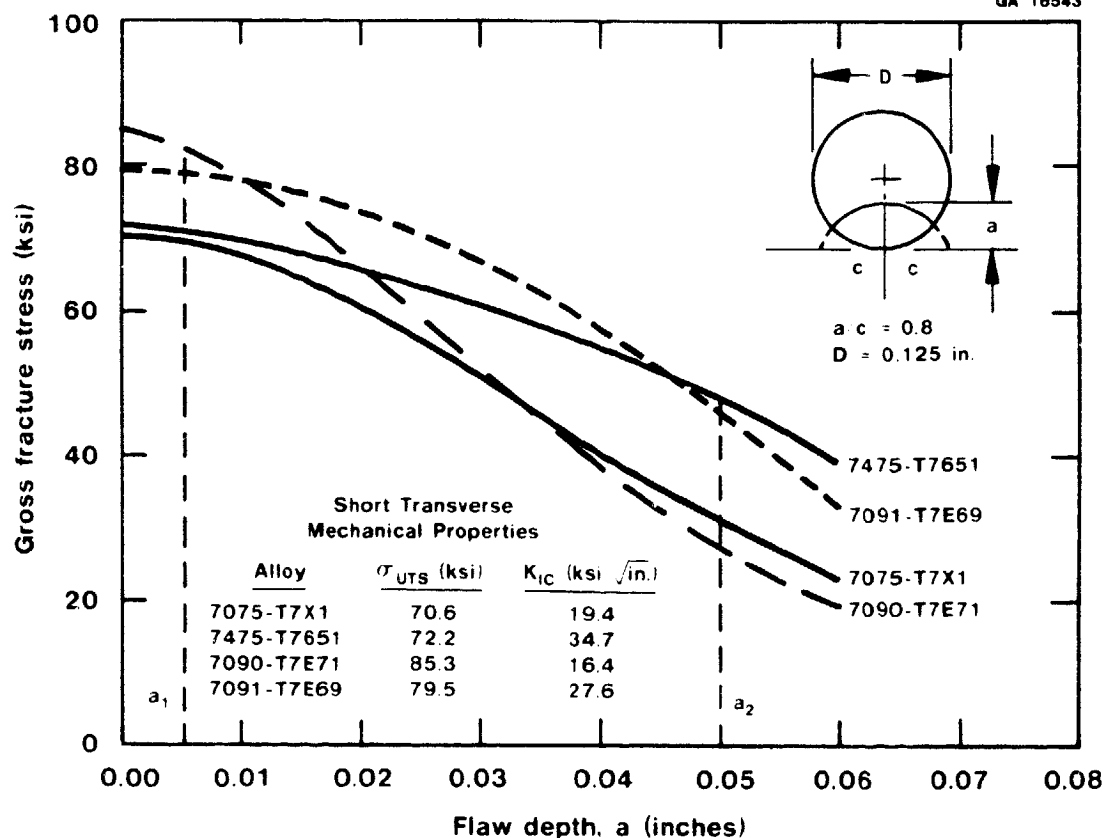


Breaking Stress-Flaw Relationships Developed from EPFM Wide-Range Estimates Showing Effects of Alloy Toughness (7075-T7X1 vs. 7475-T7651) and Strength (7075-T651 vs. 2014-T651) on Results of 0.125 in. Diameter Tension Specimens which Contain an Elliptical Partial Thickness Crack ($a/c = 0.8$).

Figure 71

ORIGINAL
OF POOR QUALITY

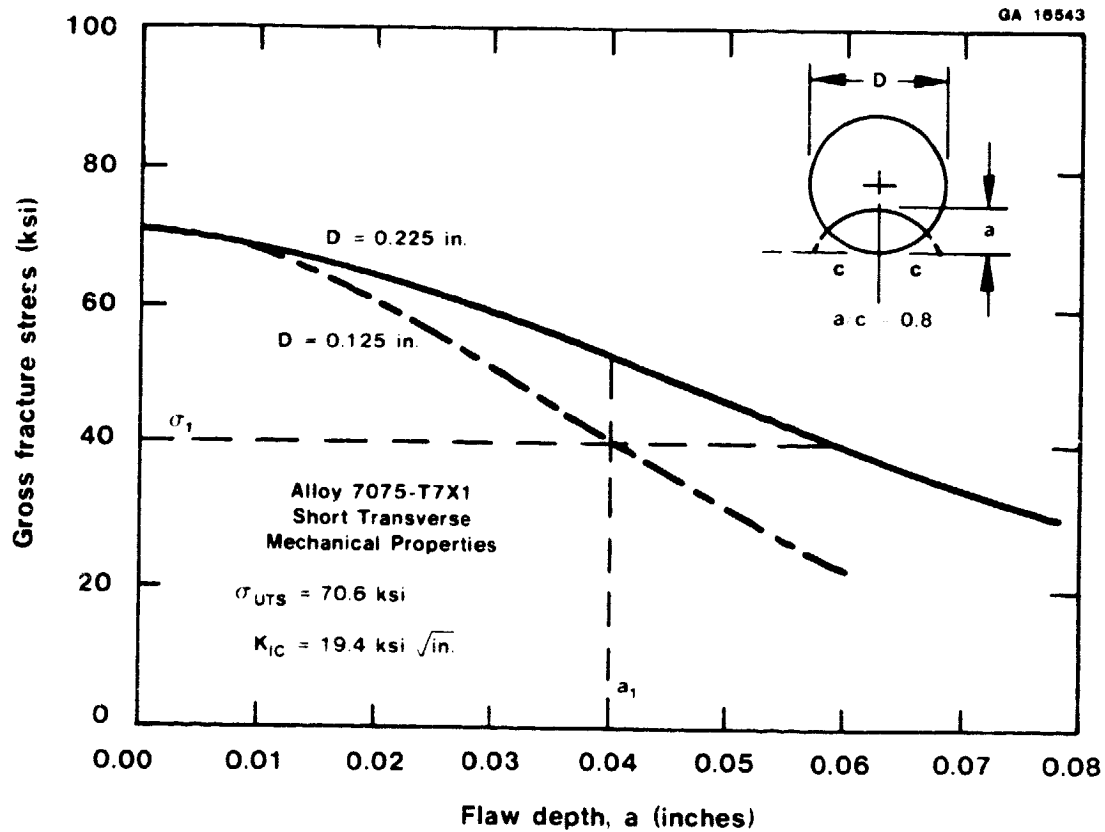
QA 16543



Estimated Gross Fracture (Breaking) Stress-Flaw Size Behaviors
for Various I/M and P/M 7XXX Series Alloys aged to a T7 Type Temper
Condition. Specimen Configuration: 0.125 in. Diameter Tension Specimen
Containing an Elliptical Partial Thickness Crack of Depth a
and Aspect Ratio $a/c = 0.8$

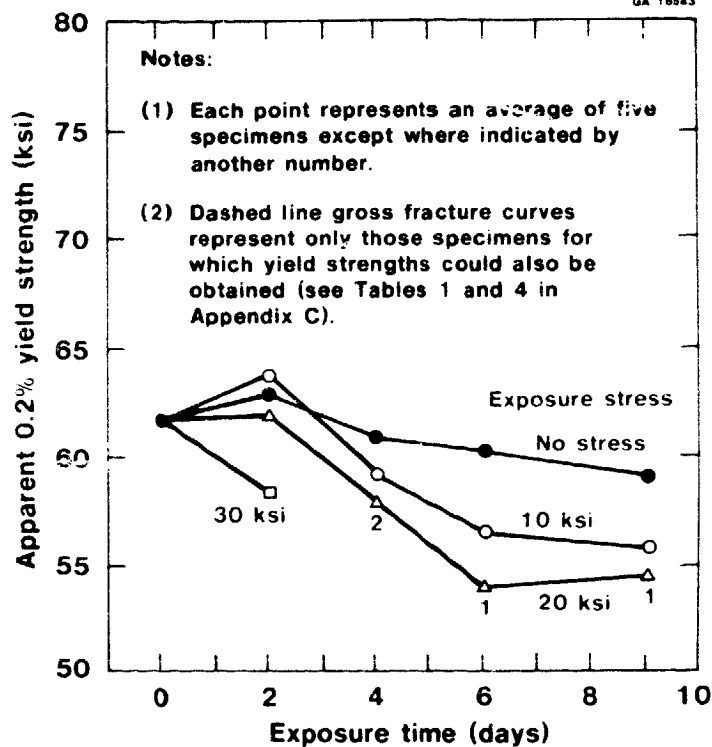
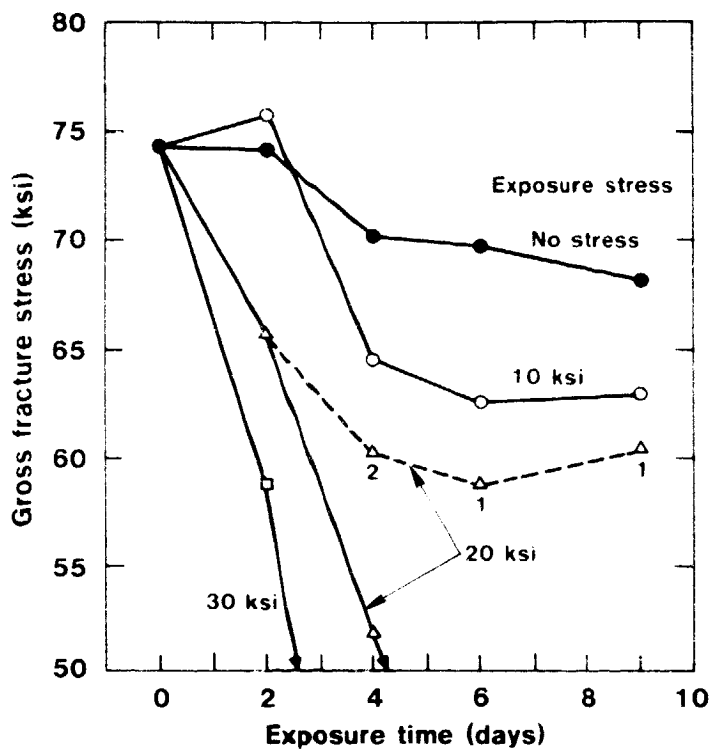
Figure 72

CRACK
OF 90°

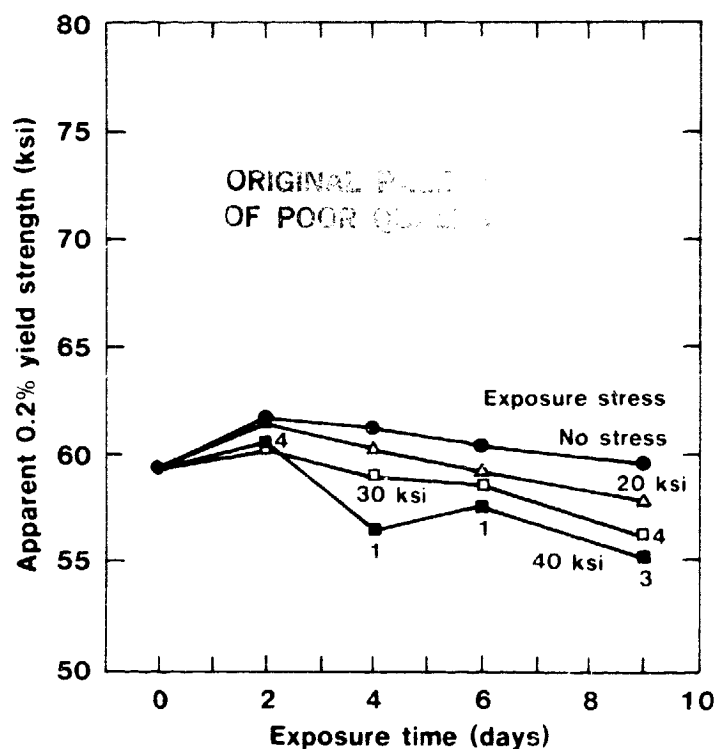
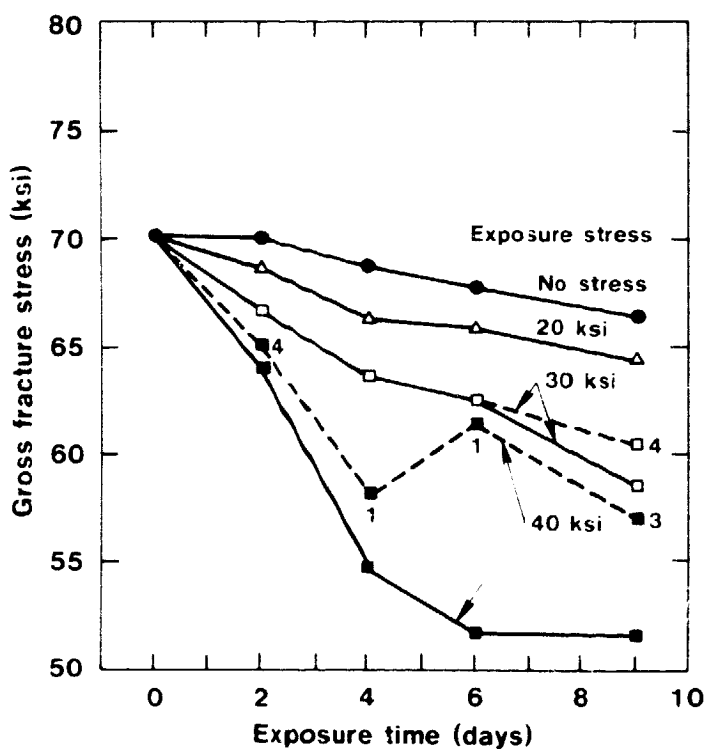


Effect of Specimen Diameter (0.125 in. vs. 0.225 in.) on Predicted EPFM Wide Range Estimated Behavior of Breaking Stress-Flaw Size Behavior in 7075-T7X1 Tension Specimens Containing an Elliptical Partial Thickness Crack ($a/c = 0.8$).

Figure 73



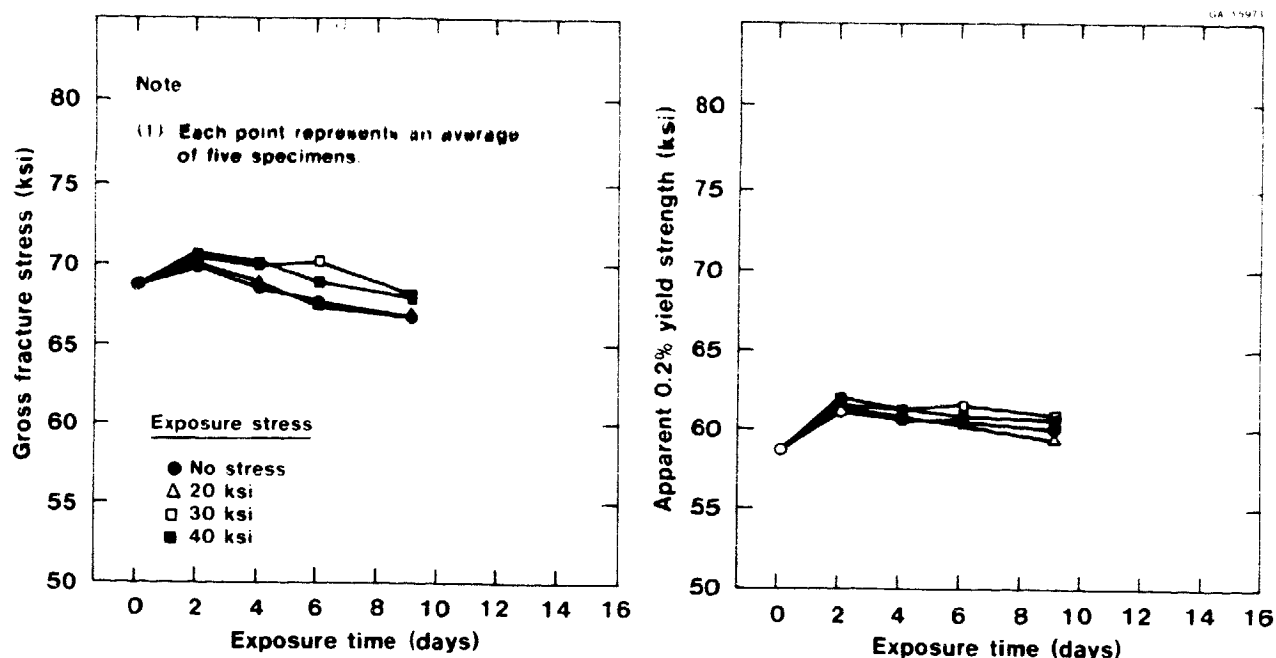
(a) 7075-T651



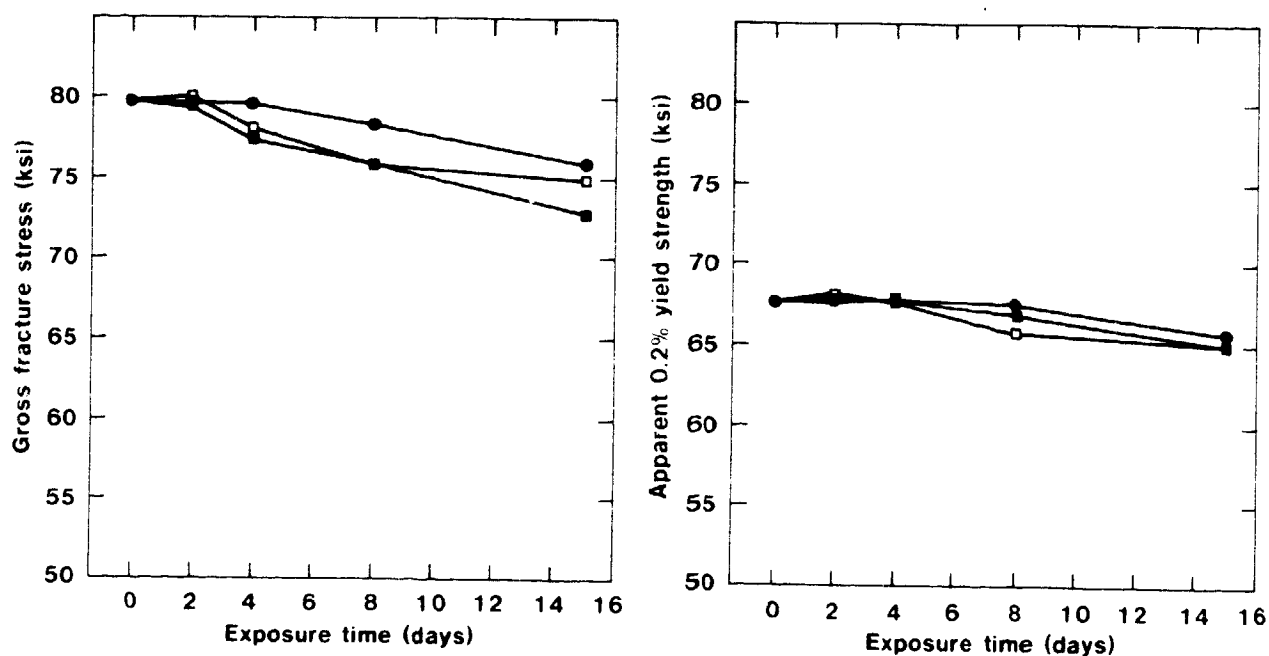
(b) 7075-T7X1

Comparative Trends of Mean Breaking Stress and Mean Apparent Yield Strength for 7075-T651 and 7075-T7X1 Short Transverse 0.125 in. Diameter Tension Specimen Exposed to 3.5% NaCl Solution by Alternate Immersion (ASTM G44). Specimens were Exposed at the Indicated Exposure Stress for Various Times and then Tensile Tested.

Figure 74



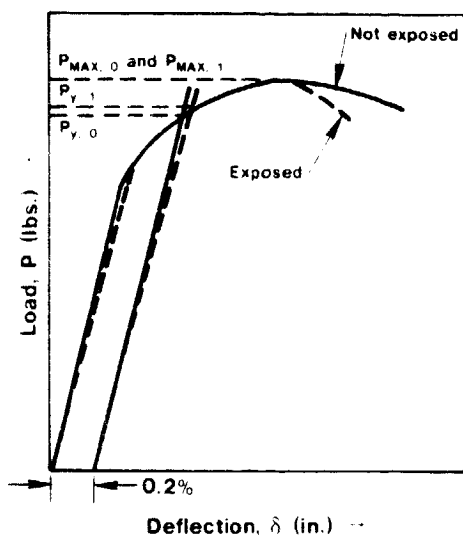
(a) Short transverse, 0.125 in. diameter 7075-T7X2 specimens



(b) Long transverse, 0.225 in. diameter 7075-T651 specimens

Comparative Trends of Mean Breaking Stress and Apparent Yield Strength of Short Transverse 0.125 in. Diameter Specimens of 7075-T7X2 and Long Transverse 0.225 in. Diameter Specimens of 7075-T651. Specimens were Exposed to 3.5% NaCl Solution by Alternate Immersion (ASTM G44) at the Indicated Exposure Stress for Various Times and then Tensile Tested.

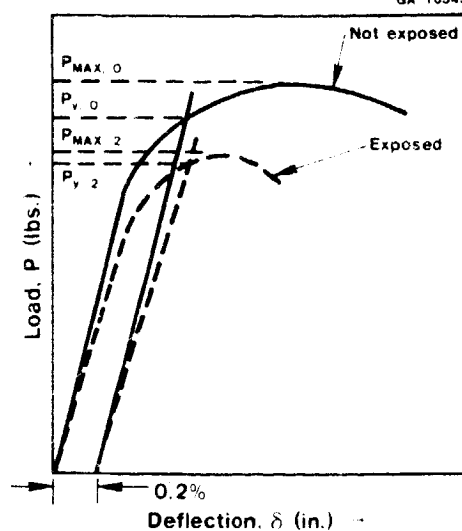
Figure 75



(a) Directional pitting and shallow fissures (multiple sites).

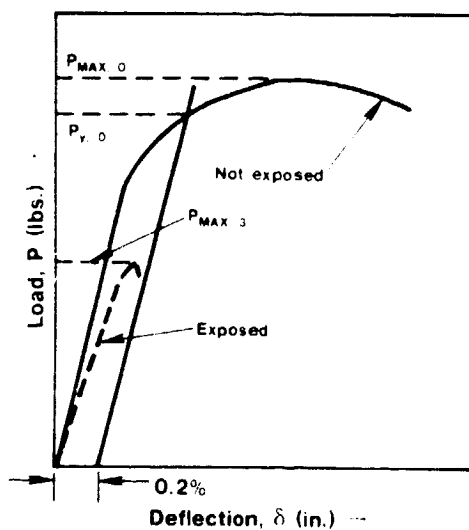
Slight loss of specimen, elastic stiffness resulting in an apparent increase in load to 0.2% deflection.

Maximum load of exposed and unexposed specimens equivalent, but total energy to fracture (area under the P vs. δ curve) will be greater for the unexposed specimen.



(b) Directional pitting plus mild to moderate SCC (multiple sites).

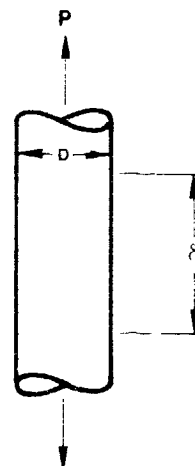
Modest loss in apparent tensile and yield strengths, elastic stiffness and energy to fracture (area under the P vs. δ curve).



(c) Directional pitting plus severe SCC attack (deep flaw(s)).

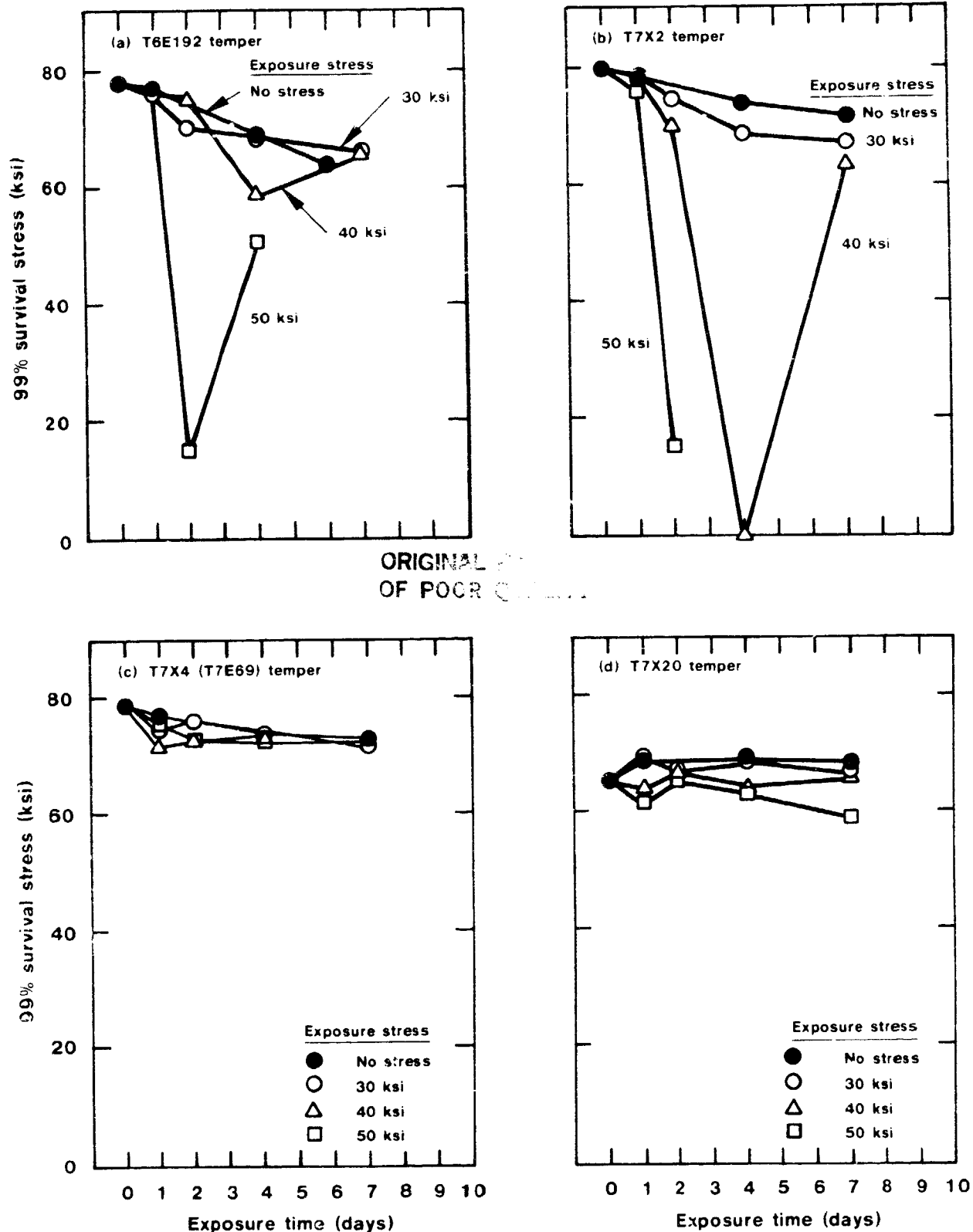
Appreciable losses in strength, elastic stiffness and energy to fracture (area under the P vs. δ curve). Insufficient elongation to develop 0.2% offset load.

ORIGINAL
OF POOR QUALITY



Influence of Progressive Amounts of Corrosion and SCC Damage on Load vs. Deflection Behavior of Breaking Load Test Specimens

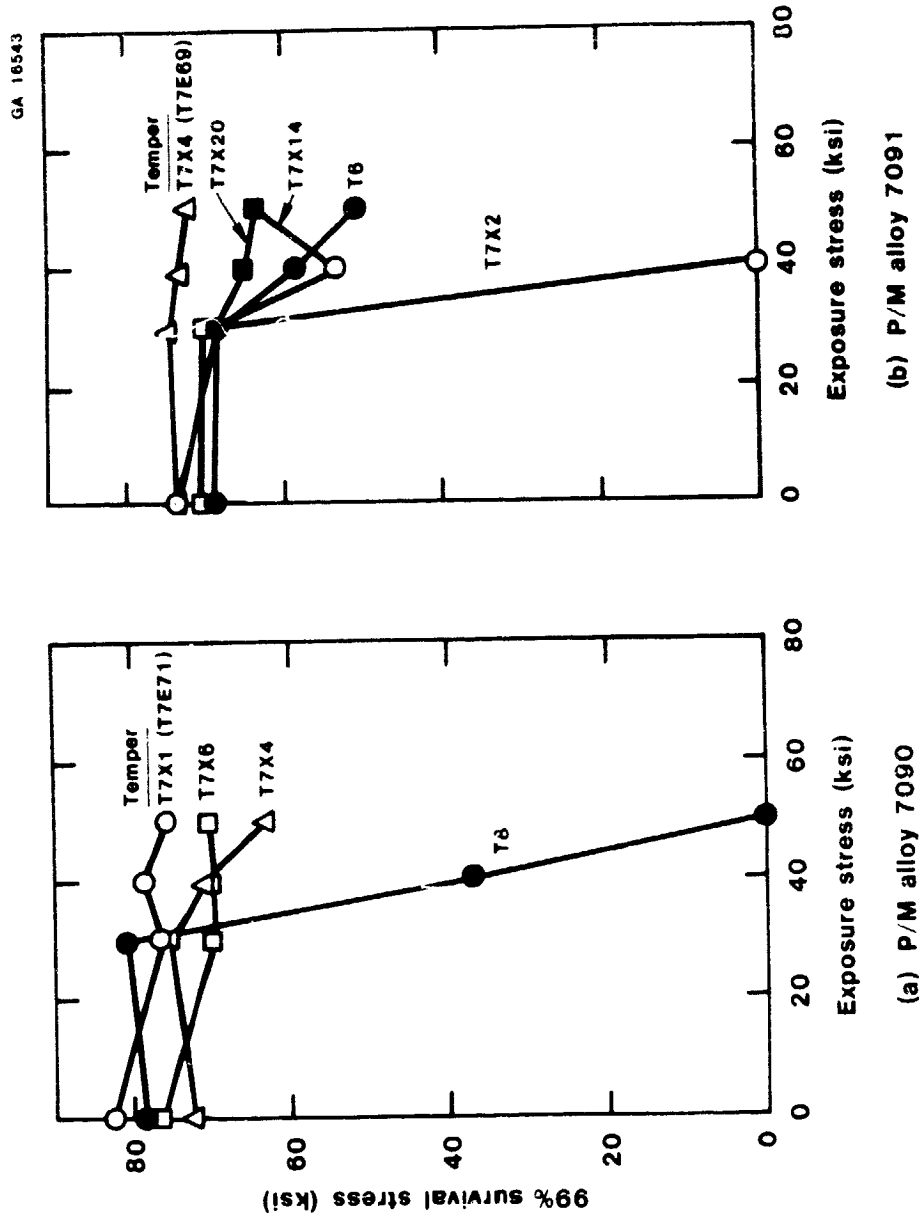
Figure 76



Short transverse 0.125 in. diameter tension specimens exposed to 3.5% NaCl solution by alternate immersion (ASTM G44) for various exposure times and then tensile tested.

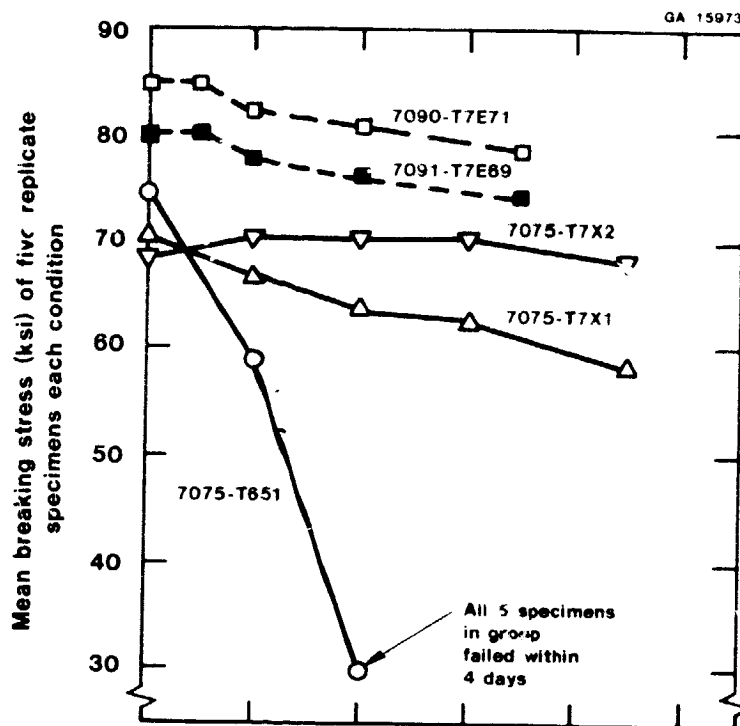
Comparative SCC Performances of Various Tempers of P/M Alloy 7091.
Figure 77

ORIGINAL PAGE IS
OF POOR QUALITY

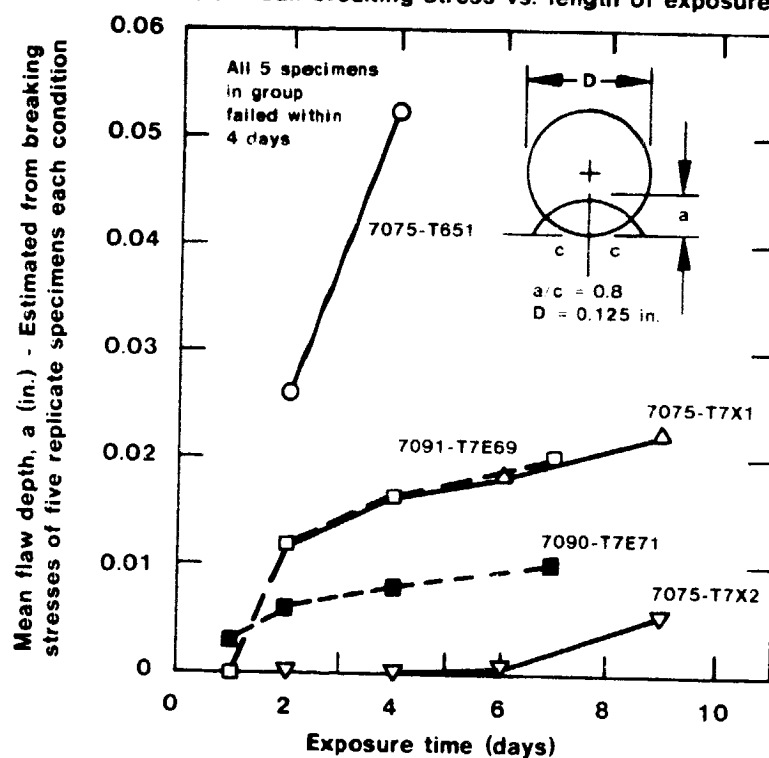


Short transverse 0.125 in. diameter tension specimens exposed 4 days to 3.5% NaCl solution by alternate immersion (ASTM G44) and then tensile tested.

Comparative Performances of P/M 7090 and 7091 in Various Tempers
at Several Exposure Stress Levels.
Figure 78



(a) Mean breaking stress vs. length of exposure

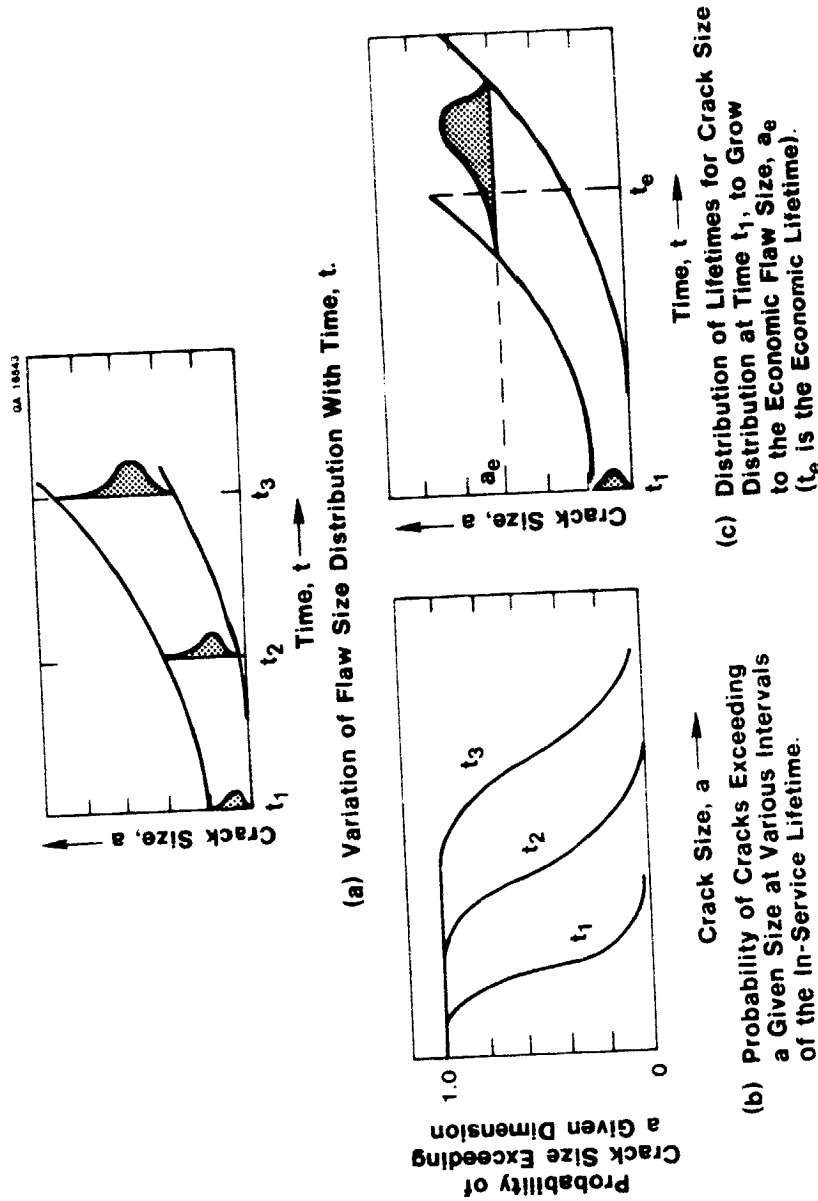


(b) Effective depth of SCC penetration vs. length of exposure

Comparison of Breaking Load Test Results from 0.125 in. Diameter Short Transverse Tensile Specimens of I/M and P/M Aluminum Alloys Exposed to 3.5% NaCl Solution at 30 ksi Exposure Stress by Alternate Immersion (ASTM G44) for Various Times and Then Tensile Tested.

Figure 79

ORIGINAL QUALITY
OF POOR QUALITY



Conceptual Use of Small Crack Data for Durability Life Assessment
Figure 80

APPENDIX A
Glossary of Symbols

a	Depth of flaw (crack).
A_c	Flawed area of the specimen cross section.
a_e	Depth of annular flaw corresponding to the flawed area, A_c .
a_{max}	Maximum depth of flaw penetration from the surface.
A_{net}	Unflawed area of the specimen cross section.
a_{99}	The SCC flaw depth that would not be exceeded in 99 percent of the specimens, as calculated from the 99 percent survival stress and the analytical wide range estimate for flaw size and breaking load.
c	One half the major axis of an elliptical flaw (crack) (The flaw dimension that characterizes surface length of an elliptical partial thickness crack); refer to Figure 22(a).
D	Specimen diameter.
da/dt	Crack propagation rate.
E	Modulus of elasticity.
G	Strain-energy release rate.
K	Stress intensity factor.
K_I	Stress intensity factor, for opening mode I.
K_c	Critical fracture toughness.
K_{Ic}	Critical plane strain fracture toughness.
K_o	Stress intensity in SCC test specimen at beginning of environmental exposure.
K_{th}	Threshold stress-intensity factor for SCC--The stress intensity below which SCC is not propagated under specified test conditions.
N	Sample size.
P	Probability of survival; Equation [2].
q, s	Weighting exponents in the wide-range fracture stress-flaw size relationship; Equation [8].
R	Specimen radius.

$S, \hat{\mu}, \hat{\sigma}$	Stress, location, and scale parameters, respectively, for the extreme-value distribution; Equations [2a, 2b and 3].
S_{99}	99% survival stress; Equation [3].
Z	Reduced variate for Gompertz equation; Equation [2].
\bar{S}, δ	The sample mean and standard deviation from replicate specimen breaking stress values; Equation [2b].
κ, n	Strain hardening coefficients.
σ_L	Fracture stress predicted by the limit load failure criterion.
σ_{EPFM}	Gross fracture stress predicted by the EPFM failure criterion; Equation [8].
σ_{LEFM}	Gross fracture stress predicted by the LEFM failure criterion; Equation [8].
σ_{max}	The gross fracture stress corresponding to the maximum load in the breaking load test.
σ_{net}	Net section stress.
σ_{th}	Threshold stress for SCC--The gross section stress below which SCC failure will not occur under specified test conditions.
σ_N, \bar{Y}_N	Extreme value distribution parameters; Equation [2b].
σ_{UTS}	Ultimate tensile strength.
ν	Poisson's ratio.
θ	One half of the central angle subtended by an elliptical or chord crack; refer to Figure 22.

APPENDIX B

Calculation of a Statistically Defined Threshold

Stress from Breaking Load Test Data

The threshold stress (σ_{th}) has been traditionally thought of as the test stress below which specimen failure will not occur. Since the zero probability of specimen failure implied by this definition can never be demonstrated experimentally, this concept of a threshold stress is not practical. The problems associated with an implied probability of zero can be avoided by applying a statistical definition to the threshold stress. A suggested definition of a statistical threshold stress would be the test stress for which it can be demonstrated with 95 percent confidence that the probability of specimen failure under specified testing conditions is less than one percent. While this may be an improvement in the threshold concept, it really provides only limited relief to the problem of determining threshold stresses with reasonable confidence. For example, to obtain 95 percent confidence of a probability of failure of less than one percent requires about 300 replicate tests. One procedure used by Alcoa to determine a statistical threshold stress considers smooth specimen testing at various stresses, both above and below the expected threshold. A small number of replicate specimens are tested each stress level. As the test results are accumulated, the test stresses are adjusted to obtain a balance between failing and passing specimens, and the threshold stress for a selected exposure period is determined from the cumulative pass-fail

results at each test stress. This procedure typically requires thousands of tests to quantify claims of improved SCC resistance and to establish criteria for lot acceptance (B1, B2).*

An advantage of the breaking load test procedure is that it can be used to determine threshold stresses for small sample sizes. An extreme-value statistical treatment has been shown to estimate the stress that 99 percent of a population would be expected to withstand in a tension test without failure after being exposed to 3.5% NaCl alternate immersion for a given set of test conditions. The 99% survival stress can also be used to define a statistical threshold stress. Point estimates for the statistical threshold were made by plotting the 99% survival stresses as a function of exposure stress for each exposure period as in Figures B1-B3. The estimate of the threshold stress was taken at the point where the trend in the data intersected the 1:1 line indicating equal exposure stresses and survival stresses. The intersection point estimates the exposure stress that would produce a 99% survival stress at the test time considered.

Figure B1 demonstrates the estimation procedure for the 0.125 inch diameter short transverse specimens of alloy 7075-T651. For the 6-day and 9-day exposure periods, specimen failures during exposure at 20 ksi did not permit statistical calculations. A

* Refers to references listed at the end of the section.

conservative estimate of the 99% survival stress was taken to be zero because no failures would be expected at zero stress. The estimated threshold stress was about 17 ksi for exposure periods of 4, 6, and 9 days. Figure B2 shows the data for the 0.125 inch diameter short transverse specimens of 7075-T7X1 alloy. Estimated threshold stresses of 30 to 34 ksi were obtained for the 6 and 9-day exposure periods. The data for the 0.225 inch diameter specimens of 7075-T7X1 in Figure B3 also gave estimated threshold stresses of about 32 to 35 ksi for the 6 and 9-day exposure periods.

A treatment was made of the 99% survival stress data to estimate threshold stresses and is summarized in Table B1. The 99% survival stresses were determined for the highest two exposure stresses between two and twelve days exposure to obtain a point estimates of the threshold stress as described above. For the 7075-T7X1 and 7075-T7X2 alloys, exposure stresses of 30 and 40 ksi were used. The threshold stresses for these materials were also estimated by using the 20 and 40 ksi exposure stress data to obtain an indication of the sensitivity of the threshold stress estimates to the data grouping used. The estimates of the threshold stress for the 7075-T7X1 material did not reveal any significant difference due to the two specimen diameters. Although estimates of the threshold stress tended to decrease with increased test time, conservative average estimates were made by generally accepting "worst case" values, as indicated in Table B1.

The estimates of threshold stresses appeared to be insensitive to the range of breaking load test conditions employed in the analysis.

The threshold stresses in Table B1 are point estimates. To estimate the stress for which there is 95 percent confidence of a probability of failure of one percent or less (a statistical definition for the threshold stress), the lower limit of the 90 percent confidence band for the point estimates was determined. The statistical threshold stress values calculated from the point estimates of Table B1 are given in Table B2 for each of the test materials.

REFERENCES

- B1. B. M. Ponchel, "Lot Acceptance Criteria for 7050-T736 Alloy Products," 1980 January 19.
- B2. B. M. Ponchel, "Lot Acceptance Criteria for 7050-T76 Alloy Products," 1980 May 28.

ORIGINAL PAGE IS
OF POOR QUALITY

APPENDIX B

TABLE B-1

CALCULATED THRESHOLD STRESSES (POINT ESTIMATES) DETERMINED FROM BREAKING
LOAD TEST RESULTS OBTAINED ON THREE TEMPER VARIANTS OF ALLOY 7075 EXPOSED
TO 3.5% NaCl SOLUTION BY ALTERNATE IMMERSION

Alloy/ Temper	Orientation	Specimen Dia. (in.)	Exposure Time (days)	Stress Range(ksi)		Fitted Line Coefficients(c)		Estimated Threshold Stress(d) ksi
				S_{exp} (a)	S_{99} (a)	b	m	
7075-T651	LT	0.225	2	30-40	73.3-72.3	76.3	-0.10	69.4
			4	30-40	73.1-67.2	90.8	-0.59	57.1(e)
			8	30-40	71.2-72.1	68.5	+0.09	75.3
			15	30-40	67.8-63.7	80.1	-0.41	56.8(e)
			60	30-40	59.3-59.4	59.0	+0.01	59.6(e)
7075-T651	ST	0.125	2	20-30	40.0-22.3	75.4	-1.77	27.2
			2	10-30	69.7-22.3	93.4	-2.37	27.2
			4	10-20	49.9-0.0	99.8	-4.99	16.7(e)
			6	10-20	56.8-0.0	113.6	-5.68	17.0(e)
			9	10-20	56.7-0.0	113.4	-5.67	17.0(e)
7075-T7X1	ST	0.125	2	30-40	61.7-38.0	132.8	-2.37	39.4
			2	20-40	62.1-38.0	86.2	-1.20	39.1
			4	30-40	48.1-35.2	86.8	-1.29	37.9
			4	20-40	61.3-35.2	87.4	-1.30	37.9
			6	30-40	52.8-0.0	211.2	-5.28	33.6(e)
			6	20-40	61.8-0.0	123.6	-3.09	30.2(e)
			9	30-40	31.3-0.8	122.8	-3.05	30.3(e)
			9	20-40	61.5-0.8	122.2	-3.04	30.3(e)
7075-T7X1	ST	0.225	2	30-40	57.8-65.2	35.6	+0.74	136.9
			2	20-40	60.2-65.2	55.2	+0.25	73.6
			4	30-40	48.7-42.1	68.5	-0.66	41.3
			4	20-40	57.0-42.1	71.9	-0.74	41.2
			6	30-40	45.8-21.2	119.6	-2.46	34.6(e)
			6	20-40	46.6-21.2	72.0	-1.27	31.7(e)
			9	30-40	37.9-27.0	70.6	-1.09	33.8(e)
			9	20-40	59.8-27.0	92.6	-1.64	35.1(e)
			12	30-40	55.9-56.8	53.2	+0.09	58.5
			12	20-40	58.0-56.8	59.2	-0.06	55.8
			60	20-30	46.3-0.0	138.9	-4.63	24.7
7075-TX2	ST	0.125	2	30-40	66.5-68.1	61.7	+0.16	73.5
			2	20-40	69.0-68.1	69.9	-0.04	66.9
			4	30-40	68.3-66.6	73.4	-0.017	62.7(e)
			4	20-40	67.5-66.6	68.4	-0.04	65.6(e)
			6	30-40	68.5-63.8	82.6	-0.47	56.2(e)
			6	20-40	65.3-63.8	66.8	-0.08	62.1(e)
			9	30-40	63.0-62.2	65.4	-0.08	60.6(e)
			9	20-40	64.2-62.2	66.2	-0.10	60.2(e)
			60	30-40	48.1-31.0	99.4	-1.71	36.7

- NOTES: (a) S_{exp} = Exposure stress.
 (b) S_{99} = 99% survival stress, from tabulated values in Appendix C.
 (c) Straight line equation of S_{99} vs. S_{exp} ; $S_{99} = m S_{exp} + b$.
 (d) Estimated at the intersection of the regressed line and the 1:1 line, ref. Figures B1-B3.
 (e) Accepted Estimate.

APPENDIX B

TABLE B-2

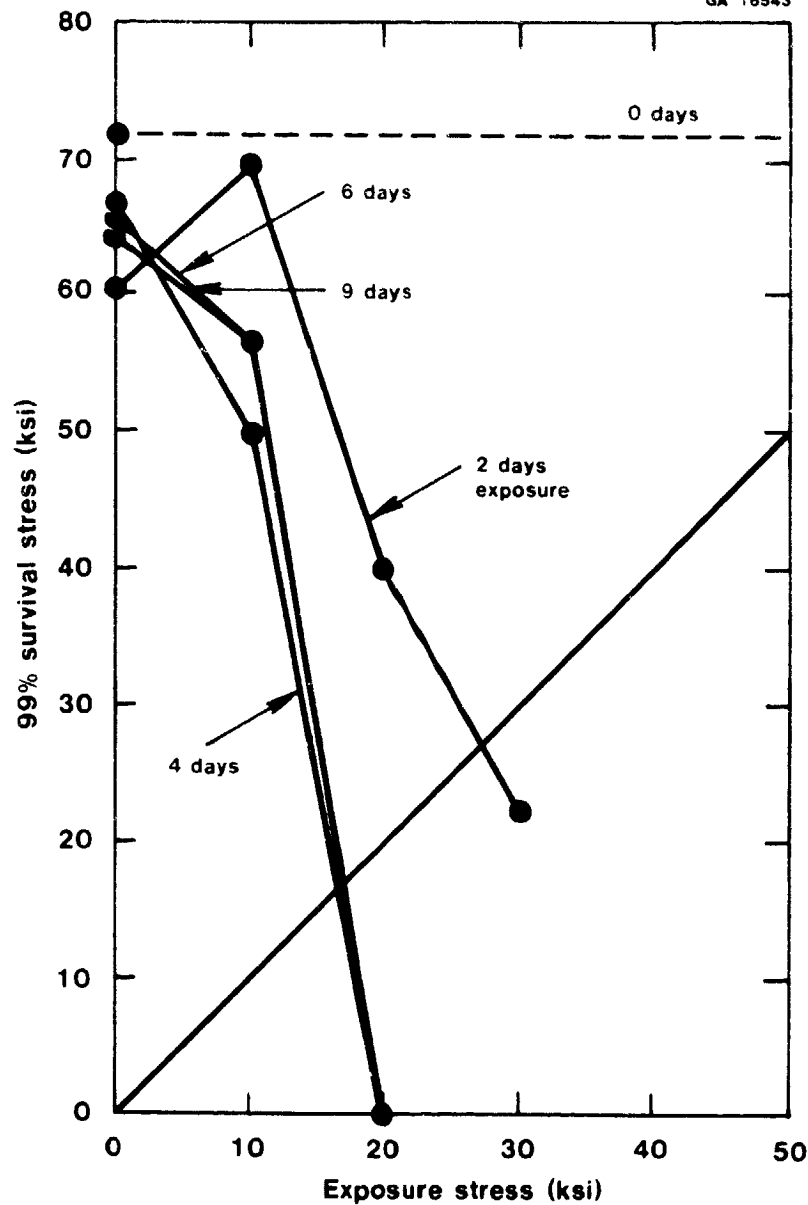
ESTIMATION OF STATISTICAL THRESHOLD STRESS FROM BREAKING LOAD TEST
RESULTS OBTAINED ON THREE TEMPER VARIANTS OF ALUMINUM ALLOY 7075
EXPOSED TO 3.5% NaCl SOLUTION BY ALTERNATE IMMERSION

Alloy/Temper	Orientation	Exposure Time (days)	Exposure Stress Range (ksi)	Threshold Point Estimate (a) (ksi)	Mean	Standard Deviation	Statistical Threshold (b) (ksi)
7075-T651	LT	4	30-40	57.1	57.8	1.54	55.2
		15	30-40	56.8			
		60	30-40	59.6			
7075-T651	ST	4	10-20	16.7	16.9	0.173	16.6
		6	10-20	17.0			
		9	10-20	17.0			
7075-T7X1	ST	6	30-40	33.6	33.1	1.90	30.9
		9	30-40	30.3			
		6	30-40	34.6(c)			
		9	30-40	33.8(c)			
7075-T7X2	ST	4	30-40	62.7	59.8	3.32	54.2
		6	30-40	56.2			
		9	30-40	60.6			

NOTES: (a) Accepted values from Table B1.
(b) Determined as the lower limit of the 90% confidence interval (two-tailed) of the student's t distribution.
(c) 0.225-in. specimen diameter; all other values from 0.125-in. diameter specimen.

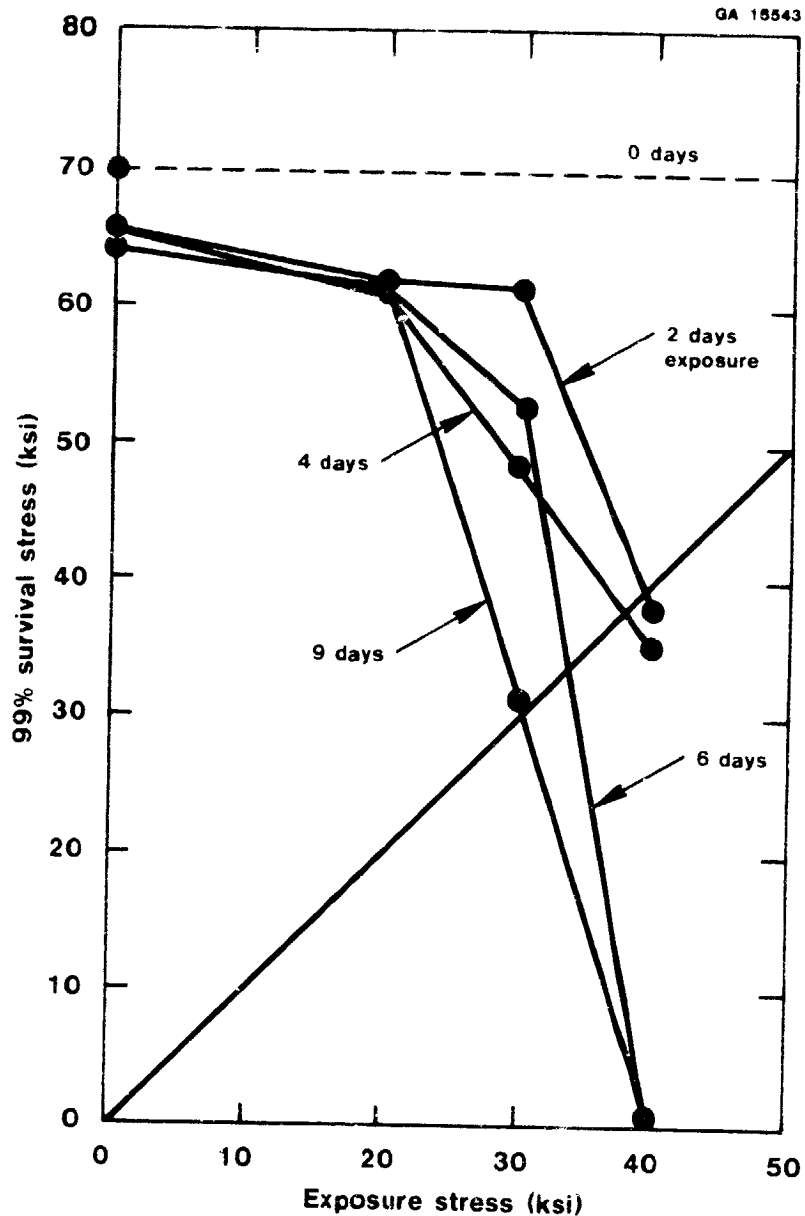
ORIGINAL PAGE 1
OF FOUR

GA 16543



Calculated 99% Survival Stress vs. Exposure Stress for 0.125 in. Diameter 7075-T651 Tension Specimens. Specimens were Exposed to 3.5% NaCl Solution by Alternate Immersion (ASTM G44) at the Indicated Exposure Stress for Various Exposure Times and then Tensile Tested. The 99% Survival Stress is the Stress Below Which 99% of the Specimens are Expected to Survive the Tensile Test.

Figure B1

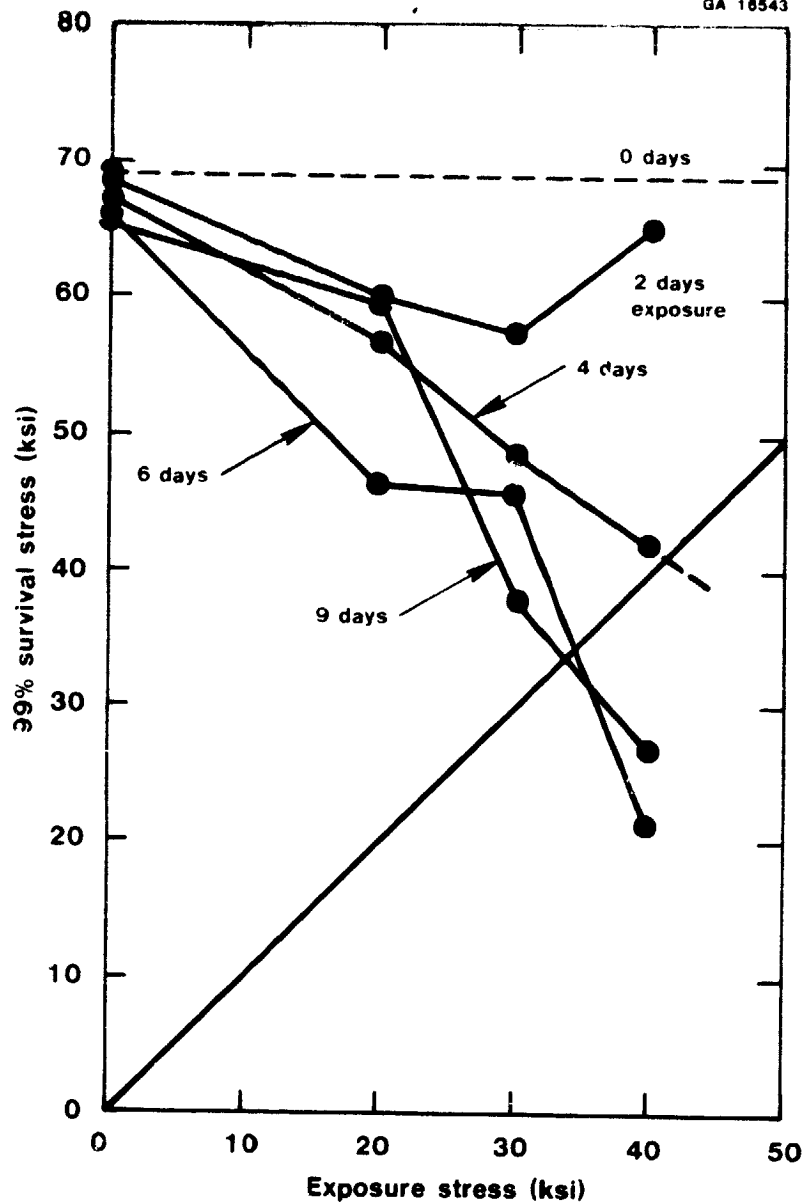


Calculated 99% Survival Stress vs. Exposure Stress for 0.125 in. Diameter 7075-T7X1 Tension Specimens. Specimens were Exposed to 3.5% NaCl Solution by Alternate Immersion (ASTM G44) at the Indicated Exposure Stress for Various Exposure Times and then Tensile Tested. The 99% Survival Stress is the Stress Below Which 99% of the Specimens are Expected to Survive the Tensile Test.

Figure B2

ORIGINAL PAGE
OF POOR QUALITY

GA 16543



Calculated 99% Survival Stress vs. Exposure Stress for 0.225 in. Diameter 7075-T7X1 Tension Specimens. Specimens were Exposed to 3.5% NaCl Solution by Alternate Immersion (ASTM G44) at the Indicated Exposure Stress for Various Exposure Times and then Tensile Tested. The 99% Survival Stress is the Stress Below Which 99% of the Specimens are Expected to Survive the Tensile Test.

Figure B3

APPENDIX C

DETAILED BREAKING LOAD SCC TEST RESULTS AND A DESCRIPTION OF THE PROBABILITY PLOTTING METHOD USED TO STATISTICALLY ANALYZE BREAKING LOAD DATA

1. Breaking Load Test Results

The tensile properties determined from individual tension tests performed on each of the exposed material and specimen conditions examined are given respectively in Tables C-1, 4, 7, 10, and 13. The tensile property mean and standard deviation values calculated from the above tables for each group of five replicate specimens subjected to identical exposure conditions are given in Tables C-2, 5, 8, 11, and 14. Results of the extreme value statistical analysis of breaking load tests data are presented in Tables C-3, 6, 9, 12, and 15, respectively, for each of the material conditions studied. The latter series of tables includes the survival probabilities, 99% survival stress and 99% penetration limit (flaw depth, a_{99}) estimated from the extreme value analysis.

2. Description of the Probability Plotting Method for Determining the Extreme Value Distribution Parameters $\hat{\mu}$ and $\hat{\sigma}$.

Probability plotting is a graphical method for determining distribution parameters and for determining whether a specific distribution appropriately describes the statistical variation of a data set. Briefly, the method involves ranking replicate observations in order and plotting these ordered values against

the expected value of each observation for the distribution of interest (Ref. C-1). The resulting data should lie approximately on a straight line if the distribution is appropriate. Distribution parameters can be determined from the slope and intercept of the line.

Probability plotting is especially useful for truncated data sets (Ref. C-2), such as for test groups which contain specimens that failed prior to tensile testing. To determine $\hat{\mu}$ and $\hat{\sigma}$ for the extreme value distribution of smallest breaking strengths, the values for the five specimens in a data set (test group) are ranked in descending order and are plotted against the expected value of each ranked value. Specimens for which no breaking strengths are available are assumed to belong to the distribution but are not available for plotting. These values would fall at the low end of the ranked values (having breaking strengths below the exposure stress) and are not used.

The expected value of i^{th} observation is estimated by the R^{th} fractile of the distribution, where $R_i = (i-1/2)/N$ and N is the sample size ($N=5$). For the extreme value distribution of smallest values, the expected value of the i^{th} observation is $E_i = -\ln[-\ln(R_i)]$. If extreme value probability paper is available, plotting R_i against the ranked values should yield a linear relationship.

A straight line fit to the plotted data provides estimates of $\hat{\mu}$ and $\hat{\sigma}$ for a distribution of large sample size, as will be shown below. These estimates are then adjusted to account for the reduced precision of the finite sample size. This method provides conservative estimates of $\hat{\mu}$ and $\hat{\sigma}$ compared to using equation 2b, even for complete data sets. The probability plotting method was used to analyze the breaking load data, and results are tabulated in Tables 3, 6, 9, 12, and 15 in this Appendix.

As an illustration of the probability plotting method, data from the six-day, 40 ksi exposure stress test group of 7075-T7X1 (0.125 in. diameter specimens) are analyzed in detail here. One specimen in this group of five failed during exposure, and the remaining specimens had breaking strengths of 57.4, 56.6, 61.4, and 45.2 ksi (Ref. Table C-4). Ranking these values in descending order along with the expected value of the i^{th} observation results in the data pairings shown below:

i	$R_i = \frac{(i-1/2)}{N}$	Y	X
		Expected Value of i^{th} Observation, $E_i = -\ln(-\ln(R_i))$	Ranked Breaking Strengths, (ksi)
1	0.1	-0.834	61.4
2	0.3	-0.186	57.4
3	0.5	0.367	54.6
4	0.7	1.031	45.2
N=5	0.9	2.250	-- (<40)

Fitting a straight line of the form $y = mx+b$ by linear regression* to the four available data points yields the estimates $m = -0.112$, $b = 6.20$. Estimates of $\hat{\mu}$ and $\hat{\sigma}$ for a large sample size (denoted by $\hat{\mu}_{\infty}$ and $\hat{\sigma}_{\infty}$) are obtained from the following equations:

$$\hat{\mu}_{\infty} = -\frac{b}{m} = 55.5$$

$$\hat{\sigma}_{\infty} = -\frac{1}{m} = 8.93$$

To convert these to parameters which describe the distribution for a finite sample size, equation [2b] is used. Since that relationship holds for various N , then:

$$\text{and} \quad \hat{\sigma}_N = \delta/\sigma_N; \quad \hat{\mu}_N = \bar{S} + \hat{\sigma}_N \bar{Y}_N$$

$$\hat{\sigma}_{\infty} = \delta/\sigma_{\infty}; \quad \hat{\mu}_{\infty} = \bar{S} + \hat{\sigma}_{\infty} \bar{Y}_{\infty}$$

where σ_N and \bar{Y}_N can be found in the following table for $N = 2$ to $N = 7$, $\sigma_{\infty} = \pi/\sqrt{6}$, and $\bar{Y}_{\infty} = 0.577$ (Ref. 47).

Means and Standard Deviations of Reduced Extremes Extrapolated from Gumbel (Ref. 47).

<u>N</u>	<u>σ_N</u>	<u>\bar{Y}_N</u>
2	0.5247	0.3819
3	0.6503	0.4185
4	0.7334	0.4410
5	0.7932	0.4565
6	0.8388	0.4681
7	0.8748	0.4771

* The simple least squares regression method is not strictly applicable in this situation because the ordered observations are not independent. The more difficult technique of generalized least squares should be used, but the additional effort is not justified because a subjective decision must still be made [Ref. C-1].

Eliminating δ and \bar{S} from the previous equations yields estimates of $\hat{\sigma}$ and $\hat{\mu}$ for describing the extreme value distribution of smallest values for a finite sample size determined from $\hat{\sigma}_{\infty}$ and $\hat{\mu}_{\infty}$ values obtained from the probability plot.

$$\hat{\sigma} = \hat{\sigma}_N = \hat{\sigma}_{\infty}(\sigma_{\infty}/\sigma_N)$$

$$\hat{\mu} = \hat{\mu}_N = \hat{\mu}_{\infty} - \hat{\sigma}_{\infty}Y_{\infty} + \hat{\sigma}_N\bar{Y}_N$$

To be conservative, since only four data points were used to determine $\hat{\mu}_{\infty}$ and $\hat{\sigma}_{\infty}$ in this example, $\hat{\sigma}_4$ and \bar{Y}_4 are used to find $\hat{\sigma}$ and $\hat{\mu}$.

$$\hat{\sigma} = 8.93(\pi/\sqrt{6})/0.7334 = 15.6$$

$$\hat{\mu} = 55.5 - 8.93 \times .577 + 15.6 \times 0.4410 = 57.2$$

These now described (conservatively) the appropriate extreme value distribution of smallest breaking strength values.

The probability of survival at the exposure stress (40 ksi) can be determined by equation [2] and [2a].

$$Z = \frac{S - \hat{\mu}}{\hat{\sigma}} = \frac{40.0 - 57.2}{15.6} = -1.102$$

$$P = \exp [-e^Z] = 0.717$$

The 99% survival stress is calculated from equation [3] in the text:

$$\begin{aligned} S_{99} &= \hat{\mu} + \hat{\sigma} (\ln[\ln(0.99)^{-1}]) \\ &= \hat{\mu} - 4.60 \hat{\sigma} \\ &= 57.2 - 4.60 (15.6) \\ &= -14.6 \end{aligned}$$

The 99% survival stress is negative because the distribution is not limited to positive values and $\hat{\sigma}$ (scale parameter) is large relative to $\hat{\mu}$ (the location parameter of the distribution). Consequently, in Table C-6, the value of S_{99} is reported as zero, and the 99% penetration limit, a_{99} , is reported as infinity.

REFERENCES

- C-1 G. J. Hahn and S. S. Shapiro, Statistical Models in Engineering, John Wiley & Sons, New York (1968).
- C-2 W. Weibull, Fatigue Testing and Analysis of Results, published for AGARD NATO by Pergamon Press, New York (1961), pp. 159-167.

APPENDIX C

ORIGINAL PAGE
OF POOR QUALITY

TABLE C-1

APPARENT TENSILE PROPERTIES OF 0.125 INCH DIAMETER SHORT TRANSVERSE SPECIMENS
OF 7075-T651 ALLOY EXPOSED TO 3.5 PERCENT SODIUM CHLORIDE SOLUTION BY
ALTERNATE IMMERSION

Exposure Time (days)	Exposure Stress							
	No Stress		10 ksi		20 ksi		30 ksi	
	Tensile(1) (ksi)	Yield(2) (ksi)	Tensile(1) (ksi)	Yield(2) (ksi)	Tensile(1) (ksi)	Yield(2) (ksi)	Tensile(1) (ksi)	Yield(2) (ksi)
0	73.9	61.6						
0	74.8	62.0						
0	74.8	61.6						
0	74.2	61.1						
0	74.3	62.4						
2	76.1	63.5	76.5	63.4	65.5	62.2	68.0	61.7
2	76.3	63.3	76.7	64.0	72.2	63.2	53.9	53.9
2	75.1	63.7	76.4	63.7	62.1	59.5	56.5	(3)
2	71.7	61.8	75.5	63.8	66.9	63.3	60.5	59.7
2	72.0	62.6	74.2	64.3	62.5	61.8	55.6	(3)
4	70.2	60.7	65.2	60.0	59.3	58.7	(F4d)	--
4	69.2	60.8	64.6	58.5	61.3	57.2	(F3d)	--
4	70.8	61.4	60.5	59.1	52.2	(3)	(F3d)	--
4	69.8	60.8	65.9	59.1	51.4	(3)	(F3d)	--
4	70.7	61.3	67.1	59.7	35.0	(3)	(F3d)	--
6	70.7	61.0	61.7	56.4	58.9	54.0	(F6d)	--
6	68.9	60.2	63.0	58.5	(F6d)	--	(F3d)	--
6	70.3	60.8	63.8	56.7	(F5d)	--	(F3d)	--
6	69.7	60.2	63.0	55.4	(F5d)	--	(F3d)	--
6	69.4	59.5	61.6	55.7	(F5d)	--	(F3d)	--
9	69.0	59.3	61.5	54.8	60.5	54.6	(F3d)	--
9	68.9	59.3	63.3	55.2	(F5d)	--	(F3d)	--
9	68.0	58.9	63.4	56.9	(F5d)	--	(F3d)	--
9	67.4	59.8	64.4	56.9	(F5d)	--	(F3d)	--
9	68.0	58.3	62.4	55.5	(F5d)	--	(F3d)	--
60			41.5	38.7				
60			38.5	36.7				
60			34.3	(3)				
60			42.0	37.9				
60			29.9	(3)				

- NOTES: (1) Gross fracture stress corresponding to maximum tensile load.
 (2) Gross section stress corresponding to 0.2% permanent offset.
 (3) Failed before reaching 0.2% offset.
 (4) (Fxd) means specimen failed after x days of exposure.

APPENDIX C

TABLE C-2

MEAN AND STANDARD DEVIATION OF TENSILE PROPERTIES FOR 0.125 INCH DIAMETER
SHORT TRANSVERSE SPECIMENS OF 7075-T651 EXPOSED TO 3.5 PERCENT SODIUM
CHLORIDE SOLUTION BY ALTERNATE IMMERSION

Exposure Time (days)	Exposure Stress (ksi)	Tensile (ksi)			Yield (ksi)		
		No. of Survivors	Mean(b)	Std. Dev.(b)	No. of Values	Mean	Std. Dev.
0	0	5	74.4	0.394	5	61.7	0.488
2	0	5	74.2	2.23	5	63.0	0.779
2	10	5	75.9	1.04	5	63.8	0.336
2	20	5	65.8	4.09	5	62.0	1.54
2	30	5	58.9	5.64	3(c)	58.4	4.05
4	0	5	70.1	0.662	5	61.0	0.324
4	10	5	64.7	2.51	5	59.3	0.585
4	20	5	51.8	10.4	2(c)	58.0	1.06
4	30	0	-- (30.0)	-- (0)	-	--	--
6	0	5	69.8	0.714	5	60.3	0.590
6	10	5	62.6	0.945	5	56.5	1.21
6	20	1	58.9(27.8)	-- (17.4)	1	54.0	--
6	30	0	-- (30.0)	-- (0)	-	--	--
9	0	5	68.3	0.667	5	59.1	0.559
9	10	5	63.0	1.10	5	55.9	0.981
9	20	1	60.5(28.1)	-- (18.1)	1	54.6	--
9	30	0	-- (30.0)	-- (0)	-	--	--
60	10	5	37.2	5.12	3(c)	37.8	1.01

- NOTES: (a) From group of 5 replicate specimens subjected to identical exposure test conditions.
- (b) Number in parenthesis corresponds to values calculated for five specimens using the exposure stress for specimens which failed prior to tensile testing. All other calculated values are based on the survivors.
- (c) The mean tensile strengths are anomalous with respect to the mean yield strengths because yield strengths could not be obtained for some specimens (refer to Table C-1).

ORIGINAL
OF POOR

APPENDIX C

TABLE C-3

EXTREME VALUE ANALYSIS OF TENSILE PROPERTY DATA FOR 0.125 INCH DIAMETER SHORT TRANSVERSE SPECIMENS OF 7075-T651 EXPOSED TO 3.5 PERCENT SODIUM CHLORIDE SOLUTION BY ALTERNATE IMMERSION

Exposure Time (days)	Exposure Stress (ksi)	No. of Survivors Out of 5	Gross Fracture Stress(a)		Extreme Value Distribution Parameters (b)		Probability of Survival At the Exposure Stress	99 Percent Survival Stress (ksi)	99 Percent Penetration Limit, δ_{99} (in.)
			Mean (ksi)	Std. Dev. (ksi)	$\hat{\mu}$ (ksi)	$\hat{\sigma}$ (ksi)			
0	0	5	74.4	0.39	74.6	0.56	1.000	72.0	0.013
2	0	5	74.2	2.23	75.6	3.29	1.000	60.5	0.025
2	10	5	75.9	1.04	76.5	1.47	1.000	69.7	0.016
2	20	5	65.8	4.09	68.5	6.18	1.000	40.0	0.043
2	30	5	58.9	5.64	62.6	8.77	0.976	22.3	0.060
4	0	5	70.1	0.66	70.5	0.91	1.000	66.3	0.020
4	10	5	64.7	2.50	66.2	3.53	1.000	49.9	0.034
4	20	5	51.8	10.4	58.0	14.6	0.929	0	∞
4	30	0	--(30.0)	--(0)	--	--	0	0	∞
6	0	5	69.8	0.71	70.2	0.99	1.000	65.6	0.020
6	10	5	62.6	0.94	63.2	1.39	1.000	56.8	0.029
6	20	1	58.9(27.8)	--(17.4)	--	--	0.200	0	∞
6	30	0	--(30.0)	--(0)	--	--	0	0	∞
9	0	5	68.3	0.68	68.7	0.98	1.000	64.2	0.022
9	10	5	63.0	1.10	63.6	1.52	1.000	56.7	0.029
9	20	1	60.5(28.1)	--(18.1)	--	--	0.200	0	∞
9	30	0	--(30.0)	--(0)	--	--	0	0	∞
60	10	5	37.2	5.12	40.3	7.11	0.986	7.5	--

NOTES: (a) Numbers in parenthesis correspond to values calculated for five specimens using the exposure stress for specimens which failed prior to tensile testing. All other values are based on the survivors.
(b) $\hat{\mu}$ and $\hat{\sigma}$ are the location and scale parameters, respectively, which define the extreme value distribution of gross fracture stresses. These parameters were determined by probability plotting using probability scales adjusted for the sample size (number of survivors). This method allows the estimation of correct distribution parameters for truncated sample sizes due to specimen failures, as outlined in Section III.D.2.b.

APPENDIX C

TABLE C-4

APPARENT TENSILE PROPERTIES OF 0.125 INCH DIAMETER SHORT TRANSVERSE SPECIMENS
OF 7075-T7X1 ALLOY EXPOSED TO 3.5 PERCENT SODIUM CHLORIDE SOLUTION BY
ALTERNATE IMMERSION

Exposure Time (days)	Exposure Stress							
	No Stress		20 ksi		30 ksi		40 ksi	
	Tensile(1) (ksi)	Yield(2) (ksi)	Tensile(1) (ksi)	Yield(2) (ksi)	Tensile(1) (ksi)	Yield(2) (ksi)	Tensile(1) (ksi)	Yield(2) (ksi)
0	70.1	59.5						
0	70.1	60.3						
0	70.5	59.1						
0	69.3	59.1						
0	70.5	59.5						
2	70.9	61.9	68.3	61.7	67.6	60.3	67.9	61.1
2	70.1	62.3	70.0	61.9	66.8	60.1	63.4	59.9
2	69.0	61.0	69.5	61.5	67.1	60.5	68.6	62.3
2	70.2	62.3	68.4	61.7	65.3	60.7	60.1	58.9
2	69.6	61.4	67.1	60.9	66.5	59.9	59.7	(3)
4	69.1	62.1	67.4	60.3	59.2	58.1	52.7	(3)
4	69.3	61.7	66.1	60.7	65.0	59.5	56.6	(3)
4	68.3	61.5	66.3	59.9	65.9	59.5	56.3	(3)
4	68.5	60.9	66.3	60.1	63.7	59.9	58.1	56.6
4	68.0	60.5	65.1	60.5	64.0	58.9	49.9	(3)
6	67.9	61.3	65.8	59.5	64.0	59.3	57.4	(3)
6	68.1	61.3	64.9	58.5	61.6	59.1	54.6	(3)
6	67.4	60.3	66.7	60.1	61.9	58.3	61.4	57.7
6	66.7	59.7	65.4	59.1	60.6	58.5	45.2	(3)
6	68.0	60.5	66.2	59.7	64.3	58.7	(F5d)	--
9	65.7	59.7	64.5	57.2	59.3	56.2	53.4	52.8
9	66.7	60.1	63.6	57.4	63.0	57.4	59.2	57.4
9	66.3	59.3	64.6	58.5	61.8	57.4	47.5	(3)
9	66.2	59.5	64.4	58.3	57.0	55.0	58.0	56.2
9	66.2	60.1	63.8	58.7	51.1	(3)	(F4d)	--
60			43.6	42.8				
60			46.9	42.8				
60			46.6	44.4				
60			44.8	(3)				
60			46.6	(3)				

- NOTES: (1) Gross fracture stress corresponding to maximum tensile load.
(2) Gross section stress corresponding to 0.2% permanent offset.
(3) Failed before reaching 0.2% offset.
(4) (Fxd) means the specimen failed after x days of exposure.

APPENDIX C

TABLE C-5

MEAN AND STANDARD DEVIATION OF TENSILE PROPERTIES FOR 0.125 INCH
DIAMETER SHORT TRANSVERSE SPECIMENS OF 7075-T7X1

Exposure Time (days)	Exposure Stress (ksi)	Tensile (ksi)			Yield (ksi)		
		No. of Survivors(a)	Mean(b)	Std. Dev.(b)	No. of Values	Mean	Std. Dev.
0	0	5	70.1	0.490	5	59.5	0.490
2	0	5	70.0	0.709	5	61.8	0.572
2	20	5	68.7	1.13	5	61.5	0.385
2	30	5	66.7	0.862	5	60.3	0.316
2	40	5	63.9	4.20	4	60.6	1.47
4	0	5	68.6	0.546	5	61.3	0.639
4	20	5	66.2	0.817	5	60.3	0.316
4	30	5	63.6	2.59	5	59.2	0.701
4	40	5	54.7	3.34	1(c)	56.6	--
6	0	5	67.6	0.581	5	60.6	0.687
6	20	5	65.8	0.696	5	59.1	0.610
6	30	5	62.5	1.60	5	58.8	0.415
6	40	4	54.7(51.7)	6.89(8.86)	1(c)	57.7	--
9	0	5	66.2	0.356	5	59.7	0.358
9	20	5	64.2	0.449	5	58.0	0.676
9	30	5	58.4	4.71	4(c)	56.5	1.15
9	40	4	54.5(51.6)	5.31(7.96)	3(c)	55.5	2.39
60	20	5	45.7	1.44	3(c)	43.3	0.924

- NOTES: (a) From group of 5 replicate specimens subjected to identical exposure test conditions.
- (b) Numbers in parenthesis correspond to values calculated for five specimens using the exposure stress for specimens which failed prior to tensile testing. All other calculated values are based on the survivors.
- (c) The mean tensile strength is anomalous with respect to the mean yield strength because yield strengths could not be obtained for some specimens (refer to Table C-4).

APPENDIX C

TABLE C-6

EXTREME VALUE ANALYSIS OF TENSILE PROPERTY DATA FOR 0.125 INCH DIAMETER SHORT TRANSVERSE SPECIMENS OF 7075-T7X1 EXPOSED TO 3.5 PERCENT SODIUM CHLORIDE SOLUTION BY ALTERNATE IMMERSION

Exposure Time (days)	Exposure Stress (ksi)	No. of Survivors Out of 5 Exposed	Gross Fracture Stress(a)		Extreme Value Distribution Parameters(b)		Probability of Survival at the Exposure Stress	99 Percent Survival Stress (ksi)	99 Percent Penetration Limit, a_{99} (in.)
			Mean (ksi)	Std. Dev. (ksi)	$\hat{\mu}$ (ksi)	$\hat{\sigma}$ (ksi)			
0	0	5	70.1	0.49	70.4	0.70	1.000	67.2	0.011
2	0	5	70.0	0.71	70.4	0.98	1.000	65.9	0.013
2	20	5	68.7	1.13	69.3	1.58	1.000	62.1	0.018
2	30	5	66.7	0.86	67.2	1.19	1.000	61.7	0.019
2	40	5	63.9	4.20	66.6	6.21	0.986	38.0	0.043
4	0	5	68.6	0.55	69.0	0.78	1.000	65.4	0.014
4	20	5	66.2	0.82	66.7	1.18	1.000	61.3	0.019
4	30	5	63.6	2.59	65.1	3.69	1.000	48.1	0.033
4	40	5	54.7	3.35	56.7	4.66	0.973	35.2	0.046
6	0	5	67.6	0.58	68.0	0.82	1.000	64.2	0.016
6	20	5	65.8	0.70	66.2	0.96	1.000	61.8	0.019
6	30	5	62.5	1.60	63.5	2.32	1.000	52.8	0.028
6	40	4	54.7(51.7)	6.89(8.86)	57.2	15.66	0.717	0	∞
9	0	5	66.2	0.36	66.4	0.51	1.000	64.1	0.016
9	20	5	64.2	0.45	64.5	0.64	1.000	61.5	0.019
9	30	5	58.4	4.71	61.2	6.49	0.992	31.3	0.050
9	40	4	54.5(51.6)	5.31(7.96)	56.5	12.12	0.774	0.8	--
60	20	5	45.7	1.44	46.6	2.06	1.000	37.1	0.044

NOTES: (a) Numbers in parenthesis correspond to values calculated for five specimens using the exposure stress for specimens which failed prior to tensile testing. All other values based on the survivors.

(b) $\hat{\mu}$ and $\hat{\sigma}$ are the location and scale parameters, respectively, which define the extreme value distribution of gross fracture stresses. These parameters were determined by probability plotting using probability scales adjusted for the sample size (No. of survivors). This method allows the estimation of correct distribution parameters for truncated sample sizes due to specimen failures, as outlined in Section III.D.2.b.

ORIGINAL PAGE IS
OF POOR QUALITY

APPENDIX C

TABLE C-7

APPARENT TENSILE PROPERTIES OF 0.125 INCH DIAMETER SHORT TRANSVERSE SPECIMENS
OF 7075-T7X2 ALLOY EXPOSED TO 3.5 PERCENT SODIUM CHLORIDE SOLUTION BY
ALTERNATE IMMERSION

Exposure Time (days)	Exposure Stress							
	No Stress		20 ksi		30 ksi		40 ksi	
	Tensile(1) (ksi)	Yield(2) (ksi)	Tensile(1) (ksi)	Yield(2) (ksi)	Tensile(1) (ksi)	Yield(2) (ksi)	Tensile(1) (ksi)	Yield(2) (ksi)
0	69.3	59.1						
0	69.3	59.5						
0	69.3	58.7						
0	69.3	58.7						
0	66.8	57.9						
2	70.3	60.3	70.2	61.8	70.1	61.1	71.1	62.1
2	69.3	61.5	70.1	61.7	70.3	61.4	70.6	62.0
2	70.2	61.0	70.6	62.1	70.2	61.5	71.3	62.3
2	70.1	62.0	70.2	61.3	70.5	61.5	70.4	62.3
2	69.7	61.5	70.3	61.1	71.5	62.1	70.4	61.6
4	68.3	60.5	68.8	60.9	69.7	61.9	70.2	61.7
4	68.2	61.0	69.3	60.9	70.2	61.3	70.5	60.9
4	68.4	60.3	69.2	60.9	70.1	60.9	70.2	61.5
4	69.6	60.9	68.9	60.9	70.2	61.1	69.2	60.9
4	68.9	61.1	68.8	61.1	69.7	61.3	70.8	61.9
6	68.0	61.1	67.9	60.5	70.6	61.9	69.4	61.1
6	67.7	60.7	67.7	60.7	70.3	61.3	69.2	60.9
6	68.4	60.5	68.0	60.3	70.6	62.1	67.6	60.1
6	67.6	59.9	67.0	59.8	70.1	61.5	69.7	61.3
6	67.1	60.5	67.7	60.2	69.9	61.3	69.4	60.9
9	65.8	59.5	66.5	59.5	67.5	60.3	68.4	61.1
9	66.0	59.9	67.1	59.2	69.3	61.8	68.9	60.7
9	67.1	60.3	66.2	59.2	68.7	60.5	68.9	60.7
9	67.6	60.3	66.9	59.7	67.1	60.9	66.5	60.3
9	67.2	60.3	67.3	59.8	68.4	61.1	67.8	60.7
60					52.3	48.1	48.1	45.6
60					51.6	49.5	43.0	(3)
60					53.1	51.3	44.9	(3)
60					52.4	49.1	42.3	(3)
60					53.6	51.3	45.6	43.6

- NOTES: (1) Gross fracture stress corresponding to maximum tensile load.
(2) Gross section stress corresponding to 0.2% permanent offset.
(3) Failed before reaching 0.2% offset.

APPENDIX C

TABLE C-8

MEAN AND STANDARD DEVIATION OF TENSILE PROPERTIES FOR 0.125 INCH
DIAMETER SHORT TRANSVERSE SPECIMENS OF 7075-T7X2

Exposure Time (days)	Exposure Stress (ksi)	Tensile (ksi)			Yield (ksi)		
		No. of Survivors	(a) Mean	Std. Dev.	No. Tests	Mean	Std. Dev.
0	0	5	68.8	1.12	5	58.8	0.593
2	0	5	69.9	0.415	5	61.3	0.643
2	20	5	70.3	0.192	5	61.6	0.400
2	30	5	70.5	0.568	5	61.5	0.363
2	40	5	70.8	0.416	5	62.1	0.288
4	0	5	68.7	0.581	5	60.8	0.344
4	20	5	69.0	0.234	5	60.9	0.089
4	30	5	70.0	0.259	5	61.3	0.374
4	40	5	70.2	0.602	5	61.4	0.460
6	0	5	67.8	0.483	5	60.5	0.434
6	20	5	67.7	0.391	5	60.3	0.339
6	30	5	70.3	0.308	5	61.6	0.363
6	40	5	69.1	0.836	5	60.9	0.456
9	0	5	66.7	0.793	5	60.1	0.358
9	20	5	66.8	0.447	5	59.5	0.278
9	30	5	68.2	0.894	5	60.9	0.585
9	40	5	68.1	1.00	5	60.7	0.283
60	30	5	52.6	0.771	5	49.9	1.41
60	40	5	44.8	2.29	2(b)	44.6	1.41

NOTES: (a) From group of 5 replicate specimens subjected to identical exposure test conditions.

(b) The mean tensile strength is anomalous with respect to the mean yield strength because yield strengths could not be obtained for some specimens (refer to Table C-7).

APPENDIX C

TABLE C-9

EXTREME VALUE ANALYSIS OF TENSILE PROPERTY DATA FOR 0.125 INCH DIAMETER SHORT TRANVERSE SPECIMENS OF 7075-T7X2 EXPOSED TO 3.5 PERCENT SODIUM CHLORIDE SOLUTION BY ALTERNATE IMMERSION

Exposure Time (days)	Exposure Stress (ksi)	No. of Survivors Out of 5 Exposed	Gross Fracture Stress Mean (ksi)	Gross Fracture Stress Std. Dev. (ksi)	Extreme Value Distribution Parameters (a) $\frac{\mu}{\sigma}$ (ksi)	Probability of Survival At the Exposure Stress	99 Percent Survival Stress (ksi)	99 Percent Penetration Limit, a_{99} (in.)
0	0	5	68.8	1.12	69.6	1.87	61.0	0.018
2	0	5	69.9	0.41	70.2	0.58	67.5	0.008
2	20	5	70.3	0.19	70.4	0.30	69.0	0.004
2	30	5	70.5	0.57	70.9	0.96	66.5	0.010
2	40	5	70.8	0.42	71.0	0.64	68.1	0.007
4	0	5	68.7	0.58	69.1	0.91	64.9	0.013
4	20	5	69.0	0.23	69.2	0.36	67.5	0.008
4	30	5	70.0	0.26	70.1	0.39	68.3	0.006
4	40	5	70.2	0.60	70.5	0.85	66.6	0.010
6	0	5	67.8	0.48	68.0	0.67	65.0	0.013
6	20	5	67.7	0.39	67.9	0.56	65.3	0.012
6	30	5	70.3	0.31	70.5	0.44	68.5	0.006
6	40	5	69.1	0.84	69.6	1.25	63.8	0.015
9	0	5	66.7	0.79	67.2	1.14	62.0	0.017
9	20	5	66.8	0.45	67.1	0.62	64.2	0.014
9	30	5	68.2	0.89	68.7	1.25	63.0	0.016
9	40	5	68.1	1.00	68.7	1.41	62.2	0.017
60	30	5	52.6	0.77	53.1	1.08	48.1	0.032
60	40	5	44.8	2.29	46.2	3.30	31.0	0.050

NOTE: (a) μ and σ are the location and scale parameters, respectively, which define the extreme value distribution of gross fracture stresses. These parameters were determined by probability plotting using probability scales adjusted for the sample size (No. of survivors). This method allows the estimation of correct distribution parameters for truncated sample sizes due to specimen failures, as outlined in Section II.D.2.b.

APPENDIX C

TABLE C-10

APPARENT TENSILE PROPERTIES OF 0.225 INCH DIAMETER SHORT TRANSVERSE SPECIMENS
OF 7075-T7X1 ALLOY EXPOSED TO 3.5 PERCENT SODIUM CHLORIDE SOLUTION BY
ALTERNATE IMMERSION

Exposure Time (days)	Exposure Stress							
	No Stress		20 ksi		30 ksi		40 ksi	
	Tensile(1) (ksi)	Yield(2) (ksi)	Tensile(1) (ksi)	Yield(2) (ksi)	Tensile(1) (ksi)	Yield(2) (ksi)	Tensile(1) (ksi)	Yield(2) (ksi)
0	70.3	61.9						
0	70.4	61.1						
0	70.4	61.9						
0	70.7	61.6						
0	70.2	61.1						
2	69.7	61.9	69.0	61.6	68.8	61.0	68.8	62.0
2	69.7	61.5	69.8	62.1	68.9	61.0	69.4	62.9
2	69.9	61.4	70.4	61.5	65.6	61.5	69.8	63.4
2	69.7	60.9	69.8	61.9	67.0	61.9	70.9	63.6
2	70.0	61.6	66.6	61.9	66.0	61.1	70.2	62.8
4	69.5	61.6	68.9	63.9	64.9	60.4	63.9	63.1
4	69.3	62.1	67.0	61.1	60.5	59.9	66.4	62.4
4	69.3	61.9	67.4	61.6	63.8	61.0	59.1	(3)
4	68.8	61.4	64.4	61.1	64.6	61.1	69.4	61.9
4	69.7	62.1	68.4	61.1	60.2	60.1	63.0	62.1
6	69.2	62.4	66.0	60.9	63.3	60.1	60.7	(3)
6	68.4	61.6	67.8	61.6	63.4	60.4	64.6	64.1
6	69.2	61.1	67.0	61.6	65.4	61.6	58.7	(3)
6	69.7	61.9	67.7	60.9	62.1	60.4	64.8	62.9
6	69.3	61.4	60.4	60.4	57.8	(3)	48.9	(3)
9	68.2	60.9	65.4	60.4	64.9	59.9	63.1	60.9
9	68.3	61.4	66.9	59.4	56.3	(3)	59.0	(3)
9	67.7	60.9	65.0	59.4	61.4	58.1	(F7d)	--
9	68.5	61.1	67.0	60.1	63.4	58.9	55.2	(3)
9	67.5	60.9	65.3	59.9	57.1	(3)	60.0	(3)
12	66.4	60.7	65.4	60.4	65.3	59.1	63.9	62.1
12	68.4	60.7	65.1	59.6	64.5	59.6	67.8	61.4
12	68.0	60.4	64.1	58.6	63.9	59.1	66.6	62.1
12	67.8	60.6	67.5	60.6	65.4	59.6	64.7	--
12	67.4	60.4	65.8	59.6	61.9	59.2	66.1	60.9
60			58.6	53.3	38.4	(3)	47.0	(3)
60			56.5	51.8	43.6	(3)	--	--
60			55.5	53.6	50.9	50.8	(F15D)	--
60			57.7	54.8	51.6	50.0	(F12d)	--
60			54.1	52.1	(F37d)	--	(F37d)	--

- NOTES: (1) Gross fracture stress corresponding to maximum tensile load.
(2) Gross section stress corresponding to 0.2% permanent offset.
(3) Failed before reaching 0.2% offset.
(4) (Fxd) means specimen failed after x days exposure.

APPENDIX C

TABLE C-11

MEAN AND STANDARD DEVIATION OF TENSILE PROPERTIES FOR 0.225 INCH
DIAMETER SHORT TRANSVERSE SPECIMENS OF 7075-T7X1

Exposure Time (days)	Exposure Stress (ksi)	No. of Survivors(a)	Tensile (ksi)		No. Tests	Yield (ksi)	
			Mean(b)	Std. Dev.(b)		Mean	Std. Dev.
0	0	5	70.4	0.187	5	61.5	0.403
2	0	5	69.8	0.141	5	61.5	0.365
2	20	5	69.1	1.49	5	61.8	0.245
2	30	5	67.3	1.54	5	61.3	0.394
2	40	5	69.8	0.795	5	62.9	0.623
4	0	5	69.3	0.335	5	61.8	0.311
4	20	5	67.2	1.75	5	61.8	1.22
4	30	5	62.8	2.28	5	60.5	0.534
4	40	5	64.4	3.85	4(c)	62.4	0.525
6	0	5	69.2	0.472	5	61.7	0.497
6	20	5	65.8	3.09	5	61.1	0.517
6	30	5	62.4	2.83	4(c)	60.6	0.665
6	40	5	59.5	6.49	2(c)	63.5	0.849
9	0	5	68.0	0.422	5	61.0	0.219
9	20	5	65.9	0.952	5	59.8	0.439
9	30	5	60.6	3.80	3(c)	59.0	0.902
9	40	4	59.3(55.4)	3.26(9.09)	1(c)	60.9	--
12	0	5	67.6	0.762	5	60.6	0.152
12	20	5	65.6	1.24	5	59.8	0.793
12	30	5	64.2	1.43	5	59.3	0.259
12	40	5	65.8	1.54	4(c)	61.6	0.585
60	20	5	56.5	1.78	5	53.1	1.21
60	30	4	46.1(42.9)	6.29(9.04)	2(c)	50.4	0.566
60	40	1(d)	47.0(41.4)	-- (3.13)	-	--	--

- NOTES: (a) From group of 5 replicate specimens subjected to identical exposure test conditions.
- (b) Numbers in parenthesis correspond to values calculated for five specimens using the exposure stress for specimens which failed prior to tensile testing. All other calculated values are based on the survivors.
- (c) The mean tensile strengths are anomalous with respect to the mean yield strengths because yield strengths could not be obtained for some specimens (refer to Table C-10).
- (d) One survivor out of four specimens tested.

ORIGINAL PAGE IS
OF POOR QUALITY

APPENDIX C

TABLE C-12

EXTREME VALUE ANALYSIS OF TENSILE PROPERTY DATA FOR 0.225 INCH DIAMETER SHORT TRANSVERSE SPECIMENS OF 7075-T7X1 EXPOSED TO 3.5 PERCENT SODIUM CHLORIDE SOLUTION BY ALTERNATE IMMERSION

Exposure Time (days)	Exposure Stress (ksi)	No. of Survivors Out of 5 Exposed	Gross Fracture Stress(a)		Extreme Value Distribution Parameters(b)		Probability of Survival at the Exposure Stress	99 Percent Survival Stress (ksi)	99 Percent Penetration Limit, a_{99} (in.)
			Mean (ksi)	Std. Dev. (ksi)	$\hat{\mu}$ (ksi)	$\hat{\sigma}$ (ksi)			
0	0	5	70.4	0.19	70.5	0.28	1.000	69.2	0.007
2	0	5	69.8	0.14	69.9	0.24	1.000	68.8	0.009
2	20	5	69.1	1.49	70.0	2.14	1.000	60.2	0.027
2	30	5	67.3	1.54	68.2	2.26	1.000	57.8	0.032
2	40	5	69.8	0.79	70.3	1.10	1.000	65.2	0.018
4	0	5	69.3	0.33	69.5	0.47	1.000	67.4	0.013
4	20	5	67.2	1.75	68.3	2.44	1.000	57.0	0.033
4	30	5	62.8	2.27	64.2	3.37	1.000	48.7	0.046
4	40	5	64.4	3.85	66.6	5.33	.993	42.1	0.057
6	0	5	69.2	0.47	69.4	0.68	1.000	66.3	0.015
6	20	5	65.8	3.09	67.7	4.59	1.000	46.6	0.050
6	30	5	62.4	2.83	64.1	3.98	1.000	45.8	0.051
6	40	5	59.5	6.49	63.4	9.17	.925	21.2	0.096
9	0	5	68.0	0.42	68.3	0.59	1.000	65.6	0.017
9	20	5	65.9	0.95	66.5	1.47	1.000	59.8	0.028
9	30	5	60.6	3.80	62.9	5.44	0.998	37.9	0.064
9	40	4	59.3 (55.4)	3.26 (9.09)	60.5	7.28	0.942	27.0	0.083
12	0	5	67.6	0.76	68.0	1.05	1.000	63.2	0.022
12	20	5	65.6	1.24	66.3	1.81	1.000	58.0	0.031
12	30	5	64.2	1.42	65.0	2.00	1.000	55.9	0.035
12	40	5	65.8	1.54	66.7	2.15	1.000	56.8	0.033
60	20	5	56.5	1.78	57.5	2.44	1.000	46.3	0.050
60	30	4	46.1 (42.9)	6.29 (9.04)	48.5	14.49	0.757	0.0	∞
60	40	1(c)	47.0 (41.4)	-- (3.13)	--	--	0.250	0.0	∞

- NOTES: (a) Numbers in parenthesis correspond to values calculated for five specimens using the exposure stress for specimens which failed prior to tensile testing. All other values are based on the survivors.
- (b) $\hat{\mu}$ and $\hat{\sigma}$ are the location and scale parameters, respectively, which define the extreme value distribution of gross fracture stresses. These parameters were determined by probability plotting using probability scales adjusted for the sample size (number of survivors). This method allows estimation of the correct distribution parameters for truncated sample sizes due to specimen failures, as outlined in Section III.D.2.b.
- (c) One survivor out of four specimens tested.

APPENDIX C

TABLE C-13

APPARENT TENSILE PROPERTIES OF 0.225 INCH DIAMETER LONG TRANSVERSE SPECIMENS OF 7075-T651 ALLOY EXPOSED TO 3.5 PERCENT SODIUM CHLORIDE SOLUTION BY ALTERNATE IMMERSION

Exposure Time (days)	Exposure Stress					
	No Stress		30 ksi		40 ksi	
	Tensile(1) (ksi)	Yield(2) (ksi)	Tensile(1) (ksi)	Yield(2) (ksi)	Tensile(1) (ksi)	Yield(2) (ksi)
0	78.6	66.4				
0	81.0	68.9				
0	79.0	66.6				
0	78.6	66.1				
0	80.9	68.7				
2	79.6	66.4	80.9	69.8	79.0	66.6
2	79.1	66.8	79.1	66.6	79.0	67.7
2	81.1	69.4	79.3	67.2	80.9	69.9
2	79.0	66.9	81.1	69.4	78.8	66.4
2	78.8	67.4	79.2	66.9	79.0	67.4
4	80.5	68.9	77.8	67.2	78.7	68.7
4	78.8	66.6	78.7	68.7	76.6	66.9
4	78.3	66.4	77.0	65.9	76.0	66.4
4	80.7	69.2	77.3	66.4	79.2	69.2
4	78.8	66.4	78.7	68.7	75.8	66.4
8	77.3	66.6	74.9	64.6	75.5	65.9
8	79.6	69.2	75.2	65.6	76.2	68.2
8	77.7	66.1	76.8	67.4	75.6	65.9
8	77.5	66.1	75.8	65.1	74.9	65.9
8	79.2	68.4	75.7	65.1	76.5	67.4
15	76.1	65.1	75.5	66.1	73.3	64.9
15	76.1	65.6	74.3	64.4	72.8	64.4
15	76.7	67.3	74.7	64.4	74.7	67.4
15	75.5	65.8	76.5	65.9	71.4	63.1
15	75.0	63.8	73.3	63.1	71.0	63.9
60			65.9	57.9	64.0	60.6
60			65.4	(3)	63.8	58.3
60			64.6	(3)	64.8	58.9
60			63.9	57.8	65.4	59.6
60			66.5	59.9	63.4	58.6

- NOTES: (1) Gross fracture stress corresponding to maximum tensile load.
 (2) Gross section stress corresponding to 0.2% permanent offset.
 (3) Failed before reaching 0.2% offset.

APPENDIX C

TABLE C-14

MEAN AND STANDARD DEVIATION OF TENSILE PROPERTIES FOR 0.225 INCH
DIAMETER LONG TRANSVERSE SPECIMENS OF 7075-T651 EXPOSED TO 3.5 PERCENT
SODIUM CHLORIDE SOLUTION BY ALTERNATE IMMERSION

Exposure Time (days)	Exposure Stress (ksi)	Tensile (ksi)			Yield (ksi)		
		No. of Survivors	(a) Mean	Std. Dev.	No. Tests	Mean	Std. Dev.
0	0	5	79.6	1.23	5	67.3	1.35
2	0	5	79.5	0.931	5	67.4	1.18
2	30	5	79.9	0.991	5	68.0	1.50
2	40	5	79.3	0.876	5	67.6	1.39
4	0	5	79.4	1.10	5	67.5	1.42
4	30	5	77.9	0.784	5	67.4	1.29
4	40	5	77.3	1.58	5	67.5	1.33
8	0	5	78.3	1.06	5	67.3	1.43
8	30	5	75.7	0.726	5	65.6	1.09
8	40	5	75.7	0.627	5	66.7	1.08
15	0	5	75.9	0.650	5	65.5	1.26
15	30	5	74.9	1.21	5	64.8	1.24
15	40	5	72.6	1.49	5	64.7	1.63
60	30	5	65.3	1.03	3(b)	58.5	1.19
60	40	5	64.3	0.807	5	59.2	0.919

NOTES: (a) From group of 5 replicate specimens subjected to identical exposure test conditions.

(b) The mean tensile strength is anomalous with respect to the mean yield strength because yield strengths could not be obtained for some specimens (refer to Table C-13).

APPENDIX C

TABLE C-15

EXTREME VALUE ANALYSIS OF TENSILE PROPERTY DATA FOR 0.225 INCH DIAMETER
LONG TRANSVERSE SPECIMENS OF 7075-T651 EXPOSED TO 3.5 PERCENT SODIUM
CHLORIDE SOLUTION BY ALTERNATE IMMERSION

Exposure Time (day)	Exposure Stress (ksi)	No. of Survivors Out of 5 Exposed	Gross Fracture Stress		Extreme Value Distribution Parameters(a)		99 Percent Survival Stress (ksi)
			Mean (ksi)	Std. Dev. (ksi)	$\hat{\mu}$ (ksi)	$\hat{\sigma}$ (ksi)	
0	0	5	79.6	1.23	80.5	1.96	71.4
2	0	5	79.5	0.93	80.2	1.54	73.1
2	30	5	79.9	0.99	80.6	1.60	73.3
2	40	5	79.3	0.88	80.1	1.70	72.3
4	0	5	79.4	1.10	80.1	1.68	72.4
4	30	5	77.9	0.78	78.4	1.14	73.1
4	40	5	77.3	1.58	78.3	2.41	67.2
8	0	5	78.3	1.06	79.0	1.64	71.4
8	30	5	75.7	0.73	76.1	1.07	71.2
8	40	5	75.7	0.63	76.1	0.87	72.1
15	0	5	75.9	0.65	76.3	0.90	72.1
15	30	5	74.9	1.21	75.6	1.69	67.8
15	40	5	72.6	1.49	73.5	2.14	63.7
60	30	5	65.3	1.03	65.9	1.42	59.3
60	40	5	64.3	0.81	64.8	1.17	59.4

NOTE: (a) $\hat{\mu}$ and $\hat{\sigma}$ are the location and scale parameters, respectively, which define the extreme value distribution of gross fracture stresses. These parameters were determined by probability plotting using probability scales adjusted for the sample size (number of survivors). This method allows estimation of the correct distribution parameters for truncated sample sizes due to specimen failure, as outlined in Section III.D.2.b.

APPENDIX D

DETAILED TEST DATA AND ANALYTICAL PROCEDURES FOR THE
FRACTURE MECHANICS TYPE STRESS CORROSION TESTS

APPENDIX D

DETAILED TEST DATA AND ANALYTICAL PROCEDURES FOR THE FRACTURE MECHANICS TYPE STRESS CORROSION TESTS

- Table D-1. Environmental Crack Growth Data for 7075-T651, DCB Specimen SL-1.
- Table D-2. Environmental Crack Growth Data for 7075-T651, DCB Specimen SL-2.
- Table D-3. Environmental Crack Growth Data for 7075-T7X1, DCB Specimen SL-1.
- Table D-4. Environmental Crack Growth Data for 7075-T7X1, DCB Specimen SL-2.
- Table D-5. Environmental Crack Growth Data for 7075-T7X2, DCB Specimen SL-1.
- Table D-6. Environmental Crack Growth Data for 7075-T7X2, DCB Specimen SL-2.
- Table D-7. Comparison of Data Reduction Methods for Calculating Crack Growth Rates in DCB Specimens.
- Table D-8. Summary of Crack Length Measurements and Stress Intensity Factor Calculations for Ring-Loaded WOL Specimens Exposed to 3.5% NaCl Solution Introduced Dropwise into the Crack Three Times a Day.

APPENDIX D

TABLE D-1

Environmental Crack Growth Data for 7075-T651, DCB Specimen SL-1

STRESS INTENSITY CALCULATIONS OF DCB TYPE SPECIMENS
AVERAGE OF 2 SURFACES AND 3 INTERIOR PLANES

ENVIRONMENT -SALT DROP
ALLOY + TEMPER - 7075T651
S NUMBER-DASH - 5476198L1
PRODUCT TYPE - PLATE THICKNESS - 2.5 INCHES
MODULUS OF ELASTICITY - .103E+08
TOTAL V, D1-D0 - .265E-01 INCHES
NOTCH DEPTH - 1 INCHES
BEAM HEIGHT - .991 INCHES

DAYS	CRACK INCHES	LENGTH MM	CRACK INCHES	GROWTH MM	K VALUE	
					PSI $\sqrt{\text{IN}}$	MPA $\sqrt{\text{M}}$
0	1.182	30.03	0.0000	0.00	17604.05	19.4877
1	1.186	30.11	0.0034	0.09	17527.75	19.4032
2	1.190	30.22	0.0074	0.19	17438.61	19.3045
3	1.193	30.29	0.0104	0.26	17372.20	19.2310
4	1.218	30.93	0.0356	0.90	16828.92	18.6296
7	1.252	31.81	0.0700	1.78	16127.27	17.8529
9	1.272	32.32	0.0902	2.29	15735.38	17.4191
11	1.288	32.72	0.1060	2.69	15438.66	17.0906
14	1.324	33.62	0.1414	3.59	14803.37	16.3873
16	1.356	34.44	0.1736	4.41	14258.75	15.7844
18	1.363	34.61	0.1804	4.58	14147.55	15.6613
21	1.392	35.36	0.2098	5.33	13681.36	15.1453
23	1.392	35.36	0.2098	5.33	13681.36	15.1453
28	1.398	35.52	0.2162	5.49	13582.91	15.0363
30	1.414	35.92	0.2320	5.89	13344.33	14.7722
39	1.508	38.31	0.3262	8.29	12043.36	13.3320
46	1.611	40.93	0.4292	10.90	10825.95	11.9843
52	1.655	42.03	0.4726	12.00	10367.27	11.4766
63	1.709	43.42	0.5272	13.39	9830.22	10.8821
71	1.743	44.28	0.5612	14.25	9516.47	10.5347
77	1.793	45.54	0.6108	15.51	9084.85	10.0569
*	1.815					

* AVERAGE CRACK LENGTH MEASURED ON THE FRACTURED SURFACE AFTER
CONCLUSION OF EXPOSURE

ORIGINAL PAGE 10
OF POOR QUALITY

APPENDIX D

ORIGINAL PAGE 10
OF POOR QUALITY

TABLE D-2

Environmental Crack Growth Data for 7075-T651, DCB Specimen SL-2STRESS INTENSITY CALCULATIONS OF DCB TYPE SPECIMENS
AVERAGE OF 2 SURFACES AND 3 INTERIOR PLANES

ENVIRONMENT -SALT DROP

ALLOY + TEMPER - 7075T651

S NUMBER-DASH - 547619SL2

PRODUCT TYPE - PLATE THICKNESS - 2.5 INCHES

MODULUS OF ELASTICITY - .103E+08

TOTAL V, D1-D0 - .23E-01 INCHES

NOTCH DEPTH - 1 INCHES

BEAM HEIGHT - .992 INCHES

DAYS	CRACK INCHES	LENGTH MM	CRACK INCHES	GROWTH MM	K VALUE	
					PSI $\sqrt{\text{IN}}$	MPA $\sqrt{\text{M}}$
0	1.125	28.59	0.0000	0.00	16468.53	18.2307
1	1.131	28.74	0.0060	0.15	16338.29	18.0865
2	1.152	29.27	0.0268	0.68	15898.48	17.5996
3	1.176	29.87	0.0506	1.29	15416.55	17.0661
4	1.185	30.10	0.0598	1.52	15236.09	16.8663
7	1.221	31.02	0.0960	2.44	14555.71	16.1132
9	1.222	31.03	0.0964	2.45	14548.44	16.1051
11	1.253	31.84	0.1280	3.25	13991.28	15.4884
14	1.294	32.86	0.1682	4.27	13327.28	14.7533
16	1.333	33.85	0.2074	5.27	12724.01	14.0855
18	1.337	33.97	0.2120	5.38	12655.90	14.0101
21	1.394	35.42	0.2690	6.83	11855.07	13.1236
23	1.400	35.57	0.2750	6.98	11775.19	13.0351
28	1.425	36.21	0.3000	7.62	11450.84	12.6761
30	1.449	36.79	0.3232	8.21	11161.60	12.3559
39	1.491	37.88	0.3658	9.29	10658.10	11.7985
46	1.595	40.52	0.4698	11.93	9562.25	10.5854
52	1.667	42.34	0.5414	13.75	8902.56	9.8551
63	1.742	44.25	0.6168	15.67	8278.56	9.1644
71	1.777	45.14	0.6516	16.55	8012.33	8.8696
77	1.835	46.61	0.7096	18.02	7596.13	8.4089
*	1.865					

* AVERAGE CRACK LENGTH MEASURED ON THE FRACTURED SURFACE AFTER
CONCLUSION OF EXPOSURE

APPENDIX D

TABLE D-3

Environmental Crack Growth Data for 7075-T7X1, DCB Specimen SL-1

STRESS INTENSITY CALCULATIONS OF DCB TYPE SPECIMENS
AVERAGE OF 2 SURFACES AND 3 INTERIOR PLANES

ENVIRONMENT -SALT DROP
ALLOY + TEMPER - 7075T7X1
S NUMBER-DASH - 550915SL1
PRODUCT TYPE - PLATE THICKNESS - 2.5 INCHES
MODULUS OF ELASTICITY - .103E+08
TOTAL V, D1-D0 - .305E-01 INCHES
NOTCH DEPTH - 1 INCHES
BEAM HEIGHT - .9915 INCHES

DAYS	CRACK INCHES	LENGTH MM	CRACK INCHES	GROWTH MM	K VALUE	
					PSI \sqrt{IN}	MPA \sqrt{M}
0	1.225	31.13	0.0000	0.00	19196.21	21.2502
1	1.226	31.13	0.0002	0.01	19191.43	21.2449
2	1.227	31.16	0.0014	0.04	19162.79	21.2132
3	1.234	31.35	0.0090	0.23	18982.89	21.0141
4	1.235	31.36	0.0092	0.23	18978.19	21.0089
7	1.239	31.48	0.0140	0.36	18865.90	20.8845
9	1.239	31.48	0.0140	0.36	18865.90	20.8845
11	1.239	31.48	0.0140	0.36	18865.90	20.8845
14	1.255	31.87	0.0292	0.74	18516.77	20.4981
16	1.255	31.87	0.0294	0.75	18512.25	20.4931
18	1.255	31.88	0.0296	0.75	18507.72	20.4880
21	1.257	31.93	0.0316	0.80	18462.53	20.4380
23	1.257	31.93	0.0316	0.80	18462.53	20.4380
28	1.257	31.93	0.0316	0.80	18462.53	20.4380
30	1.259	31.98	0.0336	0.85	18417.51	20.3882
39	1.262	32.04	0.0362	0.92	18359.22	20.3237
46	1.271	32.28	0.0456	1.16	18150.78	20.0929
52	1.272	32.32	0.0470	1.19	18120.03	20.0589
63	1.273	32.34	0.0480	1.22	18098.12	20.0346
71	1.278	32.45	0.0522	1.33	18006.52	19.9332
*	1.352					

* AVERAGE CRACK LENGTH MEASURED ON THE FRACTURED SURFACE AFTER
CONCLUSION OF EXPOSURE

ORIGINAL COPY
OF POOR QUALITY

APPENDIX D

ORIGINAL
OF POC

TABLE D-4

Environmental Crack Growth Data for 7075-T7X1, DCB Specimen SL-2

STRESS INTENSITY CALCULATIONS OF DCB TYPE SPECIMENS
AVERAGE OF 2 SURFACES AND 3 INTERIOR PLANES

ENVIRONMENT -SALT DROP
 ALLOY + TEMPER - 7075T7X1
 S NUMBER-DASH - 550915SL2
 PRODUCT TYPE - PLATE THICKNESS - 2.5 INCHES
 MODULUS OF ELASTICITY - .103E+08
 TOTAL V, D1-D0 - .28E-01 INCHES
 NOTCH DEPTH - 1 INCHES
 BEAM HEIGHT - .993 INCHES

DAYS	CRACK INCHES	LENGTH MM	CRACK INCHES	GROWTH MM	K VALUE	
					PSI $\sqrt{\text{IN}}$	MPA $\sqrt{\text{M}}$
0	1.158	29.41	0.0000	0.00	19228.62	21.2861
1	1.158	29.42	0.0002	0.01	19223.63	21.2806
2	1.159	29.44	0.0012	0.03	19198.71	21.2530
3	1.159	29.44	0.0012	0.03	19198.71	21.2530
4	1.159	29.44	0.0012	0.03	19198.71	21.2530
7	1.160	29.46	0.0018	0.05	19183.78	21.2364
9	1.160	29.46	0.0018	0.05	19183.78	21.2364
11	1.168	29.66	0.0096	0.24	18991.23	21.0233
14	1.170	29.72	0.0120	0.30	18932.56	20.9583
16	1.171	29.74	0.0128	0.33	18913.07	20.9368
18	1.171	29.74	0.0130	0.33	18908.20	20.9314
21	1.171	29.75	0.0134	0.34	18898.46	20.9206
23	1.171	29.75	0.0134	0.34	18898.46	20.9206
28	1.192	30.29	0.0344	0.87	18397.80	20.3664
30	1.202	30.54	0.0444	1.13	18166.31	20.1101
39	1.212	30.79	0.0544	1.38	17939.14	19.8586
46	1.244	31.59	0.0858	2.18	17252.68	19.0987
52	1.269	32.23	0.1108	2.81	16733.76	18.5243
63	1.277	32.44	0.1192	3.03	16564.61	18.3370
71	1.281	32.54	0.1232	3.13	16484.95	18.2488
77	1.303	33.10	0.1450	3.68	16060.71	17.7792
*	1.332					

* AVERAGE CRACK LENGTH MEASURED ON THE FRACTURED SURFACE AFTER
CONCLUSION OF EXPOSURE

APPENDIX D

ORIGINAL PAGE IS
OF POOR QUALITY

TABLE D-5

Environmental Crack Growth Data for 7075-T7X2, DCB Specimen SL-1STRESS INTENSITY CALCULATIONS OF DCB TYPE SPECIMENS
AVERAGE OF 2 SURFACES AND 3 INTERIOR PLANES

ENVIRONMENT -SALT DROP
 ALLOY + TEMPER - 7075T7X2
 S NUMBER-DASH - 5476208L1
 PRODUCT TYPE - PLATE THICKNESS - 2.5 INCHES
 MODULUS OF ELASTICITY - .103E+08
 TOTAL V, D1-D0 - .275E-01 INCHES
 NOTCH DEPTH - 1 INCHES
 BEAM HEIGHT - .9935 INCHES

DAYS	CRACK INCHES	LENGTH MM	CRACK INCHES	GROWTH MM	K VALUE	
					PSI $\sqrt{\text{IN}}$	MPA $\sqrt{\text{M}}$
0	1.146	29.11	0.0000	0.00	19187.49	21.2406
1	1.148	29.16	0.0020	0.05	19137.41	21.1851
2	1.152	29.27	0.0060	0.15	19037.82	21.0749
3	1.155	29.33	0.0086	0.22	18973.51	21.0037
4	1.160	29.45	0.0134	0.34	18855.62	20.8732
7	1.161	29.48	0.0146	0.37	18826.32	20.8407
9	1.161	29.49	0.0148	0.38	18821.44	20.8353
11	1.161	29.49	0.0148	0.38	18821.44	20.8353
14	1.162	29.51	0.0158	0.40	18797.08	20.8084
16	1.162	29.51	0.0158	0.40	18797.08	20.8084
18	1.162	29.51	0.0156	0.40	18801.95	20.8138
21	1.162	29.51	0.0158	0.40	18797.08	20.8084
23	1.162	29.51	0.0158	0.40	18797.08	20.8084
28	1.164	29.58	0.0182	0.46	18738.82	20.7439
30	1.164	29.58	0.0182	0.46	18738.82	20.7439
39	1.164	29.58	0.0182	0.46	18738.82	20.7439
46	1.164	29.58	0.0182	0.46	18738.82	20.7439
52	1.165	29.59	0.0186	0.47	18729.13	20.7331
63	1.165	29.59	0.0186	0.47	18729.13	20.7331
71	1.165	29.59	0.0188	0.48	18724.29	20.7278
77	1.169	29.69	0.0228	0.58	18627.89	20.6211
*	1.185					

* AVERAGE CRACK LENGTH MEASURED ON THE FRACTURED SURFACE AFTER
CONCLUSION OF EXPOSURE

APPENDIX D

ORIGINAL
OF POOR QUALITY

TABLE D-6

Environmental Crack Growth Data for 7075-T7X2, DCB Specimen SL-2STRESS INTENSITY CALCULATIONS OF DCB TYPE SPECIMENS
AVERAGE OF 2 SURFACES AND 3 INTERIOR PLANES

ENVIRONMENT -SALT DROP
 ALLOY + TEMPER - 7075T7X2
 S NUMBER-DASH - 547620SL2
 PRODUCT TYPE - PLATE THICKNESS - 2.5 INCHES
 MODULUS OF ELASTICITY - .103E+08
 TOTAL V, D1-D0 - .31E-01 INCHES
 NOTCH DEPTH - 1 INCHES
 BEAM HEIGHT - .9945INCHES

DAYS	CRACK INCHES	LENGTH MM	CRACK INCHES	GROWTH MM	K VALUE	
					PSI $\sqrt{\text{IN}}$	MPA $\sqrt{\text{M}}$
0	1.096	27.83	0.0000	0.00	23157.40	25.6352
1	1.099	27.92	0.0038	0.10	23038.95	25.5041
2	1.109	28.17	0.0134	0.34	22743.69	25.1773
3	1.115	28.31	0.0190	0.48	22574.05	24.9895
4	1.115	28.33	0.0198	0.50	22549.97	24.9628
7	1.120	28.46	0.0248	0.63	22400.34	24.7972
9	1.121	28.46	0.0250	0.64	22394.39	24.7906
11	1.122	28.51	0.0268	0.68	22340.90	24.7314
14	1.124	28.54	0.0282	0.72	22299.44	24.6855
16	1.127	28.62	0.0310	0.79	22216.85	24.5941
18	1.127	28.62	0.0312	0.79	22210.97	24.5875
21	1.127	28.63	0.0314	0.80	22205.09	24.5810
23	1.127	28.63	0.0314	0.80	22205.09	24.5810
28	1.128	28.64	0.0320	0.81	22187.46	24.5615
30	1.130	28.69	0.0340	0.86	22128.86	24.4967
39	1.131	28.72	0.0352	0.89	22093.82	24.4579
46	1.155	29.33	0.0590	1.50	21415.45	23.7069
52	1.155	29.34	0.0594	1.51	21404.32	23.6946
63	1.165	29.60	0.0696	1.77	21123.29	23.3835
71	1.165	29.60	0.0698	1.77	21117.83	23.3774
77	1.167	29.64	0.0714	1.81	21074.26	23.3292
*	1.178					

* AVERAGE CRACK LENGTH MEASURED ON THE FRACTURED SURFACE AFTER
CONCLUSION OF EXPOSURE

APPENDIX D

TABLE D-7

Comparison of Data Reduction Methods for Calculating Crack Growth Rates in DCB Specimens

Method	Degree of Smoothing	Comments
Graphical	Subject to choice	<ul style="list-style-type: none"> - Simple to calculate. - Degree of smoothing depends on the choice of region used to determine rates. - Very subjective.
Secant	Low	<ul style="list-style-type: none"> - Simple to calculate. - Should use minimum crack growth increment. - Crack growth rates retain high degree of noise, but with no sacrifice of filtering small perturbations from results.
Curve Fitting	High	<ul style="list-style-type: none"> - Generally, complex calculations required. - Amount and type of smoothing depends on choice of curve to fit and method of fitting. - Fit curve often not statistically sound. - Often requires judgement to choose appropriate curve to fit. - Smoothing often results in shift in location of inflection points (typical of high degree of filtering).
Incremental Polynomial	Moderate	<ul style="list-style-type: none"> - Moderately complex calculation and data handling. - Only smooths data locally, major trends maintained. - Least subjective of the smoothing techniques. - Used extensively in fatigue crack growth testing, and is a generally accepted method used by a large body of testing technology. - As with most smoothing techniques, extremes of the crack growth rates are sacrificed (ie. no rates can be calculated at the low and high ends of the curve).

APPENDIX D

TABLE D-8

SUMMARY OF CRACK LENGTH MEASUREMENTS AND STRESS INTENSITY FACTOR CALCULATIONS FOR RING-LOADED WOL SPECIMENS EXPOSED TO 3.5% SODIUM CHLORIDE SOLUTION INTRODUCED DROPWISE INTO THE CRACK THREE TIMES A DAY

Specimen	a ₀	P ₀	K ₀	a _f	P _f	K _f	K _{IC}	K ₀ /K _{IC}	K _f /K _{IC}	Start Date	End Date	Notes	
547619 1	7075-T651	0.861*	1995	9.42	1.467	1850	15.90	19.3	0.49	0.82	11/30	02/04	Removed from test 83-02-04, fracture test run, closure evident; definite crack growth.
2		0.916*	1398	6.90	1.175	1384	8.53	19.3	0.36	0.44	12/10	03/07	Removed from test 83-03-07, fracture test run, closure evident; definite crack growth.
3		0.910*	801	3.97				19.3	0.21		12/10	02/04	No growth evident on 83-02-04, precracked additional amount.
		0.922*	1608	7.89	1.182	1493	9.26	19.3	0.41	0.48	02/08	03/07	Crack length at start in question, fracture tests run, closure evident; definite crack growth.
550915 1	7075-T7X1	0.880	1401	6.72	0.880	1424	6.83	19.4	0.35	0.35	12/10	02/04	No growth evident on 83-02-04, precracked add'l amt., but specimen broke upon reloading.
2		0.857*	2001	9.42	0.857	1996	9.40	19.4	0.49	0.48	11/30	02/09	Removed for metallurgical sectioning. No growth indicated by monitoring equipment.
3		0.851*	3000	14.00	0.883	2990	14.40	19.4	0.72	0.74	11/30	03/07	Fracture test run, little or no closure evident; no crack growth indicated by monitoring equipment.
547620 1	7075-T7X2	0.932*	2990	14.94	0.932	2969	14.84	20.2	0.74	0.73	11/30	02/04	Removed for metallurgical sectioning. No growth indicated by monitoring equipment.
2		0.883*	3200	15.40	0.850	3203	15.00	20.2	0.76	0.74	11/30	03/07	Fracture test run, little or no closure evident; no crack growth indicated by monitoring equipment.
3		0.918*	3800	18.80	0.923	3740	18.60	20.2	0.93	0.92	11/30	02/04	Fracture test run, little or no closure evident; possible crack growth indicated by monitoring equipment.

NOTE: * From initial compliance, otherwise measured, may not agree with surface measurements.

ORIGINAL PAGE IS
OF POOR QUALITY

END

DATE

FILMED

JAN 10 1985